C1 Chemistry for the Production of Ultra-Clean Liquid Transportation Fuels and Hydrogen

Annual report
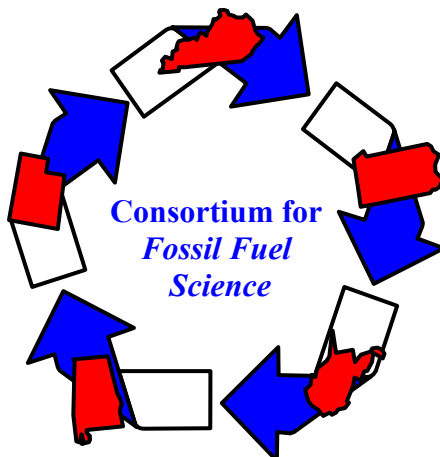**Research conducted October 1, 2002-September 30, 2003**
U.S. Department of Energy Contract No. DE-FC26-02NT41594
Prepared by the Consortium for Fossil Fuel Science
Gerald P. Huffman, Director
CFFS / University of Kentucky
533 S. Limestone Street, Suite 107
Lexington, KY 40506
Phone: (859) 257-4027
FAX: (859) 257-7215
E-mail: huffman@engr.uky.edu

Consortium for Fossil Fuel Science
University of Kentucky
West Virginia University
University of Pittsburgh
University of Utah
Auburn University

Consortium for
*Fossil Fuel
Science*

C1 Chemistry for Production of Clean Liquid Transportation Fuels and Hydrogen

Abstract

The Consortium for Fossil Fuel Science (CFFS) is a research consortium with participants from the University of Kentucky, University of Pittsburgh, University of Utah, West Virginia University, and Auburn University. The CFFS is conducting a research program to develop C1 chemistry technology for the production of clean transportation fuel from resources such as coal and natural gas, which are more plentiful domestically than petroleum. The processes under development will convert feedstocks containing one carbon atom per molecular unit into ultra clean liquid transportation fuels (gasoline, diesel, and jet fuel) and hydrogen, which many believe will be the transportation fuel of the future. These feedstocks include synthesis gas, a mixture of carbon monoxide and hydrogen produced by coal gasification or reforming of natural gas, methane, methanol, carbon dioxide, and carbon monoxide. Some highlights of the results obtained during the first year of the current research contract are summarized below.

➢
➢ Terminal alkynes are an effective chain initiator for Fischer-Tropsch (FT) reactions, producing normal paraffins with C numbers ≥ to that of the added alkyne.
➢ Significant improvement in the product distribution towards heavier hydrocarbons (C_5 to C_{19}) was achieved in supercritical fluid (SCF) FT reactions compared to that of gas-phase reactions.
➢ Xerogel and aerogel silica supported cobalt catalysts were successfully employed for FT synthesis. Selectivity for diesel range products increased with increasing Co content.
➢ Silicoaluminophosphate (SAPO) molecular sieve catalysts have been developed for methanol to olefin conversion, producing value-added products such as ethylene and propylene.
➢ Hybrid Pt-promoted tungstated and sulfated zirconia catalysts are very effective in cracking n-C_{36} to jet and diesel fuel; these catalysts will be tested for cracking of FT wax.
➢ Methane, ethane, and propane are readily decomposed to pure hydrogen and carbon nanotubes using binary Fe-based catalysts containing Mo, Ni, or Pd in a single step non-oxidative reaction.
➢ Partial dehydrogenation of liquid hydrocarbons (cyclohexane and methyl cyclohexane) has been performed using catalysts consisting of Pt and other metals on stacked-cone carbon nanotubes.
➢ An understanding of the catalytic reaction mechanisms of the catalysts developed in the CFFS C1 program is being achieved by structural characterization using multiple techniques, including XAFS and Mössbauer spectroscopy, XRD, TEM, NMR, ESR, and magnetometry.

Table of Contents

C1 Chemistry for Production of Clean Liquid Transportation Fuels and Hydrogen

Executive Summary

Introduction

The Consortium for Fossil Fuel Science (CFFS) is a research consortium with participants from five universities – the University of Kentucky, University of Pittsburgh, University of Utah, West Virginia University, and Auburn University. The CFFS universities are collaborating in a research program to develop C1 chemistry processes to produce clean transportation fuel from resources such as coal and natural gas, which are more plentiful domestically than petroleum. The processes under development will convert feedstocks containing one carbon atom per molecular unit into ultra clean liquid transportation fuels (gasoline, diesel, and jet fuel) and hydrogen, which many believe will be the transportation fuel of the future. The feedstocks include syngas, a mixture of carbon monoxide and hydrogen produced by coal gasification or reforming of natural gas, methane, methanol, carbon dioxide, and carbon monoxide. An Industrial Advisory Board with representatives from Chevron, Eastman Chemical, Energy International, the Department of Defense, Conoco, and Tier Associates provides guidance on the practicality of the research.

The major objectives of the program are to develop C1 technology for the production of:
- Ultra-clean, high efficiency, liquid transportation fuels; and
- Hydrogen, the zero-emissions transportation fuel of the future.

The current report contains results obtained during the first year of the current CFFS research contract with the U.S. Department of Energy, Office of Fossil Energy, on C1 chemistry. Some of the more interesting results obtained during the year (October 1, 2002 – September 30, 2003) are briefly summarized below. More detailed reports on each research project may be found on the indicated pages.

Fischer-Tropsch synthesis

FT synthesis using acetylenic probe molecules (pp. 11-20)
Alkynes initiate FT reactions much more effectively than olefins. Alkyne-initiated FT reactions can occur at temperatures as low as 100 ^{o}C, where normal FT reactions do not occur. It indicates that chain initiation in the FT synthesis might be the rate-determining step. It is postulated that chain initiation entity consists of two carbons that have an unsaturated bond, similar to surface-bound acetylene. The phenyl group of phenyl acetylenes is an excellent marker to differentiate the products from normal FT and FT reactions initiated by acetylenic probe molecules.

Terminal alkynes are the most effective chain initiator for FT reactions and produce normal hydrocarbons, which are similar to normal FT products but start from the alkynes. Internal alkynes can also initiate FT reactions but less effectively than terminal alkynes and produce mostly branched with some normal hydrocarbons. Chain initiation is strongly associated with the position of the triple bonds in the added alkyne.

Jet and diesel fuel from FT wax (pp. 21-30)

The hydroconversion of n-C_{36} to transportation fuels, especially to middle range products, such as jet and diesel fuel, was investigated. PtWZr, PtSZr catalysts and a series of PtWZr/SZr hybrid catalysts and the effect of hydrogen pressure were studied. The results indicate that hydroisomerization and hydrocracking of n-C_{36} are strongly influenced by hydrogen pressure. Pt promoted tungstated and sulfated zirconia respond to hydrogen pressure differently. Interesting results have been obtained with hybrid catalysts consisting of PtWZr and SZr components. The behavior of the hybrid catalysts with various component ratios suggests active interactions. With hydrogen pressures from 100 psi to 300 psi, the reactivities and yields of middle distillates with the hybrid catalysts demonstrated the existence and variety of the interactions.

Optimum yields of middle range fuel products can be achieved using catalysts with appropriately balanced hydroisomerization and hydrocracking abilities. Our results suggest that hydrogen pressure is an effective method to control the reactivities of tungstated and sulfated zirconia catalysts. Advantage can be taken of the active interactions between PtWZr and SZr components in hybrid catalysts. Hybrid catalysts can combine the isomerization activity of PtWZr with the cracking activity of SZr for higher yields of middle range products.

Optimization of Fischer-Tropsch Synthesis under Supercritical Fluid Conditions: Solvent Effects on Reaction Performance (pp. 31-52)

Fischer-Tropsch synthesis (FTS) reaction has been investigated over a 15% Co/ Al_2O_3 catalyst in supercritical fluid (SCF) media. The conventional gas phase FTS reaction was used as the base line for comparison with the supercritical phase FTS results under the same reaction conditions. The goal is to identify optimum operating conditions to maximize production of middle distillate hydrocarbons (e.g. C_5-C_{19}) while maintaining good reactants conversion rates. The findings in the current year are summarized below:

1. Significant improvement in the product distribution towards heavier hydrocarbons (high α-value) was obtained in SCF-FTS compared to that of the gas-phase reaction. This was also accompanied by high selectivity towards α-olefins and suppression of CH_4 and CO_2 production rates.

2. In SCH-FTS and SCP-FTS, high reaction temperatures increase the rates of reactants consumption and shift product selectivity towards light hydrocarbons and gasoline fractions. Low reaction temperatures promote chain growth and therefore favor the production of diesel fractions and wax. Maximum yield of diesel fractions was obtained in SCH-FTS at an optimum temperature of 250 °C, where the selectivity towards CH_4 and CO_2 at 250 °C did not exceed 15%, and 2% respectively. At the same temperature in the gas phase reaction, CH_4, and CO_2 selectivity can go as high as 39%, 14% respectively.

3. Re-adsorption of α-olefins is believed to enhance chain growth probability under supercritical phase operation.

4. Interestingly, both SCP and SCH-FTS performed nearly identically at a common density in terms of hydrocarbon product distribution. However, significantly higher conversions were observed in SCP due to the much higher pressure (kinetic effect). Secondary reactions such as isomerization and oxygenation were significantly suppressed in SCH-FTS, while in SCP-FS considerable amount of isomers and oxygenates were detected, especially in the lower hydrocarbon fractions (C_2-C_{11}).

5. Changing the gas fed composition (H_2/CO ratio) has a more pronounced influence in the supercritical phase than in the gas phase reaction especially at high hydrogen concentration (ratio 2/1). This indicates that easy extraction of products from inside the catalyst pores and enhanced solubility in the SCF creates more active site vacancies for the hydrogen to dissociate and thus increase the reaction rates (Elbashir et al., 2003).

Fischer-Tropsch synthesis using Co supported on silica xerogels and aerogels (pp. 53-64)
A series of xerogel and aerogel catalysts containing metallic cobalt has been prepared, characterized, and tested for Fischer-Tropsch activity. BET surface area measurements indicated that increases in the loading of cobalt lead to lower surface area, presumably due to the filling of micropores of the xerogel support. The average pore size of the support increased as a function of cobalt loading from 2.21 nm for the 4.91% Co catalyst to 4.52 nm for the 19.7% Co catalyst. TEM micrographs indicate the presence of uniform 7 nm diameter metallic cobalt particles in the 9.83% Co catalyst. However, TEM micrographs of the 19.7% Co catalyst indicate increased cobalt particle size heterogeneity. The lowest loading of cobalt on silica xerogel, 4.91%, showed no activity while the most heavily loaded catalyst, 19.7% Co, generated a 13.4% CO conversion. The selectivity towards diesel range hydrocarbon products increased as a function of increased cobalt loading reaching a maximum value of 41.4% for the C_8+ fraction. An aerogel supported cobalt catalyst yields a lot of olefinic product.

Development of Single-Site Metallic Catalysts for Fischer-Tropsch Reactions (pp. 65-71)
This is a new project initiated about halfway through the current year. The main goals of the work are as follows:
1. To develop approaches to the incorporation of single-site metal centers into aerogels (or other supports). This appears to have been accomplished for Fe and Ru, and Co.
2. To characterize the natures of the initially incorporated metal species, and to confirm the occurrence of a second protonation step for open-metallocene-derived species. Collaborative efforts with other consortium groups are already planned or underway in the areas of ESR, Mössbauer, solid state NMR, and XAFS spectroscopies as well as powder XRD measurements.
3. To convert the initial metal-supported species into single-site and agglomerated oxides. The natures of both types of oxides will be studied by the methods above and the conditions required for agglomeration will be determined.
4. To determine the behaviors of both single site and agglomerated metal-laden aerogel catalysts in the F-T process, initially focusing on Co. Collaborative efforts under both traditional and supercritical conditions will be initiated once the appropriate aerogels have been obtained.
5. The use of $Fe(2,4-C_7H_{11})_2$ and $Fe(C_5H_5)(2,4-C_7H_{11})$ complexes as a suppressor of diesel soot emissions will be studied shortly as part of another Consortium project in collaboration with Prof. Adel Sarofim at the University of Utah.

7

Value-Added Products

Development of Microporous Shape-Selective Catalysts for Ethylene, Propylene and other Value-Added Products via C-1 Chemistry (pp. 72-88)
We are exploring the use of silicoaluminophosphate (SAPO) molecular sieves in C1 chemistry reactions to produce value-added products. In methanol to olefin (MTO) reactions, the highest conversions to C2-C4 olefins were observed on SAPO-18 (92 %) and SAPO-34 (94 %) catalysts. C2–C4 olefins selectivity on various SAPO's is in the order: SAPO-34 > SAPO-18 > SAPO-47> SAPO-44> SAPO-17>SAPO-56. Ethylene selectivity on various SAPO's takes the following order: SAPO-34>SAPO-17>SAPO-47>SAPO-18> SAPO-44> SAPO-56. Lifetime of various SAPO's takes the following order: SAPO-34> SAPO-18> SAPO-17> SAPO-47= SAPO-56> SAPO-44. Particle size plays a significant role in activity and selectivity in MTO reaction as demonstrated on SAPO's-34, 18, and 44. Methane formation at high temperatures (> 450°C) can be reduced substantially by metals modification. Olefin selectivity is high in Fischer-Tropsch reaction on Co/SAPO34 catalyst; however, conversion is low.

Hydrogen

Hydrogen production by catalytic decomposition of ethane, propane and cyclohexane (pp. 89-97)
Non-oxidative, catalytic decomposition of lower alkanes is an alternative, one-step process to produce pure hydrogen with no production of carbon oxides or higher hydrocarbons. Our earlier work demonstrated that nanoscale, binary Fe-based catalysts supported on high surface area alumina (M-Fe/Al$_2$O$_3$, M=Mo, Pd or Ni) exhibit high activity for the catalytic decomposition of undiluted methane into pure hydrogen and carbon. Under proper reaction conditions, these binary catalysts promote the growth of carbon nanotubes which transport carbon away from the catalyst surfaces, thereby increasing the lifetime of the catalysts while producing a potentially valuable by-product.

During the current year, we have demonstrated that these binary catalysts are equally effective for the catalytic dehydrogenation of ethane and propane. Methane, ethane, and propane are the common hydrocarbon constituent of natural gas and the major compounds produced in the light products of Fischer-Tropsch synthesis. Therefore, this approach should a very effective of producing hydrogen from natural gas, F-T light products, coalbed methane, or landfill methane.

We have also begun to explore the potential applications of the carbon nanotube (CNT) by-products produced in the catalytic dehydrogenation process that are relevant to this program. Specifically, we are exploring the use of stacked-cone CNT for hydrogen storage and as catalyst supports. The initial results obtained for both applications are quite promising.

Characterization of the catalysts by XAFS and Mössbauer spectroscopy, high resolution TEM, and XRD indicates that the active phase is an Fe–M–C austenitic metallic alloy and that the catalyst particles are anchored to the alumina support by an Fe-aluminate, hercynite. The catalysts exhibit good time on stream behavior because the Fe-M-C phases are very effective in stabilizing carbon in the form of CNT, which efficiently carry the carbon away from the active alloy particle surfaces.

Conversion of Methane to Syngas (pp. 98-105)

Currently, most hydrogen production begins with the reforming of methane to synthesis gas. Because many natural gas deposits contain substantial amounts of CO_2, it is of interest to identify catalysts that exhibit high activity and good lifetimes for reforming of methane by CO_2. It has been established that a commercially available bimetallic carbide (Nanodyne, Inc., η-Co_6W_6C) is a precursor for a catalyst that is at least as good as, or better than, supported Ni or unsupported Mo_2C for the dry reforming (CO_2) of methane. Similar catalysts have been prepared in CFFS laboratories at WVU that exhibit good activities and time on stream (TOS) behavior. Future work will attempt to determine the active surface species on bimetallic carbide catalysts.

Analytical characterization of catalyst structures

Science behind Catalysis in C1 Reactions: Catalyst Characterization and Determination of Active Species (pp. 106-117)

Magnetic and ESR measurements indicate that the Co in cobalt-loaded xerogel catalysts is not completely reduced to Co^0, perhaps limiting its effectiveness in the Fischer – Tropsch synthesis. Longer reduction times may be necessary to achieve the complete reduction to Co^0.

Magnetic studies have determined the Ni loadings in Ni/SAPO catalysts and shown that higher loadings lead to precipitation of Ni as nanoparticles. Working with the Guin group, we will attempt to determine the role of Ni in the catalytic conversion of methanol to olefin.

Our basic studies on the nanoparticles of CuO and doped and undoped ferrihydrites have established the important role played by the uncompensated surface spins of Cu^{2+} and Fe^{3+} in the measured properties and hence in catalytic reactions involving nanoparticle catalysts.

Science behind catalysis in C1 reactions: XAFS studies of metal-doped SAPO and aerogel/xerogel catalysts (pp. 118-130)

XAFS spectroscopy has been used to investigate the local structure around the elements, Ni, Co and Mn that have been added to the SAPO catalyst formulations to promote higher reactivity. Preliminary analysis of the XAFS data suggests that Ni and Co are more likely to be in an octahedral coordination by oxygen anions rather than a tetrahedral coordination.

XAFS and Mössbauer spectroscopy have been used to speciated the Fe and Co in a xerogel catalyst doped with Fe as the major element and Co as a secondary element were predominantly present in the form of a metallic bcc Fe-Co alloy. A small amount of fayalite (Fe_2SiO_4) containing ~5% of the total Fe was also observed. The xerogel and aerogel materials have been examined by ultra-small angle x-ray scattering (USAXS) methods in order to obtain information on the short –to-long-range order in these materials, which can be related to details of the porosity or metal precipitate size. USAXS has provided new information on the long-range structure of these materials. Such structure is significantly altered by the introduction of cobalt into the aerogel material.

Investigation of Fischer-Tropsch (F-T) Catalysts using Solid State NMR Methods (pp. 131-138)
The conclusions reached from investigation of silica aerogel catalysts by ^{29}Si NMR spectroscopy are summarized below.

1. The ^{29}Si NMR data clearly delineate the presence of three types of Q sub-unit structures (Q_2 middle group, Q_3 branching group and Q_4 cross-linking group) in silica aerogel samples without calcination.
2. The calcining process and the loading of metal compounds (cobalt and iron compounds) increase the inhomogeneity of the aerogel structure, which results in the disappearance of the three distinct spectral lines from the Q sub-units. However, the chemical shift regimes of the three Q sub-units are still present, which suggests the silica tetrahedral sub-units do not collapse during these processes.
3. From the relative intensities of the ^{29}Si NMR spectra, it can be seen that Q_3 (branching group) and Q_4 (cross-linking group) are the dominant components in the aerogel samples with minor amounts of Q_2 middle group.
4. No distinct difference in the ^{29}Si NMR spectra is apparent between 2% and 10% cobalt loaded silica aerogel sample.
5. The ferrocene molecule exhibits a fast tumbling motion in the silica aerogel support based on the ^{13}C NMR data. Its behavior resembles a structure in the gas or liquid-like state.
6. The loading of metal compounds has a significant influence on the ^{29}Si spin lattice relaxation time. The interactions between the loading metal compounds and silica aerogel are still under investigation.

Characterization of Molybdenum and Tungsten Alcohol-Synthesis Catalysts using Temperature-Programmed Reduction and In Situ X-Ray Diffraction (pp. 139-143)
In situ x-ray diffraction has shown how several molybdenum and tungsten alcohol-synthesis catalysts are reduced stepwise from the starting oxides to metals and metal carbides. Potassium promoted molybdenum-on-carbon catalysts show intermediate Mo(III) and Mo(IV) oxides that are absent when potassium is absent. The alkali metal is also necessary to produce alcohols with molybdenum catalysts. Without an alkali promoter, only hydrocarbons are produced. This correlation suggests that the observed Mo(III) and Mo(IV) oxide phases are important in alcohol synthesis.

Fischer-Tropsch Mechanism Studies Using Acetylenic Molecules as Probes

Y. Zhang, L. Hou, J. Tierney and I. Wender
Chemical Engineering Department, University of Pittsburgh

Introduction

Petroleum is the chief source of transportation fuels at the present time. We now import about half of the petroleum and this need for imported oil will likely increase. This affects our balance of payments while making our supply of transportation fuels precarious. There is little possibility that we can increase petroleum production in the US.

We can, however, depend on our indigenous coal resources for future transportation fuels – essentially via gasification to syngas (CO/H_2) which is then converted to clean liquid fuels via the Fischer-Tropsch (FT) process. Natural gas is also a good resource for FT production but it may be in short supply in the United States.

Fischer-Tropsch (FT) synthesis converts syngas, which can be produced from coal, natural gas, coal and biomass and any carbonaceous materials, into long chain hydrocarbons. The hydrocarbons can be further processed to produce gasoline, jet and diesel, as well as bulk and specialty chemicals. FT synthesis was used in Germany during World War II to produce fuels from coal, and has been employed in SASOL, South Africa since the 1950s to produce fuels and chemicals. Shell has built a plant in Malaysia as a showcase of modern FT technology based on natural gas. Recently California air and energy officials in a California Air Resources Board (CARB) symposium praised the potential for gas-to-liquids (GTL), essentially FT synthesis, to make a significant future contribution to the state's diesel supply while reducing emissions and dependence on petroleum-based fuels. GTL is the most cost-effective diesel fuel alternative to reduce undesirable emissions and is backed by engine makers to enable them to build new, cleaner combustion engines.

Another driving force for FT synthesis is the new fuel regulations which require <15ppm sulfur in diesel in the near future. Deep hydrodesulfuration is needed to remove sulfur from petroleum distillates and this will drive up the cost of petroleum-based fuel. Fuels from the FT synthesis are essentially sulfur-free and have a high cetane number; they can be used as blending agents to meet the sulfur restrictions on clean diesel fuels.

FT synthesis has been considered as a portable fuel producer for the military because the diverse sources of syngas, the reactants for the FT synthesis, can be made from local resources. The US military has identified JP-8 as a single fuel for military use. The base oil of JP-8 is the kerosene fraction of hydrocarbons which can be made from FT products with high yields.

The FT synthesis is also a hydrogen storage method in which hydrogen is packaged in hydrocarbons in liquid form where they can be transported and stored in the same way as current fuels. Hydrogen can be extracted either by decomposition to carbon and hydrogen or by steam reforming. It is compatible with the current infrastructure for transport and storage. In addition, it is more easily processed than petroleum based fuels because it is free of sulfur and aromatics.

The hydrogen storage capacity is 14% (wt.) when decomposition to carbon and hydrogen is used to extract hydrogen, and 42% (wt.) hydrogen can be obtained when steam reforming is used.

Iron, cobalt and ruthenium are the best catalysts for FT synthesis. Iron catalysts are employed in SASOL FT plants. Iron catalysts are the best fit for coal-based FT synthesis because iron is a good water-gas-shift (WGS) catalyst. Low H_2/CO ratio syngas, which is produced by coal gasification, can be directly converted into hydrocarbons and CO_2 on iron catalysts. Production of CO_2 instead of water improves the activity and stability of the catalyst. Cobalt catalysts are preferred in FT synthesis in which natural gas based syngas with higher H_2/CO ratio is used. Cobalt catalysts do not have WGS activity and so H_2/CO ratios need to be adjusted to about 2/1 before feeding into the reactor. Syngas based on natural gas has a higher H_2/CO, suitable for cobalt catalysts. In addition, higher activity, stability and selectivity to middle distillates make cobalt catalysts very attractive. Shell's plant in Malaysia employs cobalt catalysts. Ruthenium catalysts have excellent FT reactivity; however, no commercial ruthenium catalyst has ever been used, mainly due to its high cost. Ruthenium has been used as a promoter to improve the reduction and reactivity of cobalt catalysts.

The FT mechanism has been studied for more than 70 years. It is generally agreed that the FT synthesis is a polymerization reaction in nature and that the product follows the Anderson-Shultz-Flory (ASF) distribution. However, it is still under debate in terms of the monomer, chain initiation and chain termination steps, due to the complexity of surface structures of catalysts, surface intermediates and fouling of pore structures by long chain products. It is interesting that iron catalysts become iron carbides and iron oxides, while cobalt and ruthenium catalysts remain in metal form during the synthesis reactions.

Incorporation of probe molecules has been used widely in elucidating the mechanism of FT reactions. Several C1 probes such as diazomethane CH_2N_2 [1,2], methyl chlorides CH_xCl_{4-x} [3] and methyl nitrite CH_3NO_2 [4-6] for FT reactions have been studied. Results suggest that C1 species can be incorporated into the FT reaction and serve as monomers for chain growth.

Incorporation of olefins into FT synthesis has been used to study the FT mechanism [7-17]. Schulz et al.[17] investigated the incorporation of small amounts of ^{14}C labeled olefins with different chain lengths during FT synthesis with cobalt and precipitated iron catalysts. They found that the extent of incorporation depends on the chain length of the olefin. Incorporation of ethylene is much greater than that of propylene. It was observed that the added olefins acted as chain initiators. A fraction of the added propylene was incorporated into the FT products to form monomethyl branched compounds. They pointed out that co-feeding of olefins during synthesis is useful in the investigation of individual pathways of secondary reactions.

Maitlis et al.[10,14,18,19] have extensively studied incorporation of ^{13}C probe molecules containing a carbon-carbon double bond into the FT synthesis. Results indicate that the probe molecules initiate chain growth. However, they are not incorporated in the middle of a hydrocarbon chain. The degree of incorporation decreased with increasing molecular mass of the hydrocarbon. They also observed that no significant ^{13}C was incorporated into the C1 and C2 oxygenates and suggested that these products are formed by a different path. They proposed an alkenyl mechanism for the FT synthesis. Chain initiation and propagation involves an alkenyl

intermediate rather than an alkyl intermediate. Recently, a quantum calculation[20] presented evidence that the alkyl intermediate route has a higher energy barrier than the hydrogen deficient alkenyl intermediate.

Loktev et al.[21-23] studied the incorporation of highly unsaturated hydrocarbons, such as acetylenes, to carbon monoxide hydrogenation reactions on fused iron catalysts developed for synthesis of higher alcohols. They observed that small amounts of acetylene can increase the reaction rate and selectivity to oxygenates. The space-time yields of liquid products could be two or three times higher than normal FT reactions under identical conditions. It is suggested that acetylene is inserted only once per molecule of alcohol formed. This indicates that acetylene can initiate chain growth but does not participate in chain growth. They proposed this as a new type of reaction involving CO, H_2 and acetylene in which acetylene plays the role of initiator of chain growth.

The FT synthesis consists of a series of complex reactions in which very little is known of the chain initiation step. FT mechanistic studies mainly focus on the chain growth step and suppose that the chain initiation and chain growth share the same scheme. However, Maitlis et al.[24] noted differences between chain initiation and chain growth and proposed an alkenyl mechanism. In our previous study, we found that alkynes can be incorporated more easily than alkenes. In this study, we propose that surface-bound acetylenes act as chain initiators in FT synthesis based on results of incorporation of a variety of alkynes.

Currently, we are focusing on cobalt catalysts because of their simpler reaction scheme, superior activity and stability, which make them more commercially viable at this time. As far as we know, there is no report of incorporation of acetylenes into the FT synthesis on a cobalt catalyst. Incorporation of acetylenic compounds could reveal chain initiation and chain growth mechanisms in the FT synthesis. We are also interested in extending this study to other CO hydrogenation catalysts, such as Ni catalysts (methanation), Pd catalysts (methanol synthesis) and Cu/ZnO catalysts (methanol synthesis).

Experimental

Catalyst preparation

Cobalt catalysts were prepared by the incipient wetness impregnation technique. Vista B alumina was calcined at 500 ^{o}C for 10 hours before impregnation. Cobalt nitrate was dissolved in a suitable amount of distilled water, then impregnated on calcined alumina support. The catalyst was dried in an oven at 110 ^{o}C overnight, and calcined at 300 ^{o}C for two hours. Ni/Al_2O_3 preparation followed the same procedure and nickel nitrate was used instead of cobalt nitrate. Lanthanum nitrate hydrate was dissolved in distilled water; then ammonium hydrate was added until pH=10 to precipitate $La(OH)_3$. The precipitate was aged for 30 minutes at room temperature. Then it was filtered and washed using distilled water. It was dried at 120°C overnight and calcined at 400°C for 2 hours. Palladium nitrate hydrate was dissolved in distilled water, and then La_2O_3 was added with vigorous stirring. Then it was placed under a infrared lamp and stirred frequently to eliminate the excess water, dried at 120°C overnight and then calcined at 400°C for 2 hours. The catalyst then was pelletized to 20-60 mesh and was ready to use.

Cu/ZnO/Al$_2$O$_3$ catalyst was prepared by coprecipitation of copper nitrate, zinc nitrate and aluminum nitrate solution by sodium carbonate solution at 80°C. Then, the precipitate was dried at 120 ^{o}C overnight and calcined at 350°C for 2 hours. The powder then was pelletized to 20-60 mesh.

FT reactions

The FT reaction was carried out in a computer controlled fixed bed reactor. The reactor was stainless-steel with i.d. 3/8 inches. Probe molecules can be added into the FT reaction continually by a syringe pump or by a saturator placed in the reactant gas stream, or intermittently by a syringe. A thermocouple was inserted into the middle of the catalyst bed in the reactor. 0.5 gram of cobalt catalyst was mixed with 1 gram of quartz sand and loaded on the isothermal stage of the reactor. The catalyst then was activated by pure H$_2$ at a rate of 50 ml/min, with temperature program ramping from room temperature to 350°C at 1°C/min, holding at 350°C for 10 hours. After reduction, the temperature of the reactor was lowered to the reaction temperature in H$_2$. Then, the gas stream was switched to argon. The FT reaction was slowly started by gradually increasing the CO and H$_2$ flow rate and, at the same time, decreasing the argon flow rate in two hours to avoid the temperature surge due to the active sites present in the fresh catalyst. Wax product was collected by a hot trap at about 200°C. Liquid product was collected by a cold trap in an ice-water bath. A stream of effluent gas was removed between the hot trap and the cold trap and went through three sampling valves controlled by a computer and analyzed by two GCs (HP6890, HP5890) controlled by a HP Chemstation equipped with three GC columns, i.e., HP-5, Porapak Q, and Carbonsphere, for analysis of all products except for heavy waxes, hydrocarbon gases and reactant gases, separately. The liquid product collected in the cold trap was analyzed by HP GC-MS.

The pump and the transfer lines of the reaction system were washed by pentane after each experiment to reduce possible interference by any material remaining from the previous run. Conversions were kept below 5% to reduce the condensation of the heavier hydrocarbons in the transfer lines. Lower conversion is also beneficial in evaluating the incorporation of the alkynes.

Results and Discussion

Incorporation of terminal acetylenes (RC≡CH)

It has been shown that terminal alkenes (RCH=CH$_2$) can be incorporated into the FT synthesis and produce linear hydrocarbons. Terminal alkynes have been incorporated into the FT synthesis on cobalt catalysts in this study and results show that terminal alkynes can initiate chain growth much more effectively than do terminal olefins. At 120 ^{o}C, which is 100 ^{o}C below the normal FT synthesis temperature on cobalt catalysts, CO conversion is essentially zero without alkyne addition. However, C7+ products are produced when 1-hexyne is added. Clearly, 1-hexyne can initiate the chain growth of CO hydrogenation even at very low temperatures. At 150 ^{o}C, CO conversion is 0.02% in normal FT reactions; only very small amounts of C1 to C6 hydrocarbons are observed. With addition of 1-hexene, some C7+ products are obtained, showing some degree of incorporation of 1-hexene. 1-Heyxne is incorporated about an order of magnitude more than is 1-hexene.

At higher temperatures, both the normal FT synthesis and alkyne initiated FT reactions occur simultaneously. Enhancement of C7+ products are observed for both 1-hexene and 1-hexyne addition. 1-Hexyne again shows a higher rate of incorporation than 1-hexene.

Differentiation of products from alkyne-induced and normal FT reactions
Addition of 1-hexyne into FT can initiate chain growth; however, it is difficult to distinguish the products of the normal FT synthesis and the alkyne initiated FT synthesis. This problem was solved by using phenyl substituted alkynes. The phenyl group in these alkynes is a marker to indicate the source of certain products. Phenylacetylene and 4-phenyl-1-butyne, which have terminal alkyne groups, are incorporated into FT reactions. Results show that the phenyl group does not hinder the ability of alkyne to initiate chain growth. The GC chromatogram of incorporation of 4-phenyl-1-butyne at 220 ^{o}C is shown in Figure 1. It can be observed that a spectrum of products with a phenyl group was obtained. The FT reaction can be initiated by the alkyne chain with the intact phenyl group. Normal FT products (normal hydrocarbons) and 4-phenyl-1-butyne initiated FT products (products with a phenyl group) are clearly distinguished. It should be pointed out that using the phenyl marker has advantages over using a radioactive marker. Products are analyzed effectively by using conventional GC-MS without dealing with radioactive materials. Position of the phenyl marker in the hydrocarbon chain can be resolved much more easily than with a radioactive marker. 4-phenyl-1-butyne is more like a normal alkyne because the phenyl group is two-carbons away from the carbon-carbon triple bond. In order to investigate the effect of the phenyl group on the alkyne incorporation, phenylacetylene was used. Results show that phenylacetylene can effectively initiate the FT reaction to produce phenyl substituted hydrocarbons.

Incorporation of internal alkynes (RC≡CR′)
Internal alkynes do not have a hydrogen atom attached to the carbon-carbon triple bond. Incorporation of internal alkynes is quite interesting in a number of ways. An internal alkyne can only be adsorbed in a direction parallel to the surface. One would expect branched products to be formed when an internal alkyne initiates chain growth. It has been shown that incorporation of internal alkynes is less rapid than incorporation of terminal alkynes, probably due to steric inhibition. When internal alkynes are incorporated, in addition of enhancement of straight chain FT products, branched products are obtained; for instance, incorporation of 2-hexyne produces 2-methyl-1-hexene and 2-methylhexane. Incorporation of 1-phenyl-1-propyne (Ph-C≡C-CH$_3$) produces a very complex spectrum of products, as shown in Figure 2. Besides the straight chain hydrocarbons from normal FT reactions, both branched and straight chain substituted benzenes are produced. It indicates that some internal alkynes may isomerize to terminal alkynes and then be incorporated into the FT reaction. However, internal alkynes can also be incorporated directly into the FT products to form branched products. Chain growth starts from the position of the triple bond of the alkyne probe.

Mechanism of chain initiation
Our results show that chain initiation and chain growth in FT synthesis may proceed differently. FT reactions may be initiated by an unsaturated and acetylene-like two-carbon identity; chain growth may proceed by stepwise addition of CH$_2$ monomers. Schulz et al.[17] noted that incorporation of ethylene is more than an order of magnitude higher than propylene, which shows the special role of the two-carbon entity. Formation of the chain initiator may be the

controlling step at low temperatures. Such chain initiations can be produced by adsorption of acetylenic probes, a much easier route than coupling of two adsorbed surface methylidynes. Coupling of two CH groups has been shown to produce acetylenic structures[25]. Maitlis et al.[10,26] also noticed the differences between chain initiation and chain growth and proposed an alkenyl mechanism for FT reactions based on model organometallic compound chemistry and incorporation of radioactive labelled probes. However, we cannot provide the exact surface structure of the chain initiator due to the complexity of surface intermediates and their dynamically changing properties.

Mechanism of oxygenate formation

It can be seen from Table 1 that incorporation of 1-hexyne produces 1-heptanal and 1-heptanol. Figure 1 shows that 5-phenyl-1-pentanol is produced with incorporation of 4-phenyl-1-butyne. Similarly, oxygenates (alcohols and aldehydes) with one carbon more than the incorporated alkynes are observed for most of the alkyne probes. It has been shown that the primary oxygenated products are aldehydes which are then hydrogenated to alcohols. Since these products are very similar to hydroformylation products, we added thiophene and pyridine separately to the system to elucidate the mechanism of oxygenate formation. Results clearly show that such oxygenates are formed by a hydroformylation type of reactions which are less sensitive to sulphur compounds, while sensitive to large amount of pyridine. It should be noted that the formation of oxygenates is enhanced with Time-on-Stream (TOS); while alkyne initiated chain growth proceeds immediately after addition of alkyne probes. The different trends with TOS also indicate a different mechanism for oxygenate formation.

Incorporation of 1-hexyne into CO hydrogenation on Cu, Pd, and Ni catalysts

The effect of 1-hexyne incorporation has been extended to CO hydrogenation on methanol synthesis catalysts ($Cu/ZnO/Al_2O_3$, Pd/La_2O_3 and $Pd/La_2O_3/SiO2$), and the methanation catalysts (Ni/Al_2O_3). A common characteristic of these catalysts is lack of chain growth capability. The aim of this study is to reveal the characteristics in CO dissociation, chain initiation and chain growth on different metals.

The Pd/La_2O_3 catalyst is active for methanol synthesis and has good activity and selectivity to methanol. $Cu/ZnO/Al_2O_3$ is a better methanol synthesis catalyst in terms of both activity and selectivity. With addition of 1-hexyne, these two catalysts show similar hydrocarbon products, such as heptane, dodecane, and 5-methylundecane. Both catalysts exhibit high hydrogenation ability and most of the added 1-hexyne was converted to hexane which indicates that the hydrogenation is not affected by CO adsorption on those catalysts. Incorporation of 1-hexyne into CO hydrogenation on Pd/La_2O_3 catalyst also produce C7 oxygenates, such as 1-heptanol and 2-methyl-1-hexanol, which cannot be observed on $Cu/ZnO/Al_2O_3$ catalysts. Methanol synthesis activity on Pd/La_2O_3 decreased with addition of 1-hexyne and returned after 1-hexyne addition stopped. Addition of 1-hexyne has little effect on methanol synthesis activity on $Cu/ZnO/Al_2O_3$ catalysts. It could be postulated that adsorption of alkynes does not occur on methanol synthesis centers, proposed to be Cu+ sites.

Activity decreased rapidly when 1-hexyne was added in CO hydrogenation on Ni/Al_2O_3 catalysts. It showed little incorporation of the 1-hexyne.

16

A common characteristic of higher hydrogenation activity can be observed from Cu, Pd and Ni catalysts which do not show chain growth in CO hydrogenation reactions. The ratios of hexane/1-hexene products from CO hydrogenation on Co, Fe, Ni, Pd and Cu based catalysts are shown in Table 2. The hexane/1-hexene ratio can be used to measure the hydrogenation capability in the presence of CO, which is different from hydrogenation ability of these metals in the absence of CO. It can be clearly seen that Co and Fe catalysts, which are excellent FT catalysts, have much lower hexane/1-hexene ratios. Cu, Pd catalysts, which are methanol synthesis catalysts, produce essentially no 1-hexene. The added 1-hexyne is hydrogenated to hexane. The Ni/Al_2O_3 catalyst shows a moderate hydrogenation activity. It can be postulated that hydrogenation ability is a very important factor for chain growth. CO is associatively adsorbed on Cu and Pd catalysts. Adsorption of hydrogen is not hindered on these catalysts by a weaker CO adsorption. CO adsorption on Ni catalysts is dissociative. However, CO adsorption on Ni catalysts is less strong than CO adsorption on Fe and Co catalysts. Hence, the inhibition effect of CO on hydrogen adsorption on Ni catalysts is less effective than that on Fe and Co catalysts. The stronger hydrogenation capability of Ni catalysts turns the surface intermediates into CH_3 which is then hydrogenated into CH_4. It has been shown that surface intermediates of the co-adsorption of CO and H_2 on metals, such as Fe, Co and Ni, which dissociatively adsorb CO, consist of CHx (x=0-3). CHx intermediates are in equilibrium under reaction conditions and the x depends on hydrogenation capability of the catalysts. Less hydrogenation activity is essential to keep the equilibrium to the unsaturated CH and CH_2 for chain growth.

Conclusions

Alkynes initiate FT reactions much more effectively than olefins. Alkyne initiated FT reactions can occur at very low temperatures, as low as 100 ^{o}C at which temperature normal FT reactions do not occur. It indicates that chain initiation in the FT synthesis might be the rate determining step. We postulate that chain initiation identity consists of two carbons which have an unsaturated bond, similar to a surface-bound acetylene.

The phenyl group of phenyl acetylenes is an excellent marker to differentiate the products from normal FT and acetylenic molecule initiated FT reactions.

Terminal alkynes are the most effective chain initiator for FT reactions and produce normal hydrocarbons which are similar to normal FT products but starting from the alkynes. Internal alkynes can also initiate FT reactions but less effectively than terminal alkynes and produce mostly branched with some normal hydrocarbons. Chain initiation is greatly associated with the position of the triple bonds in the added alkyne.

Alkynes do not incorporate in CO hydrogenation on $Cu/ZnO/Al_2O_3$, Pd/La_2O_3 or Ni/Al_2O_3 catalysts due to their higher hydrogenation activity.

Balance between CO and H_2 adsorption to keep the catalyst surface rich in CH and CH_2, the unsaturated surface intermediates, is essential for FT synthesis, as the case of cobalt and iron catalysts. The higher hydrogenation activity of Ni may drive the equilibrium to CH_3 and produce methane.

17

Papers presented

1. L. Hou, Y. Zhang, J. W. Tierney and I. Wender, Fischer-Tropsch Studies Using Acetylenic Molecules as Probes, Pittsburgh-Cleveland Catalysis Society 41st meeting, June, 2003, Pittsburgh. Miss Hou won the Best Student Presentation Award of Meeting.
2. Y. Zhang, L. Hou, J. W. Tierney and I. Wender, Acetylenes as Probes in the Fischer-Tropsch Reaction, ACS Annual Meeting, September, 2003, New York.

Future work

Future work will involve the addition of small amounts (1%) of acetylene itself (HC≡CH) to cobalt catalyzed reactions. We expect the acetylene to initiate the FT synthesis and to increase the rate of reaction as well as the yield of liquid products. The effect of adding 1% of acetylene on the nature of the FT products and the rate of reaction at low temperatures of will be studied. It may be that acetylene, added in very small amounts, will have a great influence on the nature of the FT synthesis and could provide an entirely new way to the FT synthesis.

The effect of acetylene on iron catalysts will also be explored since iron catalysts are used for coal based syngas. Unlike Loktev et al.'s study which focused on alcohol synthesis, we will investigate FT synthesis on iron catalysts and operate at reaction conditions which are compatible with FT reactions. Our goal is to study the mechanism of FT reactions and improve the activity and selectivity of the catalyst.

Ruthenium and rhodium catalysts may also be explored by incorporation of acetylene in the CO hydrogenation reaction. Mechanistic information could be revealed by comparison of the similarities and differences of these metals in CO hydrogenation and their responses to the incorporation of acetylene

References

1. Brady, R. C., III; Pettit, R. *J. Am. Chem. Soc.* **1980**, *102*, 6181-6182.
2. Brady, R. C., III; Pettit, R. *J. Am. Chem. Soc.* **1981**, *103*, 1287-1289.
3. Van Barneveld, W. A. A.; Ponec, V. In *J. Catal.*, 1984; Vol. 88, pp 382-387.
4. Cavalcanti, F. A. P.; Oukaci, R.; Wender, I.; Blackmond, D. G. *J. Catal.* **1990**, *123*, 270-274.
5. Cavalcanti, F. A. P.; Oukaci, R.; Wender, I.; Blackmond, D. G. *J. Catal.* **1990**, *123*, 260-269.
6. Cavalcanti, F. A. P.; Oukaci, R.; Wender, I.; Blackmond, D. G. *J. Catal.* **1991**, *128*, 311-319.
7. Hall, W. K.; Kokes, R. J.; Emmett, P. H. *J. Am. Chem. Soc.* **1960**, *82*, 1027-1037.
8. Satterfield, C. N.; Huff, G. A., Jr.; Summerhayes, R. *J. Catal.* **1983**, *80*, 486-490.
9. Percy, L. T.; Walter, R. I. *J. Catal.* **1990**, *121*, 228-235.
10. Turner, M. L.; Marsih, N.; Mann, B. E.; Quyoum, R.; Long, H. C.; Maitlis, P. M. *J. Am. Chem. Soc.* **2002**, *124*, 10456-10472.
11. Tau, L. M.; Dabbagh, H. A.; Davis, B. H. *Energy Fuels* **1990**, *4*, 94-99.
12. Hanlon, R. T.; Satterfield, C. N. *Energy Fuels* **1988**, *2*, 196-204.
13. Turner, M. L.; Long, H. C.; Shenton, A.; Byers, P. K.; Maitlis, P. M. *Chemistry-a European Journal* **1995**, *1*, 549-556.
14. Maitlis, P. M.; Quyoum, R.; Long, H. C.; Turner, M. L. *Appl. Catal. a-Gen.* **1999**, *186*, 363.

15. Matsumoto, D. K.; Satterfield, C. N. *Energy Fuels* **1989**, *3*, 287-291.
16. Schulz, H.; Claeys, M. *Appl. Catal. a-Gen.* **1999**, *186*, 91-107.
17. Schulz, H.; Claeys, M. *Appl. Catal. a-Gen.* **1999**, *186*, 71-90.
18. Maitlis, P. M. *Pure Appl. Chem.* **1989**, *61*, 1747-1754.
19. Quyoum, R.; Berdini, V.; Turner, M. L.; Long, H. C.; Maitlis, P. M. *J. Catal.* **1998**, *173*, 355.
20. Liu, Z. P.; Hu, P. *J. Am. Chem. Soc.* **2002**, *124*, 11568-11569.
21. Loktev, S. M. *J. Catal.* **1982**, *17*, 255-230.
22. Loktev, S. M. *J. Mol. Catal.* **1982**, *17*, 225-230.
23. Slivinskii, E. V.; Rumyantsev, V. Y.; Voitsekhovskii, Y. P.; Zvezdkina, L. I.; Loktev, S. M. *J. Catal.* **1990**, *123*, 333-340.
24. Maitlis, P. M.; Long, H. C.; Quyoum, R.; Turner, M. L.; Wang, Z. Q. *Chemical Communications* **1996**, 1-8.
25. Beanan, L. R.; Keister, J. B. *Organometallics* **1985**, *4*, 1713-1721.
26. Long, H. C.; Turner, M. L.; Fornasiero, P.; Kaspar, J.; Graziani, M.; Maitlis, P. M. *J. Catal.* **1997**, *167*, 172-179.

Table 1. Product distributions with/without probe addition at various temperatures

T (^{o}C)	120		150			180		220		
Probes	none	1-hexyne	none	1-hexene	1-hexyne	none	1-hexyne	none	1-hexene	1-hexyne
CO Conv. (%)	0	-	0.02	-	-	0.3	-	2.0	-	-
Product Distribution (mg/g/h)										
C1-C3	0	0	0.18	0.17	0.17	1.06	0.85	8.79	4.72	3.78
C4	0	1.1	0.04	0.13	1.16	0.32	1.19	2.18	1.77	2.23
C5	0	-	0.03	-	-	0.34	-	2.10	-	-
hexenes	0	106.8	0.02	279.1	116.9	0.24	114.6	1.57	226.3	177.7
hexane	0	25.43	0.01	0.09	24.01	0.07	26.27	0.65	34.74	24.20
C7	0	8.57	0	0.64	4.94	0.31	6.72	2.06	4.67	11.20
C8	0	2.6	0	0.17	4.71	0.27	3.09	2.34	3.38	4.92
C9	0	0.94	0	0.03	1.75	0.33	1.17	1.95	2.87	2.84
C10	0	0.5	0	0.03	3.13	0.25	2.09	2.09	2.95	2.76
C11	0	3.61	0	0.06	8.55	0.30	6.35	2.08	2.81	7.46
C12	0	89.97	0	0.41	106.14	0.33	99.24	1.90	2.51	72.87
C13	0	12.75	0	0.14	14.46	0.26	8.96	1.46	2.43	9.43
C14	0	6.24	0	0	4.78	0.27	2.62	0.94	2.13	2.62
C15+	0	14.5	0	0	9.6	1.8	6.4	10.7	15.8	15.6
heptanal	0	3.67	0	0	2.40	0	1.19	0.02	0.22	1.15
1-heptanol	0	0.13	0	0	0.84	0	2.61	0	0.02	1.95

Table 2. Hexane/1-hexene ratios on various catalysts during CO hydrogenation with 1-hexyne incorporation

Catalysts	FeKSi	Co/ Al_2O_3	Ni/ Al_2O_3	Cu/ZnO/ Al_2O_3	Pd/ La_2O_3
Main products	FT	FT	methane	methanol	methanol
Hexane/1-hexene*	0.07	0.10	1.67	>10	>10

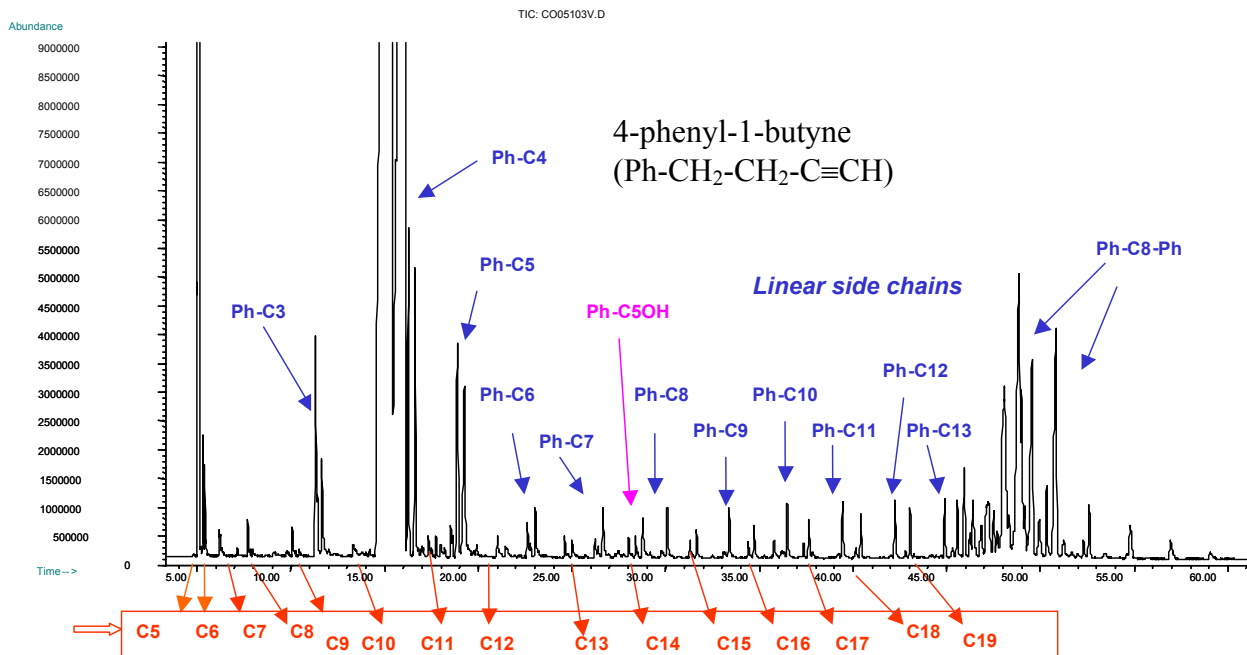*This ratio indicates the capability of hydrogenation in the presence of CO

Figure 1. GC-MS analysis of FT products with 4-phenyl-1-butyne incorporation, T=220°C, P=100 psi, $H_2/CO=2$, 2 ml/h of the solution of 10% of the probe in pentane.
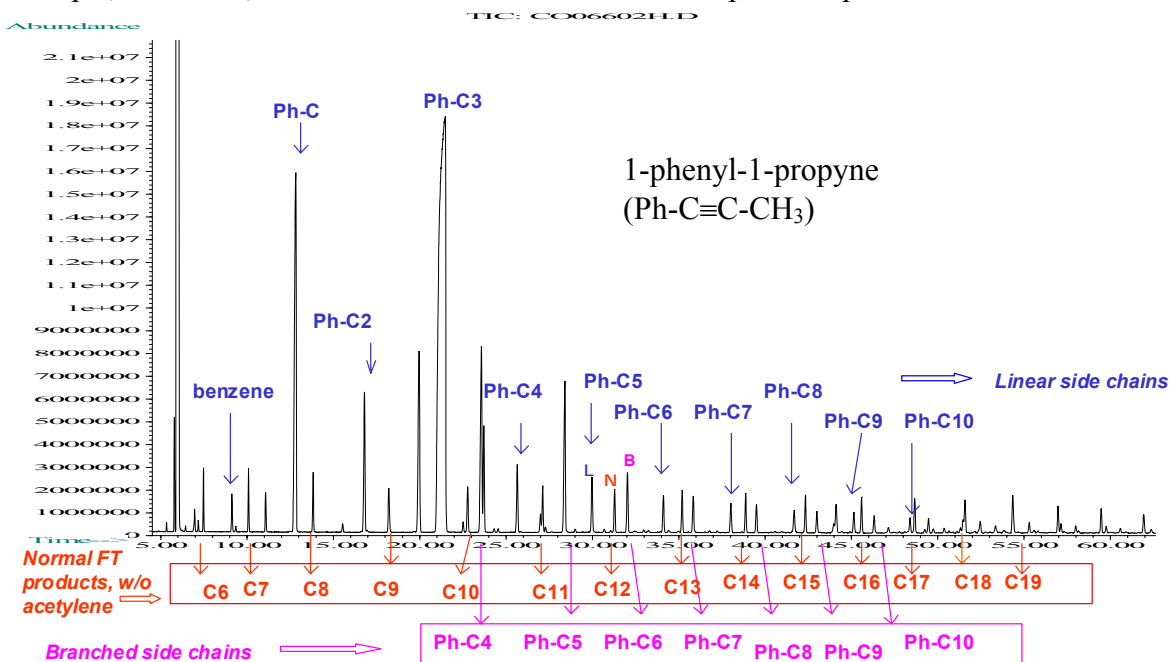

Figure 2. GC-MS analysis of products of FT with 1-phenyl-1-propyne incorporation, T=220°C, P=100 psi, $H_2/CO=2$, 2 ml/h of the solution of 10% of the probe in pentane.

Jet and Diesel Fuel from Fischer-Tropsch Wax

Z. Zhou, Y. Zhang, J. Tierney and I. Wender
Chemical Engineering Department, University of Pittsburgh

Introduction

This year's studies were aimed at converting the long-chain paraffins in Fischer-Tropsch waxes to middle distillates, such as jet and diesel fuels. Work was concentrated on two major subjects: a) the application of so-called hybrid catalysts consisting of combinations of tungstated and sulfated zirconia catalysts; and b) the effect of hydrogen pressure on reactions catalyzed by tungstated and sulfated zirconia catalysts and on the hybrid catalysts, all of which function with the presence of small amounts of platinum.

Sulfated and tungstated zirconia catalysts are solid acid catalysts and have been studied extensively in converting normal paraffins to various products through hydroisomerization and hydrocracking processes.[1-4] Structures (1) and (2) in Figure 1 are the most common structures postulated to show the surface active sites on sulfated zirconia and to explain its strong acidity. A similar structure was proposed for the interaction between zirconium and tungsten on the surface. Although the mechanisms of the reactions are still unclear, the two catalysts demonstrate very different abilities in hydrocracking and hydroisomerization. Sulfated zirconia is much stronger acid than is tungstated zirconia. With promotion by platinum, sulfated zirconia is very reactive as a cracking catalyst and therefore a good choice for converting long chain paraffins to short chain products in the gasoline range. [1,3,5,6] Iglesia et al.[1,7] and Zhang et al.[2] have reported that tungstated zirconia is more stable than sulfated zirconia and can be used to convert long-chain paraffin with high selectivity to isomerization products. This may be partly due to increased hydrogen transfer rates, which limit the lifetime of adsorbed carbenium ions.[7]

Middle distillate fuel products are important transportation fuels. High quality diesel fuel is required to meet the market demand of heavy-duty trucks and buses; JP-8, a type of kerosene blend, has been identified by U.S. Army as the Single Fuel for the Battlefield.[8,9] The increasing demand for middle distillate products has led to a growing interest in hydrocracking Fischer-Tropsch (FT) heavy feedstocks.[10] The FT synthesis converts a mixture of CO and H_2 (syngas) to a range of hydrocarbons. Coal, natural gas or any carbonaceous substance can be gasified to produce ultraclean liquid fuels and serve as an alternative to petroleum sources. In commercial practice, the low temperature FT process (~ 200°C) is best suited for the production of diesel fuels.[11] However, hydrocarbons heavier than the diesel cut, i.e. waxes, account for more than half of the total FT products in current practice. These FT waxes, major components of which are long-chain normal paraffins, contain no sulfur, nitrogen or aromatics. They are an environmentally clean source for transportation fuels and lube-base oils either alone or blended with petroleum-based products. [12]

To achieve high yields and desired properties of middle distillate fuels, a well-controlled balance of hydrocracking and hydroisomerization functions is critical. It is desirable to manipulate the balance to achieve product requirements. A hybrid catalyst, which is a physical mixture of sulfated and tungstated zirconia (See section 2.1), could provide this flexibility. We have

reported the use of hybrid catalysts made by introducing zeolite components into a Pt-promoted tungstated zirconia (Pt/WO$_3$/ZrO$_2$, 0.5 wt% Pt and 12.5 wt% W), on hydroisomerization and hydrocracking of n-C$_{24}$.[13] Although sulfated zirconia and tungstated zirconia have been studied for years, there are few reported studies using combinations of these catalysts.

We have found that hydrogen pressure affects sulfated and tungstated zirconia differently in hydroconverting long chain paraffins and that a hybrid catalyst consisting of the two zirconia catalysts provides an effective way of combining and balancing their isomerization and cracking functions.

In this year, we investigated Pt promoted tungstated and sulfated zirconia catalysts used in the hydroisomerization and hydrocracking of normal paraffins as long as n-C$_{36}$. Special emphasis was put on the conversion to middle distillate fuel products. The reactions were carried out in a microautoclave reactor under mild conditions. The influence of hydrogen pressures on reactivities and product distributions of the two catalysts were compared. Hybrid catalysts consisting of tungstated and sulfated zirconia in various ratios were used and the effects of the component ratios as well as the hydrogen pressures on converting long-chain paraffins to middle distillate products were investigated.

Experimental

Catalyst preparation and characterization
WO$_3$/ZrO$_2$ (12.5 wt% W) (noted as WZr) catalysts were from Magnesium Elektron, Ltd. (MEL XZO01044/1). SO$_4$/ZrO$_2$ (9 wt% SO$_4$) (noted as SZr) was also obtained from Magnesium Elektron, Inc (MEI FZO 999). Pt(NH$_3$)$_4$Cl$_2$·H$_2$O (Strem Chemicals) was used as the Pt precursor and loaded by incipient wetness impregnation and then calcined at 700 ºC in air to achieve the desired Pt loading.

Hybrid zirconia catalysts were prepared via mechanical mixing of PtWZr with SZr followed by calcination. Both components were ground and calcined at 550 ºC for 3 hours before mixing. They were mixed at the desired weight ratios by thorough grinding and calcination at 550 ºC in air for 3 hours. When comparing the behaviors of hybrid catalysts and pure catalysts, the same amount of catalyst sample was used in each run.

Experimental procedures

Catalytic tests were carried out in a 27 ml autoclave reaction system. The reactant used was hexatriacontane (*n*-C$_{36}$) from Aldrich Chemical Company. In a typical reaction, 0.2 g of the catalyst was activated at 550 °C for 90 minutes in air and then charged into the reactor, which was pre-dried overnight beforehand. After loading the catalyst, the reactant, typically 0.8 g, was charged. The initial hydrogen pressure was set at room temperature before heating the reactor to the desired temperature in a fluidized sand bath. Reaction temperature was 200 °C. The reactor was shaken horizontally at 180 rpm during reaction to mix the reactor contents. A computer was used to record the reaction pressure, temperature and time during the run. The reaction was ended at the desired time by quickly cooling the reactor with ice water. Reaction variables were time, temperature, hydrocarbon/catalyst ratio and hydrogen pressure. Since we used a batch

reactor system, hydrogen pressure changed because of temperature changes and reactions that occurred while the reactor was being heated or cooled. We report initial values of hydrogen pressure at room temperature.

Products in the gas phase were discharged into a collector and analyzed using an HP- 6890 gas chromatography with an HP Porapak Q 80/100 packed column and TCD detector. Liquid products in the reactor were collected in vials. When waxy products remained in the reactor, appropriate amounts of CS_2 were used to dissolve them for analysis. Liquid samples were injected into an HP-5890 gas chromatography (GC), with HP-1 Cross-linked Methyl Silicon Gum, 25m × 0.2mm × 0.33μm column and FID detector.

We used GC analysis results of the reaction products to calculate conversion and selectivity for each reaction. Conversion is the weight percent of the converted reactant in the original reactant fed to the reactor. Selectivity of a certain product is the weight percent of that product in the total products. Yield of a product is calculated by multiplying conversion by the selectivity of that product.

Results and Discussion

We grouped our reaction products in terms of transportation fuel types. In addition to gasoline and jet/diesel fuel, lube-base oil is also a desirable product from FTS long chain paraffins. We define the product ranges by their retention times in GC analysis. Hydrocarbon products (C_5 and above) with peaks before that of n-C_8 (inclusive) are reported as gasoline, products with peaks from n-C_9, up to and including n-C_{22} as middle fuel and products with peaks from n-C_{23} to n-C_{31} as lube-base oil. It is recognized that the lube-base oil product should have a low pour point (be isomerized) to be of practical use. Small amounts (< 3 wt%) of products smaller than C_5 were found and are not reported. Peaks appearing after n-C_{31} and before n-C_{36} are the isomers of the reactant n-C_{36}. (Figure 2.)

Effect of hydrogen pressure on pure PtWZr and PtSZr in hydrocracking of n-C36

Effect of hydrogen pressure using PtWZr
In a former study[2], high hydrogen pressure, 500 psig, was used. With a PtWZr catalyst, high hydrogen pressure is suitable for high selectivity to isomerization products from long chain paraffins. Decreasing hydrogen pressure from 500 psi to 100 psi resulted in an increase in conversion from 40 wt% to 95 wt%. While the selectivity to middle distillate greatly increased, selectivity to highly-branched lube base oil decreased from 98 wt% to 50 wt%. (Table 1).This result is in agreement with previous work. PtWZr catalyst may have a fast hydrogen transfer rate and therefore a low surface residence time for isomerized carbenium ions. Iglesia et al., working with n-heptane, proposed that the negative order of hydrogen pressure might arise from competitive occupation of active sites by proton and carbenium ions, which causes the coverage of the latter to decrease with increasing hydrogen pressure.[7] Zhang et al. in this laboratory observed that n-C_{16} has a similar negative reaction order with respect to hydrogen.[2]

A series of hydrogen pressures were tested for a PtWZr catalyst. Under given conditions, PtWZr demonstrated the highest reactivity and selectivity to middle distillate fuels with hydrogen pressure at about 100 psi. (Figure 3) The conversion declines for pressure above 100 psi because

of the negative order of hydrogen pressure. For hydrogen pressure lower than 100 psi, the reactivities are lower, which might be attributed to insufficient hydrogen leading to deactivation of the catalyst. In both cases, selectivity to middle distillate increased with increasing conversion.

Effect of hydrogen pressure using PtSZr

The effect of hydrogen pressure on hydrocracking of n-C_{36} using a PtSZr catalyst is shown in Table 2. It differs from that of PtWZr (shown in Table 1). With increased hydrogen pressure, PtSZr showed greatly increased conversion. However, the strong cracking function of PtSZr gives major products in the gasoline range. The selectivity to middle distillates in this case was lower than that under 100 psi hydrogen pressure.

With hydrogen pressures of 100 psi to 500 psi, (Figure 4), there was a pressure (about 300 psi) where a maximum yield to middle distillates was produced. The decrease in selectivity to middle distillates is due to severe hydrocracking reactions, which results in high selectivity to light products in the gasoline range. This is very different from the result using PtWZr (Table 1). Because PtWZr does not have a strong cracking function, the selectivity remained low (9 wt%) even at a high conversion of 95 wt%.

Producing middle distillate fuels using hybrid PtWZr/SZr catalysts

Use of PtWZr catalysts favors hydroisomerization reactions but lacks cracking ability; on the other hand, PtSZr catalyst has a much higher activity and strong hydrocracking function and readily cracks long chain paraffins into light products. To convert long-chain paraffins into middle range products, an appropriate balance between hydroisomerization and hydrocracking has to be achieved. Fujimoto et al. reported the effective hydroisomerization of n-C_5 and n-C_6 with a physical mixture and the effect of spilled over hydrogen was considered to play an important role in the regeneration of Bronsted acid sites and stabilization of intermediate carbenium ions. [14]Our observation that introducing mordenite or SZr into PtWZr can increase the activity and cracking ability of PtWZr in converting n-C24 confirmed an active interaction between the mixed components. [13]

When working under high hydrogen pressure of 500 psi, a small amount of SZr in the hybrid catalyst could result in increased conversion and selectivity to cracked products.[13] Since hydrogen pressure affects sulfated and tungstated zirconia catalysts inversely, using a hybrid catalyst is an effective method to balance the activities of the two components and take better advantage of the ability of each part of the catalysts. PtWZr/SZr catalysts with various ratios were prepared and tested in converting n-C_{36} using various initial hydrogen pressures. Conversions and yields of middle products achieved with a hybrid catalyst at 100 and 300 psi are shown in Figure 5 and Figure 6.

Variation in conversion and yield to middle products with catalyst composition is not linear, showing that strong interaction between PtWZr and SZr occurs in the hybrid catalysts. SZr (without Pt) by itself, as shown at the left end of the curve, has little reactivity. It is possible that the PtWZr component provides SZr the environment, such as spill-over hydrogen, to keep it active. At the same time, SZr provides extra cracking function for PtWZr to further convert the generated carbenium intermediates to lighter products.

Reactivity and selectivity are affected by the composition of the hybrid catalyst. Under all the tested hydrogen pressures, the change in the yields of middle distillate is much greater than the change of the conversions, especially when the hydrogen pressure is low, such as 100 psi. (Figure 5) Under low hydrogen pressure, pure PtWZr catalyst has a high activity but low selectivity due to the lack of cracking ability. In a hybrid catalyst PtWZr/SZr (3:1), 25 wt% PtWZr was replaced by SZr. The increased cracking ability led to evident improvement in the yield of middle distillate products. Since sulfated zirconia has a lower activity under low hydrogen pressure, the conversion over the hybrid catalyst did not increase as much as did the middle distillate yield. With a higher SZr fraction in the hybrid catalysts, both conversions and yields decreased. With higher hydrogen pressures, as shown in Figure 6, maxima in conversion and middle distillate yield curves move towards the left. In these cases, SZr fractions can contribute more to the reactivity so that even more PtWZr is replaced by SZr, hybrid catalysts maintain high reactivities. Under a hydrogen pressure of 300 psi, a maximum conversion was achieved with PtWZr/SZr (1:2) while the maximum yield of middle distillate fuels was achieved with PtWZr/SZr (2:1). At higher hydrogen pressure, although higher conversion can be obtained with a larger SZr fraction, middle distillate yields are not necessarily higher since extra cracking ability will result in more light products, which tends to lower the selectivity to middle distillate fuels.

Conclusions

In this work, the hydroconversion of n-C_{36} to transportation fuels, especially to middle range products, such as jet and diesel fuel, was investigated. PtWZr, PtSZr catalysts and a series of PtWZr/SZr hybrid catalysts and the effect of hydrogen pressure were studied. The results indicate that hydroisomerization and hydrocracking of n-C_{36} are strongly influenced by hydrogen pressure. Pt promoted tungstated and sulfated zirconia respond to hydrogen pressure differently. Interesting results have been obtained with hybrid catalysts consisting of PtWZr and SZr components. The behavior of the hybrid catalysts with various component ratios suggests active interactions. With hydrogen pressures from 100 psi to 300 psi, the reactivities and yields of middle distillates with the hybrid catalysts demonstrated the existence and variety of the interactions.

Optimum yields of middle range fuel products can be achieved using catalysts with appropriately balanced hydroisomerization and hydrocracking abilities. Our results suggest that hydrogen pressure is an effective method to control the reactivities of tungstated and sulfated zirconia catalysts. Advantage can be taken of the active interactions between PtWZr and SZr components in hybrid catalysts. Hybrid catalysts can combine the isomerization activity of PtWZr with the cracking activity of SZr for higher yields of middle range products.

Future work:

The tungstated and sulfated zirconia catalysts and hybrid catalysts will be applied to a series of real Fischer-Tropsch waxes. Emphasis will be on maximizing jet and diesel fuel products. Comparisons will be made with present commercial catalysts used in converting FT waxes to jet/diesel. This will include zeolite and amorphous silica-alumina supports.

Past work has been confined to the use of tungstated zirconia catalysts with 12.5 wt% tungsten. Catalysts with 6.5 wt% tungsten and newly available mesoporous tungstated zirconia catalysts containing 16 wt% tungsten will be investigated. Work on this project will terminate in 2004.

Papers printed or presented

1. "Hybrid zirconia catalysts for conversion of Fischer–Tropsch waxy products to transportation fuels", Zhong Zhou, Yulong Zhang, John W. Tierney and Irving Wender, Fuel Processing Technology, Volume 83, 2003, Pages 67-80
2. "Novel Catalysts for Hydroisomerization and Hydrocracking of Fischer-Tropsch Wax", 2003 *AIChE* Spring National Meeting, New Orleans, Louisiana
3. Paper Presentations at 38th, 39th and 40th Annual Symposium, Pittsburgh-Cleveland Catalysis Society, 2000 – 2002
4. "Anion-modified zirconia: effect of metal promotion and hydrogen reduction on hydroisomerization of n-hexadecane and Fischer–Tropsch waxes", Shuguang Zhang, Yulong Zhang, John W. Tierney and Irving Wender, Fuel Processing Technology Volume 69, 2001, Pages 59-71
5. "Structure, properties and roles of the different constituents in Pt/WOx/ZrO2 catalysts", A. Punnoosea, M. S. Seehraa, and I. Wender, Fuel Processing Technology, Volume 74, 2001, Pages 33-47
6. "Hydrocracking and hydroisomerization of long-chain alkanes and polyoleffins over metal-promoted anion-modified transition metal oxides", K. R. Venkatesh, J. Hu, J. W. Tierney, and I. Wender, US patent 6,184,430, Feb. 6, 2001
7. "Hydroisomerization of normal hexadecane with platinum-promoted tungstate-modified zirconia catalysts", Shuguang Zhang, Yulong Zhang, John W. Tierney and Irving Wender, Applied Catalysis A: General, Volume 193, 2000, Pages 155-171
8. "Hydrocracking and Hydroisomerization of Long-Chain Alkanes and Polyolefins over Metal-Promoted Anion-Modified Zirconium Oxides", K. R. Venkatesh, J. Hu, W. Wang, G. D. Holder, J. W. Tierney, and I. Wender, Energy Fuels, 10 (6), 1996, 1163 –1170

References

1. Barton, D. G.; Soled, S. L.; Meitzner, G. D.; Fuentes, G. A.; Iglesia, E. *Journal of Catalysis* **1999**, *181*, 57-72.
2. Zhang, S. G.; Zhang, Y. L.; Tierney, J. W.; Wender, I. *Applied Catalysis a-General* **2000**, *193*, 155-171.
3. Yori, J. C.; Vera, C. R.; Parera, J. M. *Applied Catalysis a-General* **1997**, *163*, 165-175.
4. Wen, M. Y.; Wender, I.; Tierney, J. W. *Energy & Fuels* **1990**, *4*, 372-9.
5. Venkatesh, K. R.; Hu, J.; Wang, W.; Holder, G. D.; Tierney, J. W.; Wender, I. *Energy & Fuels* **1996**, *10*, 1163-1170.
6. Zhang, A. H.; Nakamura, I.; Aimoto, K.; Fujimoto, K. *Industrial & Engineering Chemistry Research* **1995**, *34*, 1074-1080.
7. Iglesia, E.; Barton, D. G.; Soled, S. L.; Miseo, S.; Baumgartner, J. E.; Gates, W. E.; Fuentes, G. A.; Meitzner, G. D. *11th International Congress on Catalysis - 40th Anniversary, Pts a and B* **1996**, *101*, 533-542.

8. Edwards, T. *Air Force Research Laboratory, Presentation, Air Force Perspective on Strategic Defense Fuels Initiative* **June 2002**.
9. US_Army_TACOM-TARDEC,*"JP-8, The Single Fuel Forward (an information compenduim)"* **May 2001**.
10. Calemma, V.; Peratello, S.; Perego, C. *Applied Catalysis a-General* **2000**, *190*, 207-218.
11. Dry, M. E. *Applied Catalysis, A: General* **1999**, *189*, 185-190.
12. Dry, M. E. *Journal of Chemical Technology and Biotechnology* **2001**, *77*, 43-50.
13. Zhou, Z.; Zhang, Y.; Tierney, J. W.; Wender, I. *Fuel Processing Technology* **2003**, *83*, 67-80.
14. Fujimoto, K.; Maeda, K.; Aimoto, K. *Applied Catalysis a-General* **1992**, *91*, 81-86.

Table 1 Decreased hydrogen pressure increases the reactivity and selectivity of cracked products over PtWZr catalyst

Initial Hydrogen Pressure (psi)	Conversion (wt%)	Selectivity (wt%)			
		C_5-C_8	C_9-C_{22}	C_{23}-C_{31}	isoC$_{36}$
500	40	0	2	1	97
100	95	9	41	19	31

Catalyst: 0.25 g (0.5 wt%)Pt/WO3/ZrO2 (12.5 wt% W)
Reactant: 1.0 g n-C36;   Reaction conditions: 200 °C, 25 min.

Table 2 Increased hydrogen pressure increases the reactivity and selectivity of cracked products over PtSZr catalyst

Initial Hydrogen Pressure (psi)	Conversion (wt%)	Selectivity (wt%)			
		C_5-C_8	C_9-C_{22}	C_{23}-C_{31}	Iso-C$_{36}$
100	45	10	27	6	57
500	95	65	20	7	8

Catalyst: 0.2 g (0.5 wt%)Pt/SO4/ZrO2
Reactant: 0.8 g n-C36,   Reaction conditions: 200 °C, 20 min.
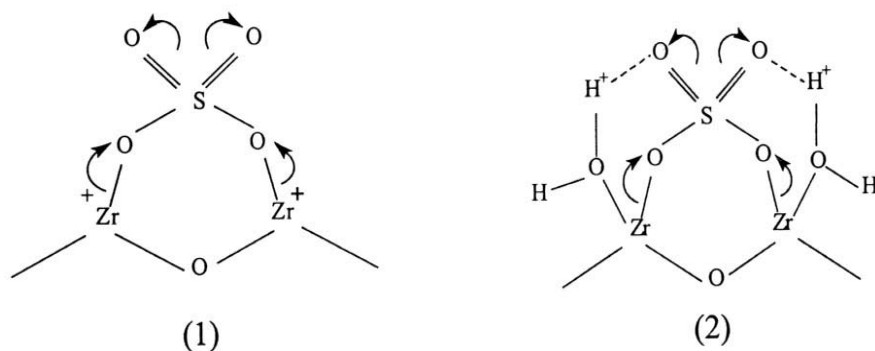
Figure 1 Postulated Structures for sulfated zirconia
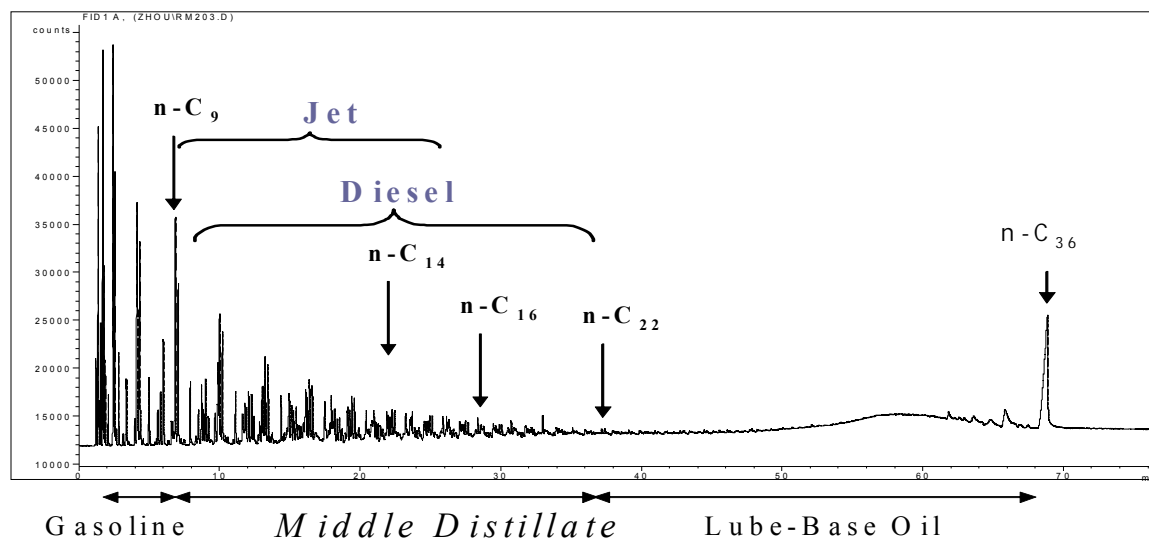
Reactant: 0.8 g n-C_{36}, Catalyst: 0.2 g PtWZr/SZr(4:1), Conversion: 93 wt%
Reaction conditions: 200 °C, 25min., initial H_2 pressure = 300psig

Figure 2 Typical product distribution from hydroisomerization and hydrocracking of n-C_{36}
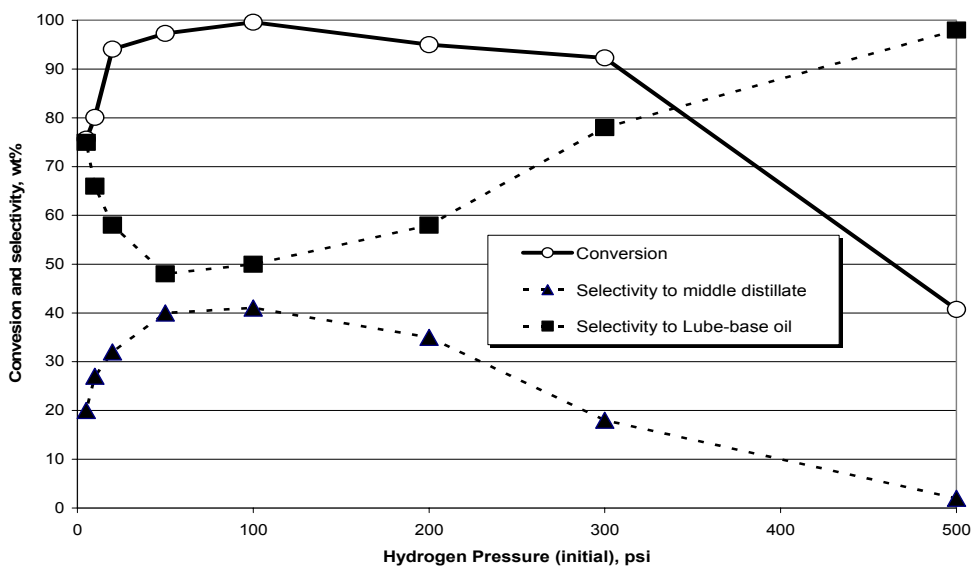
Catalyst: 0.25 g (0.5 wt%)Pt/WO3/ZrO2 (12.5 wt% W)
Reactant: 1.0 g n-C36,   Reaction conditions: 200 °C, 25 min.

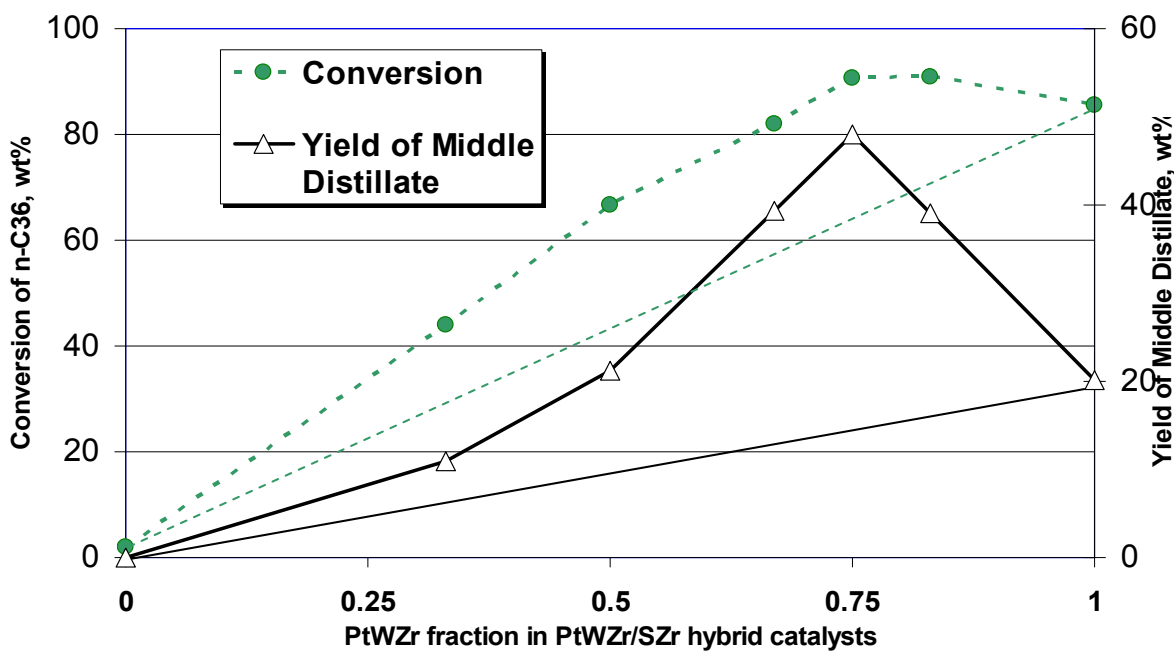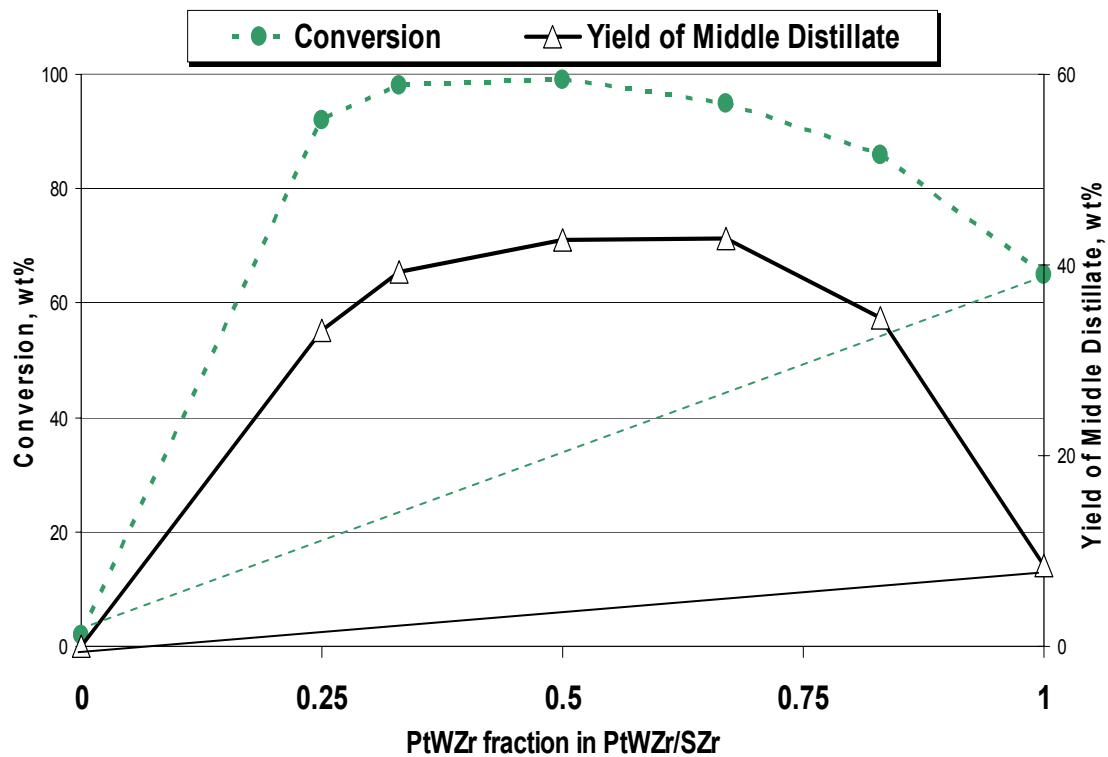Figure 3 Effect of hydrogen pressure on hydrocracking of n-C_{36} using PtWZr
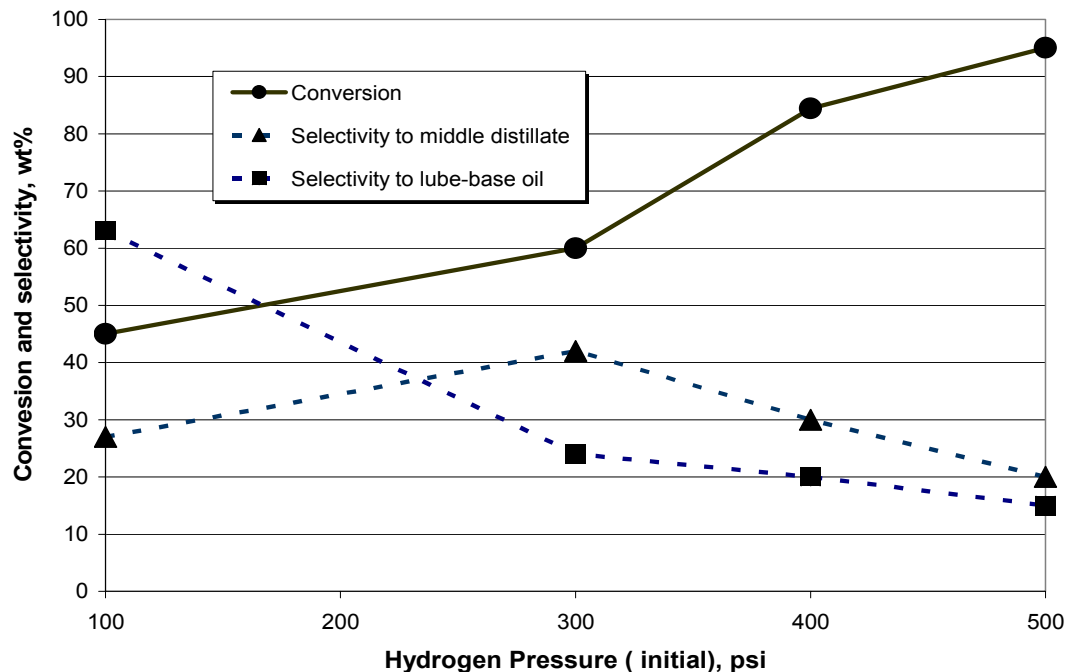
Catalyst: 0.2 g (0.5 wt%)Pt/SO4/ZrO2
Reactant: 0.8 g n-C36,   Reaction conditions: 200 °C, 20 min.

Figure 4 Effect of hydrogen pressure on hydrocracking of n-C$_{36}$ using PtSZr

Figure 5 Conversion of n-C36 using PtWZr/SZr hybrid catalysts under 100 psi hydrogen pressure

Catalyst: 0.2 g; Reactant: 0.8 g n-C36
Reaction conditions: 200 °C, 20 min.

Figure 6 Conversion of n-C$_{36}$ using PtWZr/SZr hybrid catalysts under 300 psi hydrogen pressure

Optimization of Fischer-Tropsch Synthesis under Supercritical Fluid Conditions: Solvent Effects on Reaction Performance

Nimir O. Elbashir, Xiwen Huang, Christopher B. Roberts
Department of Chemical Engineering, Auburn University

Introduction

There is significant interest in developing new technologies to improve the classical C1 chemistry routes for fuel and petrochemical production (Roberts and Elbashir 2003). In particular, the ability to better control the production of gasoline and diesel fractions from Fischer-Tropsch synthesis (FTS) is needed. Our efforts in this project are directed at utilizing the unique solvent characteristics of supercritical media in enhancing the production of middle distillate products from FTS, such as, gasoline and diesel fractions. Supercritical fluids offer several advantages for these catalytic reactions including the ability to manipulate the reaction environment through simple changes in temperature and pressure to enhance solubility of reactants and products, to eliminate interphase transport limitations, and to improve heat transfer in these exothermic reactions. Utilization of a supercritical phase medium in Fischer-Tropsch synthesis (FTS) presents a new challenge to the now 80-year old FTS technology. However, attempting commercial-scale operation of the high pressure and temperature reactors needed for supercritical fluid Fischer-Tropsch synthesis (SCF-FTS) requires improved understanding of the underlying kinetic, thermodynamic and reaction engineering issues. Nevertheless, industry has begun to focus on this SCF-FTS technology. Recently, Shell (SMDS scheme) revealed it's FTS technology in its new plant, in Bintulu, Malaysia, which employs C5 or C6 hydrocarbon injection for cooling, thus improving productivity by reducing heat transfer limitations (World Fuels Today Editorial, 2003).

In our previous report, we have demonstrated that conducting FTS under SCF conditions (using hexane as a solvent) affords unique opportunities to manipulate the reaction environment and to enhance the production of liquid fuels and value-added chemicals (such as   -olefins) from synthesis gas (Huang et al. 2002a; Huang et al. 2002b; Elbashir et al. 2003; Huang and Roberts 2003). Our results showed that varying the reaction parameters (such as pressure and temperature) have significant effect on FTS reaction performance. Generally, as the pressure is increased, the product molecular weight significantly increases as does the catalyst activity, nevertheless we noticed an existence of an optimum pressure whereby the effect of pressure on bulk diffusion and pore diffusivity is well balanced. We also reported that the product distribution in supercritical phase FTS exhibited at least two   -values (non-ASF distribution). Comparing SCF- FTS to gas phase FTS we found that the yield of heavy products (>C10) in the SCF medium is higher than that in gas phase medium. This phenomenon has been attributed to the increased solubility of hydrocarbons in the SCF medium coupled with the enhanced extraction of heavy compounds from the catalysts pores.

Proper selection of reaction conditions (such as temperature, pressure) certainly plays a vital role in producing desirable compounds with high   value at reasonable reactant conversion. As a matter of fact, varying either the temperature or the pressure of the reaction environment will significantly affect the thermo-physical characteristics of the supercritical phase (density,

diffusivity, thermal conductivity, etc.). More fundamental understanding of the process conditions is necessary to quantify the influence of the SCF environment on FTS. In this report, we examine various solvent effects on supercritical FTS under different density conditions and compare these studies to the conventional gas-phase reaction. The influence of tuning temperature and pressure (i.e. density) on the overall product distribution and on light, gasoline, diesel, and heavy hydrocarbons (wax) fractions is also reported. The activity of the catalyst was measured by CO conversion, H2 conversion and syngas (CO+H2) conversion and is reported as a function of the operating conditions. The effect of the SCF reaction media environment on CO conversion, methane selectivity, product distributions and   value was examined by adjusting the SCF reaction densities from gas-like to liquid-like through variations in temperature and pressure. Given the dramatic influence of the density dependent properties on FTS, one particular set of experiments was designed to directly compare hexane and pentane solvent effects at constant density and temperature (significantly higher pressures were required in pentane to achieve the same solvent density) in order to delineate between pressure effects on underlying kinetics and other solvent effects.

Research Objective

The objective of this project is to establish optimum operating conditions for FTS within the supercritical region that would maximize the production of middle distillate hydrocarbons such as gasoline fractions and diesel fractions and at the same time minimize the production of methane and carbon monoxide. In order to satisfy this objective we are investigating product selectivity alterations when the reaction is operated in a supercritical fluid medium vs. the conventional routes of FTS. Optimization of the FTS reactions under supercritical phase conditions requires simultaneous evaluation of the effect of the reaction media phase behavior and the bulk thermo-physical bulk properties (such as diffusivity, thermal conductivity, viscosity, etc.) that can be tuned by either the temperature or the pressure as well as the direct effect that those parameters have on the FTS reaction kinetics and chain growth-mechanism.

Our Recent Work

This study is designed to examine the effects of supercritical solvent (pentane, and hexane) at different operating conditions (temperature, pressure, syngas feed ratio, contact time, and space velocity) on FTS performance using alumina supported cobalt catalysts (15% Co/Al_2O_3 purchased from Union Carbide). The performance of supercritical phase FTS is compared to conventional gas-phase FTS. The study also covers the effect of changing the density dependent bulk thermo-physical properties (e.g. diffusivity, solubility, thermal conductivity, etc.) of the supercritical solvent-reactant mixture from liquid-like to gas-like, through either temperature or pressure tuning, on the cobalt catalyst performance (i.e. CO conversion, CH_4 and CO_2 selectivity, and hydrocarbons product distribution).

Experimental Section

High Pressure FTS Reaction Unit
In our previous report (Huang et al. 2002b) we have illustrated the basic schematic of our high pressure SCF-FTS unit that consists of three basic sections: a syngas and solvent delivery

section, a reaction section and a product separation and analysis section (as shown in Fig. 1). The supercritical solvents used were highly pure pentane (SCP) and hexane (SCH) (Fischer HPLC grade, purity >99.0%), and were used as received. Three standard gas cylinders (Air Products Company) containing certified mixtures composed of CO, N2 and H2 were used in this study. The mole percentages of the three gas mixtures in each cylinder were varied according to the following H2 /CO ratios: 2/1, 1/1, and 0.5/1. N2 served as a reference gas in each of the three cylinders for aid in chromatographic analysis and in the calculations of the activity and selectivity. The solvent hexane or pentane was pumped through the reactor system via an HPLC pump (Fischer Acuflow Series III) and the reactants (syngas) flow rate was controlled by a mass-flow controller (Brooks 5850E). The solvent and syngas streams were combined in a heated static mixer (OMEGA) before entering the reactor. The high pressure reactor (High Pressure Equipment) is a conventional down-flow fixed bed stainless steel reactor with effective volume of 32 cm3. The cobalt catalyst (15% Co/ Al2O3) was supported on a titanium disc that was fixed in the middle of the reactor. The reactor was situated in a furnace (Applied Test System Inc) with a programmed temperature controller system. A profile thermocouple with 6 detection points (OMEGA) was put thought the reactor to track the axial temperature distribution along with the length of the reactor. An 1/8" diameter hole is machined in center of the titanium disc to allow insertion of the profile thermocouple along the reactor length. The reaction pressure was controlled by a back pressure regulator (Tescom Inc.) located between the reactor and the hot trap. Two pressure indictors were located at the inlet and outlet of the reactor respectively to monitor the reaction pressure and pressure drop inside the reactor. The inlet and exit lines to and from the Back Pressure Regulator were maintained at temperature above 215 °C up to the hot trap in order to ensure no condensation of heavy hydrocarbons (waxes) prior to the hot trap and the online GC sampling system. In addition, the hot trap and its exit lines were maintained at 210 °C to condense high boiling point products. The remaining product stream was then fed to a cold trap maintained at room temperature to provide separation between liquid and gaseous products.

Analytical Methods and Measurements of the Reaction Performance
Products and reactants were analyzed by two GCs via two 6-port valves combined with two automatic injectors. One 6-port valve was located between the hot trap and the cold trap for analysis of C2 up to C40 hydrocarbons, and oxygenates in a Varian 3300 FID GC with capillary column (DB-5), and the other 6-port valve was located on the exit line of the cold trap to analyze the permanent gases (CO, H2, N2, CH4, C2H4, C2H6) in a TCD GC (Varian CP-3800) with a Hayesep-DB100/120 packed column. The response factor of N2 (assumed as unity) and the quantitative results of the TCD GC were used to calculate CO, H2, and syngas (CO+H2) conversions, in addition to CO2, CH4, C2 (ethane and ethane) selectivities. The response factor of a specific gas is a result of multiplying the mole ratio of that gas to that of N2 by the area ratio of N2 to that of the gas (as detected by the TCD). Syngas conversion (CO+H2 conversion) was defined as the molar ratio of the hydrogen and carbon monoxide consumed to those fed to the reactor, whereas selectivities of CH4, and C2 are defined as moles of the gases produced per moles of CO and hydrogen consumed. The quantitative analysis of the FID chromatogram was used to determine the weight percentage of hydrocarbons (C2 to C30) in the product stream. Due to the high concentration of the supercritical solvent in the product stream, the C5 and C6 products when using the pentane or hexane solvents, respectively, were masked and unable to be determined. The FID response factors for hydrocarbons are known to be nearly identical for the

individual species (Dietz 1967). Therefore, no correction was applied for the differences in individual responses, and the area percentages of the hydrocarbon species were used to represent their weight percentage. Normalized weight fraction is calculated as the weight of hydrocarbons (paraffin and olefin) at a specific carbon number divided by the total hydrocarbon weight (all carbon numbers) detected in that sample. Generally, the olefin selectivity is calculated as ratio of the weight of an olefin of a given carbon number to the total hydrocarbon weight at that given carbon number.

The density of the solvents (hexane or pentane) in the near-critical and supercritical region are strong function of both temperature and pressure as seen in Fig. 2.

Results and Discussion

Supercritical Phase FTS vs Gas Phase FTS

The overall product distributions of hydrocarbons from gas phase FTS and supercritical phase (hexane (SCH) or pentane (SCP)) FTS at 240 °C and partial pressure of syngas (CO+H2) ca. 20 bar whereby the supercritical solvent partial pressure is ca. 45 bar is shown in Figures 3a,b. Fig. 3 a, presents the light hydrocarbon fraction (C1-C4), gasoline fraction (C5-C11), diesel fraction (C12-C19), and wax fraction (C20+) for the product distributions from the FTS studies under the conditions stated above. As seen in Fig. 3a, the overall product distribution shifts towards heavier products in both supercritical phase hexane and pentane FTS compared to gas phase FTS.   Light hydrocarbons have not been reported for SCP due to technical difficulties in analyzing the light fractions from the FID-GC in that set of experiments. Fig. 3b illustrates non-Anderson Schulz-Flory (ASF) behavior and that the chain-growth probability (α-value) for heavier hydrocarbons (C10+) in supercritical pentane and hexane is close to 0.8 while in the gas phase it is about 0.75.

Considering the gas-phase reaction as the base line case, Fig. 3a shows that there is a significant improvement (134%) in the gasoline fraction in SCH-FTS compared to the gas phase-FTS. In SCP-FTS slight improvement was obtained in the gasoline fraction compared to gas phase-FTS with even more significant improvements in the diesel and wax fractions.   In the SCF phase reaction media, the solubility of heavy compounds is increased and as a result in-situ extraction of heavy compounds that occupy active sites on the catalyst surface increases, thereby freeing up more active sites for readsorption and enhanced chain growth. Another reason for this enhanced production of heavy components is that the enhanced solubility in SCH and SCP results in an increase in the concentration of α-olefins at the catalyst surface that promotes readsorption and further incorporation in the chain-growth process. The formation of two phases inside the catalyst pores in gas phase FTS (as result of condensation of heavy hydrocarbons) results in longer residence times of α-olefins inside the catalyst pores. This increase in residence time of α-olefins inside the catalyst pores can lead to secondary reaction of the olefins such as hydrogenation and isomerization to form normal paraffins and branched products (Yokota et al. 1990; Fan et al. 1992).   This production of paraffins and isomers terminates the chain-growth process (Iglesia et al. 1991) resulting in lower chain growth. SCF-FTS operation, on the other hand, results in elimination of multiple phases as well as improved extraction and removal of α-olefins from the catalyst pores thereby decreasing secondary reactions and promoting chain growth.

Due to the liquid-like heat capacity and thermal conductivity in SCH and SCP, the production of undesired products such as methane and carbon dioxide was significantly suppressed compared to gas phase FTS as seen in Table 1. In the gas phase reaction, local heat generation (inside the catalyst pores) during the reaction can result in temperatures that are significantly higher than the bulk temperatures measured along the length of the reactor. We have previously shown evidence of much better temperature control and improved heat distribution in SCH phase-FTS compared to gas phase-FTS (Huang et al. 2002a&b; Huang and Roberts 2003). The large amounts of heat generated in the FTS reaction can result in the cracking of long chain hydrocarbons into smaller ones if this heat is not efficiently removed from the catalyst pores (Chaumette et al. 1995). In the supercritical phase, the heat transfer rate can be improved due to the higher heat capacity and thermal conductivity.

The conversion and consumption rates of CO, as shown in Table 1, are higher in SCH and SCP than in gas phase-FTS. While it might be anticipated that conversions would be higher in gas phase FTS due to the higher diffusivities in the gas phase compared to the SCF medium (Yokota et al. 1990), we find that other density dependent factors have an important impact on the conversion in the SCF medium. The liquid-like density of the SCF medium results in high solubilities of the reactants and efficient extraction of products from the catalyst pores (Bochniak and Subramaniam 1998) thereby freeing up more active sites for enhanced conversion. Under supercritical-phase FTS conditions, the formation rate of heavy products and coke precursors is balanced by their removal rate as a result of the liquid-like solubility and in-situ extraction within the supercritical medium. The rapid desorption of the extracted and dissolved heavy hydrocarbons effectively creates more vacant reactive sites available to the reactants. It is also important to mention that at 240 °C and 65 bar the density of pentane is lower (closer to gas-like) than that of hexane (see Fig.2).

Effect of Temperature on the Supercritical Phase FTS
The distribution of light hydrocarbon, gasoline fraction, diesel fraction, and wax as function of reaction temperature for both SCP and SCH was studied at constant pressure (45 bar for SCP, and 65 bar for SCH), as shown in Fig. 4a and 4b respectively. In the case of SCP (Fig 4a), the highest reaction temperature (240 °C) favors light hydrocarbons and gasoline with less wax and heavy hydrocarbon production. At the lower temperature (210 °C) maximum yields of the diesel fraction and wax were obtained. Surprisingly, the trend in SCH medium showed an optimum temperature for each hydrocarbon fractions (see Fig 4b). For production of the gasoline fraction, 240 °C is the optimum temperature with selectivity close to 50% compared to the other fractions. At 250 °C the product shifted to the diesel fraction with selectivity close to 46%, while the wax and heavy hydrocarbons selectivity is similar for 230 °C and 250 °C. At the high temperature of 260 °C, the maximum peak of the product distribution is totally shifted towards light hydrocarbons (C1-C5) with selectivity close to 60%, however it showed a similar selectivity towards gasoline fractions as that at 250 °C.

Fig. 5 shows the profile of CO conversion and chain-growth probability in SCP-FTS at different temperatures. As the temperature is increased from 210 C to 240 C, CO conversion significantly increased, while the α-value slightly decreased with the temperature. This trend is in good agreement with the temperature effects illustrated in Fig. 4a. On the other hand the effect of

reaction temperature on activity and selectivity in SCH-FTS follows a different trend. As seen in Fig. 6a, and 6b, there is no significant effect of temperature on the syngas (CO+H2) conversion while there exits an optimum temperature (250 °C) for both chain growth probability and methane selectivity. The measured CO2 selectivity was found to be less than 1% over the range of temperature studies in SCH environment. In absence of pore diffusion limitations, the diffusion rate of CO and H2 to the active sites is very sensitive to the temperature in the SCF phase due to the dependence of density dependent properties on temperature in the near critical region. At low temperature, α-olefins readsorption dominates the competitive adsorption process facilitating the longer carbon chain propagation. High coverage of α-olefins on the catalyst surface is an obstacle to the adsorption of CO, which can result in a lower CO conversion. The results in SCH suggests that there is a very fine balance between liquid-like density needed to extract heavy hydrocarbons and wax from inside catalyst pores and gas-like diffusivity required for the reactant and olefins to reach the active sites and incorporate in the chain growth and synthesis process. Previous study has shown that there is an existence of a reversible relationship between the coverage of α-olefins on the surface and the CO conversion by adding certain α - olefins to the reaction process (Hindermann et al. 1993). Currently, we are studying the effect of temperature on chain growth probability and the phase behavior of the reaction mixture and its influence on improving diesel fractions at the optimum reaction temperature (250 °C) (Elbashir et al. 2003).

Effect of Pressure on the Supercritical Phase FTS
The effect of varying the pressure on the reaction performance of the 15% alumina supported cobalt catalyst in SCH phase is shown in Fig 7. We have observed the existence in optimum pressure (65 bar) whereby maximum CO conversion (79%) is obtained coupled with the lowest methane selectivity. Another interesting result shown in the same figure illustrates that at the constant temperature of 250 °C there is a very slight change in the chain growth probability of higher hydrocarbons (C10+) as the pressure increases from 35 (gas-like density) up to 80 bar (liquid-like density). Change of the density of the reaction media as a result of tuning the pressure would of course change the residence time of the reactant molecules in the catalyst bed. The variation in residence time with adjustments to density and pressure was estimated using the Peng-Robinson equation of state (PR-EOS) and Soave-Redlich-Kwong equation of state (SRK-EOS) setting the values of kij's of all components (reactants and solvent) equal to zero. Fig 8 shows the effect of residence time on the fraction of light hydrocarbons, fuel fraction (gasoline and diesel), and heavy hydrocarbons in SCH medium at constant temperature of 250 °C. There is no significant effect of residence time on the hydrocarbon distribution in the SCH environment whereas only slight variation has been observed in the diesel fraction (favored at higher residence time) and light hydrocarbon fractions (favored at lower residence time). However, in SCP the effect of residence time is more pronounced since as seen in Fig. 9. At lower residence time (6 s), more than 65 % of the products are in the gasoline fraction, whereby at the highest residence time (10s) more than 60% of the products are in the diesel and heavy wax fractions. According to the basic model of the chain-growth mechanism and the polymerization nature of the FTS reaction, increasing the residence time of the reactant molecules would result in an increased probability of chain growth, therefore, the weight percentage of the heavier hydrocarbon would increase (Flory 1936). The rate of secondary reactions of α-olefins (especially readsorption, and incorporation in chain growth) is also affected by the residence time; the more rapid the removal of α-olefins from the catalyst bed (lower residence time) the

lower the possibility for readsorption (Madon and Iglesia 1993). However, this is not always the case since longer residence time and readsorption of α-olefins may also result in hydrogenation to paraffins, isomerization to cis and trans-olefins, or oxygenation to alcohols, thus terminating chain growth. Besides the bed residence time and the pressure, other factors such as heat of adsorption of the light olefins, the solvent medium properties and phase behavior, and solvent-reactant feed ratio play a role in determining the degree of the incorporation of the α-olefins in the chain-growth mechanism (Elbashir et al. 2003). In the SCH environment we have not observed any formation of isomerized products or oxygenates during the FTS reaction even at pressures as high as 80 bar, and temperatures up to 250 °C, however, this was not the case for the SCP-FTS. Both GC-FID and GC-MS analysis confirms the presence of considerable amounts of isomers and oxygenates in SCP-FTS products that increased both with residence time and pressure. In SCP-FTS, the conversion steadily increased as a function of pressure, as seen in Fig. 10, up to 70 bar. This is in contrast to the trend in SCH-FTS, shown in Fig. 7, where a maximum in conversion was observed at 65 bar. This indicates that the more dense SCH medium is more effective in extracting heavy products from the interparticle pores thereby providing more active sites for higher conversion.

Comparison between SCH and SCP at constant temperature and density
The density of the supercritical fluid medium is a fundamental factor affecting the catalyst pore internal diffusion rate and -olefins readsorption. By adjusting the medium density, both bulk diffusion and internal diffusivity can be significantly changed. Increasing the medium density through isothermal pressure increases can, on one hand, enhance the internal diffusivity by strengthening in-situ extraction and removal of heavy compounds from the catalyst pores. On the other hand, this high medium density also results in lower bulk diffusion rates. An ideal balance between the positive enhancement in pore diffusivity and decrease in bulk diffusion rate with enhanced medium density should be achievable. However, if density and transport properties were the dominant factors controlling the reaction behavior, then the same medium density in two different solvents (e.g. hexane vs. pentane) should lead to similar behavior. In order to compare the influence of the two solvents at the same density, higher pressures are required in supercritical pentane in order to achieve the same density as that of hexane at a given temperature (see Fig. 2). The results presented in Fig. 11 show that there is not much difference in the hydrocarbon distributions for carbon numbers less than 20 in either SCH or SCP phase reaction at constant density. In both solvents, the maxima in the product distributions are located around C12-C15. Even though the overall hydrocarbon product distribution is almost similar at the same operating density, significant difference in α-olefins selectivity in SCH and SCP phases was observed, as seen in Fig. 13. That difference can be attributed to the high rate of isomerization in SCP phase as mentioned previously. Interestingly, the CO conversion is 92% in SCP-FTS while it is only 61% in SCH-FTS at this constant density. This suggests that there is an effect of pressure on the CO conversion rate at fixed solvent medium density and temperature.

Reactants Composition Effect
The effect of the feed composition (H_2/CO ratio) on the activity and selectivity of the 15% Co/Al_2O_3 catalyst was studied in both gas phase and supercritical phase FTS (SCH and SCP). Fig. 13 illustrates the trend of CO conversion with the feed ratio in both gas phase FTS and SCH-FTS over alumina supported cobalt catalyst at a flow rate of 100 cc/min of syngas. The results showed that there is no significant difference in activity between gas phase-FTS and

SCH-FTS at low H2/CO. However, as the H2/CO ratio is increased, higher activity was observed in SCH compared to gas phase FTS. As shown in Fig. 14, the selectivity of CH_4, and CO_2 was found to be lower in SCH than that in the gas phase reaction in all the feed ratios studied. The results illustrated in Fig. 13 and 14 are in a good agreement with most of the kinetic models available in the literature and the rates of the different reactions involved over this cobalt catalyst (Wojciechowski 1988; Sarup and Wojciechowski 1989; Patzlaff et al. 2002).

The effect of the feed gas composition on the hydrocarbon product distribution has also been investigated for FTS in SCP at 220 °C and 45 bar. Figure 15 shows that lower H_2/CO ratio leads to higher hydrocarbon content. Another observation from the same figure is that the peak maximum of the distribution curve occurs around C_8-C_{10} when a H_2/CO ratio of 2 is employed and shifts to higher carbon number, C_{14}-C_{15}, as the H_2/CO ratio changes from 2 to 0.5. On the other hand, the α-value was found to decrease as the H_2 concentration in the feed increases. This is a direct result of increasing other undesired reactions such as methanation and water-gas-shift reaction as illustrated previously in Fig. 14.

Conclusions

The center of attention of our study during the last year has been on the effects of reaction temperature, pressure, solvent type, and reaction media on FTS reaction over a 15% Co/ Al2O3 catalyst in supercritical fluid media. Our investigations mainly focused on how the density of the supercritical phase can influence the consumption rates of the reactants, propagation and chain growth probability of the hydrocarbons, and selectivity towards other reactions such as methanation, and WGS reactions. The conventional gas phase FTS reaction was used as the base line for comparison with the supercritical phase FTS results under the same reaction conditions. Variations in the product distributions of fuel fractions (gasoline, and diesel) with the density of the fluid of the reaction system was systematically evaluated. The purpose of this evaluation is to search for an optimum operating condition whereby maximum production of middle distillate hydrocarbons (e.g. C5-C19) could be obtained with minimum production of undesired products such as CH4 and CO2 at reasonable reactants conversion. The findings of this study are summarized as follows;

1. Significant improvement in the product distribution towards heavier hydrocarbons (high α-value) was obtained in SCF-FTS compared to that of the gas-phase reaction. This was also accompanied by high selectivity towards α-olefins and suppression of CH_4 and CO_2 production rates.

2. Reaction temperature has a significant influence on the thermo-physical properties of the FTS media (namely medium density) and at the same time it affects the kinetics and rates reactions. In SCH-FTS and SCP-FTS, high reaction temperatures result in increase in the rates of reactants consumption, and shift of products selectivity towards light hydrocarbons and gasoline fractions. Low reaction temperatures promote chain growth, and therefore favor the production of diesel fractions and wax. Interestingly, the temperature trend in SCH phase showed an optimum temperature of 250 °C whereby maximum yield of diesel fractions was obtained. Another important observation is that the wax content at this temperature (i.e. 250 °C) is similar to that at low temperature of 230 °C. The selectivity towards CH_4 and CO_2 at 250 °C have not exceeded 15%, and 2% respectively, while at the same temperature in the gas phase reaction, CH_4, and CO_2 selectivity can go as high as 39%, 14% respectively. It is

worth noting to mention here that this temperature was considered very high for cobalt based catalysts.

3. The reaction pressure also has a pronounced influence on the density of the media, rates of the different reactions, and the residence time of reactants and products in the catalyst bed. In SCH we observed an optimum pressure for carbon monoxide conversion (65 bar). Beyond that pressure the decrease in bulk diffusivity of the reaction mixture will overcome the enhanced pore diffusivity. CH_4 selectivity, and chain growth probability were slightly affected by the pressure in SCH-FTS and SCP-FTS.

4. Readsorption of α-olefins followed by subsequent incorporation in the chain growth process are suggested to be the main reasons behind the   enhancement of chain growth probability under supercritical phase operation. This phenomenon cannot be attributed to internal diffusion limitation effects alone. Many other factors have to be considered, such as, increased solubility in the supercritical fluid medium, increased vacant adsorption sites accessibility, and the elimination of the adsorption layer barrier.

5. Interestingly, both SCP and SCH-FTS performed nearly identically at a common density in terms of hydrocarbon product distribution, however significantly higher conversions were observed in SCP due to the much higher pressure (kinetic effect). We also observed that in SCH secondary reactions such as isomerization, and oxygenation were significantly suppressed while in SCP considerable amount of isomers and oxygenates were detected especially in the lower hydrocarbon fractions (C_2-C_{11}).

6. Changing the gas fed composition (H_2/CO ratio) has a more pronounced influence in the supercritical phase than in the gas phase reaction especially at high hydrogen concentration (ratio 2/1). This indicates that easy extraction of products from inside the catalyst pores and enhanced solubility in the SCF creates more active site vacancies for the hydrogen to dissociate and thus increase the reaction rates (Elbashir et al., 2003).

Future Work

In this report we demonstrate the ability to manipulate FTS product distributions in the supercritical phase from light hydrocarbons, up to the heavy hydrocarbons and wax by using the temperature and the pressure of the reaction medium. This illustrates the importance of simultaneous evaluation of the influence of both temperature and pressure on reaction kinetics, chain growth, and solvent/reactant/products phase behavior in supercritical phase FTS. The purpose of this evaluation is to suggest an operating condition whereby we are able to maximize the production of middle distillate hydrocarbons, specifically gasoline and diesel fractions (C5-C19), and minimize the production of light hydrocarbons and undesired product such as CH4 and CO2. Based on these objectives, future work on this project in the coming year will be carried as follows;

1. Investigate the influence of temperature and pressure on the phase behavior of the reaction mixture (reactants (CO, H_2) + solvent (hexane, or pentane) + products (hydrocarbons, CO_2, and H_2O). The phase behavior of the mixture will then be correlated with the reaction performance measured by the consumption rates of reactants and the overall hydrocarbon product distributions. That will help us to identify the best operating conditions within the supercritical phase that promotes optimum production of gasoline and diesel fractions in the supercritical media.

2. Establish a reaction pathway and chain growth mechanism that explains the consistent non-ASF phenomena observed under the supercritical phase FTS operation and identify the parameters influence this behavior. The purpose of this step is to identify the parameters that can be used to control the FTS product distributions in the supercritical phase.

3. Cobalt catalysts were known to be more sensitive towards the pressure than iron catalysts. The performance of cobalt catalysts in FTS is highly influenced by the cobalt dispersion on the support, pore volume, surface area, and the reduction methods. We have synthesized a number of cobalt catalyst systems by varying properties, such as surface area, pore volume, and cobalt dispersion. These catalysts will be tested under supercritical phase conditions. The purpose of this test is to quantify the influence of supercritical phase on the intrinsic reaction kinetics.

4. A kinetic model describing the reaction behavior in the supercritical phase FTS process will be developed. The model will be verified against the experimental results of the cobalt systems under different H_2/CO feed ratios and reaction conditions (volumetric space velocity, residence time, temperature, etc.). The purpose of this model is to simultaneously quantify the influence of parameters such as pressure and temperature on the reaction kinetics and on the phase behavior of the reaction mixture. This will provide us with basic information to better utilize the unique characteristics of the supercritical phase in performing the reaction under high catalyst activity (CO and H_2 conversion) and at the same time maximize the product distribution towards the desired products (gasoline and diesel fractions).

Publications and Presentations from this Project During the Last Year

1. Huang, X. and C. B. Roberts. "Selective Fischer–Tropsch synthesis over an Al_2O_3 supported cobalt catalyst in supercritical hexane." *Fuel Processing Technology* **83**: 81-99, (2003).

2. Huang X. , N. O. Elbashir and C. B. Roberts "Supercritical fluid Fischer-Tropsch synthesis; Influence of Solvent and Reaction conditions." To be submitted to *Ind. Eng. Chem. Res.* (2003).

3. Elbashir, N. O., X. Huang, C. B. Roberts "An Approach to understand the enhanced chain growth mechanism in supercritical hexane medium." to be submitted to *Chemical Engineering Science,* (2003).

4. Elbashir, N. O., X. Huang, and C. B. Roberts "Utilization of Supercritical Phase in Fischer Tropsch over Alumina supported Cobalt Catalysts". *Gordon Research Conference 'Hydrocarbon Resources',* Ventura, Los Angeles, Jan 12-17. (2003).

5. Roberts C. B., Elbashir N. O., and Huang X. "Influence of Solvent-Reactant Mixture Phase Behavior on Supercritical-Phase Fisher-Tropsch Synthesis" *Annual Technical Meeting of the Consortium of Fossil Fuel Science (CFFS),* Oglebay Resort and Conference Center, Wheeling WV, August 3-6 (2003).

6. Elbashir N. O. , Huang X., Boroughs D., and Roberts C. B. "An Approach to Understand the Enhanced Hydrocarbon Chain-Growth in Supercritical-Phase Fischer-Tropsch Synthesis" *Annual Technical Meeting of the Consortium of Fossil Fuel Science (CFFS),* Oglebay Resort and Conference Center, Wheeling WV, August 3-6 (2003).

7. Huang X., Elbashir N. O. , and C. B. Roberts "Fischer Tropsch Synthesis Over Cobalt Catalyst in Supercritical Hexane: Comparative Study with the FT Gas Phase Reaction" *AIChE Annual Meeting,* [Session 76] - Reactions in Compressed and Supercritical Fluids II, Indianapolis, Indiana, November 3-8 (2002).

8. Elbashir, N. O., X. Huang, D. Borough and C. B. Roberts (2003). "Enhanced Hydrocarbon Chain-Growth in Supercritical Phase Fischer-Tropsch Synthesis: Experiments and Modeling". *AIChE Annual Meeting*, San Fransicio, CA   Nov. 16-21., 2003.

References

1. Bochniak, D. J. and B. Subramaniam (1998). "Fischer-Tropsch Synthesis in Near-Critical n-Hexane: Pressure-Tuning Effects." AIChE Journal **44**(8): 1889-1896.
2. Chaumette, P., C. Verdon, et al. (1995). "Influence of the hydrocarbons distribution on the heat produced during Fischer-Tropsch synthesis." Topics in Catalysis **2**(1-4): 301-311.
3. Das, T. K., G. Jacobs, et al. (2003). "Fischer-Tropsch synthesis: characterization and catalytic properties of rhenium promoted cobalt alumina catalysts*." Fuel **82**(7): 805-815.
4. Dietz, W. A. (1967). "Response factors for gas chromatographic analyses." J. Gas Chromtogr. **5**(2): 68-71.
5. World Fuels Today Editorial (2003). "Today's Feature: 'Supercritical Phase' FT, CO2-Rich Scheme Highlights Japan SAE Conference Papers." World Fuels TODAY **July 3**: P1 & P5-6.
6. Elbashir, N. O., X. Huang, et al. (2003). "An Approach to understand the enhanced chain growth mechanisim in supercritical hexane medium." Chemical Engineering Science **to be submitted**.
7. Elbashir, N. O., X. Huang, et al. (2003). Utilization of Supercritical Phase in Fischer Tropsch over Alumina supported Cobalt Catalysts. Gordon Research Conference 'Hydrocarbon Resources', Ventura, Los Angeles.
8. Fan, L., K. Yokota, et al. (1992). "Supercritical phase Fischer-Tropsch synthesis: catalyst pore-size effect." AIChE Journal **39**(10): 1639-1648.
9. Flory, P. J. (1936). "Molecular Size Distribution in Linear Condensation Polymers." J. Am. Chem. Soc. **58**(10): 1877-1885.
10. Hindermann, J. P., G. J. Hutchings, et al. (1993). "Mechanistic aspects of the formation of hydrocarbons and alcohols from carbon monoxide hydrogenation." Catalysis Reviews - Science and Engineering **35**(1): 1-127.
11. Huang, X., C. W. Curtis, et al. (2002a). "Reaction behavior of Fischer-Tropsch synthesis in near critical and supercritical hexane media." Preprints of Symposia - American Chemical Society, Division of Fuel Chemistry **47**(1): 150-153.
12. Huang, X., N. O. Elbashir, et al. (2002b). Application of Supercritical Fluids as Reaction Medium for FTS, CFFS Annual Report, 2002.
13. Huang, X. and C. B. Roberts (2003). "Selective Fischer–Tropsch synthesis over an Al2O3 supported cobalt catalyst in supercritical hexane." Fuel Processing Technology **83**: 81-99.
14. Iglesia, E., S. C. Reyes, et al. (1991). "Transport-enhanced a-olefin readsorption pathways in ruthenium-catalyzed hydrocarbon synthesis." Journal of Catalysis **129**(1): 238-56.
15. Madon, R. J. and E. Iglesia (1993). "The importance of olefin readsorption and hydrogen/carbon monoxide reactant ratio for hydrocarbon chain growth on ruthenium catalysts." Journal of Catalysis **139**(2): 576-90.
16. Patzlaff, J., Y. Liu, et al. (2002). "Interpretation and kinetic modeling of product distributions of cobalt catalyzed Fischer-Tropsch synthesis." Catalysis Today **71**(3-4): 381-394.
17. Roberts, C. B. and N. O. Elbashir (2003). "An overview to `Advances in C1 chemistry in the year 2002'." Fuel Processing Technology **83**(1-3): 1-9.

18. Sarup, B. and B. W. Wojciechowski (1989). "Studies of the Fischer-Tropsch synthesis on a cobalt catalyst. II. Kinetics of carbon monoxide conversion to methane and to higher hydrocarbons." Canadian Journal of Chemical Engineering **67**(1): 62-74.
19. Wojciechowski, B. W. (1988). "The kinetics of the Fischer-Tropsch synthesis." Catalysis Reviews - Science and Engineering **30**(4): 629-702.
20. Yokota, K., Y. Hanakata, et al. (1990). "Supercritical phase Fischer-Tropsch synthesis." Chemical Engineering Science **45**(8): 2743-2749.

Table 1: Activity and selectivity of 15% Co/ Al_2O_3 at 240 °C in gas-phase, SCH, and SCP reaction environment. H_2/CO feed ratio is 2/1 and the VSV of syngas is 187.5 h^{-1} for 1 gram of catalyst while the flow rate of supercritical solvent is 1 ml/min.

	Gas Phase	SC-Hexane	SC-Pentane
Time on stream (h)	40	42.5	31
CO conversion %	67.6	68.435	85.6
CO consumption rate (μmol CO reacted.g_{cat}^{-1}.sec^{-1})	7.597	7.95	12.8621
H_2+CO conversion %	60.64	61.45	91.3
CH_4 Selectivity %	27.15	8.7	6.6
CO_2 Selectivity %	2.9	0	0
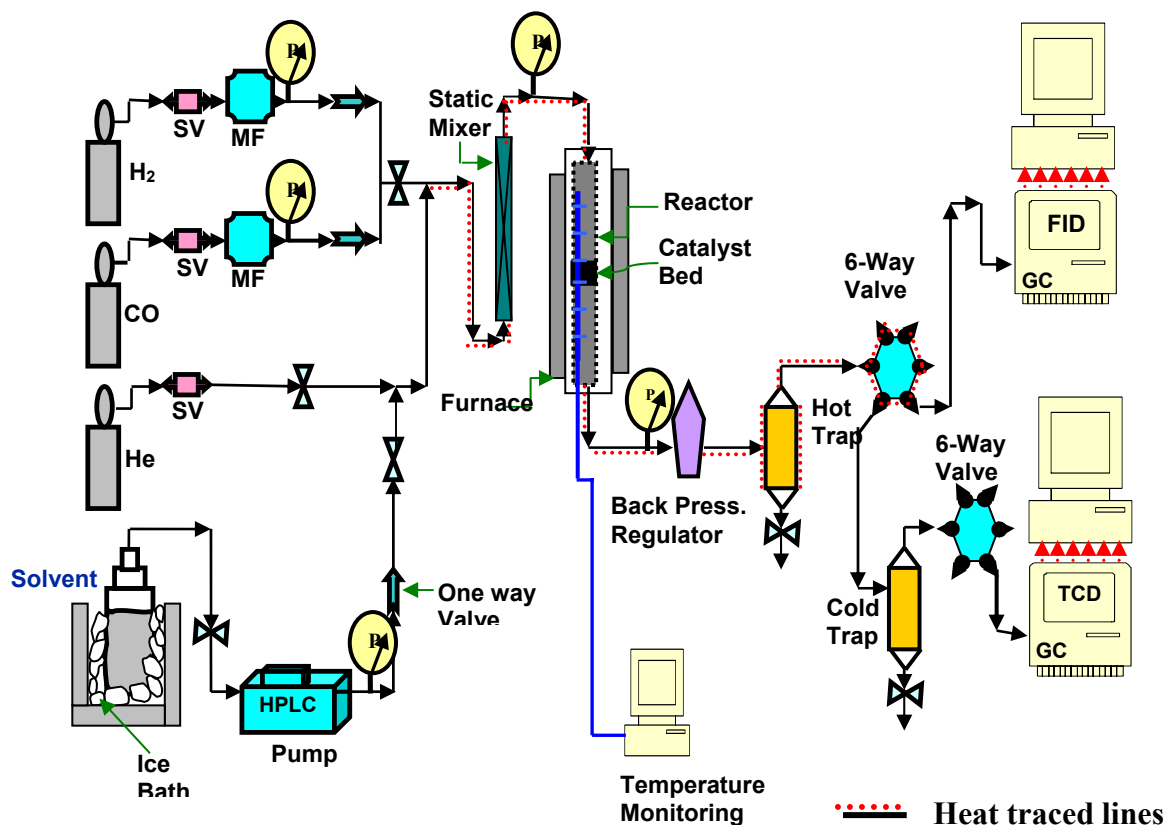
Fig.1: High pressure supercritical fluid FTS unit
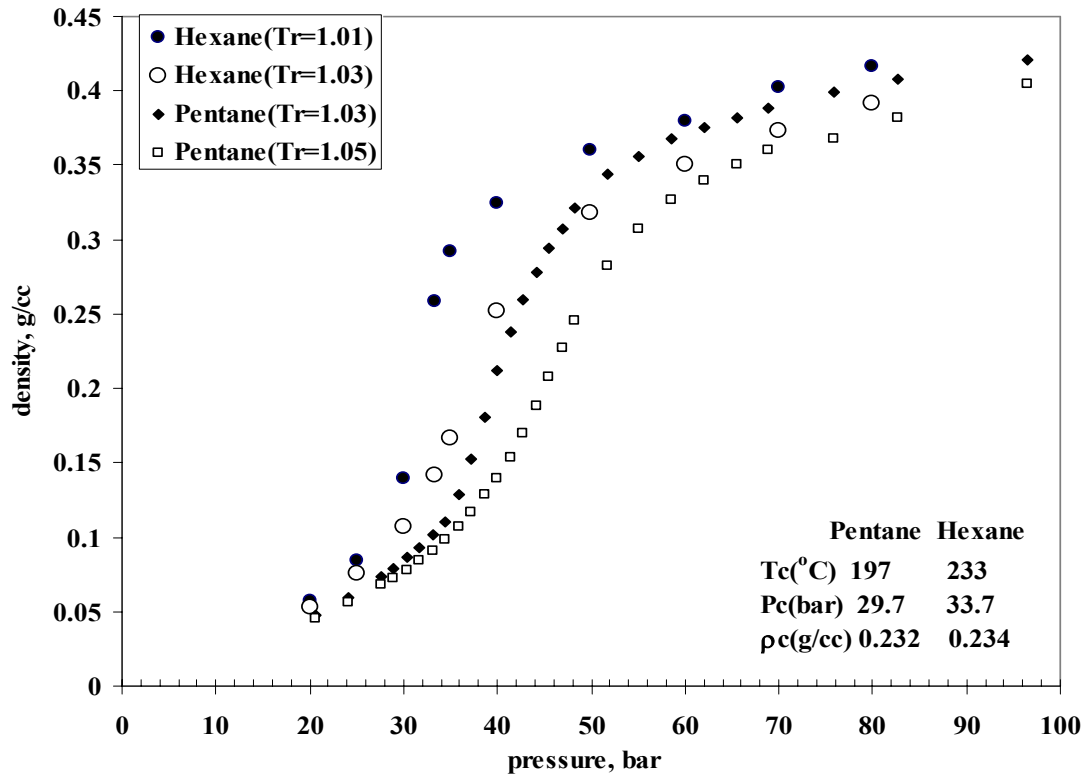
Fig. 2: P-ρ diagram of hexane and pentane at different reduced temperatures.
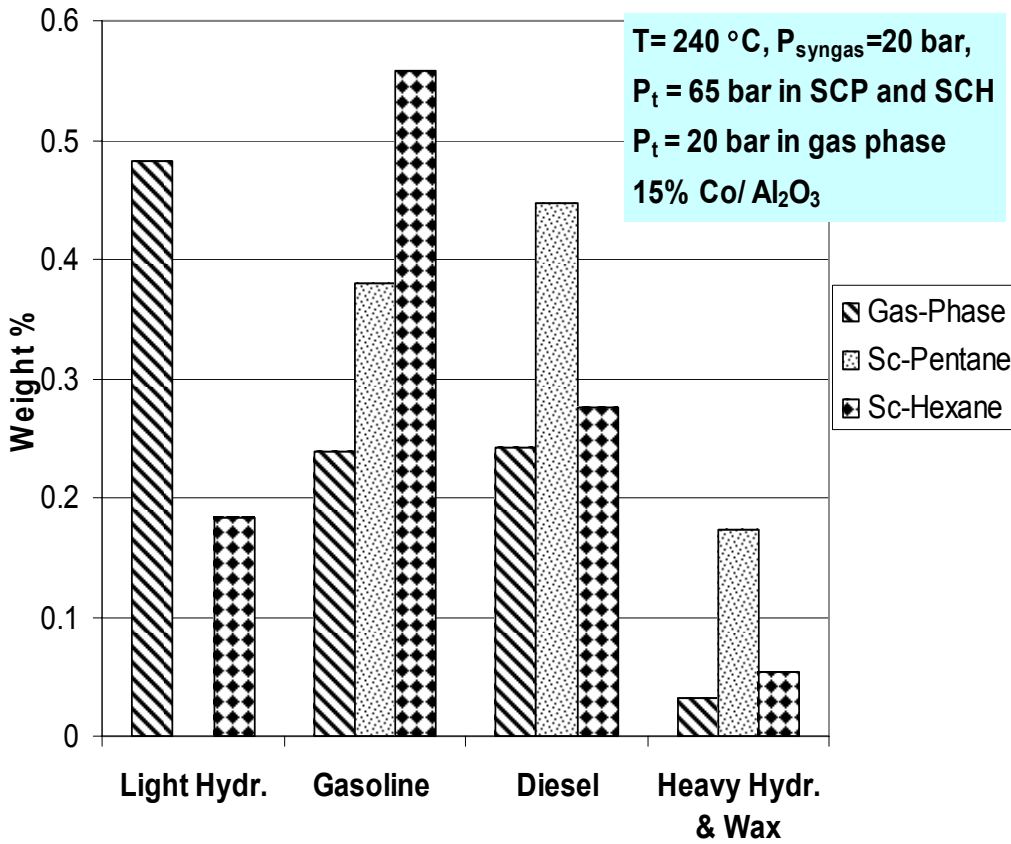
Fig 3*a*: Hydrocarbons and fuel fractions distributions in gas phase, SCH, and SCP environment at 240 °C. Catalyst is 15% Co/ Al$_2$O$_3$, H$_2$/CO feed ratio is 2/1.
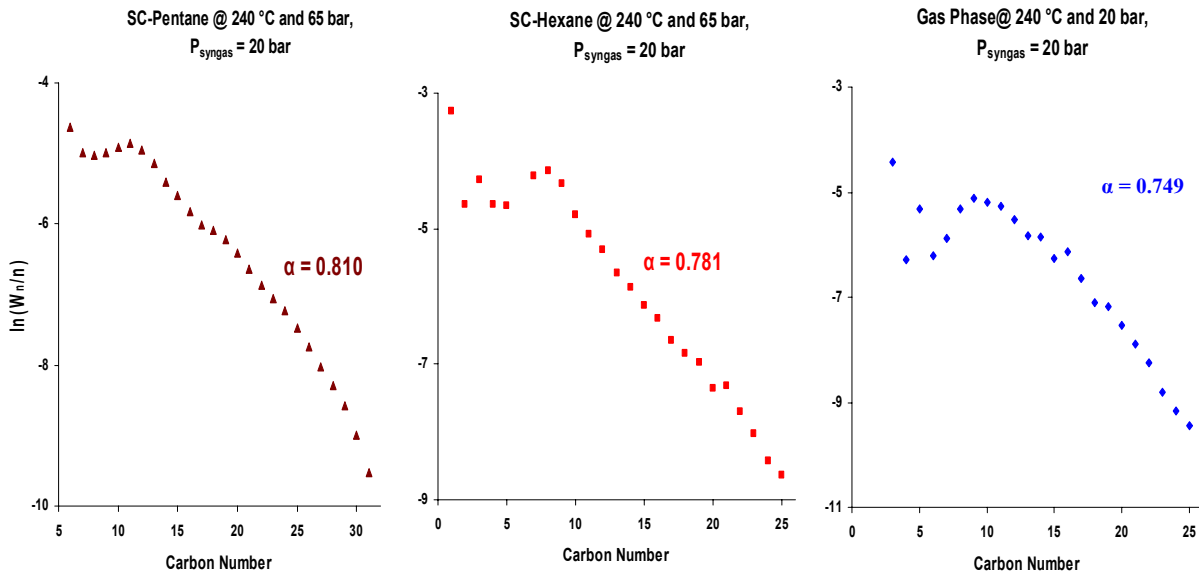
Fig. 3*b*: ASF distributions in gas-phase, SCH, and SCP reaction environment. Catalyst is 15% Co/ Al$_2$O$_3$ at 240 °C and H$_2$/CO feed ratio of 2/1.
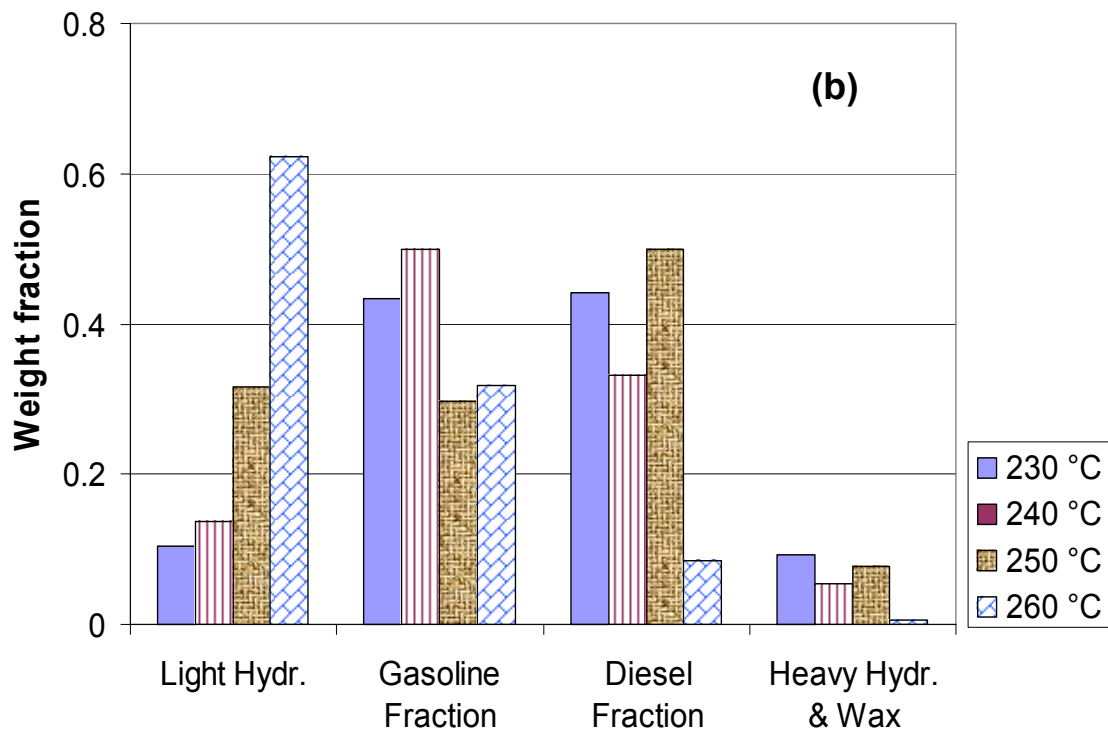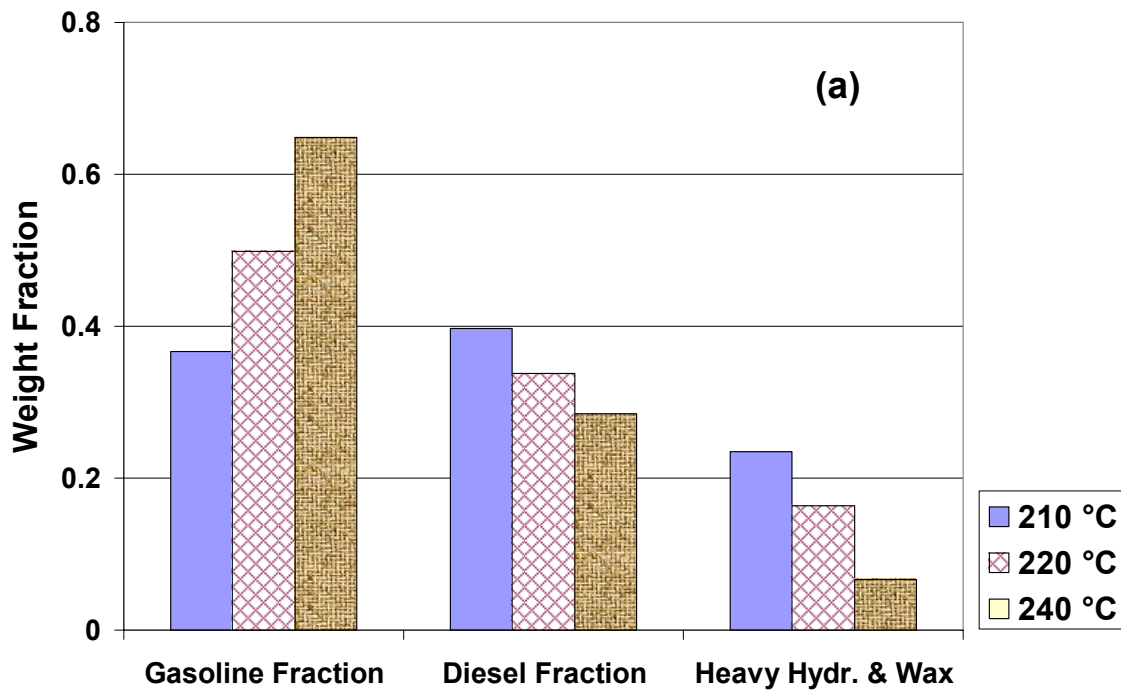
Fig. 4: Distributions of fuel fractions and heavy hydrocarbons (a) SCP-FTS environment at constant pressure of 45 bar and three different temperatures, and (b) SCH-FTS environment at constant pressure of 65 bar and four different temperatures.
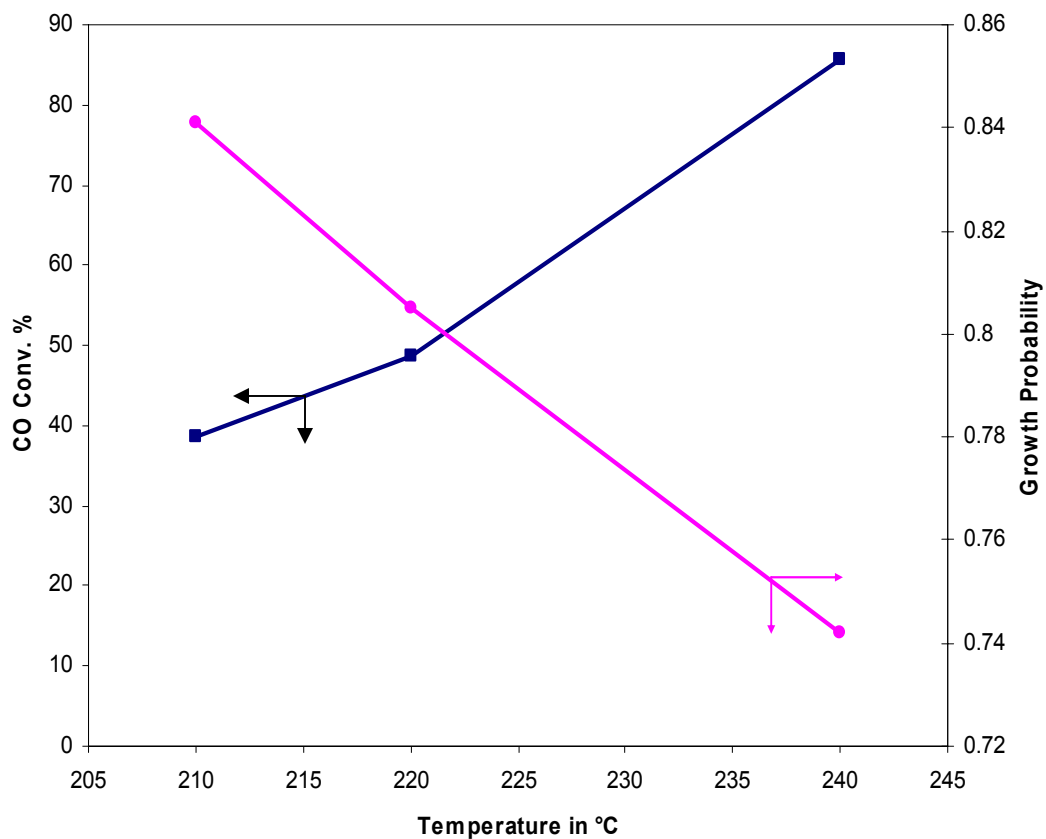
Fig. 5: Effect of reaction temperatures on carbon monoxide conversion, and chain growth probability in SCH environment at constant pressure of 45 bar.
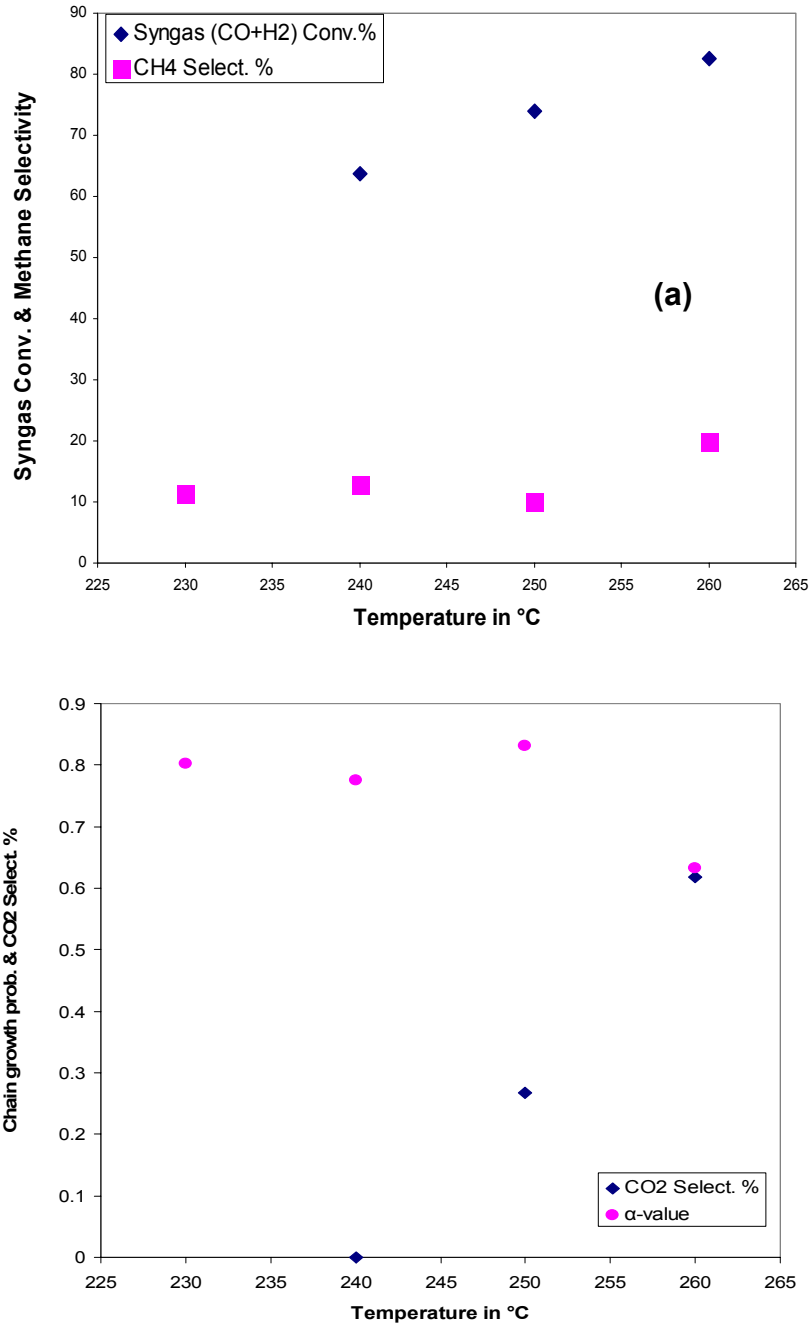
Fig. 6: Effect of reaction temperatures on (a) syngas conversion, and methane selectivity, (b) carbon dioxide selectivity and α-value for SCH phase at constant pressure of 65 bar.
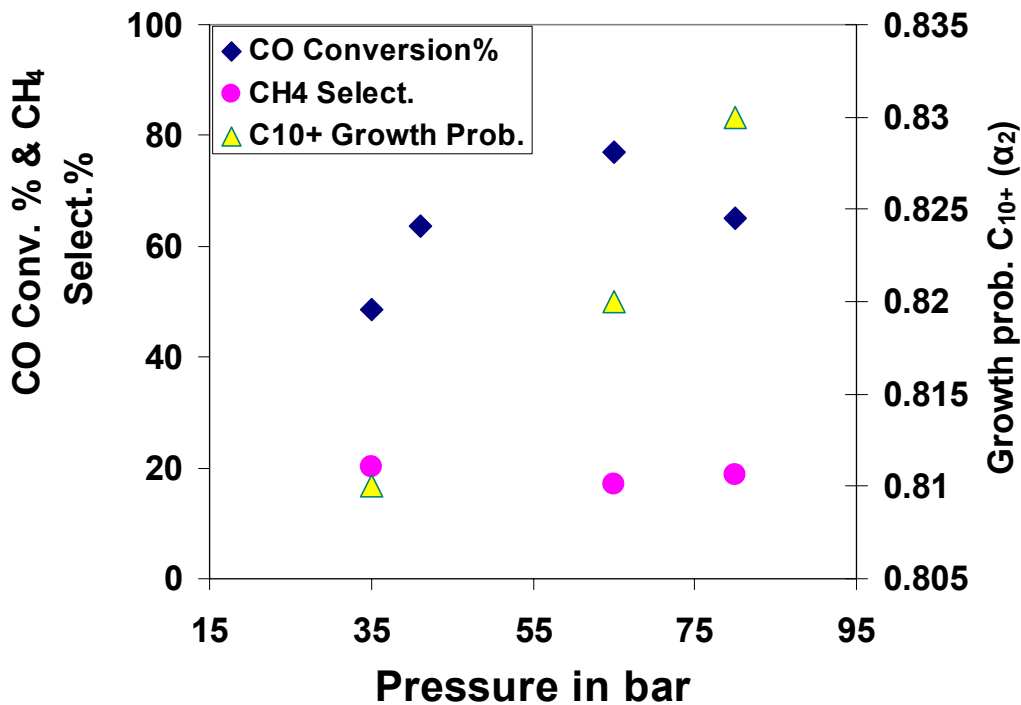
Fig. 7: Effect pressure on (CO conversion, methane selectivity chain growth probability (α-value) for SCH phase FTS at constant temperature of 250 °C.
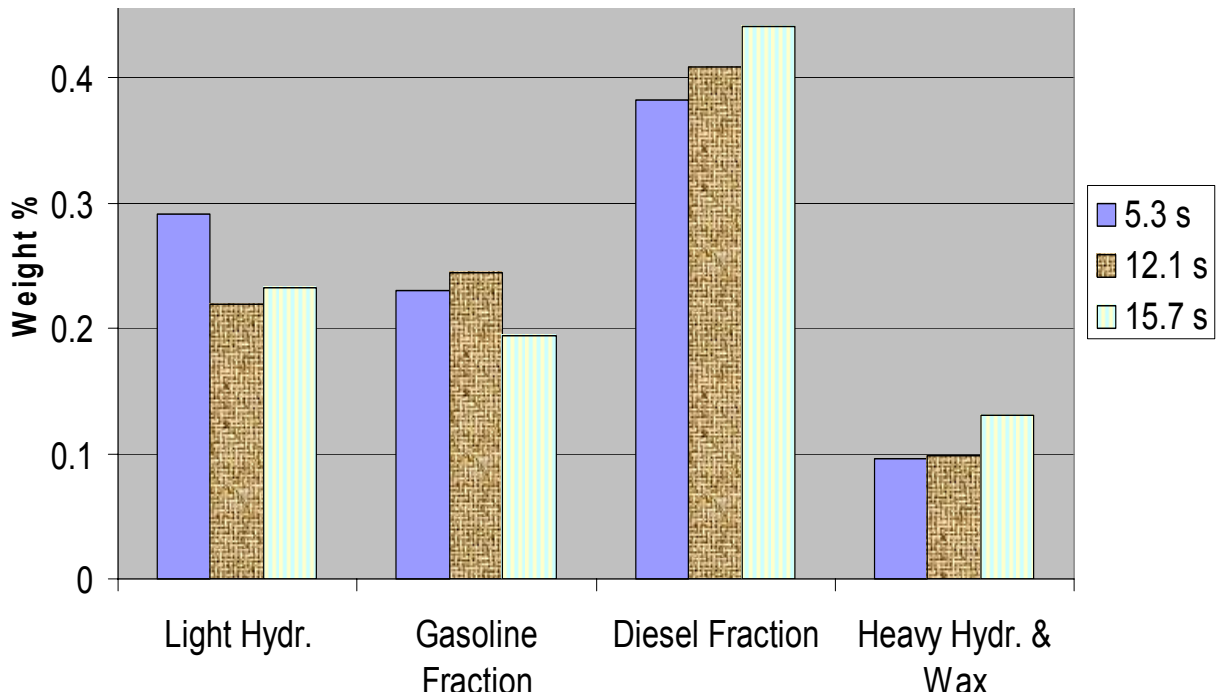
Fig. 8: Effect of the residence time on the hydrocarbon distributions in SCH environment at constant temperature of 250 °C.
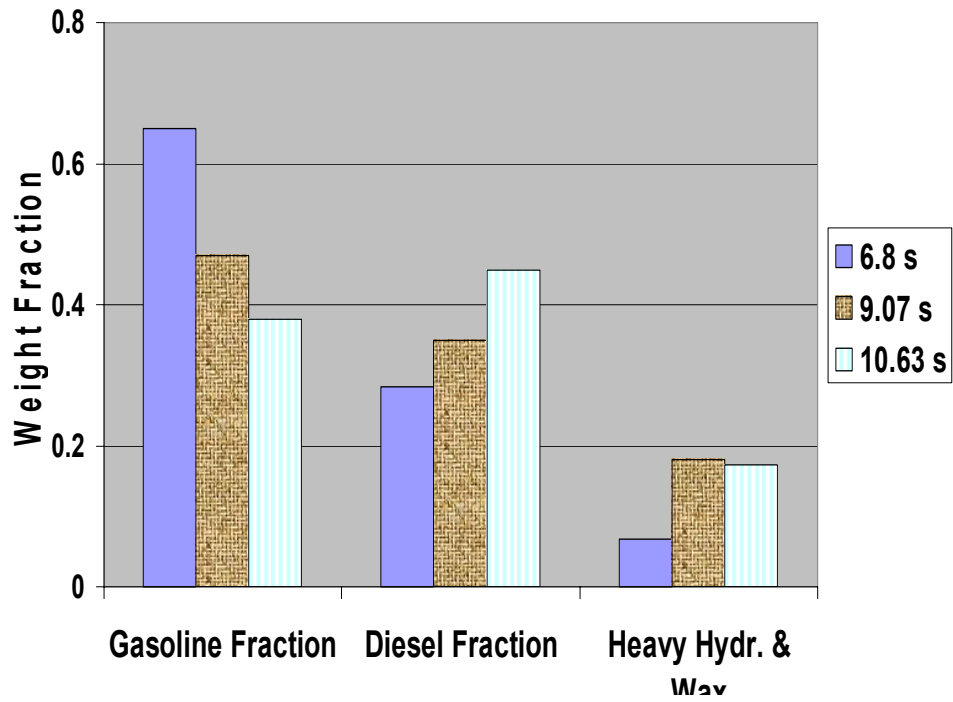
Fig. 9: Effect of the residence time on the hydrocarbon distributions in SCP environment at constant temperature of 240 °C.
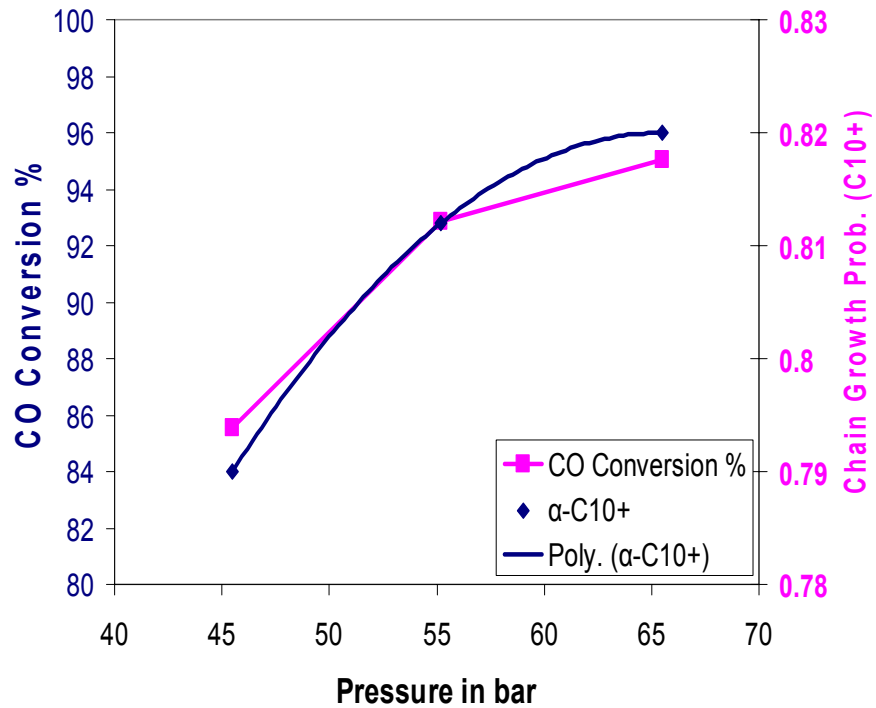
Fig. 10: Effect pressure on CO conversion and chain growth probability (α-value) of C_{10+} for SCP-FTS at constant temperature of 240 °C.
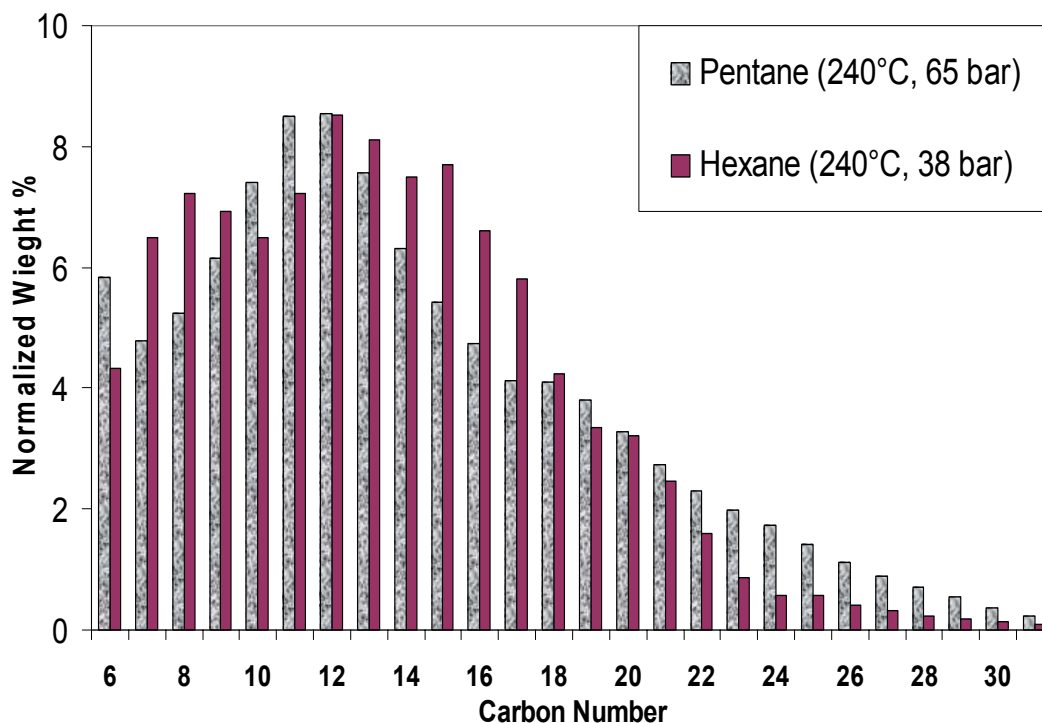
Fig. 11: Hydrocarbon distributions in both SCH, and SCP environment at a critical density of 0.334 g/cm^3 and temperature of 240 °C for H$_2$/CO feed ratio of 2:1 and SV of 93.75 hr^{-1}.
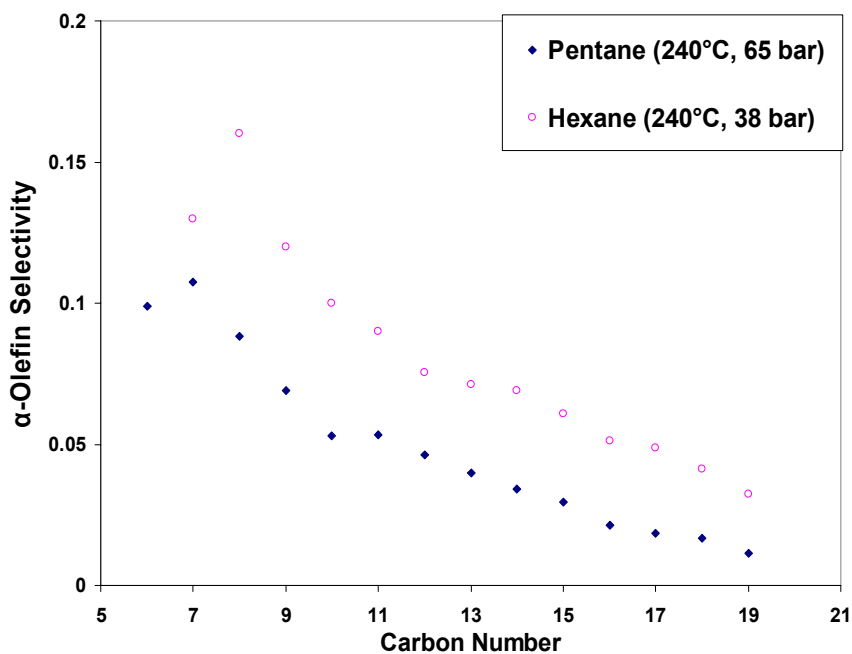
Fig. 12: α-olefin selectivity for SCH, and SCP environment at a critical density of 0.334 g/cm^3 and temperature of 240 °C for H$_2$/CO feed ratio of 2:1 and SV of 93.75 hr^{-1}.
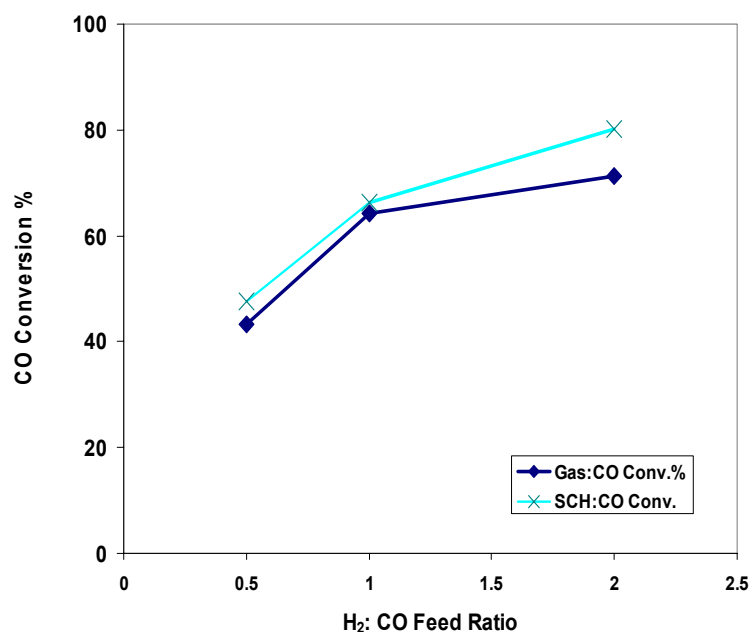
Fig. 13: Effect of H$_2$/CO feed composition on the activity of a 15% Co/Al$_2$O$_3$ in gas phase reaction and in SCH environment at reaction temperature of 240 °C and SV of 187.5 hr^{-1}.
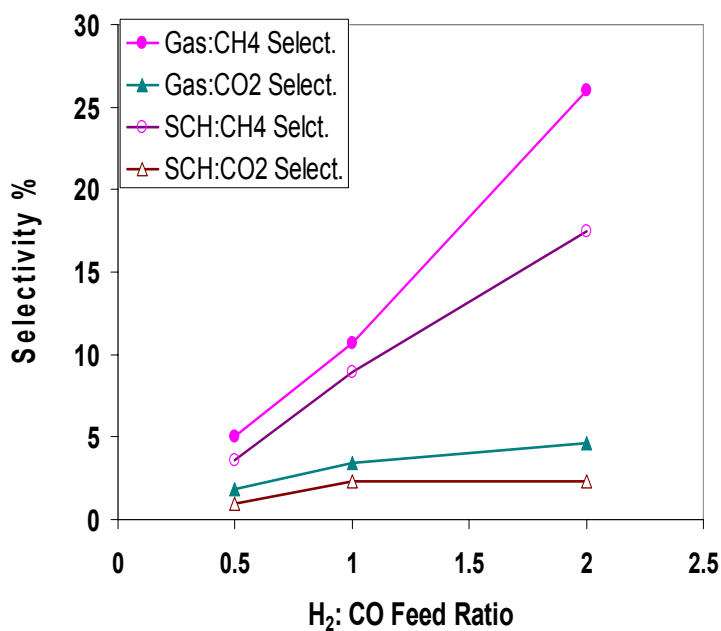
Fig. 14: Effect of H$_2$/CO feed composition on CH$_4$ and CO$_2$ selectivity of a 15% Co/Al$_2$O$_3$ catalyst in gas phase reaction and in SCH environment towards CH$_4$ and CO$_2$ at reaction temperature of 240 °C and SV of 187.5 hr^{-1}.
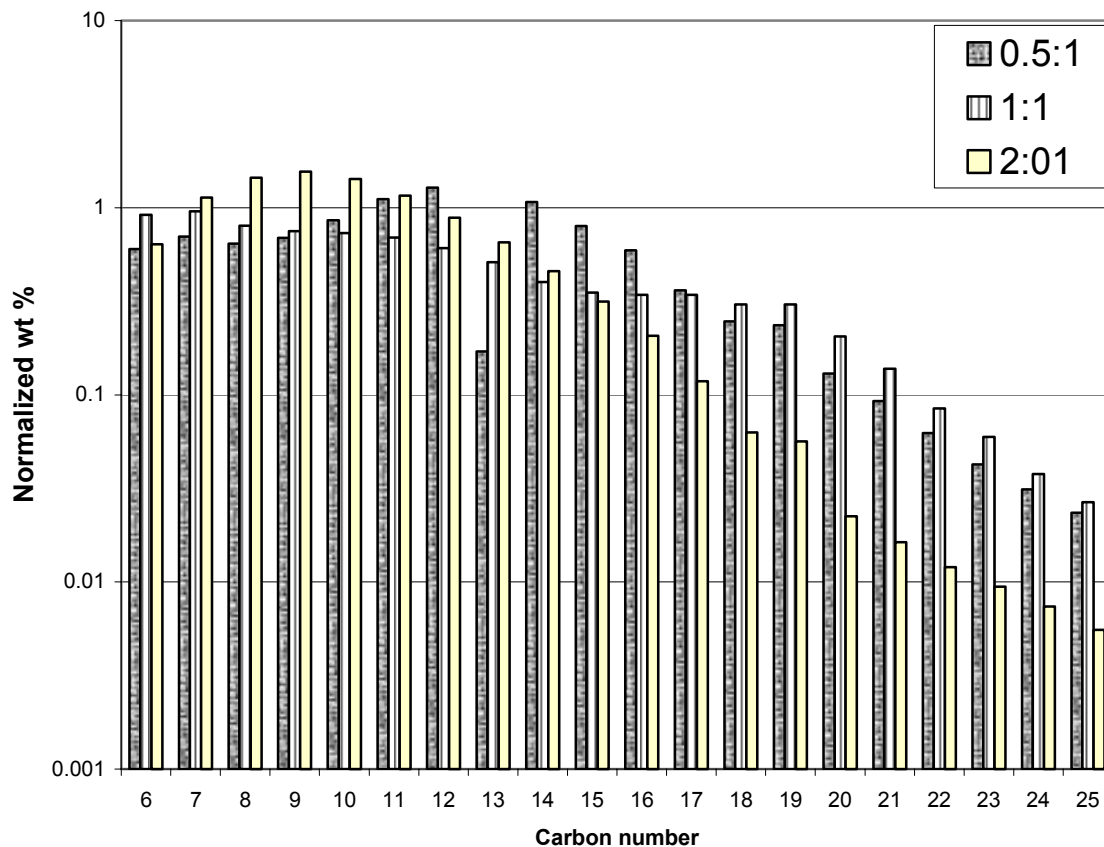
Fig. 15: Product distribution of hydrocarbons in SCP medium at 220 °C and 45 bar at different H_2/Co ratios.

Fischer-Tropsch synthesis using Co supported on silica xerogels and aerogels

Edward M. Eyring, Ronald J. Pugmire and Richard D. Ernst
Department of Chemistry, University of Utah

Introduction

C-1 Chemistry research at the University of Utah for the year beginning October 1, 2002 is reported here. The focus of this research has been the preparation and testing of novel silica supported cobalt catalysts for the Fischer-Tropsch synthesis of diesel range liquids from syngas (carbon monoxide and hydrogen). Researchers at Utah from the laboratories of Professors Richard D. Ernst, Edward M. Eyring, Henk L.C. Meuzelaar, and Ronald J. Pugmire have participated in the work described in this report. Additional research carried out in the Ernst and Pugmire laboratories is described in separate annual reports.

The preparation of silica glass by the mixing of liquid chemicals to form a sol that gradually gels was discovered over one hundred years ago.[1] Synthesis of silica xerogels and aerogels begins with the same chemicals and the same early stages of sol to gel conversion. Air drying the gel over a period of days to weeks produces a dense, porous "xerogel" glass with approximately one eighth the volume of the original sol because of surface tension effects at the internal air/gel interface. If an identical gel is dried with supercritical CO_2 or supercritical ethanol, surface tension effects are circumvented and a much more porous glass called "aerogel" results that has approximately the same volume as the original sol.

The Fischer-Tropsch (FT) synthesis of hydrocarbons by reaction of CO and H_2 ("syngas") over a heterogeneous catalyst is also an old technology.[2] Supported iron and cobalt are the usual FT catalyst choices. In the case of cobalt, low temperature (below 250 °C) FT synthesis is aimed at high wax production whereas high temperature (340 °C) FT produces alkenes, gasolines, and methane.[3] There is evidence[4] that one obtains a greater number of active sites as cobalt oxide is reduced to cobalt metal when cobalt is supported by Al_2O_3 with TiO_2, SiO_2, and ZrO_2 being steadily less effective supports in that order. One way of producing a high surface area support for a cobalt FT catalyst is to combine a cobalt salt with a silicium precursor such as tetraethoxysilane (TEOS).[5] The resulting liquid sol is dried to a gel that can be calcined and reduced. The "xerogel" thus produced contains dispersed nanoparticles of cobalt trapped in a silica glass of high porosity.

From the literature it is unclear whether or not a high porosity SiO_2 support will be favorable for diesel fuel production. It has been speculated[6] that less porosity and consequent longer reactant residence times may facilitate more hydrogenolysis and a yield of lighter hydrocarbons.

Several papers have been published by other laboratories describing preparation and use of silica xerogel supported cobalt catalysts for Fischer-Tropsch synthesis.[7-12] These studies in other laboratories have not explored the possibility of improving product yields by systematically varying the porosity of xerogel supports. This opportunity draws attention to the importance of obtaining reliable diesel range F-T yields from closed mass balance data that are unobtainable

with only a GC/MS apparatus. The problem is that a GC/MS apparatus does not quantitate the light gases (H_2, CO, CH_4) in the product stream.

Summarizing, our research objective for the year beginning October 1, 2002 was the determination of the impact of porosity of the silica support on the distribution of products in a Fischer-Tropsch reaction catalyzed by cobalt. The question of interest is the following: Can the porosity of a silica xerogel or aerogel supported cobalt catalyst be tuned to produce a more desirable range of Fischer-Tropsch hydrocarbons?

Experimental Procedure

Cobalt catalysts supported on xerogel silica were prepared by mixing tetramethoxysilane (Aldrich, 98%), methanol (Aldrich, spectrophotometric grade), water (Aldrich, HPLC grade), and $Co(NO_3)_2 \cdot 6H_2O$ in the mole ratio of 1:4:16:x where x is 0.05, 0.10, 0.15, or 0.20. The amount of liquid water added to the mixture was varied so that the total amount of water (liquid + water of hydration) remained constant. The corresponding percent by weight of the catalysts are 19.7%, 14.8%, 9.83%, and 4.91% for the 0.20, 0.15, 0.10, and 0.05 cobalt mole fraction catalysts. The sol was transferred into cylindrical glass forms, sealed with Parafilm,[TM] and gelled in approximately 30 minutes. The gels were aged in the sealed forms for two weeks, then unsealed and allowed to dry under ambient conditions for an additional two weeks. The volume of the resulting xerogel was approximately 1/8th the volume of the original wet gel. The xerogel was heated to 500 °C in static air to convert the $Co(NO_3)_2$ to Co_3O_4, then reduced in flowing hydrogen at 500 °C. The color of the xerogel changed from deep red characteristic of $Co(NO_3)_2 \cdot 6H_2O$ to black attributed to metallic cobalt. The presence of metallic cobalt was confirmed by observing the ferromagnetic character of the resulting xerogel using a hand held magnet.

The reduced xerogels were tested for catalytic activity towards Fischer-Tropsch synthesis with a pressurized gas-phase bench-top reactor. A stainless steel tube, 4-mm i.d. and 152-mm long, served as the pressurized reactor and was heated by means of a heating rope (Omega, 250 W) tightly wrapped around the tube to enhance thermal homogeneity. The reactant gases, H_2 and CO, and carrier gas, He, were delivered to the heated reactor with mass flow controllers (MKS Scientific) and mixed before entering the reaction zone. The CO stream was passed through an 8-mm i.d. by 1-m long copper tube packed with PbO/Al_2O_3 (Engelhard, provided by Irving Wender) to remove $Fe(CO)_5$ impurities that had been noticed by Henk Meuzelaar in the mass spectra of the reaction products. The H_2 contained 1% by weight Ar to serve as an internal standard. The temperature of the reaction bed was controlled by means of a thermocouple located inside the bed for maximum accuracy. A backpressure regulator maintained pressure inside the reactor. Reactant gases and products below C_5 were analyzed with an online GC/TCD (Shimadzu) and CarboPlot column (0.53 mm i.d., 30 m long). Products >C_5 were analyzed with an online GC/MS (Hewlett-Packard) and DB-5 column (0.25 mm i.d., 1 m long). A fixed-volume sampling valve (VICI) was used for sample introduction into the GC/TCD and a valveless, zero-volume Ambient Vapor Sampler (FemtoScan) was used with the GC/MS. During reaction, samples were taken every 30 minutes with the GC/TCD and every 15 minutes with the GC/MS. The GC/MS instrumentation had been borrowed from the Meuzelaar laboratory to carry out a previous diethyl carbonate study[13] funded by CFFS. Funds from Professor Pugmire and

from the University of Utah College of Science and Department of Chemistry were combined to purchase a $5,815 Shimadzu thermal conductivity detector (TCD) that was installed on a second gas chromatograph already in the lab. With the TCD detector one can compare quantitatively the amount of CO in the output stream of the chemical reactor when the catalyst is in place and when the catalyst has been removed, keeping all other conditions constant.

Undoped aerogels are comparatively easy to produce in volumes of about 20 cm^3 per batch. Spatially uniform doping of a silica aerogel with cobalt is challenging. Since water destroys aerogels, impregnation of aerogel with cobalt from aqueous cobalt nitrate solutions is not an option. Aerogels are routinely impregnated at Utah by bathing the wet gel in ethanolic solutions of cobalt nitrate and then removing the ethanol as a supercritical fluid. Professor Ernst has found an additional way to impregnate a silica aerogel with cobalt from the gas phase. His method is described in a separate report. Results of experiments with cobalt doped silica aerogel catalyst prepared in the Eyring lab are included in the present report.

Results and Discussion

Surface area and porosity properties of the four xerogel catalysts are listed in Table 1. As the loading of cobalt increases from 4.91% Co to 19.7% Co, the surface area decreases from 485.2 m^2 / g to 229.0 m^2 / g while the average pore diameter increases from 2.21 nm to 4.52 nm. The decrease in surface area is likely caused by filling in the micropores of the xerogel support with nanoparticles of either cobalt or cobalt oxide. Previous XRD and magnetometry results[14] indicate the presence of both cobalt and cobalt oxide. Cobalt oxide is formed when the xerogel containing cobalt nitrate is heated in air prior to reduction of the catalyst with hydrogen. A mixture of metallic cobalt and cobalt oxide has been detected in all of the catalyst samples with the ratio of cobalt to cobalt oxide increasing as the loading of cobalt increases.[14] A possible interpretation of the magnetic measurements is that some particles possess a cobalt oxide core surrounded by a layer of metallic cobalt. This would suggest that the reduction of the cobalt oxide to cobalt was not completed during the hydrogen reduction at 500°C. The layer of cobalt metal may hinder the transport of H$_2$ to the remaining cobalt oxide thereby preventing total reduction.[14]

The increase in average pore diameter with increasing cobalt loading was an unexpected result. The cause of this phenomenon is likely the dynamic nature of the formation of the xerogel from the wet gel. The wet gel consists of small particles of amorphous silica held together with relatively weak surface interactions.[15] As the solvent evaporates from the pores of the wet gel, stress on the surrounding particles of silica is not homogenous. Silica particles above the meniscus of the evaporating solvent are pulled inward and the process continues until evaporation of the solvent is complete. Macroscopically, this is seen as a reduction in volume of the xerogel when compared to the volume of the wet gel. Simultaneous with the collapse of the wet gel, the concentration of dissolved cobalt nitrate is increasing as the solvent evaporates. At some point, the solubility of the cobalt nitrate is exceeded and precipitation occurs. The gel continues to collapse, but must do so around the solid particles of cobalt nitrate. Increasing the amount of cobalt nitrate leads to larger particles which the silica particles must surround as the gel continues to collapse. Reduction of the cobalt nitrate particle causes a decrease in the volume of the particle, but as the solvent completely evaporates, no further collapse occurs. This process

of gel collapse concurrent with cobalt nitrate particle growth leads to the increase in average pore diameter of the final catalytic material.

The pore structure[16] of the aerogel catalyst is very different from that of the xerogel catalysts. Because little pore collapse occurs during the preparation of the aerogel, it is predicted that the pore volume of the aerogel is at least 8-fold larger than the xerogel. This corresponds to an increase in the average pore diameter of the aerogel compared to that of the xerogel by at least a factor of 2 in all three dimensions.

Transmission electron micrographs obtained by Naresh Shah and G. P. Huffman of the 9.83% Co and 19.7% Co xerogel catalyst samples are shown in Fig. 1. The metallic cobalt particles are easily distinguished from the surrounding amorphous silica by their apparent density and diffraction patterns caused by the metallic crystal lattice. The 9.83% Co sample consists in part of reasonably uniform particles with a diameter of approximately 7 nm. However, the limited field of observation may be giving a false impression of the uniformity of particle size. The 19.7% Co sample shows cobalt particles with vastly different sizes, one spherical particle about 15 nm in diameter and one oblong particle 25 nm by 37 nm. The size of the cobalt particles from the TEM images is supported by previous XRD data.[14]

The four catalysts were tested for activity in a laboratory packed-bed reactor. The H_2 and CO were introduced in a 2:1 ratio and were mixed with an inert gas, He, to moderate the conversion and prevent excessive heat generation from the exothermic F-T reaction. The CO conversion as a function of cobalt loading is presented in Fig. 2. The catalyst with the smallest amount of cobalt showed virtually no activity and the most heavily loaded catalyst showed the most activity with a CO conversion of 13.4%. This activity is considerably lower than the 84-89% conversion[12] reported for a cobalt catalyst prepared from cobalt nitrate and supported on mesoporous silica. The incorporation of helium in the present experiments along with formation of cobalt oxide subsequent to reduction both decrease the observed F-T activity.

The selectivity towards producing liquid hydrocarbons is shown in Fig. 3. As the loading of cobalt is increased, the fraction of heavier hydrocarbons increases. The C_8-C_{10} fraction increases from 16.8% to 24.2%, the C_{11}-C_{13} fraction increases from 3.8% to 12.6% and the $C_{14}+$ fraction increases from 1.8% to 4.6%. Hydrocarbons heavier than C_{17} were not detected with the present catalysts. In going from 9.83% Co to 19.7% Co the total C_8+ fraction increased from 22.3% to 41.4%. This C_8+ fraction is similar to the 30% selectivity reported[17] for the C_{10}-C_{20} fraction. The inclusion of C_8 and C_9 in the present work accounts for the apparent difference. The shift in product distributions towards larger hydrocarbons may result from the different pore size of the catalysts. It has been speculated[12,17] that severe restriction on mass transport to the active metal catalyst particle favors larger hydrocarbons. However, it appears from the present data that as the pore size of the xerogel catalysts increases, the mass transport limitations decrease, and the product distribution shifts towards larger products.

One 2% Co catalyst supported on silica aerogel was prepared and tested. Because no pore collapse occurs during the preparation of the aerogel, the bulk density is approximately 8-fold lower than that of the xerogel catalysts. The reactor was capable of holding 0.15 g of aerogel catalyst compared with 0.86 g of xerogel catalyst due to the difference in bulk densities. This

reactor loading difference along with the small amount of cobalt loaded onto the aerogel support (2%) corresponds to only about 3 mg of cobalt in the catalyst bed. The aerogel catalyst converted approximately 5% of the CO. However, the reaction conditions were different than those prevailing with the xerogel catalysts. The temperature and pressure were identical, but no He carrier gas was used with the aerogel catalyst. This change increased the partial pressures of both H_2 and CO, and decreased the space velocity. The product distribution of only the C_5+ fraction for both the xerogel and aerogel catalysts is shown in Fig. 4. The distribution has further shifted to the higher hydrocarbons, additional evidence of mass-transport limitations caused by pore structure influencing the product distribution.

An additional difference in the product distributions of the aerogel and xerogel supported catalysts was the amount of olefins produced. The majority of hydrocarbons produced with the xerogel catalysts were saturated with only a trace of olefins detected. However, with the aerogel catalyst, as much as 45% of each carbon-number product existed as the olefinic compound. Table 2 shows the fraction of olefin for the C_9 through C_{14} products. This may result from the increased mass-transport of the FT products away from the active catalyst particle. The large pores in the aerogel catalyst allow the olefins to move away from the cobalt surface quickly, so that readsorption and subsequent hydrogenation of the olefin does not occur.

The examination of connectivity of domains with xerogel and aerogel lattices using solid state NMR is documented in a separate annual report by R. J. Pugmire.

Conclusions

A series of xerogel and aerogel catalysts containing metallic cobalt has been prepared, characterized, and tested for Fischer-Tropsch activity. BET surface area measurements indicated that increases in the loading of cobalt lead to lower surface area, presumably due to the filling of micropores of the xerogel support. The average pore size of the support increased as a function of cobalt loading from 2.21 nm for the 4.91% Co catalyst to 4.52 nm for the 19.7% Co catalyst. TEM micrographs indicate the presence of uniform 7 nm diameter metallic cobalt particles in the 9.83% Co catalyst. However, TEM micrographs of the 19.7% Co catalyst indicate increased cobalt particle size heterogeneity. The lowest loading of cobalt on silica xerogel, 4.91%, showed no activity while the most heavily loaded catalyst, 19.7% Co, generated a 13.4% CO conversion. The selectivity towards diesel range hydrocarbon products increased as a function of increased cobalt loading reaching a maximum value of 41.4% for the C_8+ fraction. An aerogel supported cobalt catalyst yields a lot of olefinic product.

Future Work

CFFS funded researchers in the Eyring, Pugmire and Ernst laboratories will work on development and characterization of new solid materials that address fuel related national energy issues. The four projects listed below will be tackled first by workers in the Eyring lab with participation likely by workers in the other two labs if initial results are encouraging. (The Pugmire and Ernst groups have other new projects described under "Future Work" in their annual reports.) The following projects will in some cases be tackled simultaneously. Each project will be taken at least to a point where it is clear that an "Invention Disclosure"

transmitted to the University Technology Transfer Office will or will not be forthcoming. Preliminary experimental data obtained on the first proposed project below suggest that a published scientific paper will emerge from the first proposed project.

Proposed Project #1: Fischer-Tropsch Liquids as Hydrogen Carriers

Hydrocarbons produced via Fischer-Tropsch synthesis offer significant advantages over petroleum-based hydrocarbons when used as hydrogen carriers for fuel-cell powered vehicles. Petroleum-based hydrocarbons typically contain significant amount of impurities, such as sulfur, which must be removed before being reformed into hydrogen suitable for powering a fuel cell. Hydrocarbons synthesized using Fischer-Tropsch chemistry contain far fewer impurities and should allow their use as reformate without the need for substantial cleanup. Currently, catalysts used in the Fischer-Tropsch process yield a very wide product distribution and the products must be separated prior to use as a hydrogen carrier. We propose to investigate a new class of catalysts based on aerogel silica supported cobalt and iron which will allow strict control over the support properties. Preliminary indications are that aerogel supports of cobalt catalysts promote higher yields of Fischer-Tropsch diesel range hydrocarbons per unit weight of cobalt present. At least four aerogel supported cobalt catalyst samples with different porosities need to be reactor tested to quantify the relationship between aerogel support porosity, cobalt loading, and the narrowness of the range of hydrocarbon chain lengths being produced. Another issue to be addressed is the mechanical durability and catalyst life of the aerogel supported cobalt catalyst.

Proposed Project #2: Hydrogen Produced from Reforming Ethanol

Ethanol produced from coal-derived synthesis gas can serve as a hydrogen carrier for use in a fuel cell suitable for powering vehicles. On-board storage of hydrogen as a high-pressure gas or cryogenic liquid can be avoided by steam-reforming ethanol into hydrogen and carbon dioxide. A recent report[18] suggests that metallic cobalt catalysts on an oxide support are suitable for steam-reforming ethanol and that both the metal and the oxide are involved in the catalysis. Since the metal and oxide support are important in this reaction system, bringing the metal particle and support particle into more intimate contact may lead to more active catalysts. Traditional impregnated catalysts are composed of a small metal particle on a much larger oxide support particle and the contact between the two is limited which limits their reactivity. We propose to synthesize catalysts which have a much higher degree of contact between the metal particle and oxide support by using sol-gel techniques to create a composite material which contains metal nanoparticles and oxide particles which are similar in size. This technique has recently been employed[19] to create a very active catalyst containing gold and titania nanoparticles suitable for oxidizing carbon monoxide. A similar catalyst based on cobalt nanoparticles may prove to be very active in the steam-reforming of ethanol.

Proposed Project #3: Novel Pt/Ru Catalysts for Direct Methanol Fuel Cell

The Direct Methanol Fuel Cell provides a unique method of utilizing coal or natural gas as a power source for transportation vehicles. After the coal or natural gas is converted into methanol, the liquid fuel can be directly used in a fuel cell without the need for on-board reforming which is required in traditional H_2 / O_2 fuel cells. At present, the Direct Methanol Fuel Cell possesses

some severe limitations at the anode, namely low mass transport and high metal loadings. We propose to synthesize a new class of catalysts to increase the mass transport to the catalytically active metal site and enable higher performance with a reduced mass of precious metal. This new class of catalysts is based on Pt/Ru supported on mesoporous carbon. The mesoporous nature of the carbon support will allow increased mass transport through the catalyst layer which will provide more reactivity and this higher reactivity should allow for more efficient use of the precious metal catalyst. Mesoporous carbon can be made by decomposing a suitable carbon-containing precursor, such as acetylene, on a mesoporous silica structure. The silica is then removed by dissolving in hydrofluoric acid. This technique has been used[20] to produce carbon analogues of microporous zeolites and should be applicable to mesoporous silica aerogels. These silica aerogels are easily prepared in our laboratory and can be produced in substantial quantity.

Proposed Project #4: Palladium-Zeolite Hydrogen Permeation Membranes

One of the major obstacles to the use of hydrogen fuel cells to power automobiles is the presence of carbon monoxide gas in the hydrogen stream that poisons the heterogeneous catalyst in the fuel cell. A 0.1 mm thick palladium alloy membrane (available, for instance, from Japan Pionics Co., Ltd.) permits hydrogen diffusion but not the passage of other contaminating gases. Steven M. Kuznicki has proposed (private communication) backing an even thinner (and hence less expensive) palladium membrane with a much thicker film of a natural zeolite that also passes hydrogen more readily than other low molecular weight gases. The Eyring lab has the necessary GC and GC/MS instrumentation and can improvise a two compartment sample box to study carbon monoxide transmission through palladium, zeolite, and palladium/zeolite membranes. Eventually, one would probably need simpler detectors that can be run at every gasoline service station in the country where hydrocarbon liquids are being reformed to verify purity of resulting hydrogen coming through the supported membrane. A laser diode operating at an IR wavelength absorbed by CO might be the most reliable, cheap way to detect low level contamination of hydrogen. A possible justification for permitting the CFFS funded Utah group to collaborate with Dr. Kuznicki on the palladium/zeolite membrane evaluation project would be the resulting exposure of the Utah group to state-of-the-art fuel cell issues that could lead to further innovation within the CFFS.

References

1. Graham, T. J. Chem. Soc. **1864**, 618.
2. Fischer, F.; Tropsch, H. Brennst. Chem. **1923** 4, 276.
3. Dry, M.E. Appl. Catalysis A: General **1999**, 189, 185-190.
4. Jacobs, G.; Das, T.K.; Zhang, Y.; Li, J.; Racoillet, G.; Davis, B.H. Appl. Catalysis A: General **2002**, 233, 263-281.
5. Ernst, B.; Libs, S.; Chaumette, P.; Kiennemann, A. Appl. Catalysis A: General **1999**, 186, 145-168.
6. Lapszewicz, J.A.; Loeh, H.J.; Chipperneld, J.R. J. Chem. Soc. Chem. Commun. **1993**, 913.
7. Ernst, B.; Libs, S.; Chaumette, P.; Kiennemann, A. Appl. Cat. A **1999**, 186, 145-168.
8. Ernst, B.; Hilaire, L.; Kiennemann, A. Cat. Today **1999**, 50, 413-427.
9. Yin, D.; Li, W.; Yang, W.; Xiang, H.; Sun. Y.; Zhong, B.; Peng, S. Microporous and Mesoporous Materials, **2001**, 47, 15-24.

10. Khodakov, A.Y.; Griboval-Constant, A.; Bechara, R.; Zholobenko, V.L. J. Cat. **2002**, 206, 230-241.
11. Moradi, G.R.; Basir, M.M.; Taeb, A.; Kiennemann, A. Cat. Commun. **2003**, 4, 27-32.
12. Ohtsuka, Y.; Arai, T.; Takasaki, S.; Tsubouchi, N. Energy & Fuels **2003**, 17, 804-809.
13. Roh, N.-S.; Dunn, B.C.; Eyring, E.M.; Pugmire, R.J.; Meuzelaar, H.L.C. Fuel Processing Tech. **2003**, 83, 27-38.
14. Seehra, M.S.; Manivannan, A.; Dutta, P.; Dunn, B.C.; Cole, P.; Covington, D.J.; Eyring, E.M. Energy & Fuels, submitted for publication.
15. Celzard, A.; Mareche, J.F. J. Chem. Ed. **2002**, 79, 854-859.
16. Pietron, J.J.; Stroud, R.M.; Rolison, D.R. Nanolettters **2002**, 2, 545-549.
17. Iglesia, E. Appl. Catal. A: General **1997**, 161, 59-78.
18. Llorca, J.; Dalmon, J. A.; Piscina, P. R.; Homs, N. Appl. Cat. A, **2003**, 243, 261-269.
19. Pietron, J. J.; Stroud, R. M.; Rolison, D. R. Nano Letters, **2002**, 2, 545-549.
20. Vix-Guterl, C.; Boulard, S.; Parmentier, J.; Werckmann, J.; Patarin, J. Chemistry Letters **2002**, 10, 1062-1063.

Table 1. Surface Area and Porosity Properties of Cobalt Loaded on Silica Xerogel Catalysts

Catalyst	BET Surface Area[a] m^2 / g	BJH Pore Volume[b] cm^3 / g	Average Pore Diameter nm
5% Co	485.2	0.210	2.21
10% Co	346.3	0.281	2.91
15% Co	263.3	0.266	3.75
20% co	229.0	0.286	4.52

[a] Brunauer-Emmett-Teller determination by Micromeritics (Norcross, GA).
[b] Barrett-Joyner-Halenda method determination by micromeritics (Norcross, GA).

Table 2. Fraction of Each Carbon-Number Product Detected as an Olefinic Species with 2% Co Supported on Silica Aerogel Catalyst.

Carbon Number	% Olefin
9	21.0
10	45.9
11	42.4
12	43.3
13	37.1
14	31.4
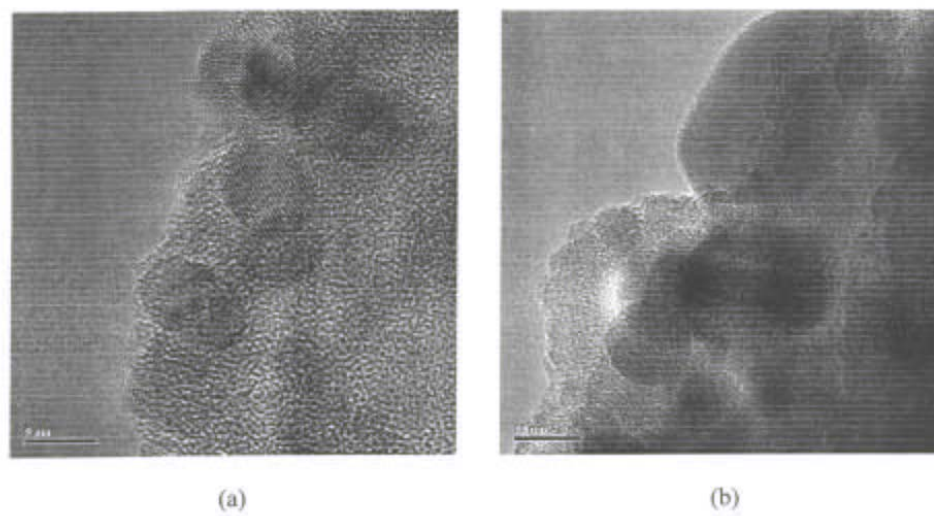
Fig. 1. TEM images of cobalt-containing xerogel catalysts after H_2 reduction.
(a) 0.10 Co at 600kx magnification. (b) 0.20 Co at 300kx magnification.
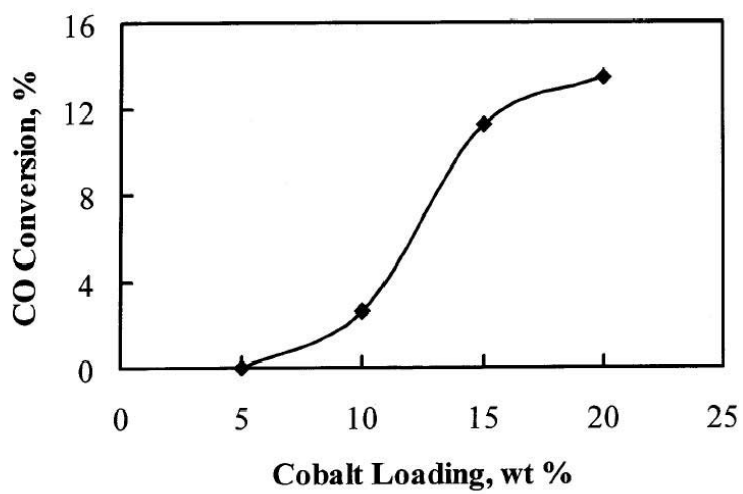
Fig. 2. Conversion of carbon monoxide into various hydrocarbons and CO_2 as a function of cobalt loading on xerogel silica. Reaction conditions: 72 sccm He, 48 sccm H_2, 24 sccm CO, 265 °C, 100 psi.
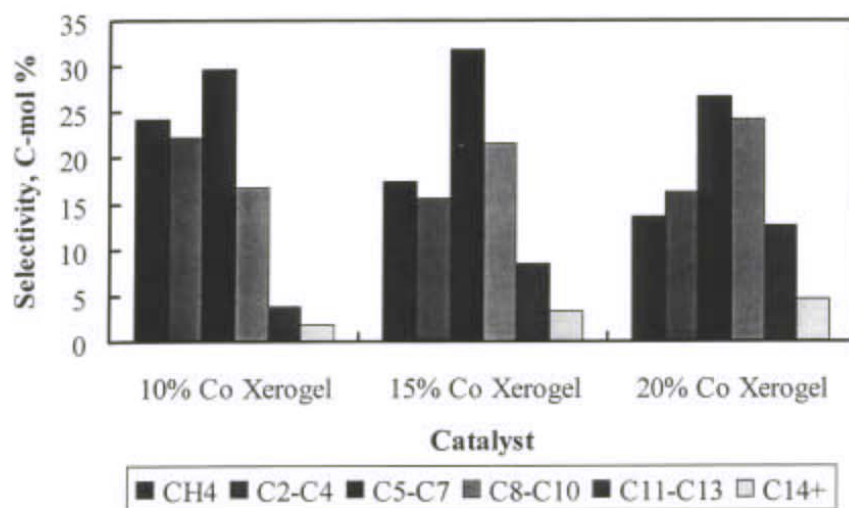
Fig. 3. Selectivity towards liquid hydrocarbon products (C_5-C_{17}) for three different loadings of cobalt on xerogel silica. Reaction conditions: 72 sccm He, 48 sccm H_2, 24 sccm CO, 265 °C, 100 psi.
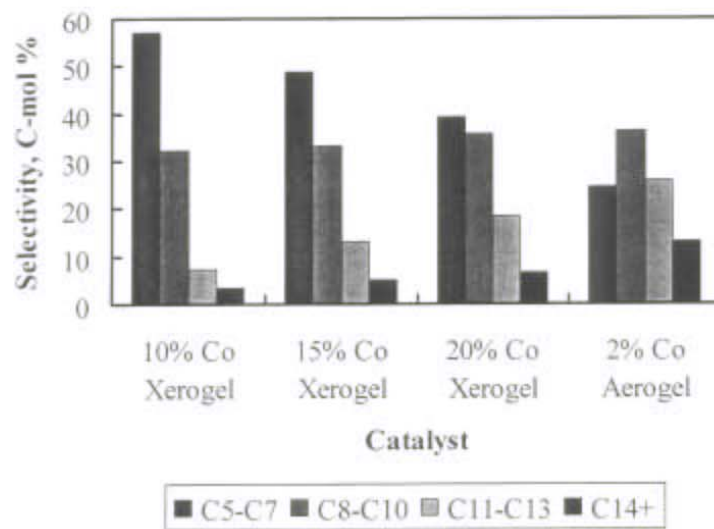
Fig. 4. Comparison of Fischer-Tropsch product selectivity using four different cobalt catalysts supported on either xerogel or aerogel silica.

Development of Single-Site Metallic Catalysts for Fischer-Tropsch Reactions

Gregory C. Turpin, Brian Dunn, Zhiru Ma, Paul Cole, Edward M. Eyring, Ronald J. Pugmire,
and Richard D. Ernst
Department of Chemistry, University of Utah

Our research efforts in the consortium began in early 2003 at a 50% level of support, and experienced some delay due to a student's call up for the Army Reserves. Nevertheless, we have already obtained results that both support our proposals and indicate a significant potential for the generation and application of supported single metal site catalysts.

INTRODUCTION

In a recent,[1] well-publicized[2] DOE-supported publication, Bell, Tilley, et al. remarked that "for many catalysts, it is apparent that desirable properties are associated with well-defined active sites containing one or only a few metal centers on the surface of a support," and they then reported their approach to generating supported single-site iron centers using the thermally unstable $Fe[OSi(OCMe_3)_3]_3(THF)$.

In a previous consulting collaboration with Phillips Petroleum Co.,[3] we demonstrated that $Cr(2,4-C_7H_{11})_2$ and $Cr(C_5H_5)(2,4-C_7H_{11})$ (C_5H_5 = cyclopentadienyl; C_7H_{11} = dimethylpentadienyl, see below) underwent protonation of a $2,4-C_7H_{11}$ ligand on contact with
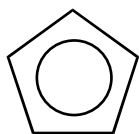
C_5H_5
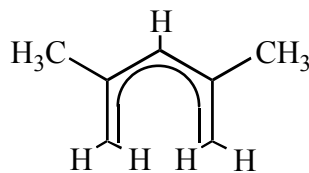
$2,4-C_7H_{11}$

aluminum phosphate supports, generating single-site chromium centers (those from the latter Cr complex being highly active ethylene polymerization catalysts). As we had succeeded also in preparing other $M(2,4-C_7H_{11})_2$ complexes (M = Ti, V, Fe, Ru, Os, Co$^+$), as well as $Zr[1,5-(Me_3Si)_2C_5H_5]_2$ and $M(2,4-C_7H_{11})_2(L)$ complexes of Zr, Hf, Nb, Mo, and W (L = CO, phosphine),[4] it appeared we had a collection of complexes suitable for the single-site depositions of a large variety of transition metals. Given that 20% of our nation's GDP is derived from catalytic processes (predominantly heterogeneous), this would likely be of some significance. It can be added that we already have developed applications of our compounds, with 3 U.S. Patents having been awarded.[5] Others have also received patents for our or related compounds, but there have been too many of these for us to follow.

Three of the above metals (Fe, Co, Ru) are well known for their high activities in Fischer-Tropsch (F-T) polymerizations.[6] In general, however, their pentadienyl complexes tend to be much more stable and less reactive than those of Cr or other early transition metals. As a result,

we did not expect Fe or Ru pentadienyl complexes to react with silica surfaces. In fact, some of these complexes can be chromatographed on silica or alumina columns. However, it seemed possible that the situation could be different with extremely porous aerogels, such as those being utilized in the Eyring group for their F-T studies.[7] As described below, this has indeed been borne out.

EXPERIMENTAL

The metallocenes,[8] open metallocenes,[9] and $Fe(C_5H_5)(2,4-C_7H_{11})$[10] were prepared by published procedures. The aerogels were kindly prepared and supplied by Dr. Brian Dunn in the Eyring group. Prior to the incorporation of metal complexes, the aerogels were heated to 200 °C and maintained at that temperature for 2 hours. They were then stored in a glovebox until needed.

Deposition into monolithic aerogels was carried out under static vacuum. The appropriate organometallic compound and the aerogel were prevented from physical contact using wire screen. For deposition into powdered samples for spectroscopic studies, a finely powdered aerogel was placed together with the appropriate compound into a Schlenk tube, which was then evacuated and rotated continuously for several hours to ensure uniform incorporation.

Solid state NMR spectroscopic studies were carried out by Dr. Zhiru Ma and Prof. Ron Pugmire. Future collaborative studies will be carried out with the other investigators named in this report.

RESULTS AND DISCUSSION

Aerogel Depositions
Our first attempt to generate single-site iron species utilized the open ferrocene, $Fe(2,4-C_7H_{11})_2$. This complex and the aerogel were placed in a Schlenk tube, which was subsequently evacuated. Under these conditions one would not observe sublimation of the compound for some time, but the aerogel immediately took on an orange coloration. This observation, and the slight color difference ($Fe(2,4-C_7H_{11})_2$ is dark red), indicated that a remarkably rapid chemical reaction was taking place, presumably as follows:

1
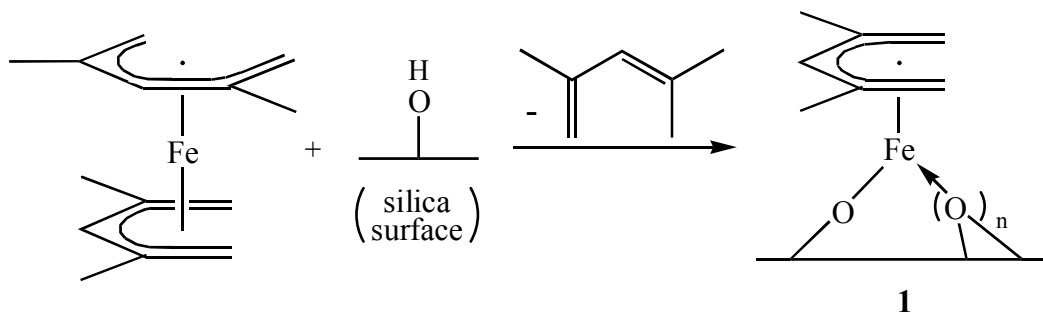
Indeed, approximately 1 equivalent of the diene was isolated, its identity being confirmed through ^{1}H NMR spectroscopy. The fact that the incorporation occurred selectively on the aerogel surface (see Fig. 1) provided further support for this proposal. Initial observations suggest we may be able to achieve 15% mass loadings of iron. In contrast, far less $Fe(acac)_3$ could be incorporated, presumably due to its greater steric bulk. This suggests that the

Bell/Tilley complex would not give high loadings either. Of additional interest is the fact that on exposure to air, these iron-laden aerogels usually smolder, leaving the material with the appearance of polished hematite (Fe_2O_3). Furthermore, samples stored under nitrogen can undergo a second color change, to more of a brown color, presumably reflecting removal of the second $2,4\text{-}C_7H_{11}$ ligand by protonation.

The possibilities of using ferrocene itself, $Fe(C_5H_5)_2$, or a half-open ferrocene, $Fe(C_5H_5)(2,4\text{-}C_7H_{11})_2$, were then considered. Due to the notorious nature of C_5H_5 as an unreactive, "stabilizing" ligand,[11] it was expected that any absorption of ferrocene would have to occur as a result of weakly favorable nonbonded interactions (giving **2**), while the single reactive $2,4\text{-}C_7H_{11}$ ligand in the half-open ferrocene should readily be protonated by the aerogel surface (giving **3**). Indeed, while ferrocene was rapidly incorporated into the aerogel, the aerogel assumed a yellow coloration similar to ferrocene; additionally, the coloration was not localized

2   **3**

on the aerogel surface, and the ferrocene could be sublimed out of the aerogel. It was observed, however, that on standing in air these aerogels slowly took on a greenish color, presumably due to the formation of the deep blue $Fe(C_5H_5)_2^+$. Notably, ferrocene can be sublimed in air on a hot plate without oxidation, revealing that its reactivity is remarkably enhanced in the aerogel. Solid state ^{13}C NMR studies by Dr. Zhiru Ma and Prof. Ron Pugmire revealed that the ferrocene molecules were behaving as though they were in the gas phase, undergoing rapid tumbling on the NMR timescale. Subsequent ESR studies with Prof. Mohindar Seehra should confirm the nature of the oxidation product as $Fe(C_5H_5)_2^+$.

Although we had an interest in trying to gain some structural and spectroscopic insight into the nature of the $Fe(2,4\text{-}C_7H_{11})_2$/aerogel product (**1**), complications exist due to the possibilities of hindered $2,4\text{-}C_7H_{11}$ rotation, its many degrees of freedom, and a second protonation step. It was therefore decided first to attempt to characterize the (**2**) $Fe(C_5H_5)(2,4\text{-}C_7H_{11})$/aerogel product (**3**), which would have the relatively unreactive, highly symmetric C_5H_5 ligand rather than $2,4\text{-}C_7H_{11}$. Indeed, the orange-red $Fe(C_5H_5)(2,4\text{-}C_7H_{11})$ was rapidly incorporated, yielding a paler, peach-colored aerogel. Despite the presence of the stabilizing C_5H_5 ligand, **3** was found to be extremely and _surprisingly_ reactive, smoldering on contact with air, which indicates that the coordination provided by the aerogel must be quite weak. In the hope of gaining some insight into the structure of this species, samples of this, and of ferrocene/aerogel to be used as a standard, were prepared as polypropylene pellets for XAFS studies with Profs. Naresh Shah and Gerald Huffman, using the Brookhaven synchrotron source. Unfortunately, the samples were sent the day before the East Coast power shortage, and must await later study. Additional structural insight for **3** should be obtainable through Mössbauer spectroscopy, which will be

carried out in collaboration with Prof. Gerald Huffman. Mössbauer studies of the open ferrocene/aerogel species (**1**) will subsequently be initiated, and should readily reveal any occurrence of a second protonation step. Based on the data we obtain, we will then evaluate the need for XAFS studies of **1**. Should the XAFS spectra of the (C_5H_5)Fe-aerogel (**3**) already be quite complicated, there would seem to be no reason for pursuing similar studies of the (2,4-C_7H_{11})Fe-aerogel (**1**). However, should the second protonation step occur, as seems almost certain, studies of the coordination environment of the resulting purely inorganic iron centers would be of value. For both **1** and **3**, solid state NMR spectroscopic studies are being undertaken with Dr. Zhiru Ma and Prof. Ron Pugmire. These should confirm the diamagnetic natures of these species, and also reveal whether the metal centers are being incorporated into essentially just one type of surface environment, or more.

While the studies of the above iron complexes will provide a fundamental picture of the nature of the iron-containing aerogel, there are good reasons to study other metals as well. Reactivity studies with iron catalysts experience complications due to the need for accompanying promoters.[6] As this would not be the case for ruthenium, which like iron forms $M(C_5H_5)_2$, $M(2,4-C_7H_{11})_2$, and $M(C_5H_5)(2,4-C_7H_{11})$ complexes, we have also initiated studies on the generation of single-ruthenium site catalysts. Indeed, like its iron analogue, the pale yellow $Ru(2,4-C_7H_{11})_2$ is rapidly incorporated into the aerogel, preferentially at the surface, yielding a pale green species. Exposure to air yields a black oxidation product. Quite clearly, then, much can be gained from spectroscopic studies of the ruthenium analogues of **1**, **2**, and **3**.

As cobalt has been the metal on which most of the F-T studies of the Eyring group have been concerned, it would be especially valuable to develop an approach to single-cobalt site centers. However, the formal $Co(2,4-C_7H_{11})_2$ complex undergoes dimerization.[12] This could later provide a convenient entry into the generation of isolated bimetallic centers, but obviously not single-site catalysts. There are possible approaches using other cobalt pentadienyl (or even allyl)[13] complexes, including $Co(C_5H_5)(2,4-C_7H_{11})^+$, but a simpler potential approach has been conceived. While ferrocene is oxidized to a cation only with difficulty, cobaltocene is a strong reducing agent, and is readily oxidized to the diamagnetic $Co(C_5H_5)_2^+$. It is quite possible that incorporation of cobaltocene into an aerogel via sublimation may spontaneously lead to its incorporation as $Co(C_5H_5)_2^+$. Even should this not occur, the unusually "rapid" (all things being relative) oxidation of ferrocene in the aerogel seems to guarantee that exposure of a $Co(C_5H_5)_2$/aerogel to air will quickly lead to oxidation, thereby preventing the cobalt from escape. Subsequent calcination should then generate the single-cobalt sites. While most of our cobalt efforts will center on its reactivity (vide infra), some cursory spectroscopic study of the cobalt-laden aerogels is called for. In particular, ESR spectroscopy can be used to detect the presence of any cobaltocene in the aerogel, while solid state NMR spectroscopy can be used to identify the cation. It would naturally be of interest to see if the cation's charge leads to slower tumbling than observed for the isoelectronic, neutral ferrocene. For purposes of comparison, ESR studies of the seemingly partially oxidized (green) ferrocene/aerogels should provide some insight into tumbling by $Fe(C_5H_5)_2^+$ (and even $Co(C_5H_5)_2$, should its incorporation not lead immediately to the cation).

Spectroscopic Studies of Single-Site Metal Oxides

Results on the previously reported single-iron site catalysts have indicated that high temperature calcination did not lead to agglomeration.[1] We therefore expect that appropriate oxidation of our

metal-containing aerogels will allow for the retention of their single site character. Of course, the temperatures achieved during the smoldering that takes place on exposure of some of our metal-containing aerogels to air could be high enough to lead to agglomeration. This possibility can probably most easily be tested by powder XD studies. Agglomeration could be useful, actually, if it turns out that single-metal site catalysts do not provide for the substantial advantages in F-T processes that one expects in many other situations. In such an event, the high and efficient loadings our method yields would at least still be a plus. Furthermore, should the smoldering process lead to agglomeration, one could either resort to other reagents (including reduction processes), or carry out the oxidation at or near calcination temperatures using dilute oxygen streams. The higher temperature would ensure that the oxygen molecules would react rapidly on contact with the metal centers, while the low oxygen concentration would extend the duration required for oxidation, thereby preventing overheating. The presence of the desired single-metal site oxides should be readily apparent by the absence of known metal oxide phases. When these situations are identified, XAFS, and in some cases ESR and/or Mössbauer, studies can provide indispensable information about the local metal environment(s).

The susceptibility of these single-metal site oxides to agglomeration can then be studied under more controlled conditions. Especially important will be their susceptibilities as a function of temperature and the presence or absence of water vapor (as opposed to liquid, which might dissolve away some of the oxides). Furthermore, the aerogel catalysts will also be studied after actual catalytic runs, to see if such conditions result in agglomeration.

Reactivity Studies
As noted above, it seems certain that we will be able to generate aerogels with single-cobalt sites using cobaltocene. The behavior of this material as a potential F-T catalyst will first be investigated under normal conditions by Dr. Brian Dunn and Prof. Ted Eyring. Also of interest will be results obtained from samples for which agglomeration has been achieved. Comparisons of these data with those already gathered by the Eyring group will begin to give us the important indications we need concerning the potential advantages of our approach to F-T catalysis. Additionally, as aerogel structures can undergo substantial alteration under non-supercritical conditions, the behaviors of these same catalysts under supercritical F-T conditions will be studied in collaboration with Prof. Chris Roberts' group.

Studies along the lines above will also be carried out for our ruthenium containing aerogels. The coordination and organometallic chemistries of cobalt differ so much from those of ruthenium that one could not assume trends observed for one of these metals would also be followed by the other. However, at present we do not plan to examine the iron species, although that could change depending on our results with cobalt and ruthenium.

SUMMARY

The main goals of our work may be listed as follows:
1. To develop approaches to the incorporation of single-site metal centers into aerogels (or other supports).
    ➢ It is already clear that we have succeeded for Fe and Ru, and Co seems almost a certainty.

2. To characterize the natures of the initially incorporated metal species, and to confirm the occurrence of a second protonation step for open-metallocene-derived species.
   - ➤ Collaborative efforts with other consortium groups are already planned or underway in the areas of ESR, Mössbauer, solid state NMR, and XAFS spectroscopies as well as powder XD measurements.
3. To convert the initial metal-supported species into single-site and agglomerated oxides.
   - ➤ The natures of both types of oxides will be studied by some of the same methods as above, while the conditions required for agglomeration will be determined.
4. To determine the behaviors of both single site and agglomerated metal-laden aerogel catalysts in the F-T process, initially focussing on Co.
   - ➤ Collaborative efforts under both traditional and supercritical conditions will be initiated once the appropriate aerogels have been obtained.

Other Consortium Projects

The use of $Fe(2,4-C_7H_{11})_2$ and $Fe(C_5H_5)(2,4-C_7H_{11})$ complexes as soot suppressors will be studied shortly in collaboration with Prof. Adel Sarofim at the University of Utah. As ferrocene itself is already used for such purposes in home heating oils in Canada and Europe,[14] it seems worth investigating our even more reactive (and soluble) open and half-open ferrocene complexes for such purposes.

REFERENCES

1. [1]C. Nozaki, C.G. Lugmair, A.T. Bell, and T.D. Tilley *J. Am. Chem. Soc.* **2002**, 124, 13194.
2. A.T. Bell *Science* **2003**, 299, 1690.
3. J.W. Freeman, D.R. Wilson, R.D. Ernst, P.D. Smith, D.D. Klendworth, and M.P. McDaniel *J. Polym. Sci.* **1987**, 25A, 2063.
4. R.D. Ernst *Chem. Rev.* **1988**, 88, 1255.
5. R.D. Ernst *Comments Inorg. Chem.* **1999**, 21, 285.
6. "Chemical Vapor Deposition Process Employing Metal Pentadienyl Complexes," J.T. Spencer and R.D. Ernst, U.S. Patent 5,352,488 (1994).
7. "Metal Complexes Containing Bridged Non-Aromatic Anionic Dienyl Groups and Addition Polymerization Catalysts Derived Therefrom," D.R. Wilson, P.N. Nickias, D.R. Neithamer, and R.D. Ernst, U.S. Patent 5,817,849 (1998) and U.S. Patent 6,034,021 (2000).
8. M.E. Dry *Appl. Catal. A: General*, **1996**, 138, 319.
9. H. Schulz *Appl. Catal. A: General*, **1999**, 186, 3.
10. B.H. Davis *Fuel Proc. Tech.* **2001**, 71, 157.
11. N. Hüsing and U. Schubert *Angew. Chem. Int. Ed.* **1998**, 37, 22.
12. "Organometallic Synthesis," Vol 1, p. 64, R.B. King, Ed., Academic Press (1965).
13. D.R. Wilson, L. Stahl, and R.D. Ernst *Organomet. Synth.* **1986**, 3, 136.
14. Ch. Elschenbroich, E. Bilger, R.D. Ernst, D.R. Wilson, and M.S. Kralik *Organometallics* **1985**, 4, 2068.
15. See, for example, the 50 year Anniversary of Ferrocene Special Commemorative issue of *J. Organometal. Chem.* **2001**, 637-639.
16. D.R. Wilson, R.D. Ernst, and M.S. Kralik *Organometallics* **1984**, 3, 1442.

17. For a promising approach to thermally stable (allyl)cobalt complexes, see J.D. Smith, T.P. Hanusa, and V.G. Young, Jr. *J. Am. Chem. Soc.* **2001**, <u>123</u>, 6455.

18. J. Raloff *Science News* **1993**, <u>144</u>, Oct. 2, p. 220.

Figure 1: Aerogel Loading Via an Open Ferrocene.
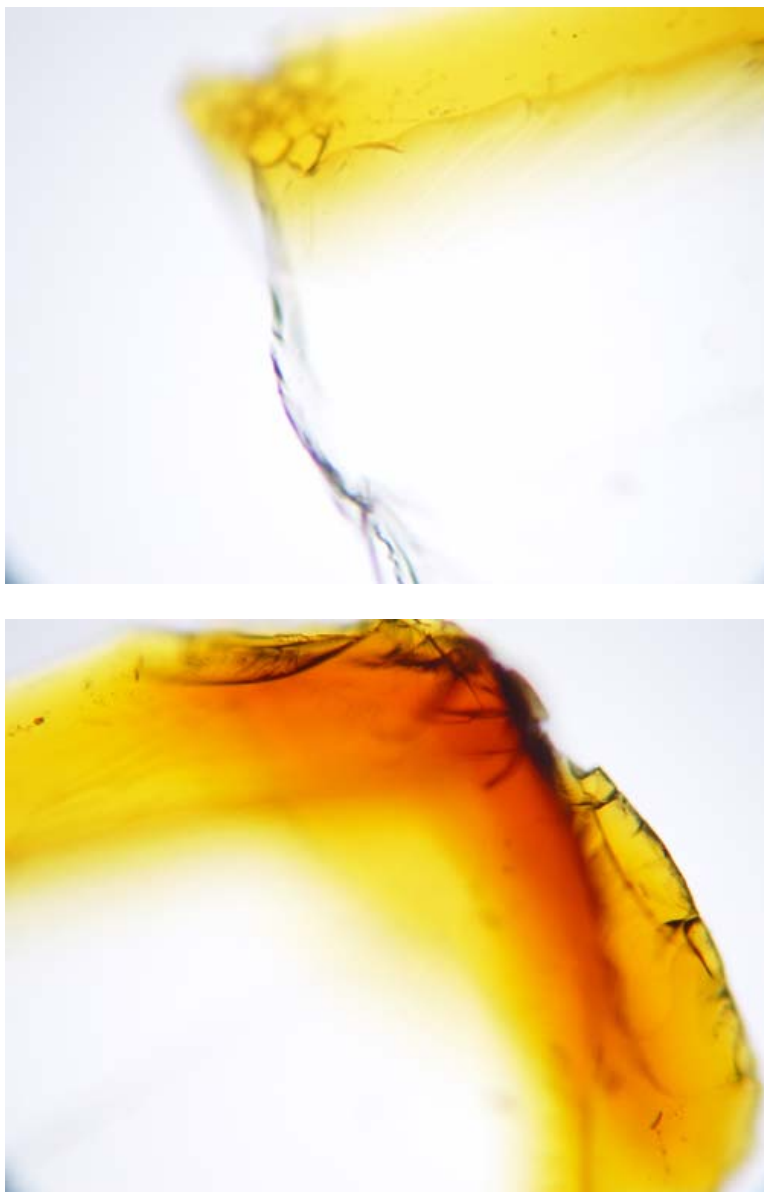
Development of Microporous Shape-Selective Catalysts for Ethylene, Propylene and other Value-Added Products via C-1 Chemistry

A. Prakash, X. Huang, D. Dubois, D. Obrzut, T. Jyothi, J. Liu, and J. Guin
Auburn University

Introduction

There is considerable interest in producing value-added products from coal and other secure U. S. energy resources. Examples of such products are ethylene and propylene, as well as higher olefins and other hydrocarbons. The first two products are particularly interesting since light olefins can be easily converted to premium clean liquid transportation fuels as well as a vast array of other value-added products including fuel additives, lubricants, and chemicals which are currently available only via a petroleum route. MTO process is one of the effective routes for the production of these value-added products such as light olefins (C2=, C3=). The typical characteristic of this process requires a shape selective catalyst for the high products yields and process activity. SAPO type catalysts, small pore silicoaluminophosphate molecular sieves, based on their specific physiochemical properties, have been demonstrated to be effective catalysts for the MTO process. In the previous two years, we have been focusing on the development of novel SAPO series catalysts and their physiochemical properties modification for a valuable light olefins production process [1-5]. Our goal is to develop a series of novel SAPO catalysts for the selective production of value-added products from methanol or syngas.

This year, silicoaluminophosphate molecular sieves SAPO-17, SAPO-18, SAPO-34, SAPO-44, SAPO-47 and SAPO-56 have been synthesized hydrothermally using various organic molecules as templates. Certain of these were modified with transition metals. These materials were characterized by X-ray powder diffraction and scanning electron microscopy to assess their crystallinity and phase purity. The materials were then studied for their activity and selectivity in the conversion of methanol to olefins. Methanol conversion was generally 100 percent on all the catalysts; however, their activity and lifetime varies significantly. Among the various structure types SAPO-34 and SAPO-18 showed the highest activities as well as lifetimes.

The SAPO-56 samples prepared with varying silicon contents showed highly uniform crystals but with different morphologies. For SAPO-56 samples prepared with varying silicon concentrations, the lifetimes tend to decrease with increased silicon content; although, no significant effect on product selectivities with silicon content was observed. Both SAPO-56 and NiSAPO-56 showed longest lifetimes and highest C_2-C_4 olefins selectivities at 350 °C compared to other temperatures. Impregnation of SAPO-34 with metal ions such as K, Cs, Pt, Ag and Ce was found to reduce the amount of methane significantly at higher temperatures thereby increasing the lower olefins selectivity.

Experimental

Synthesis
The SAPO and NiSAPO molecular sieves were synthesized by hydrothermal crystallization under autogeneous pressure using various organic templates. Syntheses were carried out in 120

cm^3 stainless steel reactor lined with Teflon material. Table 1 lists the molar composition of the reaction gel and the crystallization conditions for various SAPO molecular sieves. Similarly Table 2 lists the molar compositions and crystallization conditions for NiSAPO molecular sieves.

 SAPO-17 and NiSAPO-17.
In a typical synthesis, 27.79 g aluminum isopropoxide and 45 g water mixture were stirred for 30 minutes. Then 15.38 g phosphoric acid and 20 g of water were added, the resulting mixture was stirred 2 hours before adding 0.8 g of fumed silica and 4.7 g of water. The mixture was then stirred for 1 hour before adding 6.68 g cyclohexylamine. The final mixture was stirred for 2 hours to make the gel homogeneous. Then about 200 mg of AlPOP$_4$-17 seed crystals were added to this gel and stirred for another 30 minutes followed by being loaded into autoclave for 42 hours at 200 °C. The product appears as a fine powder and was separated from the mother liquor by centrifugation. It was then washed and dried at 70 °C overnight. Synthesis procedure of NiSAPO-17 is same as that of SAPO-17 except nickel acetate was first mixed with phosphoric acid, the solution was added to the alumina slurry.

 SAPO-18 and NiSAPO-18.
In a typical synthesis 9.71 g pseudoboehmite and 20 g water mixture was stirred for 2.5 hours followed by adding 4.15 g phosphoric acid and 10 g water, After 2.5 hours stirring of the mixture, 1.20 g fumed silica, 15 g water and 13.93 g N,N-Diisopropylethylamine were added. The final mixture was then stirred for another 2 hours. This gel mixture was heated in autoclave at 165 °C for 184 hours. After crystallization the product appears as a very fine powder and was separated from the mother liquor. It was then washed and dried at 70 °C overnight. Synthesis of NiSAPO-18 is same as above method except that nickel acetate was first mixed with phosphoric acid; the resulting solution was added to the alumina slurry.

 SAPO-34 and NiSAPO-34.
Samples of SAPO-34 have been prepared using two different organic structure-directing agents: Morpholine and Tetraethylammonium hydroxide (TEA-OH). The objective was to obtain SAPO-34 samples with different crystal sizes. The morpholine has been reported to template SAPO-34 with large crystal size, whereas TEA-OH tends to form very small crystals of SAPO-34. Following are the two procedures described separately.

SAPO-34 (Morpholine):
A 9.71 g pseudoboehmite, 20 ml water, mixture was stirred for 2 hours. Then 15.35 g phosphoric acid, 10 ml water were added and was stirred for 2 hours. In separate beaker 2.41 g silica, 11.73 g morpholine and 15 ml water was mixed well and added slowly to the above mixture. The mixture became very thick during an early stage and became dilute upon further addition. After adding 11.86 ml water, the final mixture was kept stirring for 24 hours for aging. It was then transferred to a 110 ml teflon-lined ss reactor. About 75 % of the reactor was filled with the gel. The reactor was directly kept in a convection oven at 200 °C for 49 hour. After crystallization, the solid product was separated from the mother liquor, washed several times and dried at 70 °C overnight. The synthesis procedure of NiSAPO-34 is same as that for SAPO-34 except that except that nickel acetate was first mixed with phosphoric acid, the resulting solution was added to alumina slurry.

SAPO-34 (TEA-OH):
56.06 g of TEA-OH was added slowly while stirring to 27.23 g aluminum isopropoxide in a beaker. The slurry was stirred for 2 hours. Then 1.20 g fumed silica was added slowly to this slurry and stirred for 30 minutes. 15.37 g phosphoric acid diluted in 15 g water was added followed by 7 g of water. The final mixture was stirred for 2 hours before transferring to a 130 ml autoclave. The autoclave was kept at 200 °C for 48 hours. After crystallization the product was separated from the mother liquor and washed and dried at 70 °C overnight.

 SAPO-44 and NiSAPO-44.
In a typical synthesis 15.36 g phosphoric acid was diluted with 25 g water. Then 9.71 g pseudoboehmite was added slowly to this solution over 3 hours. After adding 5 g water the mixture was stirred for 3 hours. A second mixture was prepared by mixing 2.41 g fumed silica and 12.67 g cyclohexylamine and 20 g water. This second mixture was added slowly to the first mixture under vigorous stirring. The final mixture was stirred for another 4 hours to achieve greater homogeneity. After crystallization the product was separated from the mother liquor and washed and dried at 70 °C overnight. Synthesis of NiSAPO-44 was achieved by the same procedure except that nickel acetate was first mixed with phosphoric acid.

 SAPO-47 and NiSAPO-47.
In a typical synthesis 15.38 g phosphoric acid was diluted in 30 g water. Then 9.71 g pseudoboehmite was added slowly to this solution over a 2 hours. After adding 10 g of water, the mixture was stirred for another 2 hours. Then 8.01 g colloidal silica was added slowly to this mixture followed by 10 g water. The mixture stirred for 1 hour before adding 12.11 g methylbutylamine followed by 11.48 g water. The final mixture was stirred for 2 hours to make it highly homogeneous. The gel was transferred to autoclave and heated at 200 °C for 110 hours. After crystallization, the product was separated from the mother liquor and washed, then dried at 70 °C overnight. Synthesis of NiSAPO-47 was achieved by following the same procedure except that nickel acetate was first mixed with phosphoric acid.

 SAPO-56 and NiSAPO-56.
SAPO-56 samples with varying silicon content were prepared using N,N,N',N'-tetramethyl hexane 1,6-diamine as the organic template. In preparation of the synthesis gel, the order and methodology of mixing is important as well as the composition. In a typical synthesis, 15.37 g of phosphoric acid was diluted with 30 g H_2O. To this solution 9.71 g pseudoboehmite was added in small increments over a period of 1 hour. After adding 12.78 g H2O the mixture was stirred for 2 hours. To this mixture respective amounts of silica (1.20, 2.40 and 3.60 g) were added in small quantities and stirred for about 1 h. Then 11.60 g N,N,N',N'-tetramethyl hexane 1,6-diamine was added to this mixture. The final mixture was stirred for another 3 hours before placing into 120 ml autoclaves. The autoclave was kept at 200 °C for 108, 111 and 137 hours, respectively, for the three SAPO-56 samples. After crystallization, the product was separated from the mother liquor, washed and dried at 70 °C overnight. The three SAPO-56 samples were designated as SAPO-56(0.3), SAPO-56(0.6) and SAPO-56(0.9) after the silica content in the corresponding gel.

All the SAPO materials in their as-synthesized form contain organic templates occluded in the channels and cages. The organic templates were removed by slowly heating to 550°C in air and

kept at this temperature for 12 h. This calcination process effectively converts the SAPO materials into their corresponding H-SAPO form. Synthesis of NiSAPO-56 was achieved by the same procedure except that nickel acetate was first mixed with phosphoric acid and to the solution pseudoboehmite was added.

Characterization

All the samples were characterized by room temperature x-ray diffraction (XRD) using a Rigaku diffractometer with CuK$_\alpha$ radiation. The morphology and particle size of the samples were studied by scanning electron microscopy on a Zeiss DSM940 microscope. Samples were coated with gold before SEM observations.

Reactions Procedure

The reaction system is fixed bed. Temperature was monitored by a thermocouple inserted into a thermowell in the catalyst bed. 0.5g catalyst was employed in each reaction. Methanol flow rate was varied between 0.005 – 0.015 mL/min with makeup nitrogen added to maintain the total gas flow at 60 ml/minute. These conditions result in methanol feed partial pressures of *ca*. 5 - 15 kPa, respectively. Gas samples were collected and analyzed via chromatography with Gas-Pro and Plot-Q capillary columns for hydrocarbons and oxygenates, respectively, with FID detection. Product compositions were calculated based on standard gas mixtures (Scotty, Aldrich).

Results and Discussion

X-ray powder diffraction.

All the as-synthesized SAPO and NiSAPO samples were pure phase as evidenced from their corresponding XRD patterns. As one typical example of these samples XRD patterns, Figures 1 shows powder patterns for SAPO-17 and SAPO-34. These patterns in terms of line positions match well with the pattern reported for the corresponding structure types. High crystallinity is evidenced from these patterns. No additional lines due to any possible second phases were observed in any of the SAPO samples. The X-ray diffraction patterns for NiSAPO samples are very similar to the corresponding SAPO molecular sieves.

Scanning electron microscopy.

Scanning electron microscopic analysis of the various products provided the crystallinity, phase purity and morphology of the SAPO and NiSAPO molecular sieves. Figure 2 shows the typical SEM micrographs of SAPO-34, and SAPO-56. SAPO-34 synthesized with both morpholine and TEA-OH has well defined cubic morphology. The major difference between these two routes is the particle size. With morpholine, large crystals with particle size around 20 μm were observed. On the other hand, SAPO-34 with TEA-OH crystallized in highly uniform cubic crystallites of sizes in the range 1-2 μm. The narrow size distribution for particles is evident from the SEM micrographs in both cases.

SAPO-56 crystallizes in either hexagonal plates or circular disk–like morphologies depending on the amount of silicon in the gel. The observed effect of silica concentration on crystal morphology and crystal size is very prominent. At low silica concentrations crystals are well defined, highly uniform, hexagonal plates having size in the range 50-60 μm. As the silica concentration increases, the morphology gradually evolves from hexagonal to more circular disk-

like. At higher silica concentration as in the case of SAPO-56(0.9), the crystallites are more of a "doughnut" shape with sizes in the range 110-125 μm. Whereas the hexagonal and disk-like morphologies have been reported earlier for SAPO-56 [6,7], the "doughnut" morphology observed here is new.

Methanol Conversion on SAPO Molecular Sieves.
Various SAPO catalysts were tested for their performance in MTO reaction under same reaction conditions. The temperature was 400 °C and methanol flow rate was 0.005 ml/min. These conditions were selected based on our earlier study on SAPO-34 that showed the highest olefins selectivity under these conditions.

Figure 3 shows the product distribution on SAPO-18 catalyst. The catalyst was active for a long time on TOS. Methanol conversion was 100% for up to about 20 hours. During the initial 20 hours, amount of C_2-C_4 olefins was nearly 90 percent. The activity dropped dramatically after 28 hours. The maximum C_2-C_4 olefin was 92 percent observed at 5 hours. The maximum ethylene selectivity was about 45 percent at 20 hours. Methane formation was very low (2-3 mol %) initially and reaches a maximum of 10 mol %.

Figure 4 shows the product distribution on SAPO-44 catalyst. Methanol conversion was 100% for up to about 4 hours. During the initial 4 hours the amount of C_2-C_4 olefins in the product was around 85 percent. The activity dropped significantly after 4 hours. The maximum C_2-C_4 olefins were 86 percent observed at 3.5 hours. The maximum ethylene selectivity was about 46 percent at 3.5 hours. Methane formation was very low (3 mol %) throughout the lifetime of the catalyst.

Figure 5 shows the product distribution on SAPO-47 catalyst. Methanol conversion was 100% only up to 4 hours. During the initial 4 hours, the amount of C_2-C_4 olefins in the product reached a maximum of 88 percent and then decreased rapidly. The maximum ethylene selectivity was about 49 percent at 4 hours. Methane formation was initially about 4 mol % and then decreased to less than 1 mol % in 10 hours.

Figure 6 shows the product distribution on SAPO-34 (TEA-OH) catalyst. The catalyst was active for moderately long time(30 hours). Methanol conversion was 100% only up to about 3 hours. The amount of C_2-C_4 olefins in the product reached a maximum of 88 percent and then decreased continuously after that. The maximum ethylene selectivity was about 47 percent at 3 hours. Methane formation was very low.

Figure 7 shows the product distribution on SAPO-34 (Morpholine) catalyst. Of the various SAPO materials tested this SAPO-34 turned out to be longest lifetime catalyst. Methanol conversion was 100% for up to about 26 hours on TOS. Thereafter both methanol and DME increase continuously. During the initial 26 hours on TOS the amount of C_2-C_4 olefins in the product was always above 90 percent. The activity dropped dramatically after 26 hours on TOS. The maximum C_2-C_4 olefins was 94 percent observed at 4.5 hours on TOS. The maximum ethylene selectivity was about 58 percent at 20 hours on TOS. Initially methane formation was very low (2-3 mol %) and increased slowly to a maximum of 13 mol % in 45 hours.

Figures 8 to 10 show the product distribution on various SAPO-56 samples with varying silicon content. The SAPO-56 catalysts remain active for relatively short time. For SAPO-56(0.3)

76

(Figure 8) the activity decreased substantially after about 4 hours. Methanol conversion was 100 percent only up to about 4 hours . The amount of C_2-C_4 olefins was highest (70 mol %) at 1 hour . The lower olefins amount decreased to 56 mol % at 5 hours. The maximum ethylene selectivity was about 37 mol % at 2 hours. This catalyst shows very high amounts of methane production.

The activity of SAPO-56(0.6) (Figure 9) was slightly longer than SAPO-56(0.3). A substantial decrease in activity was observed after about 9 hours. Methanol conversion was 100 percent only up to about 7 hours. The amount of C_2-C_4 olefins in the product was highest (63 mol %) at 1 hour. The maximum ethylene selectivity was about 37 mol % at 1 hour. Just as in the case of SAPO-56(0.3), this catalyst also shows very high amount of methane.

For SAPO-56(0.9)(Figure 10), the activity was lower compared to both SAPO-56(0.3) and SAPO-56(0.6). A substantial decrease in activity was observed after about 2 hours . The amount of C_2-C_4 olefins was highest (59 mol %) at 2 hour. The maximum ethylene selectivity was about 34 mol % at 2 hours. Just as the other SAPO-56 catalyst, this catalyst also shows a very high amount of methane.

Figure 11 demonstrates the temperature effects on the product distribution on SAPO-34 catalyst. The production of propylene is higher than the ethylene production at 300 °C and 350 °C. The ethylene to propylene ratio increases through the five temperatures from 300 °C to 500 °C in the following manner: 0.855, 0.903, 1.310, 2.789, and 6.418. This exponential increase shows the dependency of the ethylene to propylene ratio on temperature. By increasing temperature, the ethylene production can be increased. The disadvantage of higher temperature is the methane production. Methane production is 9.6% at 300 °C. Between 350 °C and 400 °C the methane production stays around 3%. It then increases to 9.0% at 450 °C. Then in a very dramatic jump methane production increases to 60.3% at 500°C. This is a definite drawback to increasing the temperature. A catalyst which can minimize this methane production could allow for a high ethylene production with minimal unwanted products.

Figure 12 shows the effects of different metals impregnated into SAPO-34 on the products selectivity. From this Figure, it is observed that the addition of Ce helps the reduction of methane formation, and olefins selectivity is significantly increased. Also, this figure shows that there is a large effect from impregnating the selected metals.

 Figure 13 shows the product distribution on NiSAPO-44 catalyst. The catalyst was active for about 6 hours. Methanol conversion was 100 for up to about 3 hours. During the initial 3 hours, the amount of C_2-C_4 olefins was around 84 percent. The maximum C_2-C_4 olefins was 84 percent observed at 1 hour. The maximum ethylene selectivity was about 52 percent at 3 hours.

Figure 14 shows the product distribution on NiSAPO-56 catalyst. The catalyst was active for about 6 hours. The maximum C_2-C_4 olefins was about 70 mol % observed after 5 hours. The lower olefins then decreased to a value of 7 mol % at 12 hours. The maximum ethylene selectivity was about 40 mol % observed at 5 hours. Methane amount reached a maximum of about 12 mol % in 5 hours and thereafter decreased substantially.

In general, the performance of NiSAPO catalysts matches fairly closely with the corresponding unmodified SAPO catalyst. Between SAPO and NiSAPO catalysts, ethylene selectivity was slightly higher on the later. However this increase in ethylene selectivity does not necessarily improve the overall lower olefins selectivity. This is because methane formation was higher on NiSAPO catalysts.

<u>Fischer-Tropsch Synthesis on SAPO34.</u>
Figure 15 shows the hydrocarbon distribution of the Fischer-Tropsch synthesis process on cobalt SAPO-34 at 100psi, from which we can see methane production is significant. This trend follows the typical FTS reaction behavior. Because of the small pore size of this SAPO catalyst, few heavy compounds are produced, which is in line with our expectation for this kind of catalyst. Among the hydrocarbons produced from the FTS process, most are olefins as observed from this figure. For example, for C2-C4 products, olefins production amount to almost 80%. One of the possible reasons for this results from the shape selective characteristics of the SAPO catalyst.

However, when pressure increase to 240 psi, more of the products switch to paraffins (Figure 16). The selectivity of olefins decreases because the mass transport limitation increases under high pressure, which leads to an increased residence time of olefins. In addition, the concentration of hydrogen also increases as the pressure increases. These factors lead to increased hydrogenation of olefins. Therefore, olefins selectivity decreased as pressure increased.

Conclusions.

In MTO reactions the highest conversions to C2-C4 olefins were observed on SAPO-18 (92 %) and SAPO-34 (94 %) catalysts. C2–C4 olefins selectivity on various SAPO's are in the order: SAPO-34 > SAPO-18 > SAPO-47> SAPO-44> SAPO-17>SAPO-56. Ethylene selectivity on various SAPO's takes the following order: SAPO-34>SAPO-17>SAPO-47>SAPO-18> SAPO-44> SAPO-56. Lifetime of various SAPO's takes the following order: SAPO-34> SAPO-18> SAPO-17> SAPO-47= SAPO-56> SAPO-44. Particle size plays a significant role in activity and selectivity in MTO reaction as demonstrated on SAPO's-34, 18, and 44. Methane formation at high temperatures (> 450°C) can be reduced substantially by metals modification. Olefin selectivity is high in Fischer-Tropsch reaction on Co/SAPO34 catalyst; however, conversion is low.

Future Work.

Based on our efforts in the previous work, we have made the following research plans as a guide for the next year's work:
1. Synthesize and modify molecular sieve materials by either framework metal incorporation via hydrothermal route or extra-framework metals addition via impregnation and ion exchange, esp. with F-T metals such as Co, Fe, and promoters. The desired characteristics of this kind of catalysts will be directed towards high selectivity to light olefins; sufficiently active at low temperature; high surface area and thermal stability and ultrahigh component dispersion.

2. Test synthesized catalysts in direct and indirect syngas reactions to determine the performance of these catalysts as it relates to product selectivity, activity, and catalyst lifetime. Investigate the relationship between the catalyst activity and selectivity and the particle size, shape, surface structure as well as their bulk and surface composition.
3. Develop the optimum reaction strategy for production of valuable products from C-1 chemistry processes directly and indirectly from syngas using microporous and mesoporous molecular sieve catalysts.

References

1. D. Dubois, D. Obrzut, J.Liu, J.Thundimadathil, P. Adekkanattu, J. Guin , A. Punnoose, M. Seehra. Conversion of Methanol to Olefins over Cobalt, Manganese and Nickel Incorporated SAPO-34 Molecular sieves. Fuel Processing Technology, 83, (1-3), 2003, 203-218.
2. D. Obrzut, P. Adekkanattu, J. Thundimadathil, J.Liu, D. Dubois, and J. Guin. Reducing Methane Formation in Methanol to Olefins Reaction on Metal Impregnated SAPO-34 Molecular Sieve. Reaction Kinetics and Catalysis Letters, in press.
3. P.Adekkanattu, D. Dubois, D.Obrzut, J. Guin. Conversion of Methanol to Olefins on SAPO-56 and NiSAPO-56 Molecular Sieves. Applied Catalysis, A: General. Submitted
4. Conversion of Methanol to Olefins on Small Pore Silicoaluminophosphate (SAPO) Molecular Sieves, paper in preparation.
5. S. Wang and J. Guin, Catalytic Activity of Silica Supported Sulfated Zirconia Catalysts for Liquid Phase Etherification of C6 Olefins with Alcohols. Fuel Processing Technology, 84, 2003, 135-146.
6. B.M. Lok, C.A. Messina, R.L. Patton, R.T. Gajek, T.R. Cannan, E.M. Flanigen, US Pat. 4,440,871 (1984)
7. S. Ashtekar, S.V. V. Chilukuri, and D.K.Chakrabarty, Journal of Physical Chemistry, 98 (1994) 4878.

Table 1 Gel compositions and crystallization conditions for SAPO-n molecular sieves

Structure	Template (R)	Molar Gel composition	Temperature (°C)	Time (h)
SAPO-17	cyclohexylamine	1.0 Al2O3: 1.0 P2O5: 0.2 SiO2: 1.0 R: 60 H2O	200	42
SAPO-18	N,N-diisopropyl-ethylamine	1.0 Al2O3: 0.92 P2O5: 0.3 SiO2: 1.6 R: 50H2O	165	184
SAPO-34	Tetraethylammonium hydroxide	Al2O3: 1.0 P2O5: 0.3 SiO2: 2.0 R: 50 H2O	200	48
SAPO-34	Morpholine	1.0 Al2O3: 1.0 P2O5: 0.6 SiO2: 2.0 R: 60 H2O	200	49
SAPO-44	Cyclohexylamine	1.0 Al2O3: 1.0 P2O5: 0.6 SiO2: 1.9 R: 60 H2O	190	48
SAPO-47	Methylbutylamine	1.0 Al2O3: 1.0 P2O5: 0.6 SiO2: 2.0 R: 60 H2O	200	110
SAPO-56	N,N,N',N',-tetramethyl-hexane 1,6 diamine	1.0 Al2O3: 1.0 P2O5: 0.3 SiO2: 1.0 R: 40 H2O	200	111

Table 2 Gel compositions and crystallization conditions for NiSAPO-n molecular sieves

Structure	Template (R)	Molar Gel composition	Temperature (°C)	Time (h)
NiSAPO-17	cyclohexylamine	0.03NiO: 0.98 Al2O3: 1.0 P2O5: 0.1 SiO2: 1.0 R: 60 H2O	200	42
NiSAPO-18	N,N-diisopropyl-ethylamine	0.03NiO: 0.98 Al2O3: 0.92 P2O5: 0.3 SiO2: 1.6 R:50H2O	165	184
NiSAPO-34	Morpholine	0.03: 0.98 Al2O3: 1.0 P2O5: 0.6 SiO2: 2.0 R: 60 H2O	200	49
NiSAPO-44	Cyclohexylamine	0.03NiO: 0.98 Al2O3: 1.0 P2O5: 0.6 SiO2: 1.9 R: 60 H2O	190	48
NiSAPO-47	Methylbutylamine	0.03NiO: 0.98 Al2O3: 1.0 P2O5: 0.3 SiO2: 2.0 R: 60 H2O	200	110
NiSAPO-56	N,N,N',N',-tetramethyl-hexane 1,6 diamine	0.03NiO: 1.0 Al2O3: 1.0 P2O5: 0.3 SiO2: 1.0 R: 40 H2O	200	111
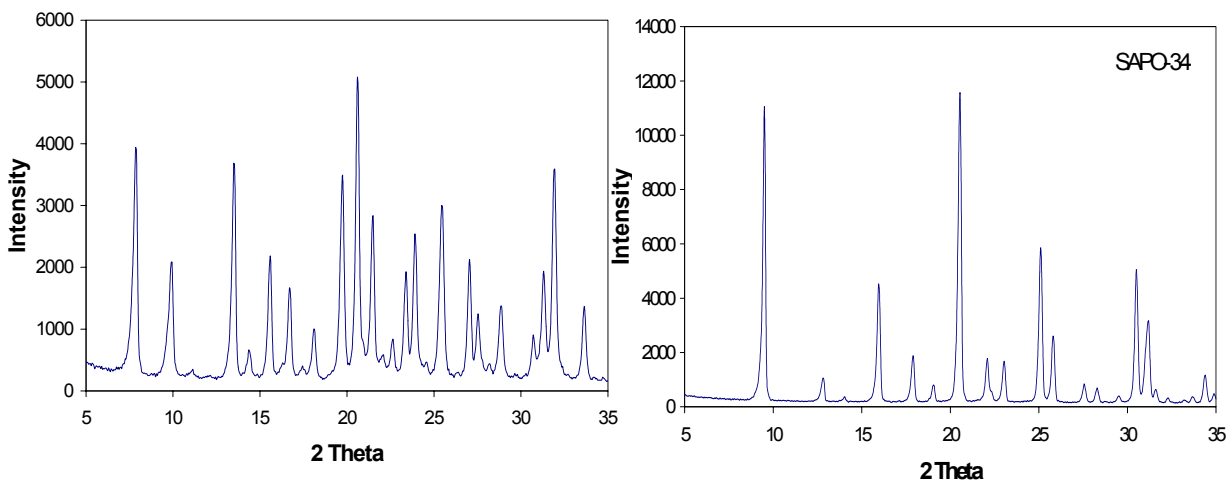
Figure 1   X-ray diffraction pattern of SAPO-17, SAPO-34 catalyst
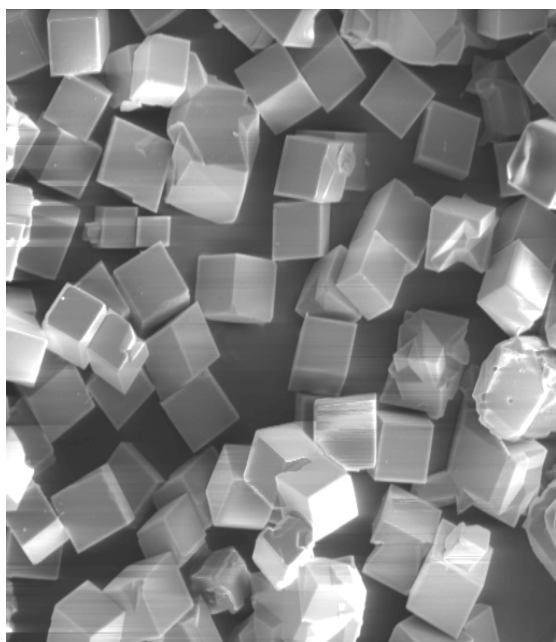
. SAPO-34 (Morpholine)
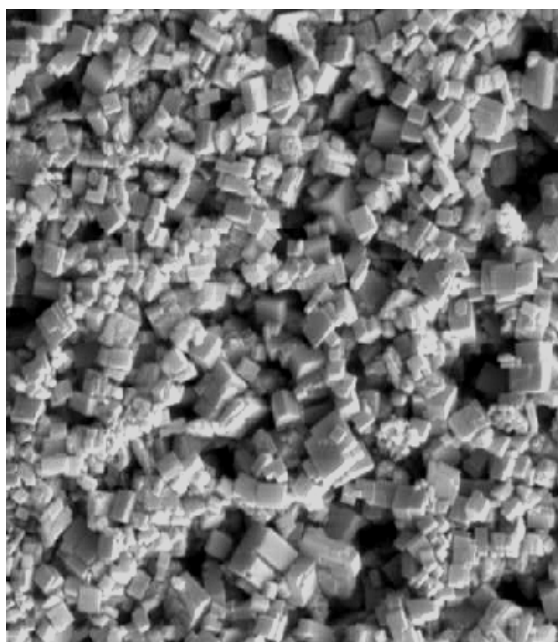
SAPO-34 (TEA-OH)
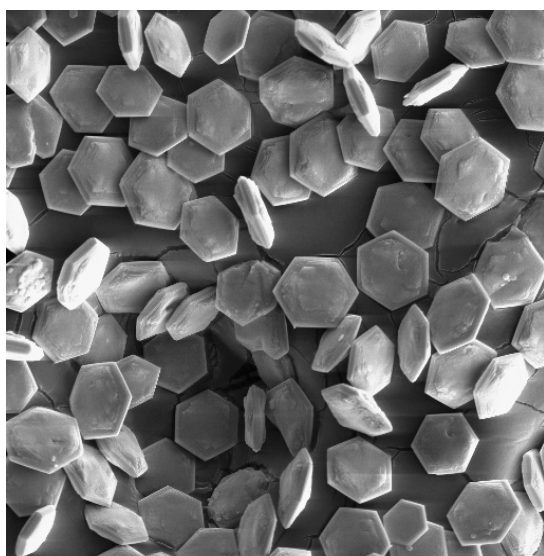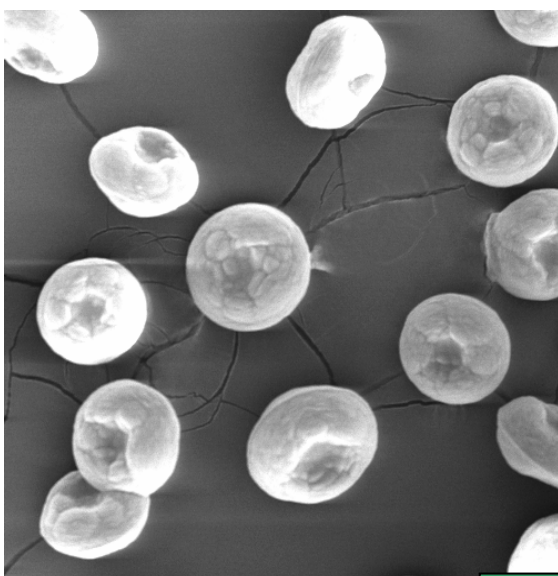
SAPO-56(0.3)   SAPO-56(0.9)

Figure 2   SEM of SAPO-34 and SAPO-56
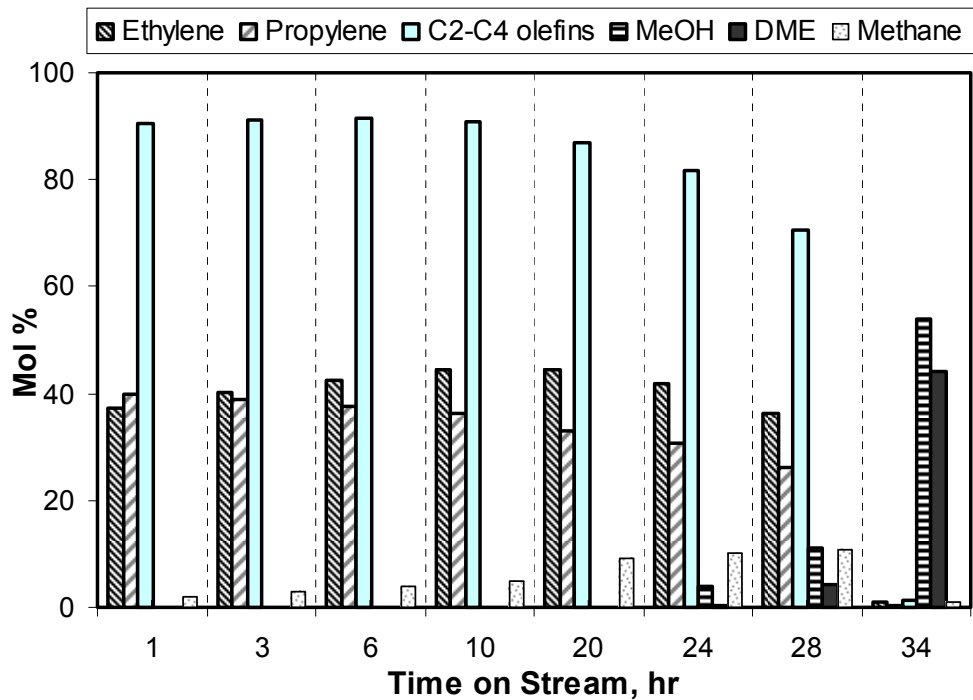
Figure 3   Product distribution in methanol conversion on SAPO-18
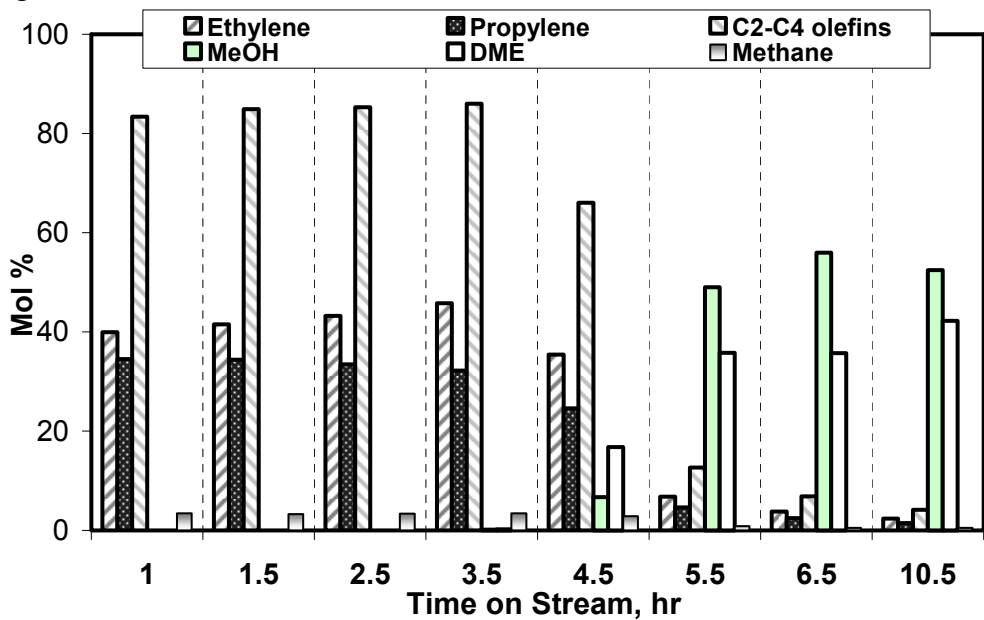
Figure 4   Product distribution in methanol conversion on SAPO-44
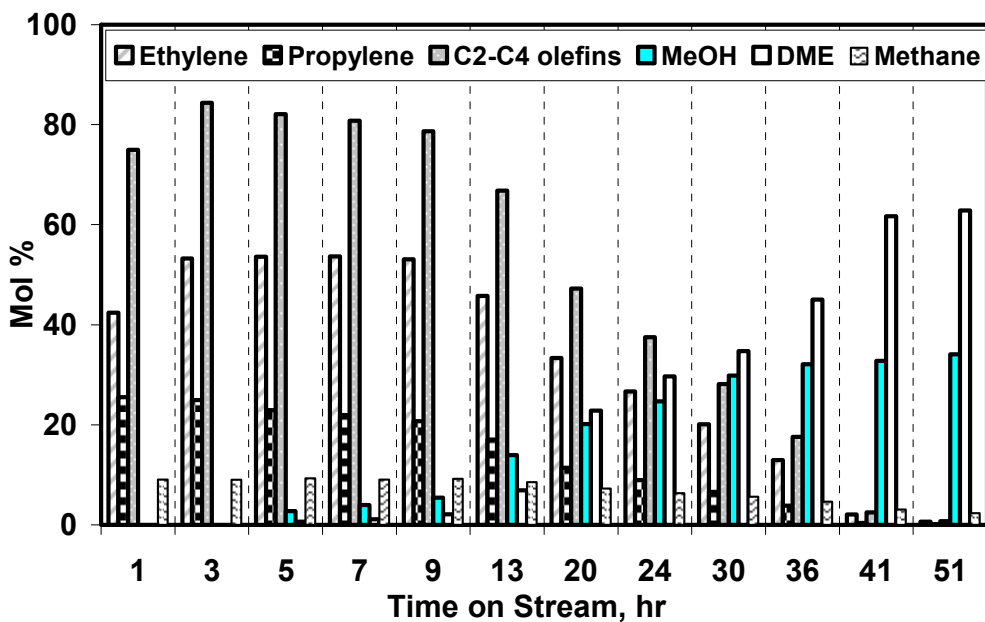
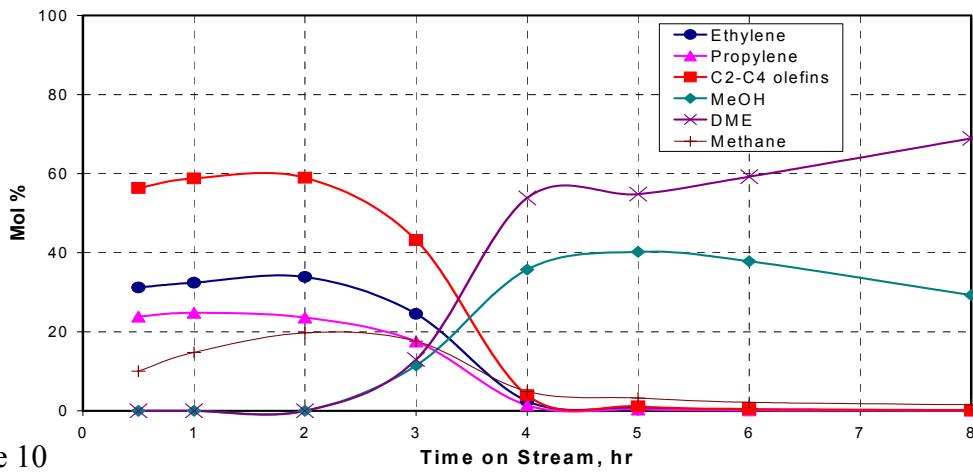Figure 5   Product distribution in methanol conversion on SAPO-47
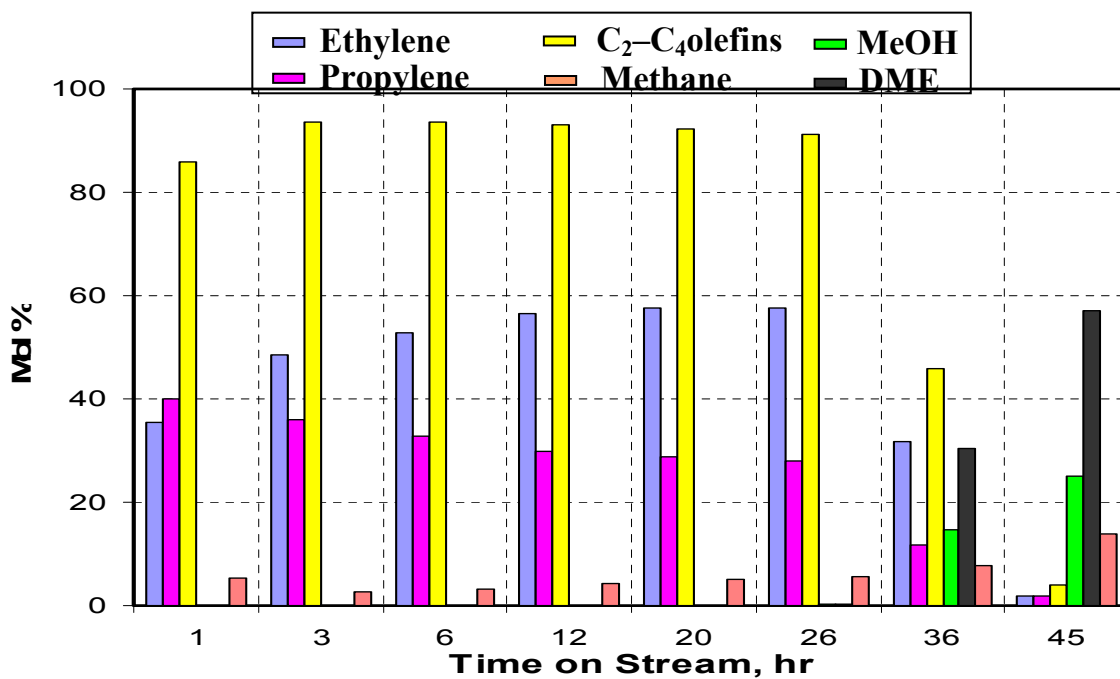
Figure 6   Product distribution in methanol conversion on SAPO-34 (TEA-OH)
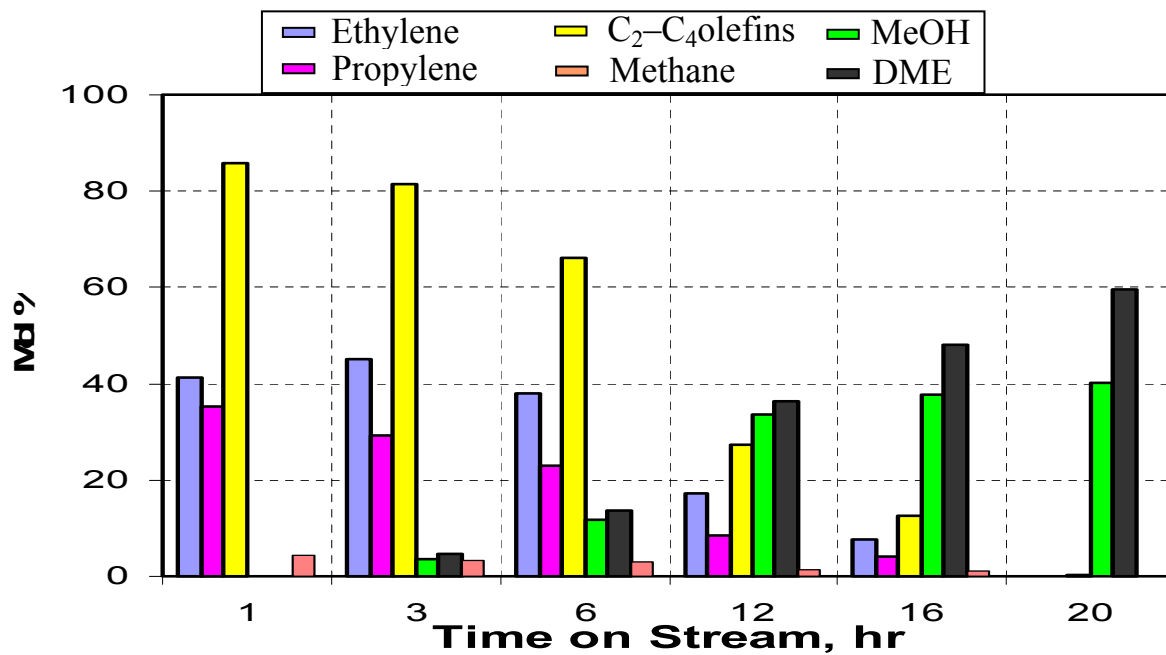
Figure 7   Product distribution in methanol conversion on SAPO-34 (Morpholine)
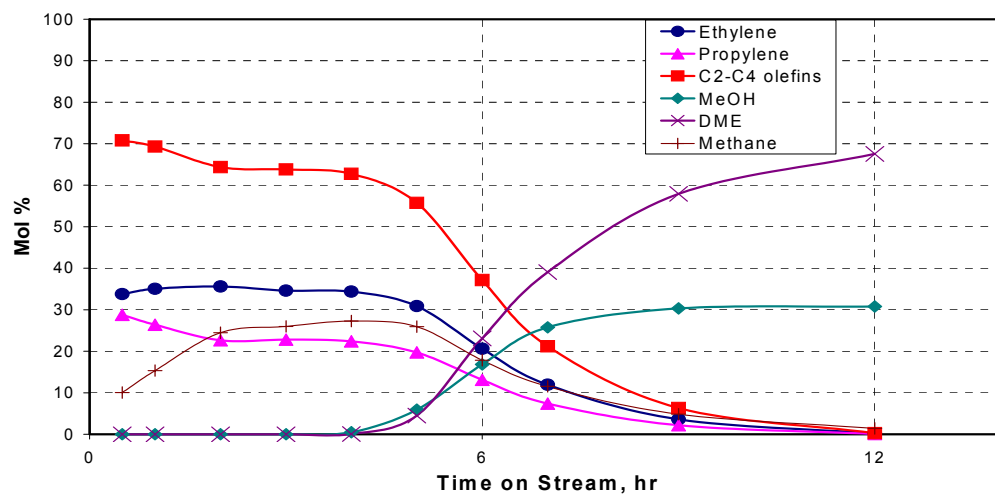
Figure 8   Product distribution in methanol conversion on SAPO-56(0.3)
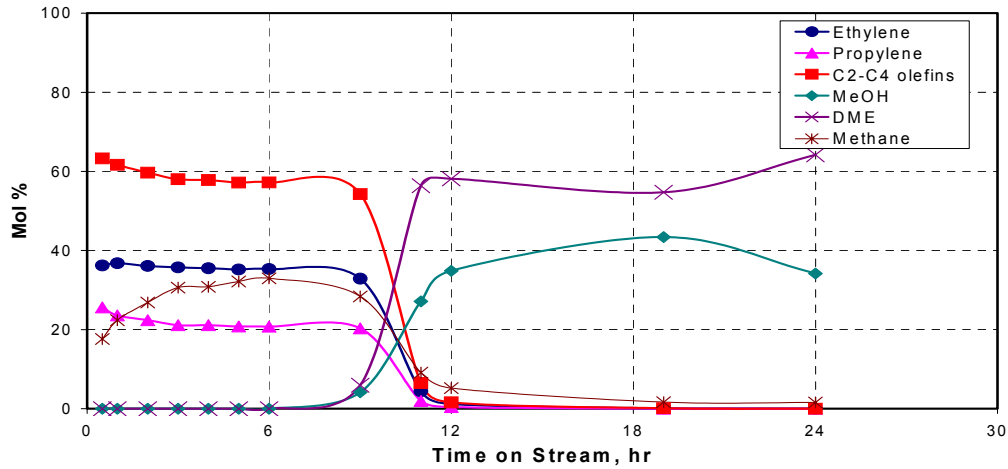
Figure 9   Product distribution in methanol conversion on SAPO-56(0.6)

Figure 10

Product distribution in methanol conversion on SAPO-56(0.9)
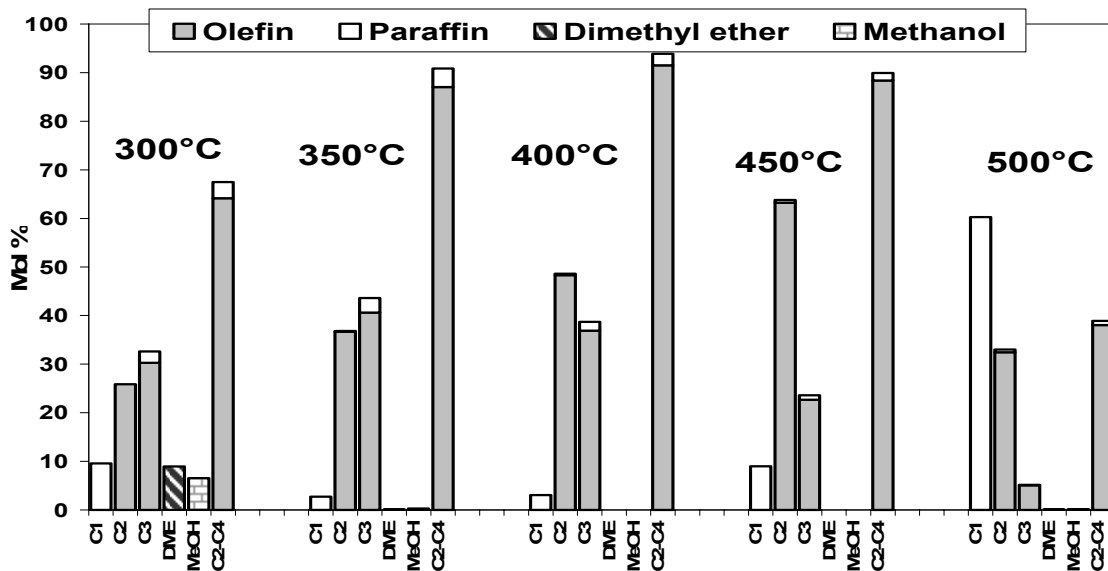
Figure 11   Product distributions on SAPO-34 under various temperatures
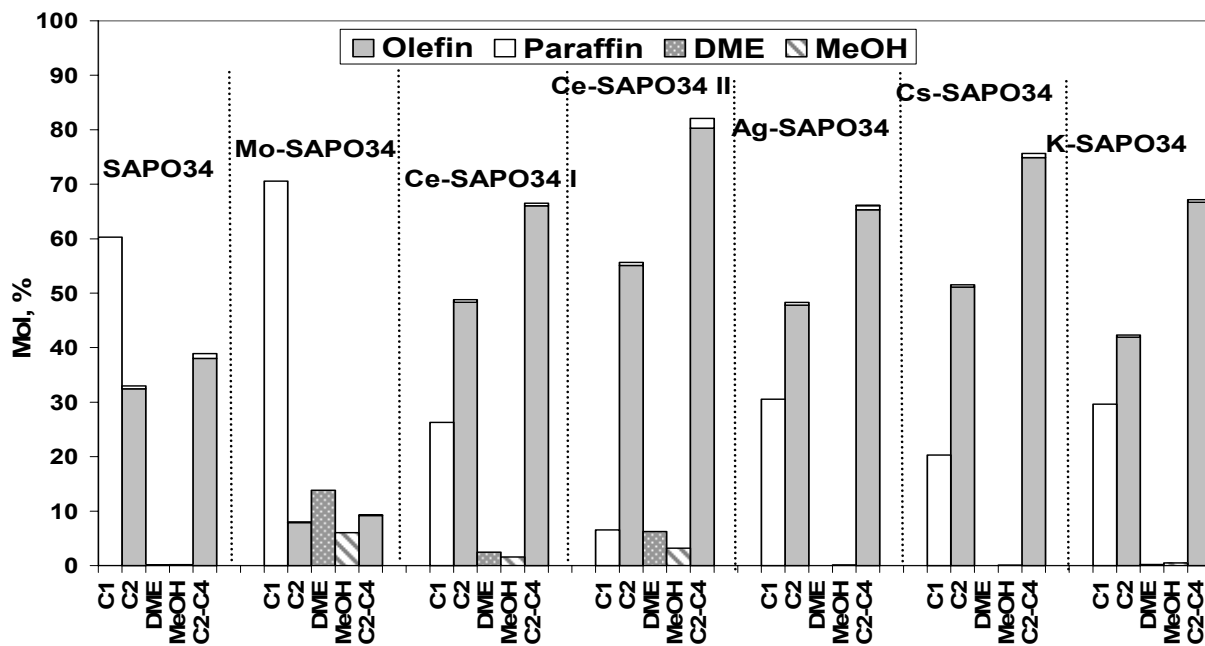
Figure 12   Product distributions on SAPO-34 and Me-SAPO34 at 500°C
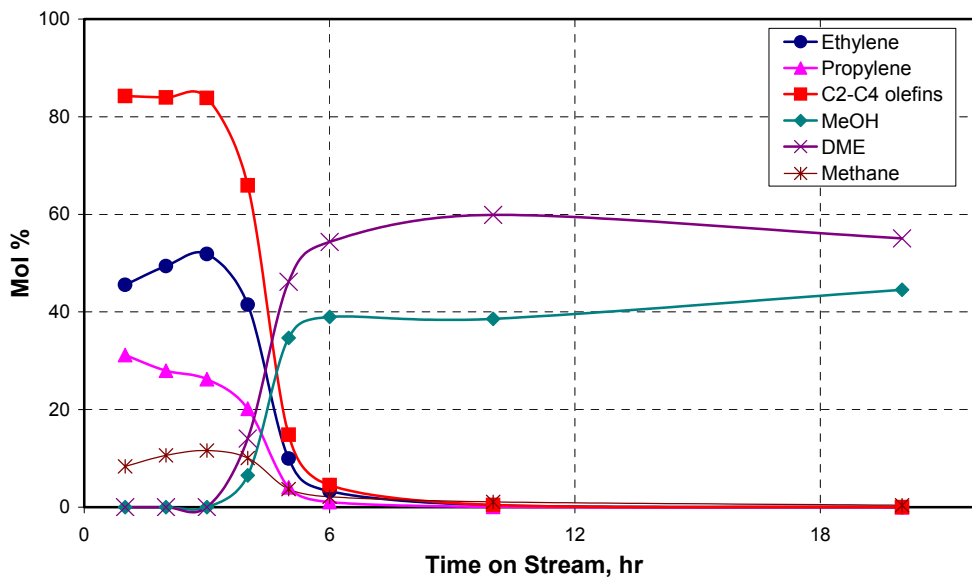
Figure 13   Product distributions on NiSAPO-44
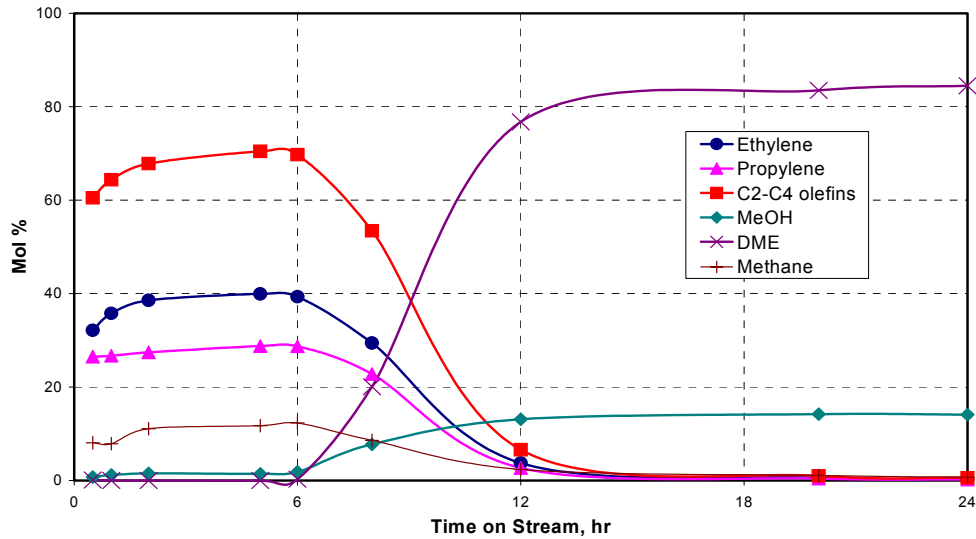
Figure 14   Product distributions on NiSAPO-56
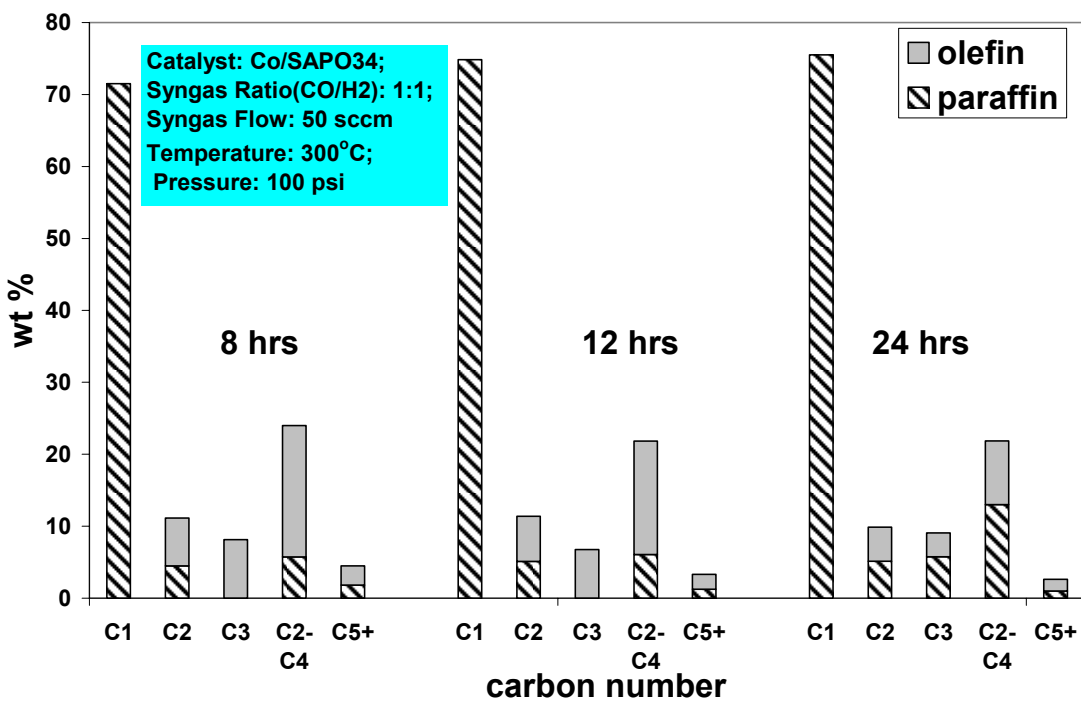
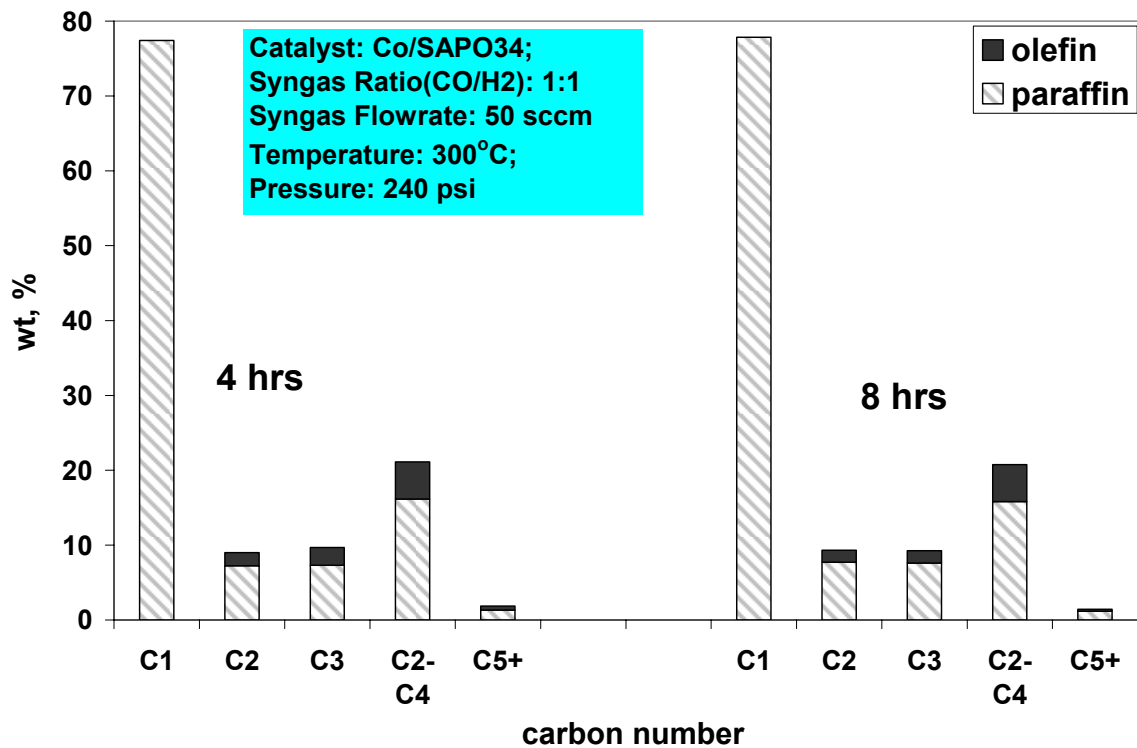Figure 15   Hydrocarbon distribution in FTS process at 100 psi

Figure 16   Hydrocarbon distribution in FTS process at 100 psi

Hydrogen production by catalytic decomposition of ethane, propane and cyclohexane

Yuguo Wang, Naresh Shah, and Gerald P. Huffman
University of Kentucky

Introduction

Non-oxidative, catalytic decomposition of hydrocarbons is an alternative, one-step process to produce pure hydrogen. Nanoscale, binary Fe-based catalysts supported on high surface area alumina (M-Fe/Al_2O_3, M=Mo, Pd or Ni) have been developed that exhibit high activity for the catalytic decomposition of undiluted methane into pure hydrogen and carbon [1]. One of the problems with non-oxidative dehydrogenation is coking of the catalyst and reactor due to carbon build up. However, under proper reaction conditions, these binary catalysts promote the growth of carbon nanotubes which transport carbon away from the catalyst surfaces, thereby increasing the lifetime of the catalysts while producing a potentially valuable by-product.

Ethane and propane are constituents of natural gas and byproducts of cracking and fractional distillation of petroleum that can also serve as hydrocarbon feedstocks to produce pure hydrogen. Methane, ethane, and propane are all present in significant amounts in Fischer-Tropsch reaction products. Non-catalytic steam cracking of ethane has been commercially used for production of ethylene [2] at reaction conditions of high (>800 C) temperature and short contact times. There are two principle uses of propane. (1) As a feedstock to produce acrylic (or propenoic, CH2=CHCO2H) acid by partial oxidation, and (2) as a fuel for residential cooking and heating. There is an established network of propane distributors throughout the country for selling and refilling propane tanks.

Partial dehydrogenation of cyclohexane to benzene avoids any solid carbon buildup on the catalysts. Thus the removal of carbon buildup and regeneration of catalyst bed is eliminated and the catalyst life is prolonged. Partial dehydrogenation of cyclohexane yields 7.143 weight % hydrogen, well above the DOE targets of 4.5 weight % by 2005 and 6 weight % by 2010 for hydrogen storage in automotive applications.

The current report summarizes results obtained to date on the catalytic decomposition of ethane, propane, and cyclohexane [3-5].

Experimental Procedure

Supported binary catalysts were produced by either incipient wetness of or co-precipitation on fine alumina powder as described previously [1, 3-5] and in previous annual reports. After in-situ pre-reduction, undiluted reactant stream was passed over the fixed catalyst bed. The entire exit stream was analyzed for reaction products and unreacted input stream by on-lined dual-TCD gas chromatographs. In the case of cyclohexane dehydrogenation, the exit stream was first analyzed with an inline FID gas chromatograph by using a heated transfer line. The exit stream from the FID GC was quenched using an in-line condenser and injected into the duel-TDC GC.

Results and Discussion

Ethane dehydrogenation
As shown in figure 1, the binary catalysts are very effective in promoting decomposition of ethane. Pre-reduction in hydrogen generates the active metallic species responsible for breaking C-C bonds.

At approximately 450 ºC, these catalysts start breaking C-C bonds in ethane to generate methane and hydrogen in substantial quantities. At 450-500 ºC, the carbon nanotubes (CNT) are produced with a "stacked traffic cone" morphology [3, 4]. At temperatures of 650 ºC and above, all of the ethane is decomposed to hydrogen (70-90 vol.%) and methane (10-30 vol.%). The CNT produced above 650 ºC are predominantly multi-walled nanotubes formed by concentric parallel-walled graphene sheets. Figure 2 shows high resolution transmission electron microscopy (HRTEM) images of the two kinds of nanotubes produced by the same catalyst used for ethane decomposition at 500 ºC and 650 ºC reactor temperatures.

Propane dehydrogenation
In thermal, non catalytic runs, propane decomposition is first noted at temperature above 525 ºC in the form of a small amount of hydrogen production (Figure 3, left). With increasing temperature, the amounts of hydrogen, methane, ethylene and ethane all increase till reactor temperature is above 650 ºC, where secondary decompositions of methane, ethane and ethylene start occurring to yield additional hydrogen. Complete thermal propane decomposition occurs only at reactor temperatures above 725 ºC.

The binary catalysts (pre-reduced at 700 ºC) initiated decomposition of propane at 350-400 ºC to hydrogen and methane. Above ~475 ºC, propane is completely converted to hydrogen (~70%) and methane (~30%). Above that temperature the subsequent catalytic decomposition of methane proceeds in essentially the same way as described in an earlier paper [1]. No propene, acetylene, benzene, or higher hydrocarbons were observed for any of the catalysts and reaction conditions.

The most active of the current suite of catalysts was the 0.5%Ni-4.5%Fe/Al_2O_3 catalyst, which yielded approximately 85 volume% of hydrogen at a fairly modest temperature of 625 ºC. Time on stream studies (TOS) were carried out at 625 ºC to determine the rate of deactivation of the various pre-reduced (at 700 °C) catalysts (Figure 4). The activities of the Mo-Fe and Ni-Fe catalysts decrease relatively slowly at rates of ~1-2% per hour. This rate of deactivation is considerably slower than that of a 5% Fe/Al_2O_3 catalyst.

The CNT structures produced by catalytic decomposition of propane were similar to those observed by catalytic decomposition of ethane. Stacked-cone CNT were produced at low temperatures and multi-walled CNT formed by parallel concentric graphene sheets were produced at high temperatures, as shown in Figure 5.

Cyclohexane dehydrogenation

Figure 6 shows the distribution of different products from cyclohexane dehydrogenation on a (0.5%Ni-4.5%Fe)/Al$_2$O$_3$ catalyst as a function of temperature. No reaction products were observed below 400 ºC and the only products produced above that temperature were methane, benzene, and hydrogen. It is evident that the Ni-Fe/Al$_2$O$_3$ catalyst mainly cleaves carbon-carbon bonds to produce hydrogen, methane and carbon nanotubes. At 475 ºC, benzene production reaches its highest point, but is still insignificant (~3 vol.%) compared to the production of methane. Consequently, it appears that the catalyst is not effective in dehydrogenating cyclohexane to benzene.

Figure 7 shows the production distribution from partial dehydrogenation of cyclohexane on Mo-Fe/Al$_2$O$_3$ catalyst as a function of temperature. There was no conversion of cyclohexane at temperatures below 400 ºC. Above 400 ºC, benzene and hydrogen were the major products. Above 550 ºC, the catalyst began to cleave carbon-carbon bonds to produce large amounts of methane in the outflow gas stream. With increasing temperature, the levels of hydrogen and benzene remained unchanged but increasing amounts of cyclohexane were converted to methane and carbon nanotubes. Just like Ni-Fe/Al2O3, Mo-Fe/Al2O3 does not seem to be very effective in dehydrogenating cyclohexane to benzene.

Experiments were also conducted using the (0.5%Pd-4.5%Fe)/Al$_2$O$_3$ for hydrogen production from cyclohexane. Figure 8 shows the distribution of different products in the outgoing gas flow from the reactor as a function of temperature. From 315 to 450 ºC, around 50 volume % of hydrogen is produced in the outgoing gas stream, benzene is about 15~17 volume %. Above 450 ºC, cyclohexane is mainly converted to methane, hydrogen and carbon nanotubes and the production of benzene decreases, just as observed for the Fe-Ni and Fe-Mo catalysts. More recent results obtained from experiments still in progress have demonstrated that dilute amounts of either Pt or Pd supported on stacked-cone CNT are very effective for catalytic decomposition of cyclohexane. These results will be submitted for publication in the near future [8].

Applications of nanotubes

The many applications of CNT have been discussed extensively (see for example references 9 and 10). We have begun to explore two possible applications that are relevant to the current program. As seen in the micrographs of Figures 2 and 5, the stacked-cone CNT have an abundance of open edges, which provide openings between graphene sheets to the interior of the structure. Additionally, they have a large density of zigzag carbene structures [10] at the cone edges on the outer circumference of the stacked-cone CNT. This unique structure offers promise both as a catalyst support and as a hydrogen storage material. Our work on using the stacked-cone CNT as catalyst supports is briefly mentioned above and will be described in a future publication [8]. The work on hydrogen storage is being conducted in collaboration with Dr. Brad Bockrath of NETL. Some initial results are shown in Figure 9. It is seen that the hydrogen storage achieved using stacked-cone CNT prepared by catalytic ethane dehydrogenation at 500 ºC after purification by treatment with NaOH are as good as the best results obtained from single-walled CNT after oxidation by CO$_2$. Additional treatments and functionalization of the stacked-cone CNT will be attempted to improve these results.

Catalyst Characterization

To better understand catalytic dehydrogenation of lower hydrocarbons, detailed investigation of catalyst structures is carried at various stages of the process. Mössbauer and XAFS spectroscopy, TEM, XRD, and magnetic measurements are being were used for this purpose. Significant findings from such analyses have been reported in earlier publications [6, 7].

Conclusions

Non-oxidative, catalytic decomposition of lower alkanes is an alternative, one-step process to produce pure hydrogen with no production of carbon oxides or higher hydrocarbons. Our earlier work demonstrated that nanoscale, binary Fe-based catalysts supported on high surface area alumina (M-Fe/Al_2O_3, M=Mo, Pd or Ni) exhibit high activity for the catalytic decomposition of undiluted methane into pure hydrogen and carbon [1]. Under proper reaction conditions, these binary catalysts promote the growth of carbon nanotubes which transport carbon away from the catalyst surfaces, thereby increasing the lifetime of the catalysts while producing a potentially valuable by-product.

During the current year, we have demonstrated that these binary catalysts are equally effective for the catalytic dehydrogenation of ethane and propane. Methane, ethane, and propane are the common hydrocarbon constituent of natural gas and the major compounds produced in the light products of Fischer-Tropsch synthesis. Therefore, this approach should a very effective of producing hydrogen from natural gas, F-T light products, coalbed methane, or landfill methane.

We have also begun to explore the potential applications of the carbon nanotube (CNT) by-products produced in the catalytic dehydrogenation process that are relevant to this program. Specifically, we are exploring the use of stacked-cone CNT for hydrogen storage and as catalyst supports. The initial results obtained for both applications are quite promising.

Future Work

Continuous dehydrogenation of lower alkanes

For practical applications of the catalytic dehydrogenation of natural gas, it will be necessary to develop a reaction system in which hydrogen and CNT can be continuously removed. To accomplish this, a closed loop, fluidized bed reactor will be developed. Because of the higher flow rate and shorter residence time, we expect a decrease in methane conversion. However, because the flow stream is recycled, the unconverted methane will continue to decompose into carbon and hydrogen in subsequent passes through the reactor. Based on some preliminary results, it is expected that fluidization of the catalyst bed will provide sufficient agitation to detach the nanotubes from the catalyst surfaces so they can be carried out of the reactor in the gas stream for collection. This process modification will improve the process both by increasing the "time on stream" of the catalyst and by isolating and capturing the valuable CNT by-product.

Partial dehydrogenation of liquid hydrocarbons

Catalytic dehydrogenation of methylcyclohexane, tetralin, decalin and F-T liquid products to produce hydrogen will be tested in the future. Pt, Pd, and other metals supported on stacked-cone CNT will be used as catalysts.

Application of nanotubes as hydrogen storage media

Exploration of possible utilization of the stacked-cone CNT for hydrogen storage has been initiated in collaboration with Brad Bockrath of NETL. The initial results are promising and this will be further pursued. To enhance storage capacity, CO_2 oxidation of the stacked-cone CNT or/and addition of hydrogen-active metals will be attempted.

Characterization of catalysts and carbon nanostructures

We plan to continue characterization of the catalysts and CNT using XAFS and Mössbauer spectroscopy and TEM.

References

1. N. Shah, D. Panjala, G.P. Huffman; *Energy & Fuels, 15(6)* (2001) 1528-34.
2. For example, US patents 5763725 and 5990370.
3. Makkuni, D. Panjala, N. Shah, and G.P. Huffman, *ACS Div. Fuel Chem. Prepr.*, **47(2)** (2002) 782-783.
4. "Production of pure hydrogen and carbon nanostructures by catalytic non-oxidative dehydrogenation of ethane", N. Shah, Y. Wang, and G.P. Huffman, submitted to *Energy & Fuels.*
   Y. Wang, N. Shah, and G.P. Huffman, *ACS Div. Fuel Chem. Prepr.*, **48(2)** (2003) 900-901.
5. N. Shah, S. Pattanaik, F.E. Huggins, D.Panjala, and G.P. Huffman, *Fuel Proc. Tech.*, **83** (2003) 163-174.
6. Punoose, N. Shah, G.P. Huffman, and M.S. Seehra, *Fuel Proc. Technology*, **83** (2003) 263-274.
7. Yuguo Wang, Naresh Shah, and Gerald P. Huffman, paper in preparation.
8. P.M. Ajayan, *Chem. Rev.*, **99** (1999) 1787-1799.
9. H. Dai, *Surface Science*, **500** (2002) 218-241.
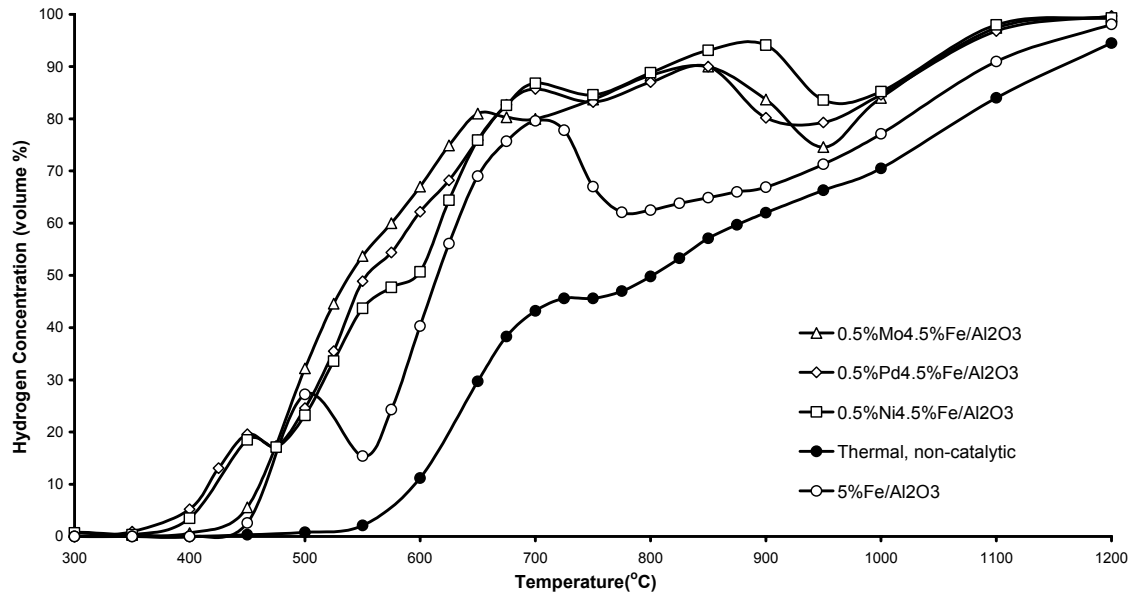10. Radovic, LR.; Bockrath, B. *ACS Div. Fuel Chem. Prepr.,47* (2) (2000) 428.

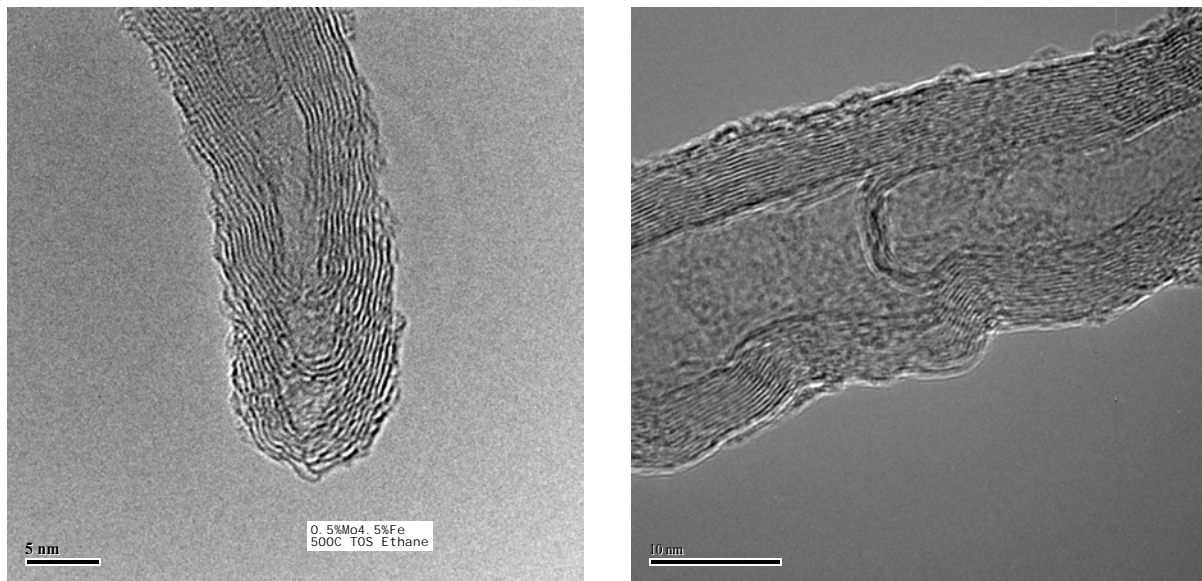Figure 1. Product distribution from thermal (non-catalytic) and catalytic cracking of ethane.

Figure 2. HRTEM images of carbon nanotubes generated on 0.5%Mo4.5%Fe/Al2O3 catalyst used for ethane dehydrogenation. Reactor temperatures were 500 ℃ (left) and 650 ℃ (right)
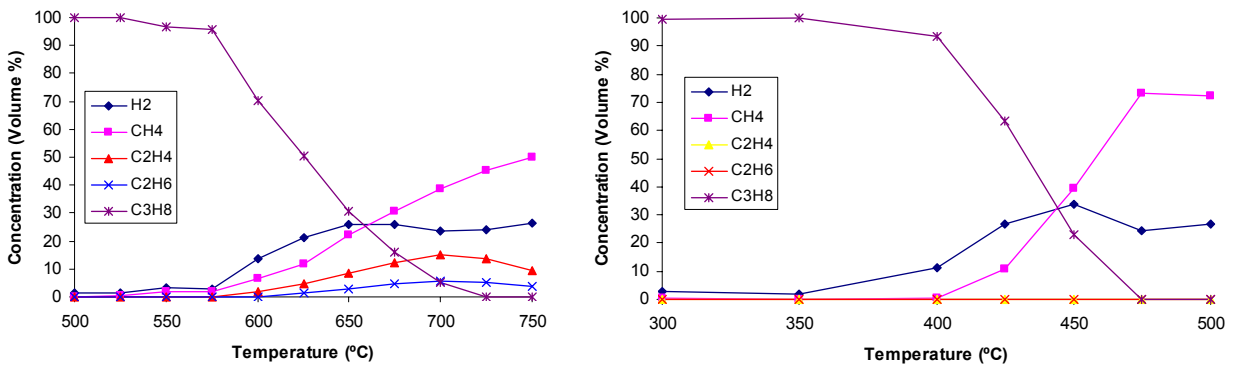
Figure 3. Product distribution of thermal (left) and catalytic (right) cracking of propane using a (0.5%Pd-4.5%Fe)/γ-Al$_2$O$_3$ catalyst.
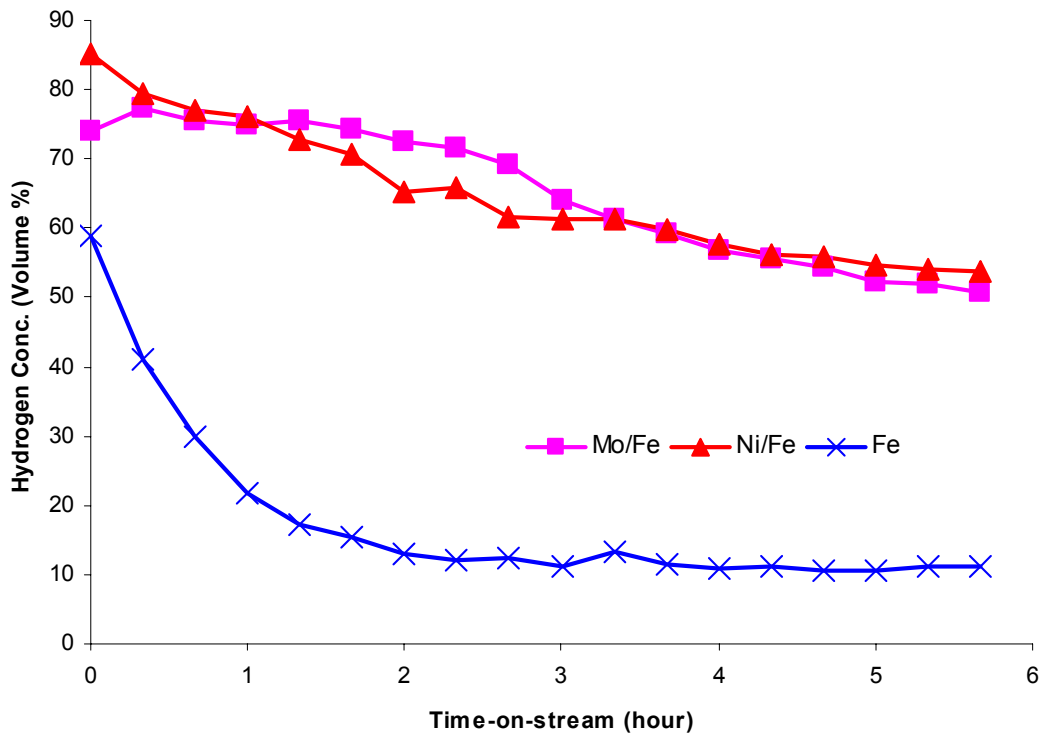

Figure 4. Time-on-stream behavior of several catalysts for decomposition of propane at 625 ºC.
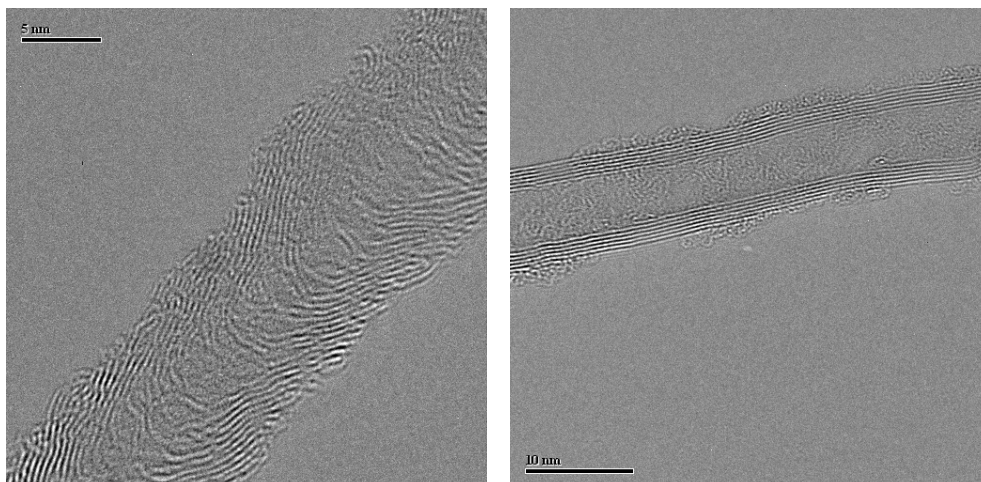
Figure 5. HRTEM images of MWNT grown by decomposing undiluted propane at 475 ºC over Pd-Fe/Al$_2$O$_3$ (left) and at 625 ºC over Mo-Fe/Al$_2$O$_3$ (right).
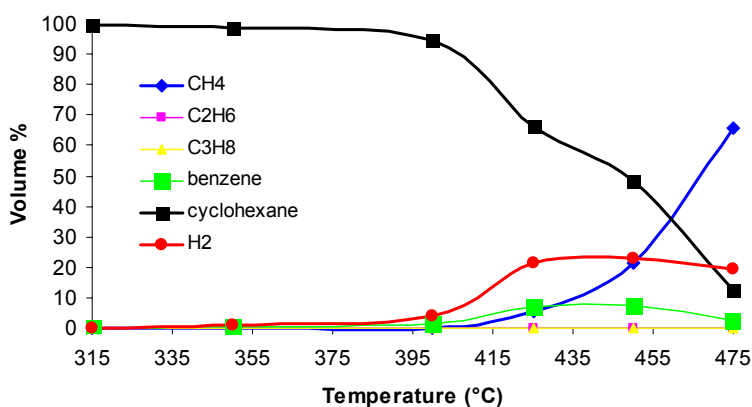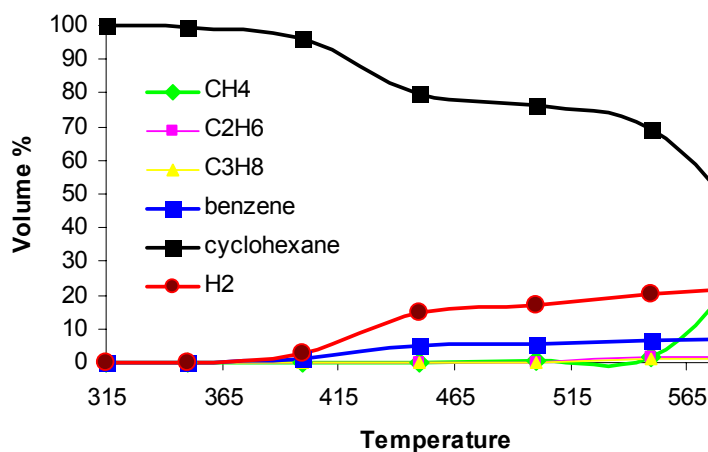

Figure 6. Product distribution of Ni-Fe/Al$_2$O$_3$ catalytic conversion of cyclohexane at different temperatures.

Figure 7. Product distribution of Mo-Fe/Al$_2$O$_3$ catalytic conversion of cyclohexane at different temperatures.
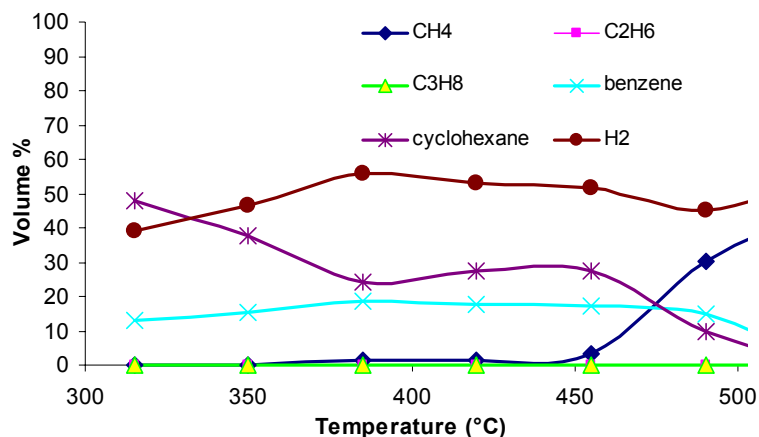
Figure 8. Product distribution of Mo-Fe/Al_2O_3 catalytic conversion of cyclohexane at different temperatures.
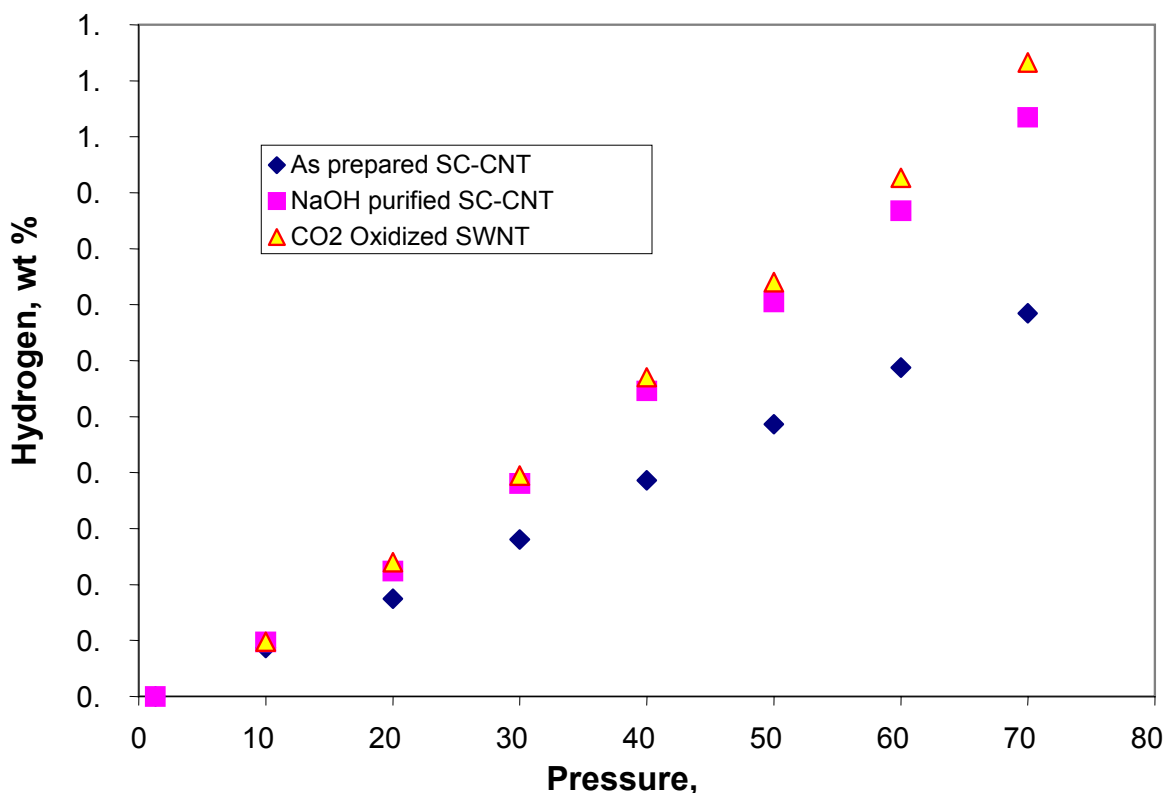

Figure 9. Room temperature weight percent hydrogen uptake as a function of pressure for as prepared (diamonds) and NaOH purified (squares) stacked-cone CNT produced by ethane dehydrogenation at 500 C over a pre-reduced (0.5%Pd-4.5%)Fe/Al_2O_3 catalyst. The results are compared with the best results achieved for acid cleaned, CO_2-oxidized single wall nanotubes (triangles) produced by the arc discharge method at Rice University.

Conversion of Methane to Hydrogen

Edwin L. Kugler and Dady B. Dadyburjor
Department of Chemical Engineering, West Virginia University

Introduction

There are many reasons to use methane as a source of value-added products and/or reactions. Methane is ubiquitous in Fischer-Tropsch processing, where it involves a significant fraction of the carbon balance; it is a greenhouse gas; it is present in coal seams; and it is the major constituent of natural gas, the reserves of which are often "stranded", i.e., found in inhospitable and/or arid locations. Dry reforming, the reaction of methane with carbon dioxide to form synthesis gas ("syngas") with a theoretical H_2/CO ratio of unity, is one such value-added reaction. It is significant for the following reasons: the other reactant (CO_2) is also a greenhouse gas, and is often found in conjunction with methane; dry reforming is one of the few reactions that actually depletes CO_2 rather than stores it; and the reaction product, syngas, is a useful feedstock for hydrocarbons and oxygenates and can be used to create a stream of H_2 for fuel or other use.

Accordingly, dry reforming of methane to syngas is the focus of the current research. Metallic catalysts such as Ni are preferred over noble metals for economic reasons, but Ni is susceptible to coking and is severely deactivated by it. Certain molybdenum and tungsten carbide catalysts offer a possible solution to this problem by being able to dissolve excess surface-carbon into the bulk to keep the surface clean. When carbon is soluble within catalytic materials, thermodynamics and kinetics determine the catalyst phase and the fate of excess carbon. Hence, carbon accumulation can be controlled. Here, tungsten-cobalt carbides are used as precursors for study as dry reforming catalysts.

We have shown [1] that a very active and stable catalyst could be produced by pretreating commercially obtained η-Co_6W_6C (Nanodyne, Inc.) with CH_4 and CO_2 at 850°C for a 24-hour period. After pretreatment, the catalyst did not deactivate for at least 100 hours. At the end of the run, the material removed from the reactor was shown to be a mixture of Co, WC and C. Micrographs showed [2] that the carbon deposited was filamentous. A reaction model was developed [3] involving Langmuir-Hinshelwood mechanics with carbon deposition, water-gas-shift and the Boudouard reaction as well as dry reforming. This was fit to kinetic data over a range of temperatures, pressures and relative amounts of CH_4 to CO_2 to obtain rate constants and activation energies for this catalytic process.

Because commercially obtained bimetallic carbides are difficult to obtain, and also because we wish to have more control over the phases present in our catalyst, we have started to develop expertise in preparing our own catalysts. Our approach has been to start with the patent literature [4,5] then modify as necessary to obtain different phases. This year, we have produced three different catalysts. These have been characterized before and after reaction. The reaction results have been correlated with the structure of the catalytic materials. The long-range plans of this work are to find bimetallic carbide-based catalysts that are at least as active, selective and stable

as those in commercial practice, and to modify these to obtain catalysts which can yield high ratios of H_2/CO in the product

Experimental Procedure

All the materials produced start with 14.5 g tungstic acid, H2WO4, added to a mixture containing 400 ml of an aqueous (1:1) NH4OH solution and 300 ml of ethylenediamine, followed by heating to 50°C and stirring to get a clear solution. Then, 13.8 g CoCl2·6H2O are dissolved in 50 ml distilled water and added into the above solution. A precipitate, Co(en)4WO4, forms when the volume of the mixture is reduced by 50 percent by evaporating and slow overhead stirring. The product is then filtered, washed and dried. The Co(en)4WO4 is then heated in an Ar-H_2 mixture to 650°C in 3h, then heated in Ar to 850°C in 0.5h, reduced in a CO_2-CO mixture at 850°C for 24h and finally cooled back to room temperature in flowing Ar.. The heating/cooling process is carried out at ambient pressure in a downflow reactor.

As mentioned above, three different materials were prepared. These corresponded to CO_2/CO ratio values of 0.75, 0.2 and 0.1. This process yields 3-5 g of material of surface areas 2 – 30 m^2/g and size 2-3μ. Some of this material was characterized by x-ray powder diffraction (XRD) in Professor Seehra's laboratory. Some material was placed in the reactor system to catalyze the CH_4 and CO_2..

The reactor system is computer-controlled with automated data logging. Details can be found in, for example, Iyer et al. [3]. In order to verify the stability of the catalysts formed, and to compare these with the commercial material, the reactor was run for at least 100 h at the highest temperature used previously, 850°C. The material showed stable catalytic behavior well before this time on stream. After the reaction, the catalyst was again analyzed by XRD. The difference between the pre-reaction XRD and the post-reaction XRD indicates the stability of the original formulation as a catalyst. The initial reactivity behavior can be correlated with the initial XRD measurement, and the final reactivity with the final XRD.

Results

It is worth comparing the bimetallic carbide material with other catalysts used in dry reforming. Comparisons are not easily obtained, however, because insufficient information is provided in many cases to calculate rates (from conversion data, say) or to relate rates to reactant concentrations. The comparisons that can be made are shown in Table I.. At low temperatures, the improvement of the bimetallic catalyst over supported Ni catalyst is by factors of 1.2 (i.e., 20%) to 5; at high temperatures, the improvements are by factors of 15 to 20. For unsupported Mo_2C, at the single temperature shown, improvements are by factors of 4 to 5. Hence it would appear that the bimetallic carbide catalyst is at least comparable, if not superior, to conventional nickel catalysts and unsupported single-metal carbides.

For the materials made in-house, the as-prepared XRD patterns are shown in Figure 1 for the three different values of CO_2/CO ratios (x): 0.75, 0.2, 0.1. The pattern for x = 0.75 corresponds closely with that of pure η-Co_6W_6C (and that of the Nanodyne material). With lower values of x, i.e., mixtures which are more reducing, the patterns change. For x = 0.2, the material appears to

consist of tungsten carbide (WC) and Co_3W_3C (or $Co_6W_6C_2$, i.e., the bimetallic carbide with an additional C atom intercalated in the molecule). This is consistent with the greater reduction of the bimetallic carbide by the CO_2/CO stream. Finally, for x = 0.1, the pattern indicates the presence of Co_3W_3C as well as elemental Co, WC and elemental C (graphite). Clearly, this material is still further reduced. It contains the components found in the Nanodyne η-Co_6W_6C after it had been pretreated and shown to be an active and stable catalyst, but it also contains some of the intercalated (and incompletely reduced) bimetallic carbide.

Figure 2 shows the results of reactivity studies with these three materials. The "carbon balance" is a measure of the carbon being deposited on the catalyst and closure of the material balance (with a fraction carbon balance of 1.0 implying no carbon being deposited and a complete material balance of carbon). All three materials go through an unsteady state, as can be seen by the changes in conversions. While the material with x = 0.75 requires about 40 h to reach steady state, the other materials require approximately 20 hours. Again, this is because the latter are more reduced during preparation.

The reactivity behavior of the material with x = 0.2 is similar to that of x = 0.75. In both cases, the ratio H_2/CO increases from the stoichiometric value of 1 to approximately 1.6 with time on stream, before decreasing back to around 1.0. The increase in the relative amount of H_2 present is consistent with the dip in the carbon balance, implying more carbon is being deposited at that time. This further implies less reverse-water-gas-shift and less reverse-Bouduard reactions. However, at steady state, the conversions of CH_4 and CO_2 are equal, consistent with the stoichiometric value of the ratio H_2/CO at that point.

The behavior of the material prepared with x = 0.1 is different. The maximum value of the ratio H_2/CO is greater than 2.0. Initially, the CO_2 conversion is less than that of CH_4, as is the case for the other two materials; however, at steady state, the CO_2 conversion is somewhat greater than that for CH_4. At least in the unsteady-state portion of the data, the catalyst is even less selective to the reverse-water-gas-shift and to the reverse-Bouduard reactions.

Given that the initial bulk structures of the materials using x = 0.2 and x = 0.1 are similar to each other, and different from those with x = 0.75, and given that the reactivity behavior of the material with x = 0.2 is more akin to that with x = 0.75 to that with x = 0.1, it would appear that the active surface structure of the material with x = 0.2 must be closer to that for the material with x = 0.75 than to that for the material with x = 0.1. This hypothesis remains to be proved.

In Figure 3 are shown the XRD patterns of the two extreme materials, corresponding to x = 0.75 and x = 0.1, after 100 h on stream. For the former material, the phases present are WC, Co and C, different from what is present before the reaction (Figure 1) and consistent with those present after the Nanodyne η-Co_6W_6C is on stream. For the material prepared with x = 0.1, the pattern in Figure 3 appears different from that for the corresponding material before reaction in Figure 1. However, the same peaks are present, but in different relative amounts: smaller amounts of Co_3W_3C, and larger amounts of WC, Co and C. The reduction of the catalytic material has continued during the reaction, but is not as complete as that for the material prepared with x = 0.75. The differences in the structure of these materials mirror the changes in their catalytic effectiveness.

100

Conclusions

The Nanodyne η-Co_6W_6C material is a precursor for a catalyst that is at least as good as, or better than, supported Ni or unsupported Mo_2C for the dry reforming of methane. The material prepared in-house with $x = 0.75$ is similarly active, selective and stable, and passes through a similar unsteady-state period. The in-house material has the structure of the commercially obtained material both before and after reaction, Co_6W_6C and $Co/WC/C$ respectively. Materials prepared using more-reducing gas streams ($x \leq 0.2$) show the intercalated carbide Co_3W_3C as part of the bulk structure, as well as Co, WC and C. After reaction, all four materials are still seen in the XRD, but there appears to be less of the intercalated carbide and more of Co, WC and C. The reactivity behavior of material prepared using $x = 0.2$ is different from that using $x = 0.1$. The behavior of the former material is closer to that using $x = 0.75$, but with perhaps a shorter unsteady-state period. Using the material with $x = 0.1$ results in an unsteady-state period with much larger H_2/CO ratios and a steady-state period with CO_2 conversion greater than CH_4 conversion. At least during the unsteady-state period, the material with $x = 0.1$ is less selective to the reverse-water-gas-shift and to the reverse-Bouduard reactions. The difference in the reactivities of the materials with $x = 0.2$ and $x = 0.1$ are hypothesized to be due to different species present on the surface of the two materials.

Future Work

Develop skills, or work with other CFFS researchers, to determine surface species on bimetallic carbides, to quantify reactivity with surface structure.
Develop preparation techniques to obtain catalyst which can produce high H2/CO ratio product stream at steady state conditions (H2/CO = 2 is possible during unsteady state).
Develop preparation techniques to prepare catalyst with high surface areas, > 50 m2/g (currently 30m2/g possible under certain conditions).

References

Iyer, M.V., L.P. Norcio, A. Punnoose, E.L. Kugler, M.S. Seehra and D.B. Dadyburjor, Catal. Lett., accepted.
Iyer, M. V. *New Catalysts for Syngas Production from Carbon Dioxide and Methane*. M.S.Ch.E. Thesis: West Virginia University, Morgantown WV, 2001.
Iyer, M.V., L.P. Norcio, E.L. Kugler and D.B. Dadyburjor, Ind & Eng Chem. Res. **42**(12) 2712 (2003).
E. L. Kugler, L. E. McCandlish, A. J. Jacobson, R. R. Chinaselli, Eta Phase Materials, Methods of Producing the Same, and Use Thereof as Catalyst for Alcohol Synthesis, Hydrocarbon Synthesis, Hydrocarbon Hydrogenation and Hydrocarbon Conversion. US Patent 5,138,111, August 11, 1992.
R.S. Polizzotti, L.E. McCandlish and E.L. Kugler, Multiphase Composite Particle Containing a Distribution of Nonmetallic Compound Particles. US Patent 5,338,330 August 16, 1994.
Lu, G.Q. and S. Wang, CHEMTECH **29**(1) 37 (1999). Data in Table I correspond to $P_{CH4,in}$ = 1.6 atm = $P_{CO2,in}$.

Tsuji, M., T. Miyao and S. Naito, Catal. Lett. **69**, 195 (2000). Data in Table I correspond to $P_{CH4,in} = 0.5$ atm $= P_{CO2,in}$.

Publications and Presentations in Current Year

1. Ref [1]
2. Ref [3]
3. Shao, H.-F., E.L. Kugler, M.V. Iyer and D.B. Dadyburjor, in Proc. Fuel Cell Topical Conference, American Institute of Chemical Engineers (2003)
4. D.B. Dadyburjor. Catalysis for Synthesis-Gas Formation from Reforming of Methane, invited lecture at 16th National Symposium, Catalysis Society of India and 1st Indo-German Conference on Catalysis, Indian Institute of Chemical Technology, India, February 2003.
5. D.B. Dadyburjor, Preparation and Pretreatment of Bimetallic Carbide Catalysts for Dry Reforming of Methane, presented at AIChE Ann. Mtg, San Francisco, November 2003

Table I Comparison of Specific Activity of Nanodyne η-Co_6W_6C-based Catalyst with Others. Based on Ref. [3]. Number is average loss rate of methane per unit surface area (of metal component, if supported) divided by the inlet partial pressure of methane and the inlet partial pressure of carbon dioxide. Data obtained when inlet partial pressures of reactants are equal.

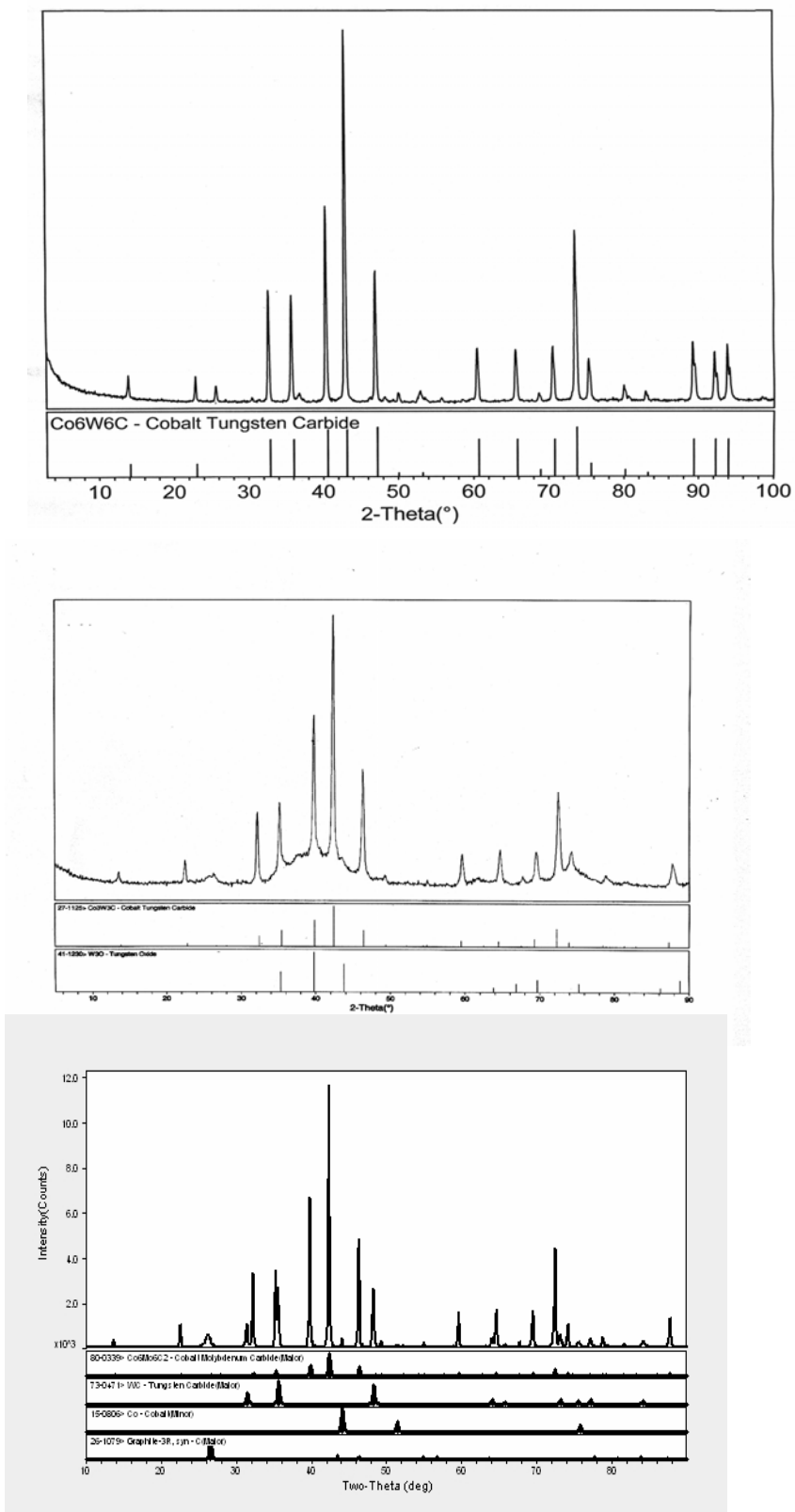| Temperature (°C)	600	650	700	750	800	850	Ref.
Catalyst	Pseudo-Second-Order Rate Constant for Loss of Methane (μmol/s/m^2/atm^2)						
Co_6W_6C (unsup)	0.47	1.25	1.79	2.67	3.72	4.31	[3]
Ni/C	0.39	0.23	0.12	0.24	0.26		[6]
Ni/C-HCl	0.18	0.16	0.19	0.21	0.32		
Ni/C-HNO$_3$	0.098	0.098	0.11	0.14	0.19		
Ni/C-HF	0.094	0.094	0.10	0.14	0.23		
Mo$_2$C (I) (unsup)						1.4	[7]
Mo$_2$C (II) (unsup)						0.89	

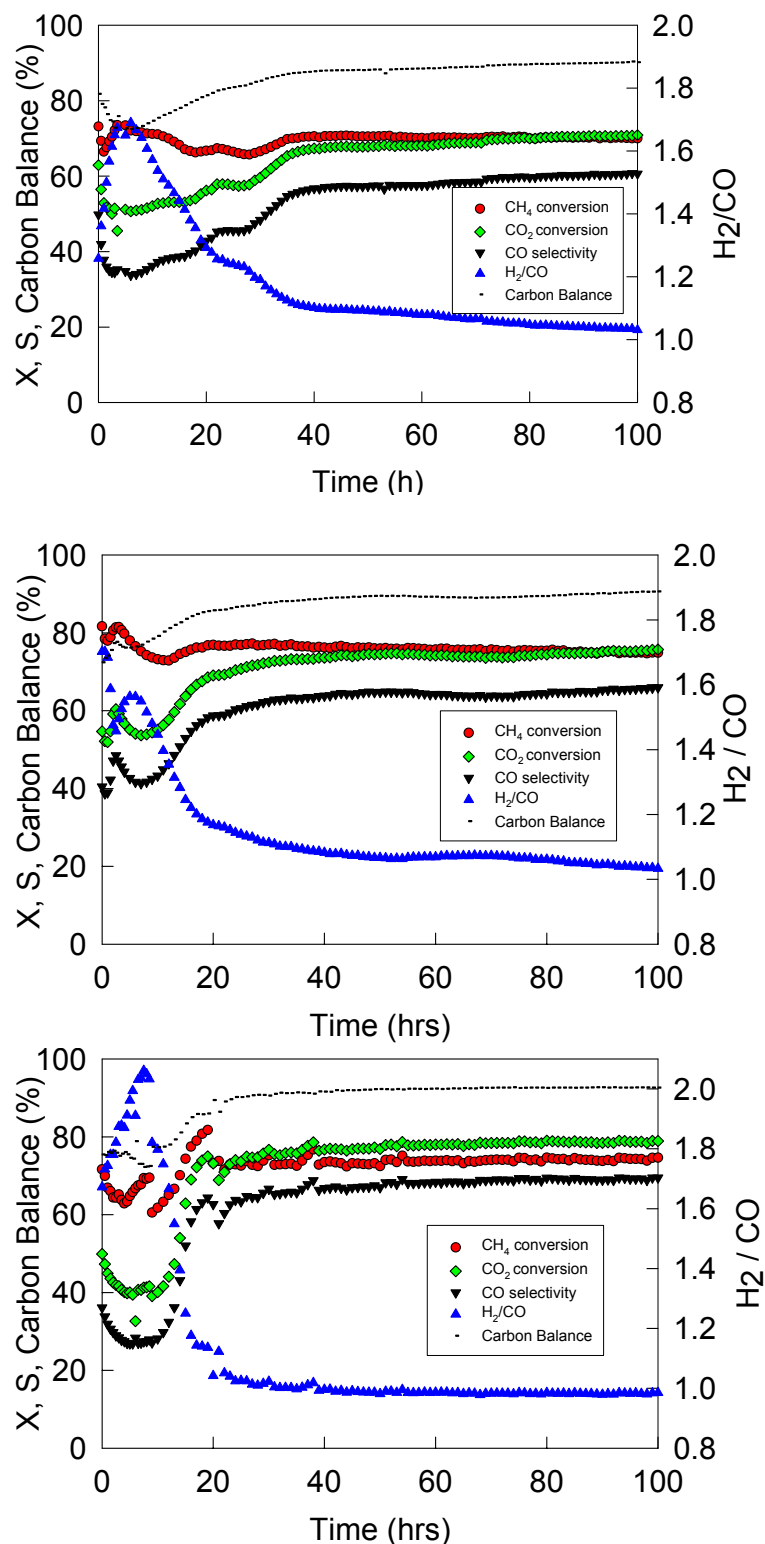Figure 1. XRD patterns of catalyst materials as-prepared. Top:.CO_2/CO Ratio used (x) = 0.75. Mid: x = 0.2. Bottom: x = 0.1

Figure 2. Reactivities of bimetallic-carbide-based catalysts: Top, x = 0.75; Middle, x = 0.2; Bottom, x = 0.1. All reactions were carried out at 850°C and 3.4 atm with $P_{CH4} = P_{CO2}$ and GHSV = 9000 h^{-1}. X, conversion; S, selectivity.
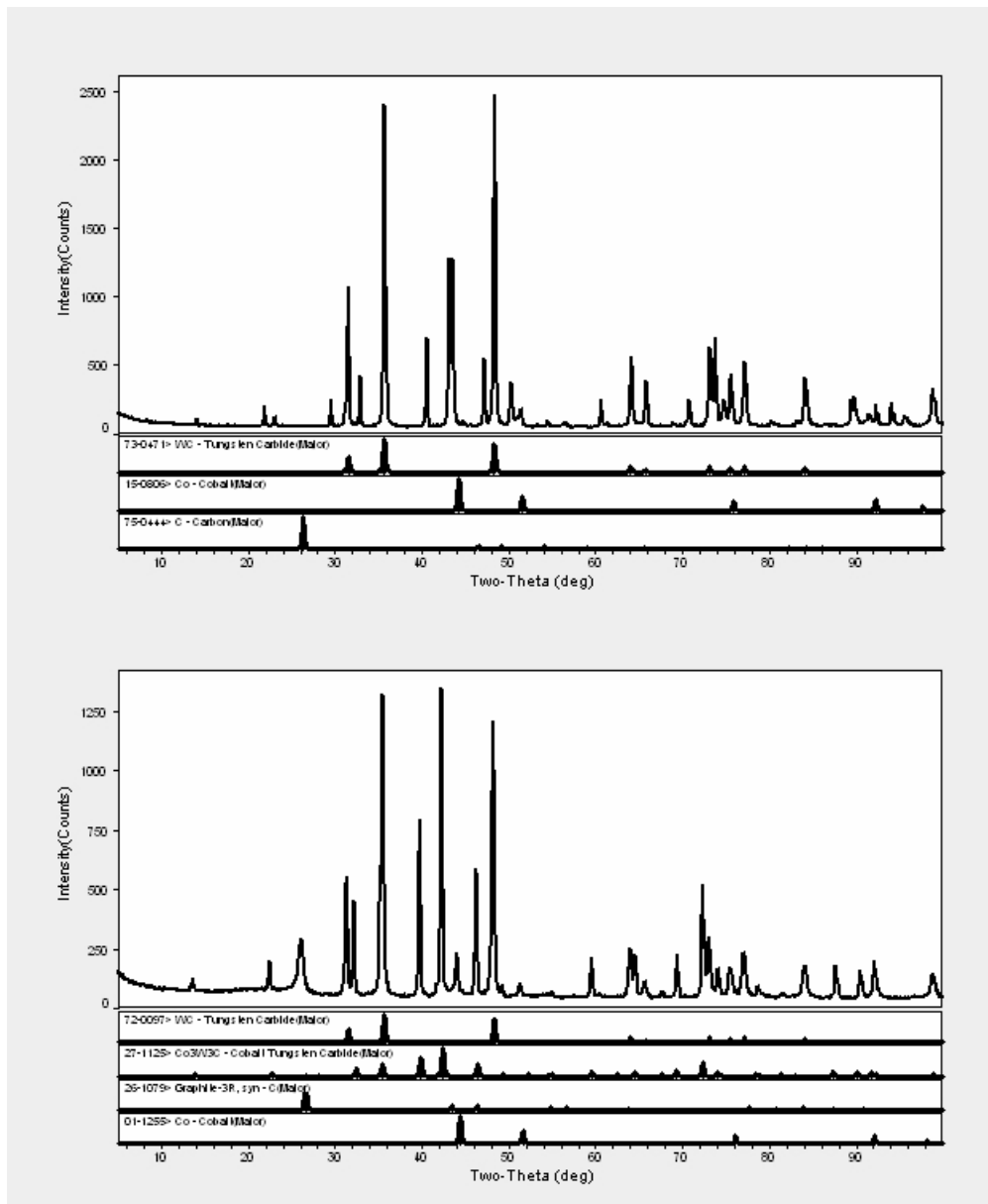
Figure 3. XRD patterns after 100 h on stream. Top, x = 0.75; Bottom, x = 0.1.

Science behind Catalysis in C1 Reactions: Catalyst Characterization and determination of Active Species.

M. S. Seehra, A. Manivannan and P. Dutta
Physics Department, West Virginia University

Introduction

The objectives under this task are to characterize the structural and electronic properties of catalysts used by the CFFS researchers for converting C-1 feedstock into clean liquid transportation fuels and high-value chemicals, and for the efficient production and storage of hydrogen obtained from syngas, hydrocarbons and coals. The measured properties of the catalysts are then correlated with the distributions of the products in an effort to determine the mechanisms of the reactions and to determine the active species and efficiency of a particular catalyst. Samples investigated in this work include those received from other CFFS researchers and some prepared in our laboratory. In this reporting period, we describe the results of our studies on the Co/xerogel catalysts obtained from Eyring et al, Ni/SAPO catalysts obtained from Guin et al, M/Fe/Al$_2$O$_3$ catalysts obtained from Huffman et al, and nanoparticles of CuO and doped and undoped ferrihydrites.

Experimental Procedure

The experimental techniques employed in these studies include the following: (i) X-ray diffraction (XRD) for determining chemical phases, their relative concentration and crystallite size; (ii) Electron magnetic resonance (EMR) for determining the valence states of active species; (iii) SQUID magnetometry to determine the valence states and concentration of magnetic compounds in the catalysts; (iv) FTIR/Photoacoustic spectroscopy for determining the surface species of the catalysts; and (v) Thermogravimetric analysis for determining the range of thermal stability of catalysts and catalyst supports. These experiments are usually carried out over a large temperature range (2K to 370K) in order to extract the useful information from the analysis of the temperature and magnetic field dependence of the data.

Results and Discussion

Results from the Utah Collaboration:
Prof. Eyring's group at Utah have synthesized Co-loaded xerogels as catalysts for the Fischer-Tropsch synthesis. Their data on the yields of alkanes for three loadings of Co show an increase in the yield with increase in Co. We received seven samples (Table I) from Prof. Eyring: three virgin samples with 5, 10 and 15% of Co loadings and four samples extracted from different parts of the reactor after FT reaction.

These samples were characterized by room temperature x-ray diffraction (XRD), and variable temperature (5K to 350K) magnetometry and EMR (Electron Magnetic Resonance) spectroscopy. Findings from these investigations, recently submitted as a research paper to Energy & Fuels [1], are summarized below.

**Table I. Summary of the Results for the Co/xerogel catalysts**

Sample	Description	XRD	Magnetic	EMR
1	0.05Co/xerogel – virgin	CoO, silica	Primarily CoO	Co° (weak), Co^{2+}
2	0.10 Co/xerogel – virgin	CoO, some Co°, silica	Co, CoO	Co° (weak), Co^{2+}
3	0.15 Co/xerogel – virgin	CoO, Co°, silica	Dominated by Co	Co°(weak), Co^{2+}
4	Front-gas entrance side, 0.05 Co	Co°, silica	Primarily Co°	Co°(strong), Co^{2+} (weak), Co^{+}
5	Back-gas exit side, 0.05 Co	Silica, CoO, Co°	Co°,with some CoO	Co°(medium), Co^{2+}, Co^{+}
6	6 hrs. used, 0.05 Co	CoO, some Co, silica	CoO, some Co°	Co° (strong), Co^{2+}
7	12 hrs. used, 0.05 Co	CoO, some Co°, silica	Co°, some CoO	Co° (strong), Co^{2+}

In Fig. 1, the XRD patterns of the seven samples are shown along with the identification of elemental Co, CoO and the broad peak due to SiO$_2$ support. Clearly, the relative amounts of Co and CoO are different in the various samples. The temperature dependence of the magnetic susceptibility χ for the seven samples is shown in Fig. 2. Since Co° is a ferromagnet with large magetization (M_s = 1400 Oe) and high ordering temperature (T_c = 1388K) whereas CoO is an antiferromagnetic (T_c = 290K) with relatively small χ = 7 x 10^{-5} emu/g at room temperature, the measured χ is dominated by Co°. In the data of Fig. 2, only sample 0.05Co/xerogel does not show the presence of Co° since χ for this sample is similar to that of bulk CoO except for the shift of T_c from 290K to about 200K because of the nanosize (~6nm) of the CoO phase. Higher the magnetic susceptibility χ, larger the amount of Co° relative to CoO. In Fig. 3, we show the hysteresis loops measured at 5K for the 12-hr used sample in ZFC (zero-field-cooled) and FC (field-cooled) conditions. The shifted loop for the FC case strongly suggests the presence of a ferromagnetic/antiferromagnetic interface, in this case Co°/CoO. This is an important observation as explained later.

In Fig. 4, we show the temperature dependence of EMR spectra for one sample, showing the temperature evolution of three EMR lines, lines 1, 2 and 3. Using the available information from literature, line 1 is identified with Co°, line 2 with Co^{2+} and line 3 with Co^{1+}. In Table I. The species observed in the other samples by EMR spectroscopy are listed. The species of Co^{2+} and Co^{1+} can only be observed from partially reduced CoO since in stoichiometric CoO, no EMR signal is observed. This important observation leads us to conclude that in none of the samples of Table I, the reduction of CoO to Co° is complete.

The above studies lead to the following model regarding the structural/electronic characteristics of the Co/xerogel catalyst. The Co(NO$_3$)$_2$ · 6H$_2$O used in the synthesis of Co/xerogel is first

reduced to Co_3O_4 under hydrogenation at 500ºC, which then further undergoes the following reactions:

$$Co_3O_4 + H_2 \rightarrow 3CoO + H_2O \qquad -----(1)$$
$$CoO + H_2 \rightarrow Co^o + H_2O \qquad . \qquad -----(2)$$
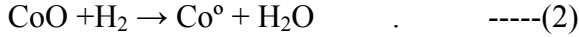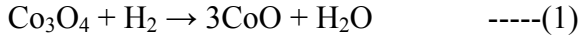
Our results show that reaction (1) is complete in our samples, whereas reaction (2) is only partially complete. Since we have observed Co/CoO interface, this leads us to suggest a core-shell model with Coº as the shell and CoO as the core. The further reduction of the CoO core is limited by the diffusion of H_2 through the Coº shell thus leading to only partial completion of reaction (2). This suggests that longer reduction time at 500ºC may be necessary for getting better yields in the FT synthesis.

Results from the Auburn Collaboration:

Prof. Guin's group have synthesized Ni doped SAPO catalysts for methanol to olefin conversion. In Table II, we list the six samples of Ni SAPO samples which we received for characterizing using magnetic and EMR studies. In EMR spectroscopy, we did not observe any signal due to Ni even at 5K. This is not completely surprising since Ni^{2+} is not always easy to detect in EMR spectroscopy. In SQUID magnetometry, we measured magnetization M and hence magnetic susceptibility $\chi = M/H$, from 2K to 350K and M vs. H at 2K in magnetic fields upto ± 55kOe. In Fig. 5, we show χ vs. T for four samples (as listed) and fit of the data to the modified Curie-Weiss law $\chi = \chi_o + C/(T - \theta)$. For the other two samples, similar data is shown in Fig. 6, where a peak in χ is observed near 5K below which there is a bifurcation of the FC and ZFC data. This is quite characteristic of nanoparticle systems, suggesting the presence of either Ni or NiO nanoparticles. The M vs. H data at 2K show symmetric hysteresis loops even when the samples are cooled in 20kOe. Thus in these samples, Ni/NiO ferromagnetic/antiferromagnetic) interface is absent. For the other four samples, M vs. H data show no hysteresis.

Another important contribution from the above studies is the determination of Ni concentration in these samples, using the magnitudes of the Curie-Weiss constant C determined from the fit of the χ vs. T data. These concentrations are listed in Table II. It is evident that for the two samples where hysteresis loops and nanoparticles are observed, the Ni concentration is higher than those of the other four samples. Correlation of these results to the product yields in the experiments of Guin et al is now underway. It is worth noting that the small concentrations of Ni determined here from magnetic studies, could not be determined from XRD studied since with XRD, one cannot observe any phases with concentrations less than 1%.

Table II: Magnetic susceptibility χ vs. T fitted to $\chi = \chi_o + C/(T - \theta)$

Samples	χ_0 (10^{-7})	C(10^{-5})	θ(K)	Wt. % Ni	Ni - NP
P-9: NiSAPO-18	6.3	2.0	0	0.093%	No
P-10: NiSAPO-34	9.3	6.0	-2	0.28 %	Small amount
P-13: NiSAPO-44	4.6	5.0	0	0.23 %	Small amount
P-32: NiSAPO-47	18.6	1.5	-1	0.07 %	No
P-30: NiSAPO-56	6.4	7.0	+4	0.33 %	Yes
P-20: NiSAPO-17	5.2	14.0	+4	0.65 %	Yes

In our recent published paper with Guin et al [2], we reported results of methanol to olefin conversion using SAPO-34 molecular sieves modified with Co, Mn and Ni. From these studies,

MnSAPO-34 was found to be the best catalyst based on catalyst lifetime. In the case of Ni-SAPO-34, in which part of the Ni exists as Ni nanoparticles outside the SAPO framework, unusually high amounts of methane were observed in the products. Further details are given in the published paper [2].

Results from the Kentucky Collaboration:
Using the reduced binary catalysts $0.5\%M/4.5\%Fe/Al_2O_3$ (M = Ni, Mo, Pd), Huffman et al at Kentucky have demonstrated efficient production of H_2 gas from methane(CH_4) at 700ºC. We have used room temperature XRD and EMR spectroscopy at 5K and 300K to determine the nature of the different phases present in these materials before and after the reaction with CH_4 at 700ºC. Details of these studies have recently appeared in a publication [3]. The main conclusions from these studies are: (i) the presence of Ni, Mo and Pd promotes the reduction of iron oxides to Fe^o which is an active catalyst and gets changed to Fe_3C in the reaction; (ii) the significant presence of Fe^{3+}/Al_2O_3 and iron oxides is detected which do not undergo any significant change in the reaction, leading to the suggestion that most of the CH_4 to H_2 conversion is perhaps facilitated by these species. For details, see Ref. [3].

Another project that is being brought to conclusion is the structural and magnetic properties of ferrihydrite nanoparticles ($FeOOH \cdot nH_2O$) doped with Ni, Mo and Ir. The binary catalysts $M/Fe/Al_2O_3$ discussed above are prepared through the ferrihydrite route, thus the interest in ferrihydrites. Our studies have shown that Ni substitutes for Fe throughout the nanoparticles whereas doping with Mo and Ir occurs primarily at the surface of the nanoparticles. The latter effect provides additional thermal stability to the doped ferrihydrites in catalytic reactions. Details of these studies are available in a detailed paper [4] which has been tentatively accepted for publication in Physical Review. The manuscript is now under revision, following suggestions by the referees.

Other Investigations:
We have collaborated with the Kugler-Dadyburjor team at WVU to investigate the Co_6W_6C based catalysts for producing syngas (CO + H_2) from methane. Details of these studies are described in the Kugler-Dadyburjor report and in the recently accepted paper [5].
The studies on the synthesis and structural/electronic properties of CuO nanoparticles which we undertook about two years ago in order to investigate their catalytic properties are being brought to conclusion. In a recently accepted paper [6], we show how the electronic properties vary systematically as the particle size D is reduced from 37nm to about 5nm. The 1/D variation reported in this paper underlines the important role of surface electron spins which is crucial in understanding catalysis.

Along the same lines, we have completed our studies on the temperature variations of EMR spectra in pure and doped ferrihydrites [7, 8]. Some of these studies were carried out at ultra high frequencies using the facilities available at the National High Magnetic Field Laboratory in Tallahassee, Florida.

Conclusions

1. For the cobalt loaded xerogel catalysts, our work has shown that Co in not completely reduced to Co^0, perhaps limiting its effectiveness in the Fischer – Tropsch synthesis. Thus larger reduction time or a different strategy is necessary to achieve the complete reduction to Co^0. We will work with Eyring et al to achieve this goal.
2. For the Ni/SAPO catalysts, our magnetic studies have determined the Ni loadings in the catalysts and shown that higher nickel loadings lead to precipitation of Ni as nanoparticles. These pieces of information were not available from any other technique. Working with Guin et al, we will next determine the role of Ni in the catalytic activity of methanol to olefin conversion.
3. For the reduced binary catalysts $0.5\%M/4.5\%Fe/Al_2O_3$ used in the production of H_2 from CH_4, our studies have shown that although a part of the activity is due to Fe^0, the dominant catalytic role is played by Fe^{3+}/Al_2O_3 and iron oxides which do not undergo any changes in the reaction. This is an important result from our work.
4. Our basic studies on the nanoparticles of CuO and doped and undoped ferrihydrites have established the important role played by the uncompensated surface spins of Cu^{2+} and Fe^{3+} in the measured properties and hence in catalytic reactions involving nanoparticle catalysts.
5. Our studies in a variety of catalysts provided by CFFS researchers described here have established the importance of multitechnique approach to catalyst characterization. Availability of a number of techniques in our laboratory, collaboration with the CFFS researchers who provide us "before" and "after" reaction samples of their catalysts and analytical skills comprise the major strength of our program.

Future Plans

The studies described above show that EMR spectroscopy is particularly useful for the detection of different valence state of cobalt such as Co^o, Co^{1+}, Co^{2+}…. Since cobalt is the primary catalyst in the Fischer-Tropsch (FT) synthesis, and a number of CFFS researchers are involved in the FT synthesis, they will provide us samples of their catalysts at different stages of the reactions for characterization. We have already received seven samples of Co/SiO_2 catalysts from Prof. Roberts' group at Auburn and other samples to be received include the following: Co/aerogel samples from Professor Eyring; Co/SAPO samples from Professor Guin and samples of Fe-based catalysts from Prof. Huffman, Prof. Wender and Prof. Ernst. Thus, analytical characterization of these samples by XRD, magnetometry, FTIR/photoacoustic spectroscopy and EMR spectroscopy, and analysis of the data will consume a large part of our effort during the coming year.

During this year, we also plan to initiate a new effort on the "development of nanocrystalline alloys for hydrogen storage." Storage of hydrogen in solids as hydrides is considered by DOE to be an important area of future research. According to a recent report (G. Gundiah et al, J. Mater. Chem. 13, 209 (2003)), reliable solid materials to store H_2 up to the 6.5wt% benchmark set by DOE have not yet been developed. In our program, we will synthesize and test nanocrystalline alloys for hydrogen storage applications. After a thorough review of the literature which is currently underway, we will select the most promising alloys for our studies. Research reported in literature suggests that alloys based on Mg, Ni and Zr in nanocrystalline form have the best

potential for applications in H_2 storage (A.Y. Esayed, J. Power Energy <u>214</u>, 669 (2000)). We will prepare the nanocrystalline alloys by mechanical alloying to yield high surface areas and improved sorption kinetics. Then alloys will be characterized by x-ray diffraction and BET surface area measurements, followed by sorption and desorption kinetics investigations by thermogravimetric analysis (TGA). Experimental facilities such as a miller/mixer for mechanical alloying and XRD and TGA studies are available in our laboratory and BET surface area measurements can be done by a commercial company. By the end of summer 2004, we expect to report results of our initial studies in this area.

<u>References</u>

1. M. S. Seehra, A. Manivannan, P. Dutta, B. C. Dunn, P. Cole, D. J. Covington and E. M. Eyring, "Characterization of Co in Co-loaded xerogels used in Fischer-Tropsch synthesis," Energy & Fuels (submitted).
2. D. R. Dubois, D. L. Obrzut, J. Liu, J. Thundimadathil, A. M. Prakash, J. A. Guin, A. Punnoose and M. S. Seehra, "Conversion of methanol to olefins over Co, Mn and Ni incorporated SAPO-34 molecular sieves," Fuel Process. Technol. <u>83</u>, 203-218 (2003).
3. A. Punnoose, N. Shah, G. P. Huffman and M. S. Seehra, "X-ray diffraction and electron magnetic resonance studies of $M/Fe/Al_2O_3$ (M = Ni, Mo and Pd) catalysts for CH_4 to H_2 conversion," Fuel Processing Technol. <u>83</u>, 263-273 (2003).
4. A. Punnoose, M. S. Seehra, N. Shah and G. P. Huffman, "Magnetic properties of ferrihydrite nanoparticles doped with Ni, Mo and Ir," Phys. Rev. B (tentatively accepted; manuscript being revised after referee review).
5. M. V. Iyer, L. P. Norcie, A. Punnoose, E. L. Kugler, M. S. Seehra and D. B. Dadyburjor, "Catalysis for synthesis gas formation from reforming of methane," Topics in Catalysis (accepted).
6. M. S. Seehra and A. Punnoose, "Size dependence of exchange-bias and coercivity in CuO nanoparticles," Solid State Commun. (accepted)
7. A. Punnoose and M. S. Seehra, "Temperature dependence of paramagnetic resonance in pure and doped ferrihydrite nanoparticles," Book chapter in "EPR in the 21st. Century: Basics and Applications to Material, Life and Earth Sciences," edited by A. Kawamori, J. Yamauchi and H. Ohta (Elsevier Sciences 2002) pp.162-167.
8. A. Punnoose, M. S. Seehra, J. van Tol and L. C. Brunel, "High-frequency electron magnetic resonance studies of ferrihydrite nanoparticles and evidence for surface spin-glass transition," (manuscript under preparation).
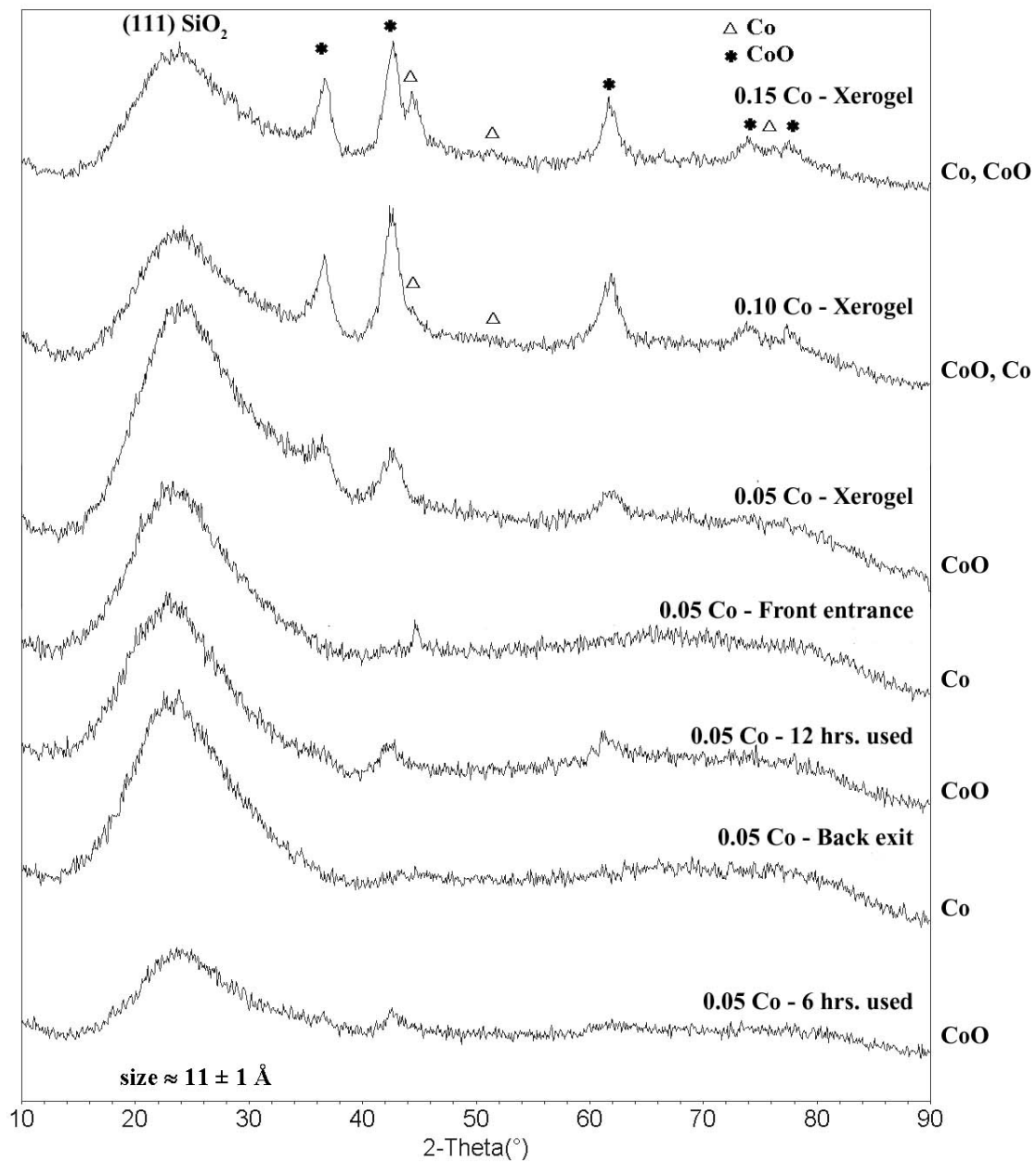
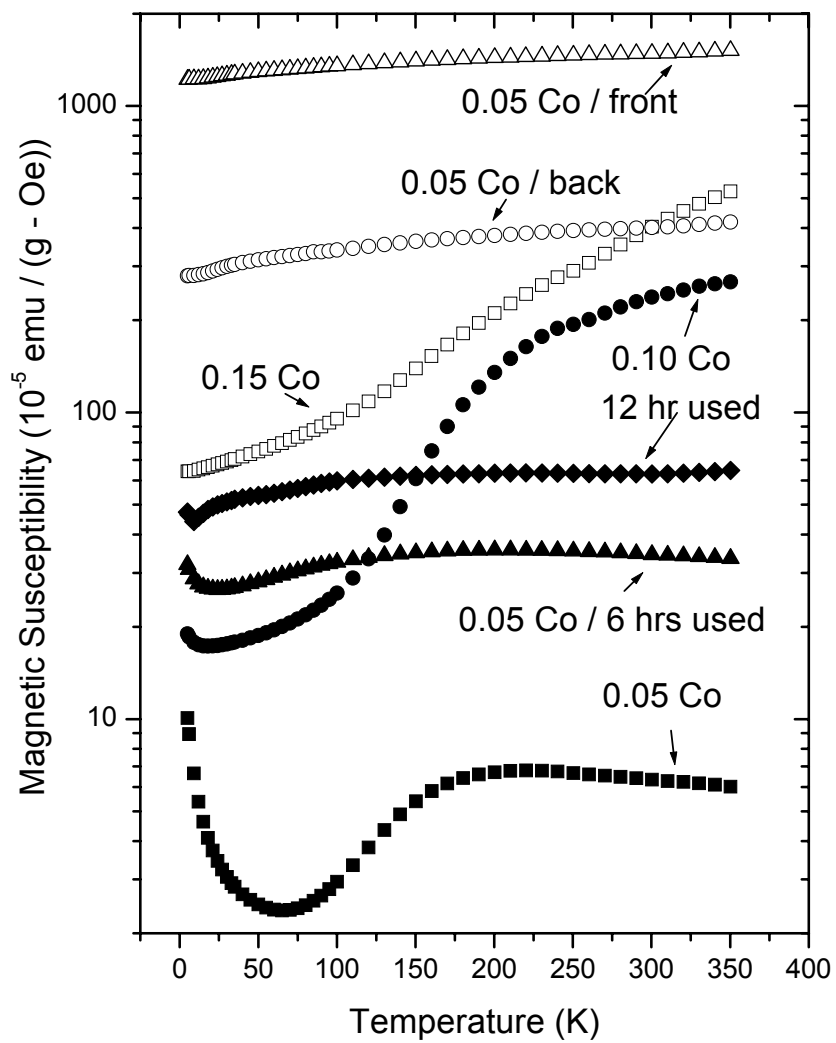Fig. 1: XRD spectra of the seven samples of Table I.

Fig. 2: Magnetic susceptibility vs. temperature for samples of Table I.
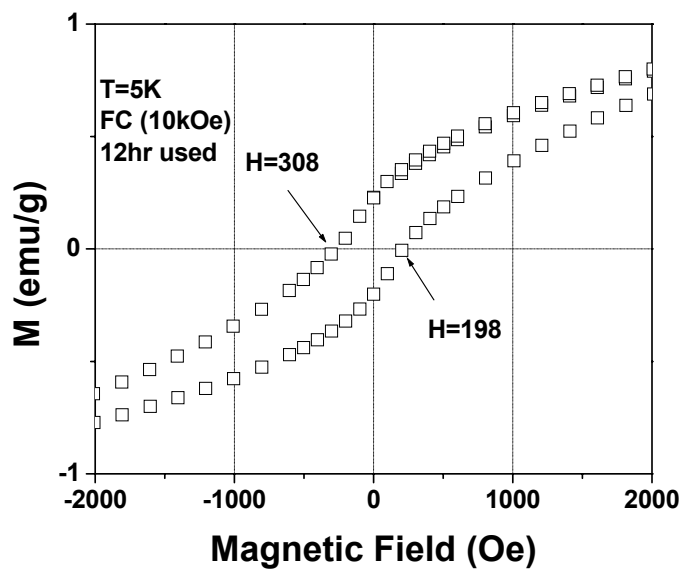
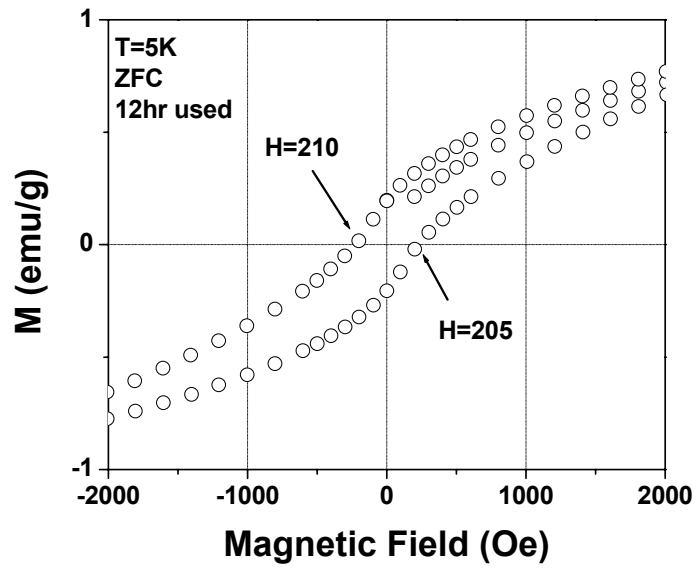Fig. 3. Hysteresis loops for the 12-hr used sample for the ZFC (upper) and the FC (lower) cases.
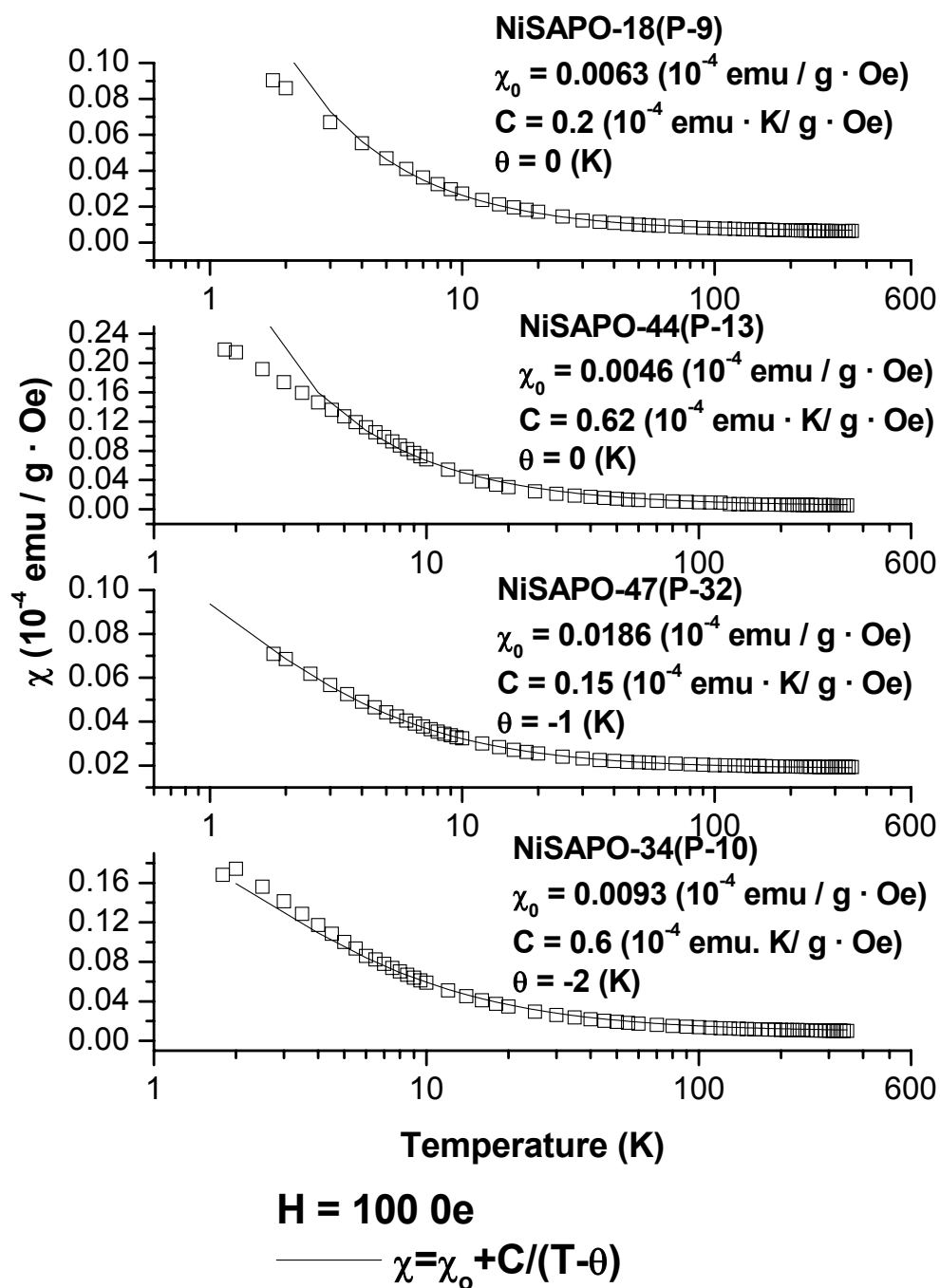
Back 0.05 Co/Xerogel

f = 9.28012 GHz

Line 1 – Co^0
Line 2 - Co^{2+} g = 4.393
Line 3 - Co$^+$ g = 2.05

2

3

7 K

18 K

28K

37 K

55 K

151 K

110 K

78 K

1

50

2550

5050

Magnetic Field (Oe)

Fig. 4. EMR spectra at different temperatures.

NiSAPO-18(P-9)

$\chi_0 = 0.0063 (10^{-4}$ emu $/$ g $\cdot$ Oe)

C = 0.2 (10^{-4} emu $\cdot$ K$/$ g $\cdot$ Oe)

$\theta = 0$ (K)

NiSAPO-44(P-13)

$\chi_0 = 0.0046 (10^{-4}$ emu $/$ g $\cdot$ Oe)

C = 0.62 (10^{-4} emu $\cdot$ K$/$ g $\cdot$ Oe)

$\theta = 0$ (K)

NiSAPO-47(P-32)

$\chi_0 = 0.0186 (10^{-4}$ emu $/$ g $\cdot$ Oe)

C = 0.15 (10^{-4} emu $\cdot$ K$/$ g $\cdot$ Oe)

$\theta = -1$ (K)

NiSAPO-34(P-10)

$\chi_0 = 0.0093 (10^{-4}$ emu $/$ g $\cdot$ Oe)

C = 0.6 (10^{-4} emu. K$/$ g $\cdot$ Oe)

$\theta = -2$ (K)

χ (10^{-4} emu $/$ g $\cdot$ Oe)

Temperature (K)

H = 100 0e

—— $\chi = \chi_o + C/(T-\theta)$

Fig. 5: χ vs. T for the samples as listed (see Table II).

116
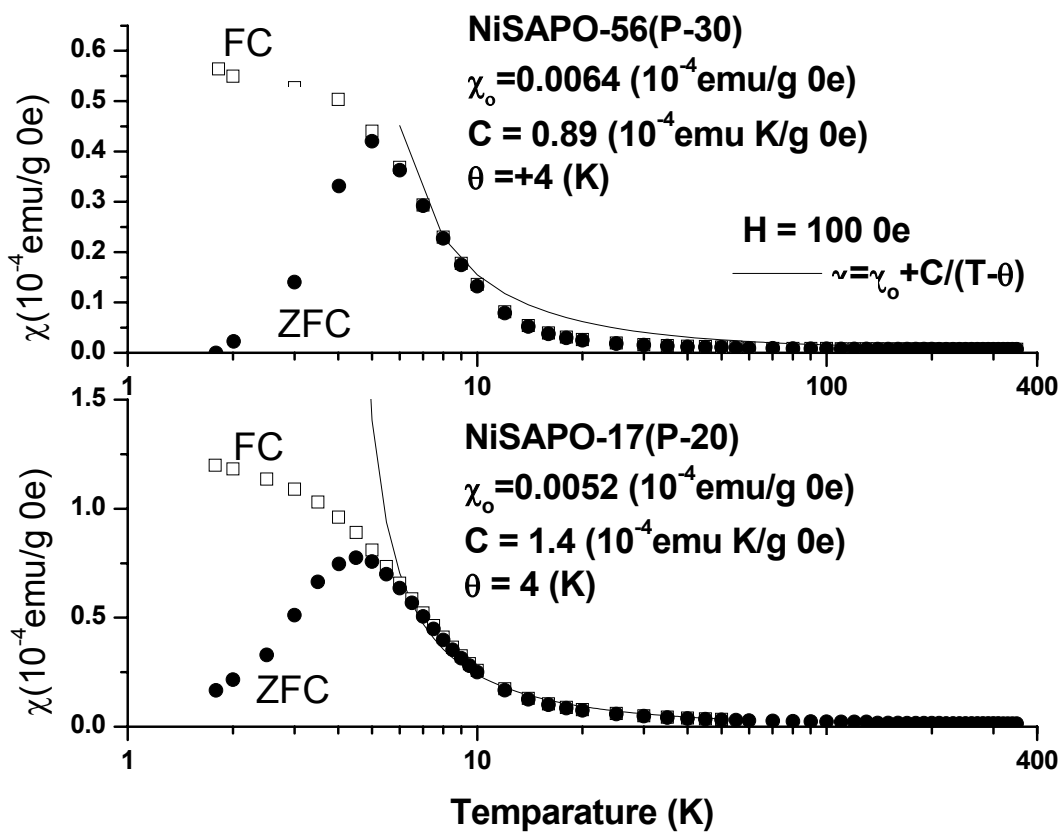
Fig. 6: χ vs. T for two samples of Table II.

Science behind catalysis in C1 reactions: XAFS studies of metal-doped SAPO and aerogel/xerogel catalysts

Frank E. Huggins and Artur Braun
University of Kentucky

Ni, Co, and Mn-doped SAPO catalysts

Introduction

In conjunction with Prof. J. Guin and co-workers (Auburn University), XAFS and other synchrotron techniques are being used to characterize the metal-doped silica-alumina-phosphate (SAPO) materials that are being synthesized at Auburn University. These materials have structural features in common with zeolites and form similar three-dimensional cages with atom and molecule-sized cavities within the framework structures. There is currently much interest in introducing metal atoms and ions in these materials for the development of new catalytic materials for possible C1 chemistry applications. The materials we have received to date from Dr Guin and his group consist of various different SAPO catalysts into which one or more cation species, such as Mn, Co and Ni, have been introduced.

Experimental Procedure:

The SAPO materials have been examined at the appropriate K-shell X-ray absorption edge using XAFS spectroscopy. Such investigations were carried out at Beamline 18B of the National Synchrotron Light Source (NSLS), Brookhaven National Laboratory. The experiments were conducted in fluorescence geometry and metallic foils were used as the primary calibration standards. Standard data reduction methods were used to convert the raw data to XANES and EXAFS/RSF spectra.

Results and Discussion:

Figure 1 shows the Ni XANES spectra obtained for four different nickel-containing SAPO catalysts. The spectra exhibit only very minor differences from each other and look quite different from that reported previously for SAPO-5 [2]. In particular, the height of the small pre-edge peak at about 0 eV is extremely small (Figure 2) and incompatible with tetrahedrally bound Ni^{2+} reported for Ni in SAPO-5 and SAPO-34 [2]. This suggests that the Ni^{2+} in the catalysts prepared at Auburn may not be contained in the framework structure (tetrahedral site), but in a centro-symmetric octahedral site. The corresponding Ni EXAFS/RSF spectra are shown in Figure 3. These spectra show just one major peak arising from a nearest neighbor shell of atoms at about 1.65 A. Such a peak is more consistent with an octahedral coordination by oxygen anions rather than a tetrahedral coordination; however, a more rigorous analysis of the EXAFS data needs to be carried out to confirm this result.

Other samples of Ni-doped SAPO-34 yield Ni XAFS data that differ from those in Figures 1-2. Figures 4 and 5, respectively, show the Ni XANES spectra of samples NJ-6 and NJ-8 and the

EXAFS/RSF spectrum for NJ-6. The Ni XANES spectra for these two samples differ from those shown in Figure 1 (note the prominent peak at about 35 eV) and, furthermore, significant differences are also seen for the RSF/EXAFS spectrum (Figure 5) for sample NJ-6 in comparison to those in Figure 3. Although there is some similarity of the data for these samples and $NiAl_2O_4$, the data for which are shown in Figure 6, there remain differences that suggest that other nickel phases are also present. These results, however, do suggest that some of the Ni is present as $NiAl_2O_4$ in these two samples

The Co XANES spectra for Co-doped SAPO materials look similar to the Ni XANES of Ni-doped SAPO materials shown in Figure 5, whereas the Mn XANES spectra for the Mn-doped SAPO phases look quite different. Indeed the two Mn-doped SAPO materials exhibit significant differences from each other (Figure 11). As for Ni, we interpret the Co XANES data (Figure 12) as indicating octahedral forms of Co, rather than tetrahedral Co forms, despite the fact that Co^{2+}, with its d^7 electron configuration, should show a much stronger tendency than Ni^{2+}, a d^8 electron configuration, to form tetrahedral-bonded species.

In addition to the XAFS data reported here, some small angle X-ray scattering (SAXS) measurements were attempted on some of the samples using beam-time at the Advanced Photon Source, Argonne National Laboratory. The SAXS data for these catalysts showed little structure and therefore did not prove to be very interesting.

Conclusions:

XAFS spectroscopy has been used to investigate the local structure around the elements, Ni, Co and Mn, that have been added to the SAPO catalyst formulations to promote higher reactivity. Preliminary analysis of the XAFS data suggests that Ni and Co are not in the tetrahedral framework sites as reported for similar previous systems [2].

Future Work

Further analysis of existing data will be attempted to confirm the conclusions reached in this preliminary study and new data will be obtained as new catalysts are prepared. There is a need to systematize the spectroscopic information and relate it to differences in the synthesis of these materials.

Reference

1. Y. Xu, J. W. Couves, R. H. Jones, R. A. Catlow, G. N. Greaves, J. Chen and J.M. Thomas, *X-ray absorption studies of framework substituted aluminium phosphate and silico-aluminium phosphate molecular sieves: the environment of nickel in NiAPO-5 and NiAPSO-34,* **J. Phys. Chem.,** 52, 1229-1234, (1991).
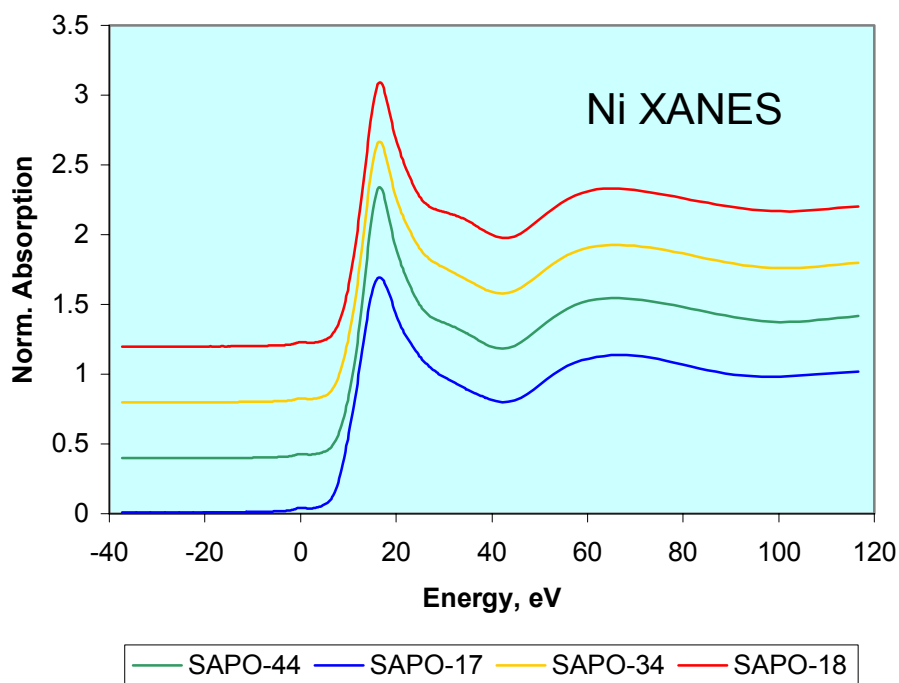
Figure 1: Ni XANES spectra of various SAPO catalysts. The numerical designation for the catalysts indicates its structural type. Zero point of energy for Ni is 8,333 eV.
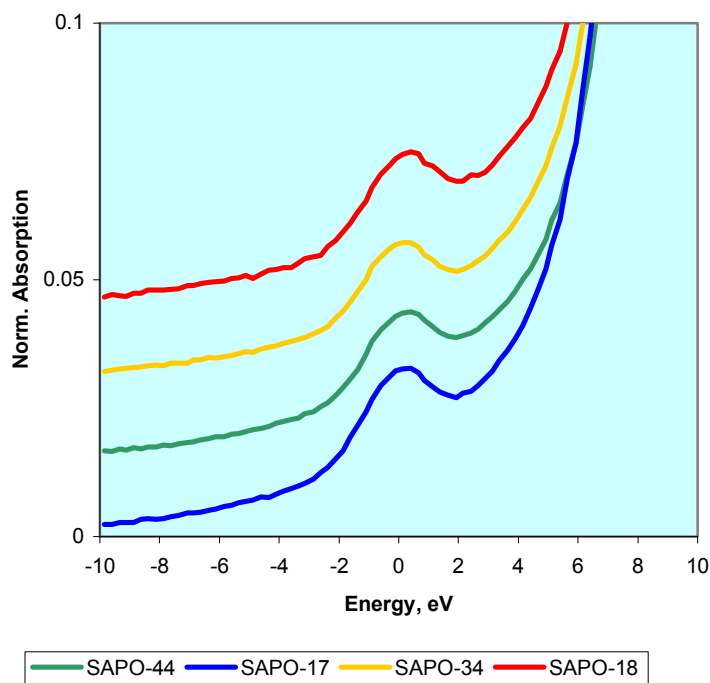

Figure 2: Detail of Ni XANES spectra indicating the small size of the pre-edge peak. Note that the vertical offsets for these curves are different than those for the corresponding XANES spectra shown in Figure 1.
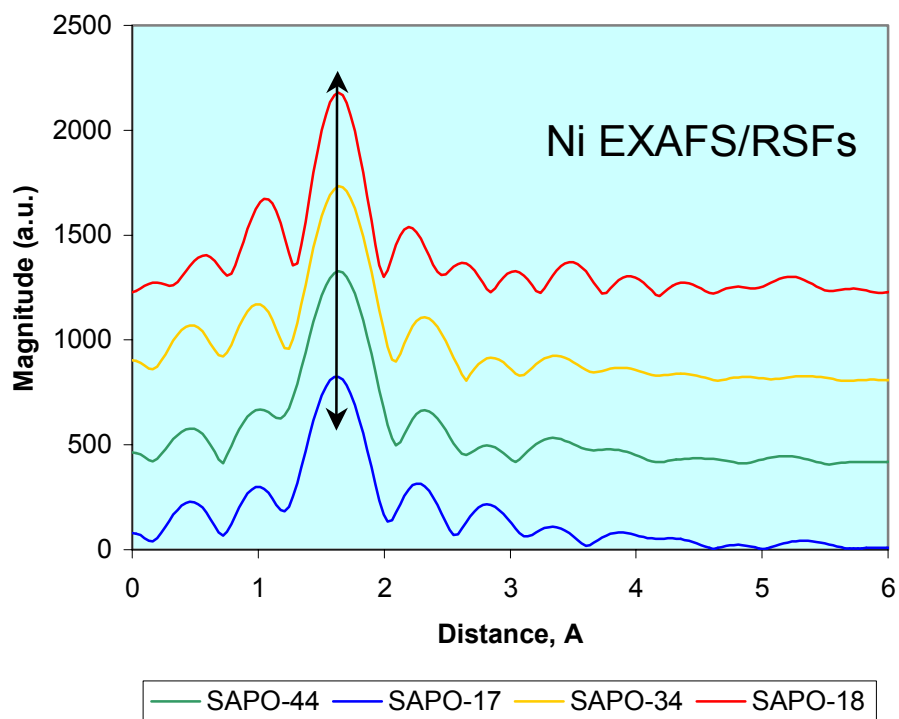
Figure 3: EXAFS/RSF spectra for Ni in various SAPO catalysts. The major peak occurs at a phase-shift uncorrected distance of ~1.65 A.

.
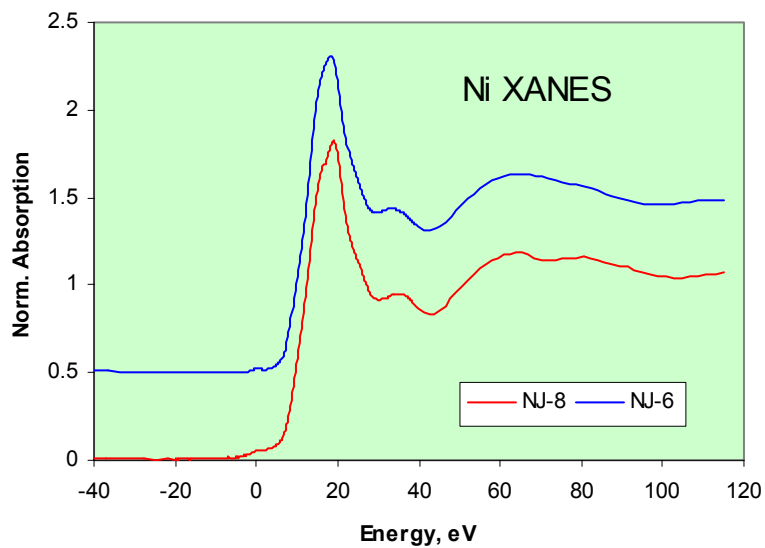
Figure 4: Ni XANES spectra for samples NJ-6 and NJ-8. Note the prominent peak at about 35 eV that is not present in any of the Ni XANES spectra shown in Figure 5.
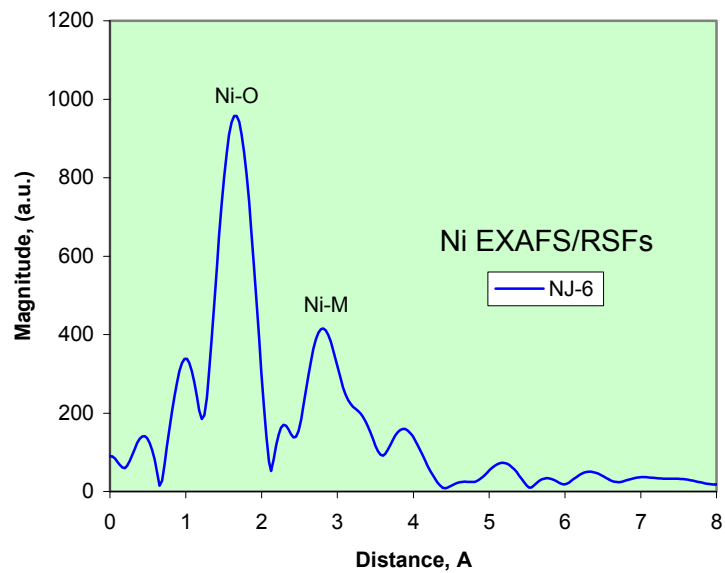
Figure 5: EXAFS/RSF spectrum for sample NJ-6. Note the prominent peak due to next nearest neighbor metal ions (M = Al, Ni) at about 2.9 A
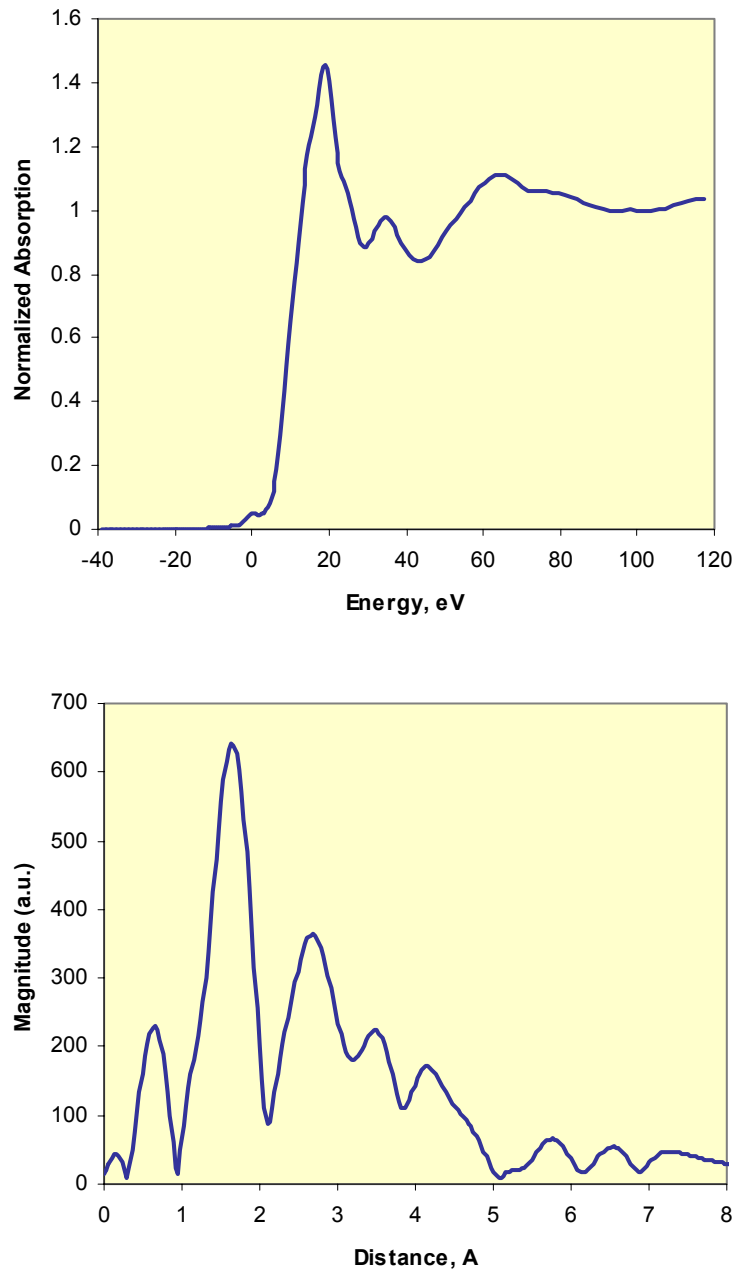
Figure 6: Comparative Ni XANES (top) and EXAFS/RSF (bottom) data for NiAl$_2$O$_4$
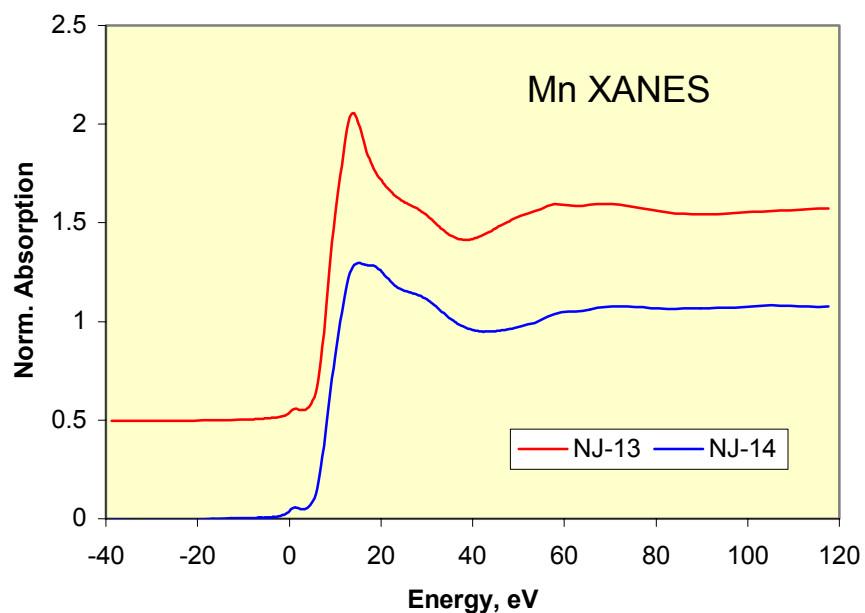
Figure 7: Mn XANES spectra of SAPO samples NJ-13 and NJ-14. Zero point of energy corresponds to 6,539 eV.
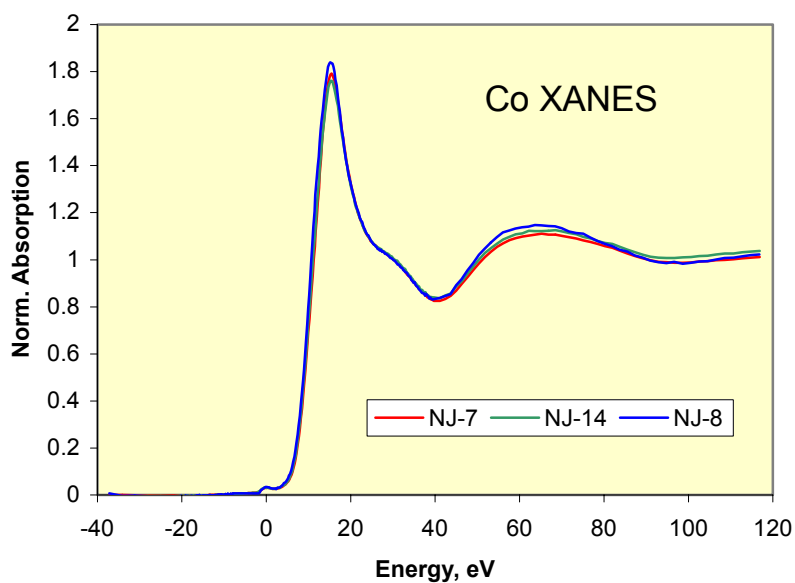

Figure 8: Co XANES spectra of SAPO samples NJ-7, NJ-8, and NJ-14. Note the similarity of the three spectra and also the small size of the pre-edge peak at about 0 eV. Zero point of energy corresponds to 7,709 eV.

Co and Fe-doped silica aerogel/xerogel catalysts

Introduction

In conjunction with Prof. Eyring, Dr. Brian Dunn, and co-workers (U. of Utah), Co and Fe XAFS and Fe Mössbauer spectroscopy and ultra-small angle X-ray scattering (USAXS) studies have been initiated of metal-doped silica xerogel and aerogel catalyst materials that are being synthesized at the University of Utah. These catalysts, which are described in more detail elsewhere in the report by Eyring et al., are being developed for possible use as catalysts for Fischer-Tropsch applications. These materials are doped with metal species, such as Co and Fe, which are then reduced to the metallic state. Such procedures not only affect the metal speciation, but may also change the structure of the aerogel and xerogel materials. The speciation changes can be followed by the spectroscopic techniques, whereas the short-range and long-range structural changes can be assessed by USAXS techniques.

Some very interesting results have been obtained by application of the USAXS technique to the undoped and Co-doped aerogel and xerogel materials.

Experimental Procedure

Cobalt and iron XAFS spectroscopy was carried out at beamline X-19A of the National Synchrotron Light Source (NSLS) at Brookhaven National Laboratory. Conventional XAFS experimental procedures were used to measure the spectra for the major iron in transmission geometry and for the lesser amounts of Co in fluorescence geometry. Standard analysis methods were used to convert the raw XAFS data to XANES and EXAFS/RSF spectra. Iron Mossbauer spectroscopy was performed at the University of Kentucky using a Co(Pd) source. Data analysis was done according to well-established procedures.

The USAXS work was carried out at beamline 33-ID at the UNICAT sector of the Advanced Photon Source (APS) at Argonne National Laboratory (ANL). At this beamline, a Bonse-Hart setup allows one to record scattering curves (SC) using a photodiode detector with an angular resolution of 0.0001 $Å^{-1}$ over a q-range from 0.0001 $Å^{-1}$ to 1.0 $Å^{-1}$. Typical data acquisition times for 150 equidistant data points over this q-range were about 15 minutes. The USAXS data are corrected for instrumental effects. Samples of the aerogel and xerogel materials, which came in cylindrical shapes (as a consequence of the way they were synthesized), were cut into about 1 cm thick fragments and taped in place in the X-ray beam.

Results and Discussion

Only one sample has been examined by the spectroscopic techniques in detail so far: a silica xerogel doped with a major amount of iron and a lesser amount of cobalt. Both Mössbauer and Co XAFS spectroscopic techniques indicate (Figures 9 and 10) that almost all of both elements are in the metallic state. About 5% of the iron was identified by Mössbauer spectroscopy as being in the form of an iron silicate (probably Fe_2SiO_4). The Mössbauer parameters for the iron metal (Table 2) indicate that the Co is substituted in the same metal phase; i.e an Fe-Co alloy is formed, rather than two separate metallic phases.

Table 2: Mössbauer parametric data for phases in an Co-Fe silica aerogel

Absorption	Isomer Shift in mm/sec	Quadrupole Splitting in mm/sec	Width, in mm/sec	Mag. Splitting, H0, in kG	% total iron in phase %Fe
Fe-Co alloy	0.01	0.01	0.31	340	67.7
Fe-Co alloy	0.02	-0.01	0.31	353	25.7
Fe^{2+}/Fe_2SiO_4	1.16	2.83	0.27	--	4.5
Austenite?	-0.04	--	0.27	--	2

Three distinct samples have been examined by USAXS. These include an undoped silica aerogel and two Co-doped aerogel formulations, before and after reduction. In addition, it was seen that the Co-doped samples had a distinct surface rind or "skin" about 1-2 mm thick on the outermost surface of the aerogel materials. This structure was also investigated by the USAXS technique.

The SC of a supercritical CO_2-dried undoped aerogel is shown in Figure 11 in a typical log-log plot of intensity against scattering vector, q. An ethanol-dried aerogel exhibited virtually the same SC. As can be seen, data collection extends from 0.0002 $Å^{-1}$ to about 1.0 $Å^{-1}$. Hence, structural information can be resolved on a length scale from about 5 Å to 15,000 Å, according to the relationship, $L = \pi/q$. Here, L is the length of an object in real space and q is the scattering vector, which relates to the scattering angle, 2θ, as $4\pi/\lambda\sin\theta$, where λ is the X-ray wavelength.

Of special interest in Figure 11 are the regions where the intensity vs. q relationship changes drastically; i.e. in those regions where there is strong curvature. As is normally done, a Guinier function,

$$I \sim \exp(-q^2R_g^2/3)$$

is fitted to the most pronounced curvature regions to obtain a value for R_g, the radius of gyration. The radius of gyration describes the center of the electron distribution in the irradiated sample and can be related to the radius of spherical objects, R, if it assumed that the scattering arose from such spherical objects, by means of the relationship:

$$R = (5/3)^{1/2}R_g$$

Hence, the least square fit values for the two prominent curved regions in Figure 11 correspond to values of R_g of 5500 Å and 50 Å; in turn, these values correspond to values of R for the equivalent spherical scatterer of 7100 Å and 64.5 Å, respectively.

Another region in the SC in Figure 11 of interest is the quasi-linear portion of the curve at q > 0.1 $Å^{-1}$. For this region of the curve, a linear fit according based on Porod's law has been attempted. The value of -3.6 obtained for the exponent of the power-law fit shows that the intensity variation for this region of the SC does not obey Porod's law, which requires a q^{-4} variation. This difference is indicative of a rough internal surface of the aerogel on this length

scale. Close inspection of the difference between the SC and the power-law fit for q larger than 0.1 Å^{-1} shows a systematic variation that can be explained as scattering from a sharp size distribution of spheres of radius 14 Å. We suspect that this structure represents an uniform microporosity   It was also observed for the ethanol-dried sample. The analysis is shown in Figure 12 and is discussed in more detail in a publication in preparation [3]. Such sharp size distributions are rarely observed and may indicate a hitherto undiscovered structural aspect of this family of aerogels.

Significant differences are seen when comparing the undoped and doped aerogel materials. The doped aerogels differ from the non-doped aerogel in terms of color and appearance. Whereas the non-doped aerogels were slightly bluish, almost transparent and diaphanous, the doped samples were brownish or greenish in color, much more opaque, and of more obvious visibility.

Figure 13 shows a comparison of the SCs for an undoped aerogel and two doped aerogels containing 2 and 10 wt% cobalt. The most striking difference is the presence of an additional structure between 0.001 and 0.006 q. Both doped samples show pronounced intensity humps with Rg of ~1750 and 1050 Å for the 2 and 10 wt% doped aerogels, respectively. For the 10% doped sample, the decay of intensity is more rapid indicative of a relatively sharp size distribution. This extra structure in the case of the doped aerogels is a result of metallic clusters formed by the Co dopant. TEM observations made by Naresh Shah (unpublished) show dendritic-like structure for metallic Co in these materials of approximately the right size to cause such scattering effects. The SC curves for the doped samples also differ in the long tail region (q > 0.4 Å) in that they show a positive deviation of the scattered intensity from their initial exponent of decay. This effect is either due to incoherent scattering from the metallic clusters in the micropores or due to fluorescence scattering because the SC were obtained at an X-ray energy close to that of the K-edge of Co. In either case, the enhanced scattering at such large q values is an indication of cobalt in the pores at this size range.

Other aspects of these materials are currently under investigation. These include the difference between reduced and non-reduced Co-doped aerogels, the structure of the rind or skin formation on the outer surface of the Co-doped samples, and the information obtained by anomalous scattering (ASAXS) in the vicinity of the Co K absorption edge. These items are being investigated in detail and will be included in a paper dealing with the SAXS data on the aerogel materials [3].

Conclusions

Spectroscopic methods such as XAFS and Mössbauer spectroscopies, with their abilities to focus on a specific element, provide important details regarding the speciation of key elements, such as Co and Fe, in xerogel and aerogel materials synthesized at the University of Utah for possible use as catalysts for Fischer-Tropsch applications. In addition, these materials have been examined by USAXS methods in order to obtain information on the short –to-long-range order in these materials, which can be related to details of the porosity or metal precipitate size in these materials. With this latter technique, new information has been obtained regarding the long-range structure of these materials. Such structure is significantly altered by the introduction of cobalt into the aerogel material.

Future Work

Further measurements will be made by both spectroscopic methods and scattering methods to complement and augment the work carried out to date. Co XAFS spectroscopy on these materials is planned for September, 2003.

Reference

1. A. Braun, J. Ilavsky, P. E. Jemian, B. Dunn, E. M. Eyring, F. E. Huggins and G. P. Huffman, *Ultra-small angle X-ray scattering of cobalt-doped silica aerogels.* **In preparation.**
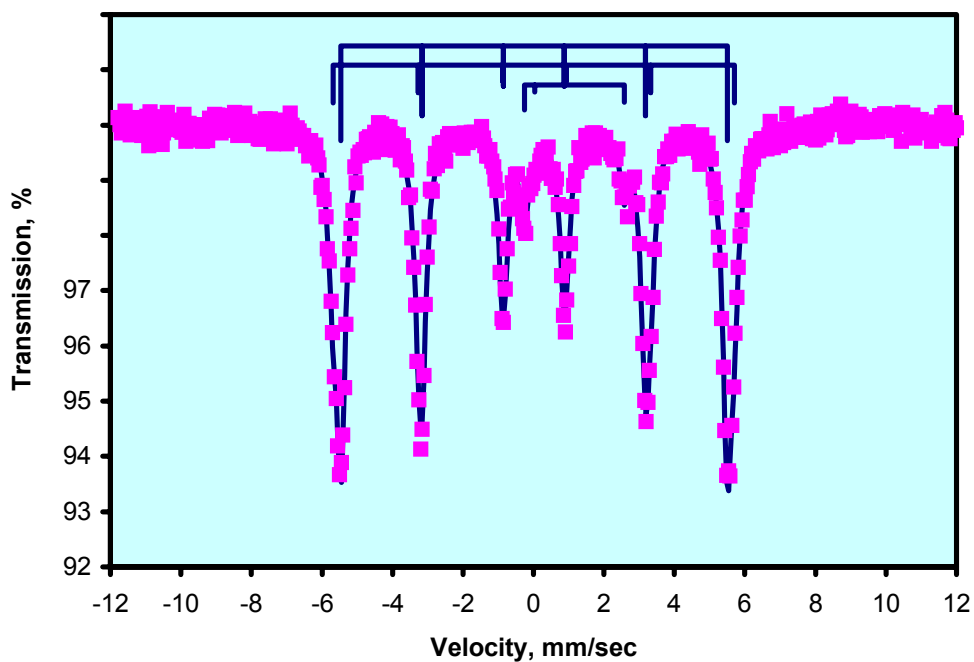
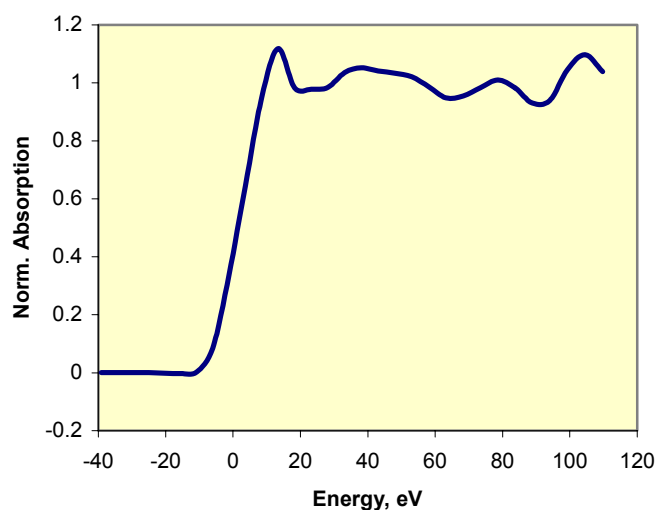Figure 9: Fe Mössbauer spectrum of a Co-Fe xerogel prepared at the Univ. of Utah.

Figure 10: Co XANES spectrum of a Co-Fe aerogel sample from the University of Utah. The spectral structure is virtually identical to that from metallic Co. Zero-point of energy corresponds to 7,709 eV.
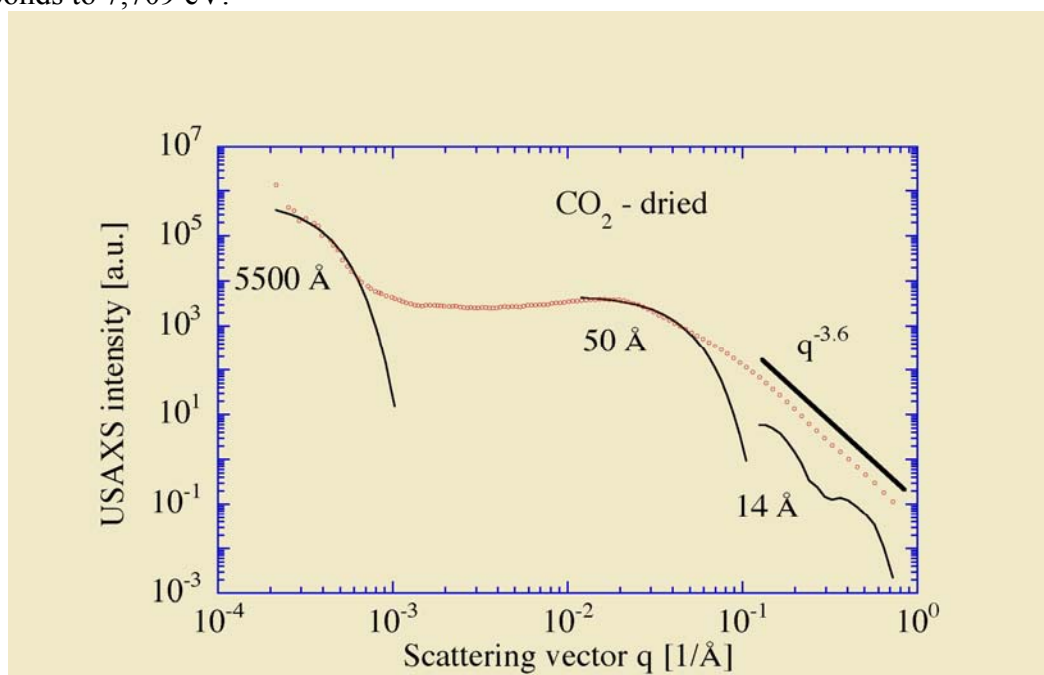

Figure 11: Log-log plot of super-critical CO_2-dried aerogel. Two least-squares fit curved regions based on the Guinier model are shown (curved black lines with radius of gyration, R_g, of 5,500 and 50 Å). The straight line shown to the right side of the apparently linear portion of the SC data is a power-law function fit to the data, with –3.6 as the exponent. The solid line shown below the straight region of the data is the residual of this region of the data with the power-law fit subtracted from the data (see Figure 16).
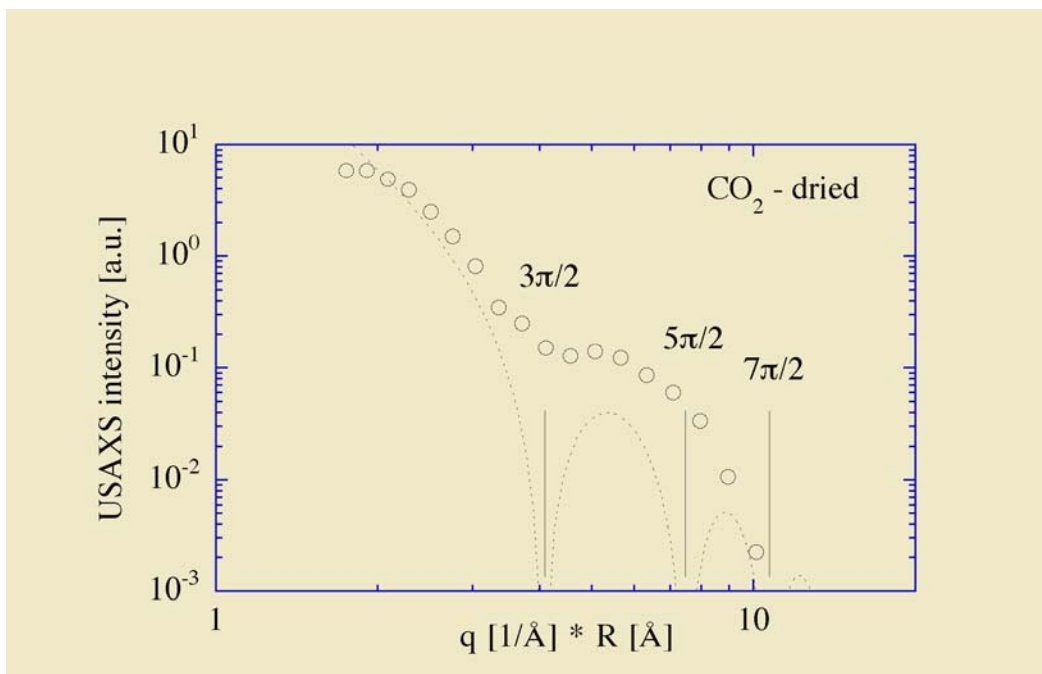
Figure 12: Comparison of micropore scattering of an aerogel and the structure function calculated for spheres of radius 14 Å. Vertical lines denote the expected positions of intensity minima
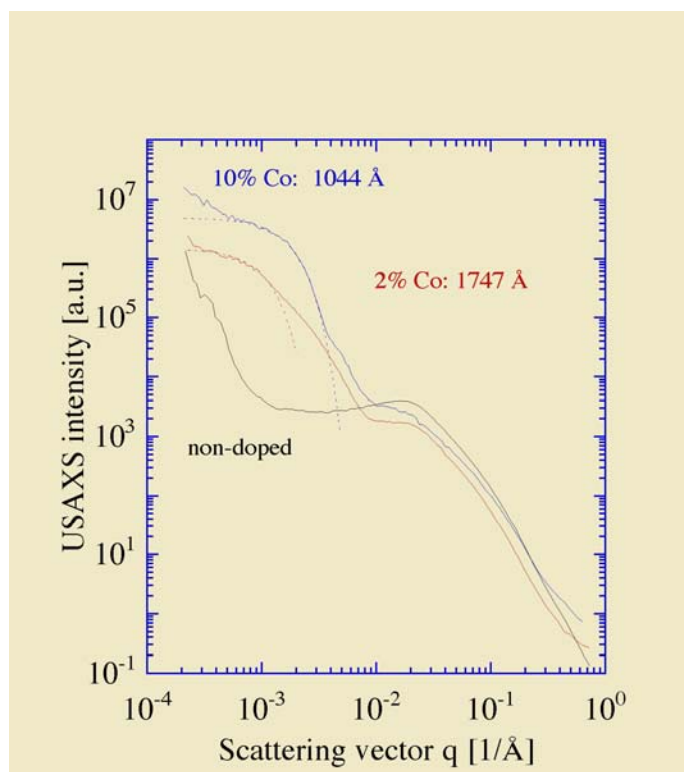

Figure 13: Comparison of scattering curves of a undoped (black line) aerogel and of 2% (red line) and 10% (green line) Co-doped aerogels. Dashed lines of the appropriate color indicate least-squares fits of the curved regions according to the Guinier function.

130

Investigation of Fischer-Tropsch (F-T) Catalysts using Solid State NMR Methods

Zhiru Ma, Brian C. Dunn, Greg Turpin, Ronald J. Pugmire, Richard D. Ernst, and Edward M. Eyring

Department of Chemistry, University of Utah

Introduction

Nuclear magnetic resonance (NMR) is a very important and powerful technique to study the structure and dynamics of various materials. Silica aerogel is a new support material for Fischer-Tropsch (F-T) catalysts; it has the advantages of high surface area, mesoporosity, and an interconnected network of mesopores. Two types of silica aerogel F-T catalysts (cobalt based catalyst provided by Prof. Eyring's lab and iron based catalyst provided by Prof. Ernst's lab) have been investigated by solid state NMR methods. In this report, the following samples are investigated using solid state ^{29}Si NMR and ^{13}C NMR methods: 1) four silica aerogel samples prepared under different conditions; 2) cobalt loaded silica aerogel samples with different Co contents under calcined and uncalcined conditions; 3) ferrocene loaded silica aerogel sample. This is the first time that solid state NMR methods have been used in the study of Co/SiO$_2$ and Fe/SiO$_2$ aerogel F-T catalysts. The silica aerogel's tetrahedral sub-unit structure and the influence of the loaded metal compounds were described by ^{29}Si NMR spectra and spin lattice relaxation time (T$_1$) measurements. The existence and motion of ferrocene in silica aerogel was investigated by ^{13}C NMR.

Experimental Procedure

Materials:
1. Four silica aerogel samples (Provided by the Prof. Eyring lab): (see Prof. Eyring's report for details of sample preparation)
   1. SiO$_2$ aerogel, supercritical CO$_2$ (40°C) processed, not calcined.
   2. SiO$_2$ aerogel, supercritical CO$_2$ (40°C) processed, calcined in static air at 500°C for 4 hours.
   3. SiO$_2$ aerogel, supercritical ethanol (300°C) processed, not calcined.
   4. SiO$_2$ aerogel, supercritical ethanol (300°C) processed, calcined in static air at 500°C for 4 hours.
2. Cobalt loaded silica aerogel samples (Provided by Prof. Eyring lab):
   Two percent and ten percent Co loaded aerogel samples were prepared by the supercritical ethanol process. Each of the loaded samples was calcined and ^{29}Si NMR spectra were obtained on both calcined and uncalcined samples.
3. Ferrocene loaded silica aerogel sample (Provided by the Prof. Ernst lab).

NMR experiments
All the NMR experiments were carried out on a Chemagnetics CMX-200 spectrometer with a 7.5mm PENCIL rotor probe. All the samples were ground into powder before packing into the rotor. Most of the samples were packed at ambient condition except the ferrocene loaded silica aerogel sample which was packed in a glove box filled with nitrogen gas. A single pulse

sequence was applied to observe ^{29}Si NMR spectra, while ^{13}C NMR spectra of the ferrocene loaded aerogel sample was obtained using CP (cross polarization) and CP/MAS (magic angle spinning) techniques. The 90 degree pulse width used for ^{29}Si was 8.0 µs, and the pulse delay for ^{29}Si was from 50 s to 400 s depending on the silica aerogel samples.

Results and Discussion

^{29}Si NMR spectra of silica aerogel samples

Figure 1 shows the ^{29}Si NMR spectra of four silica aerogel samples prepared at different conditions. The ^{29}Si solid state NMR spectrum for a silicate material can yield quantitative information in the form of the degree of Si atom coordination around bonded $Si(O_{1/2})_4$ tetrahedral units. These tetrahedral sub-units are designated Q_n. There are five possible states (designated Q_o, Q_1, Q_2, Q_3, Q_4) that can be present in the NMR spectrum. Typical chemical shift values with characteristic values in the Q region are: $Q_o = -72$ to -82 ppm; $Q_1 = -82$ to -89 ppm; $Q_2 = -92$ to -96 ppm; $Q_3 = -100$ to -104 ppm; and $Q_4 = \sim -110$ [1-5]. Q_o is designated a single tetrahedron, Q_1 an end group, Q_2 a middle group, Q_3 a branching site, and Q_4 a cross-linking group (see Figure 2).

The ^{29}Si NMR spectra of uncalcined aerogel samples (Figure 1a and c) exhibit three peaks at -92 to -96 ppm, -101 to -104 ppm, and -110 ppm. This indicates three Si tetrahedral structural units exist in the aerogel sample: Q_2 (middle group), Q_3 (branching group) and Q_4 (cross-linking group). It suggests a well defined structure exists in the uncalcined silica aerogel. The distinct spectral lines disappear in the ^{29}Si NMR spectra of calcined aerogel samples (Figure 1b and d). However, the chemical shift regimes of the three tetrahedral sub-units are still present indicating that depolymerization has probably not occurred. The calcining process probably increased the inhomogeneity of the sample; therefore the linewidth is broader than that of the sample without calcination, which leads to the disappearance of three distinct peaks.

The line width and relative intensities of three Q sub-units in four silica aerogel samples are given in Table 1. It can be seen clearly that the silica aerogel samples are dominated by Q_3 (branching group) and Q_4 (cross-linking group) sub-units with the relative intensities in the range of 28-34% and 62-67%, respectively. The amount of the Q_2 middle group is very small with its relative intensity in the range of 3-5%. The linewidths of the different Q groups in calcined samples are normally much broader than that of samples without calcination, reflecting the inhomogeneity of the calcined samples.

^{29}Si NMR spectra of cobalt loaded silica aerogel samples

Figure 3 shows the ^{29}Si NMR spectra of 2 mole percent cobalt loaded aerogel samples compared with the silica aerogel without calcination. Addition of the cobalt salt (without calcination) produced spectrum (b) with the disappearance of the three distinct spectral lines. The calcined cobalt loaded aerogel has a similar ^{29}Si NMR spectrum (c) as that of the cobalt loaded aerogel without calcination. The ^{29}Si spectra of cobalt loaded samples do not clearly delineate the structural sub-units observed in the silica areogel sample without calcination (spectrum a). However, the chemical shift regimes still exist in cobalt loaded samples indicating the cobalt loading doesn't crush the defined tetrahedral sub-unit structure in the silica aerogel support. The cobalt is randomly inserted into the aerogel pores, which increases the inhomogeneity of the

silica structure, resulting in the disappearance of the three distinct spectral lines. There are no distinct differences in the ^{29}Si NMR spectra between the calcined and uncalcined cobalt loaded sample.

The ^{29}Si NMR spectra of 10% cobalt loaded aerogel samples (calcined and uncalcined) are very similar to that of 2% cobalt loaded samples (spectra not shown). There is no distinct ^{29}Si spectral difference between 10% cobalt loaded and 2% cobalt loaded aerogel samples.

Ferrocene loaded silica aerogel sample
Figure 4 shows the ^{13}C CP spectra of a static sample of ferrocene in silica aerogel and at a spinning rate of 4 kHz. There is only one symmetric ^{13}C NMR signal from the ferrocene loaded silica aerogel. At room temperature, the ferrocene molecule is rapidly rotating about its 5-fold symmetry axis in the pure ferrocene sample. As a result of this motion, the powder pattern obtained at room temperature is axially symmetric with the unique component (δ_{33}) along the axis of rotation. The remaining two degenerate components ($\delta_{11} + \delta_{22}$) are in the plane perpendicular to the axis of rotation. Therefore, the δ_{11} and δ_{22} values of ferrocene are the same at room temperature because of the rotation along the 5-fold symmetry axis [6]. The static ^{13}C NMR spectrum of ferrocene loaded in a silica aerogel is quite different from that of pure ferrocene molecule. It looks more like the MAS spectrum at spinning rate of 4 kHz except the linewidth is much broader than the MAS spectrum, which indicates the ferrocene molecule is tumbling in the silica aerogel, and this motion averages all kinds of interactions in the molecule and leads to the symmetric static spectrum. It suggests the ferrocene molecule in the areogel is tumbling rapidly in a random fashion as in a gas or liquid state. The ^{13}C chemical shift value of the static spectrum shifts a few ppm compared to the MAS spectrum, but it is still within the ^{13}C chemical shift range of ferrocene.

The ^{29}Si NMR spectrum of a ferrocene-loaded silica areogel sample is similar to the cobalt loaded aerogel sample (spectrum not shown). The loading of ferrocene increases the inhomogeneity of the silica aerogel and results in the disappearance of three distinct spectral lines, but the chemical shift regimes of Q_2, Q_3, Q_4 sub-units still exist.

^{29}Si spin lattice relaxation time (T_1) without and with the loading of metal compounds in silica aerogel sample
Table 2 shows the ^{29}Si spin lattice relaxation times of several silica aerogel samples. It can be seen that the ^{29}Si T_1 of calcined aerogel is longer than that of aerogel without calcination. The ferrocene loaded silica aerogel has an extremely long T_1 (at least 2000 s) and it is difficult to measure accurately. The ^{29}Si T_1 of 10% cobalt loaded calcined silica aerogel is shorter (about 70 s). The influence of loading metal compounds on the ^{29}Si T_1 value is not clear and is still under investigation.

Conclusions
1. The ^{29}Si NMR data clearly delineate the presence of three types of Q sub-unit structures (Q_2 middle group, Q_3 branching group and Q_4 cross-linking group) in silica aerogel samples without calcination.
2. The calcining process and the loading of metal compounds (cobalt and iron compounds) increase the inhomogeneity of the aerogel structure, which results in the disappearance of

the three distinct spectral lines from the Q sub-units. However, the chemical shift regimes of the three Q sub-units are still present, which suggests the silica tetrahedral sub-units do not collapse during these processes.

3. From the relative intensities of the ^{29}Si NMR spectra, it can be seen that Q_3 (branching group) and Q_4 (cross-linking group) are the dominant components in the aerogel samples with minor amounts of Q_2 middle group.
4. No distinct difference in the ^{29}Si NMR spectra is apparent between 2% and 10% cobalt loaded silica aerogel sample.
5. The ferrocene molecule exhibits a fast tumbling motion in the silica aerogel support based on the ^{13}C NMR data. Its behavior resembles a structure in the gas or liquid-like state.
6. The loading of metal compounds has a significant influence on the ^{29}Si spin lattice relaxation time. The interactions between the loading metal compounds and silica aerogel are still under investigation.

Future work

Efforts will be made to:
1. Continue to study the interaction between the loadings of various metal compounds (e.g. Fe, Co, and Ru) and silica aerogel supports by measuring the spin lattice relaxation time (T_1) and silicon-29 and carbon-13 NMR spectra.
2. Search for the best iron-based F-T catalysts by modifying the ligands present in iron compounds. Investigate the iron organometallic compounds in silica aerogel supports and their interactions using ^{13}C and ^{29}Si NMR methods.
3. Try to measure the ^{59}Co NMR spectrum of cobalt loaded silica aerogel catalysts and obtain information about the conformation and state of cobalt in the silica aerogel support.

References

1. S. K. Young, W. L. Jarrett, and K. A. Mauritz, Pol. Eng. Science, **2001**, 41, 1529.
2. Lipmaa, et. al., J. Am. Chem. Soc. 1980, 102, 4889.
3. F. Babonneau, K. Thorne, and J. D. Mackenzie, Chem. Mater. **1989**, 1, 554.
4. T. M. Alum, R. A. Assink, and D. A. Loy, Chem. Mater. **1996**, 8, 2366.
5. M. P. J. Peeters, W. J. J. Wakelkamp, and A. P. M. Dentgens, J. Non-Cryst. Solids, **1995**, 189, 77.
6. A. M. Orent, J. C. Facelli, Y. J. Jiang, and D. M. Grant. J. Phys. Chem. A, **1998**, 102, 7692.

Table 1 Q results in different SiO2 aerogel samples prepared under different conditions

		Aerogel, CO_2, Not calcined(#1)	Aerogel, CO_2, calcined(#2)	Aerogel, ethanol, not calcined(#3)	Aerogel, ethanol Calcined(#4)
	δ(ppm)	-92.1	-91.0	-96.8	-91.7
Q2	LW(Hz)	213	195	147	222
	%	3.3	4.0	5.5	5.4
	δ(ppm)	-101.1	-100.1	-103.7	-100.4
Q3	LW(Hz)	230	323	211	310
	%	34	28.7	31.8	30.4
	δ(ppm)	-110.6	-108.9	-110.9	-109.2
Q4	LW(Hz)	308	410	302	393
	%	62.5	67.3	62.7	64.2

Table 2 29Si T1 values of different SiO2 aerogel samples

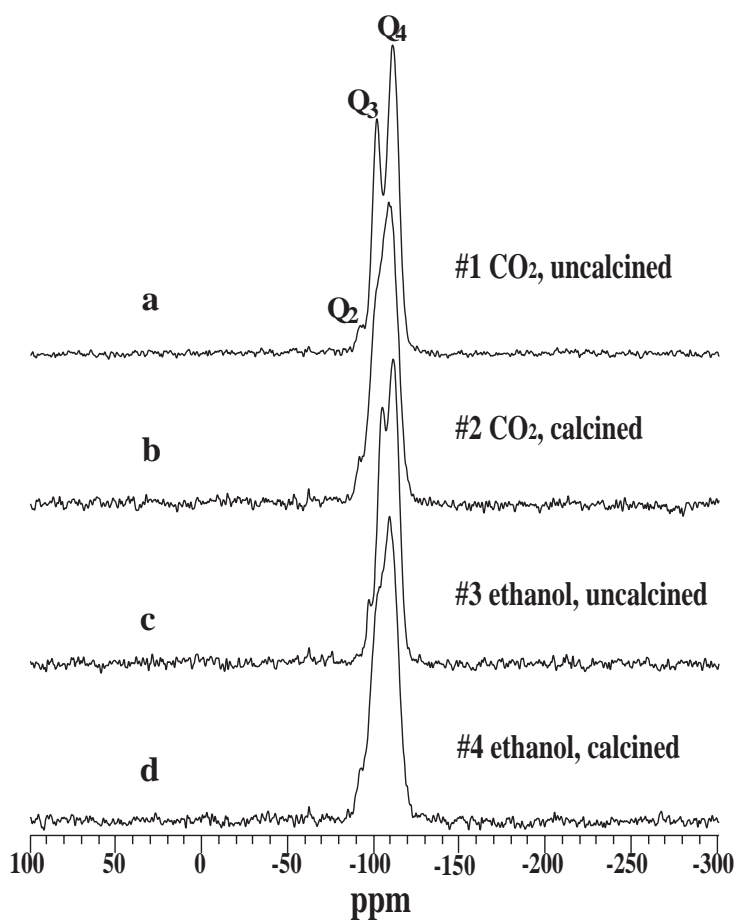| sample	^{29}Si Spin lattice relaxation time T_1 (s)
SiO_2 aerogel, ethanol, not calcined	100
SiO_2 aerogel, ethanol, calcined	400
Ferrocene in SiO_2 aerogel	>2000
10% CoO loaded, calcined	~70

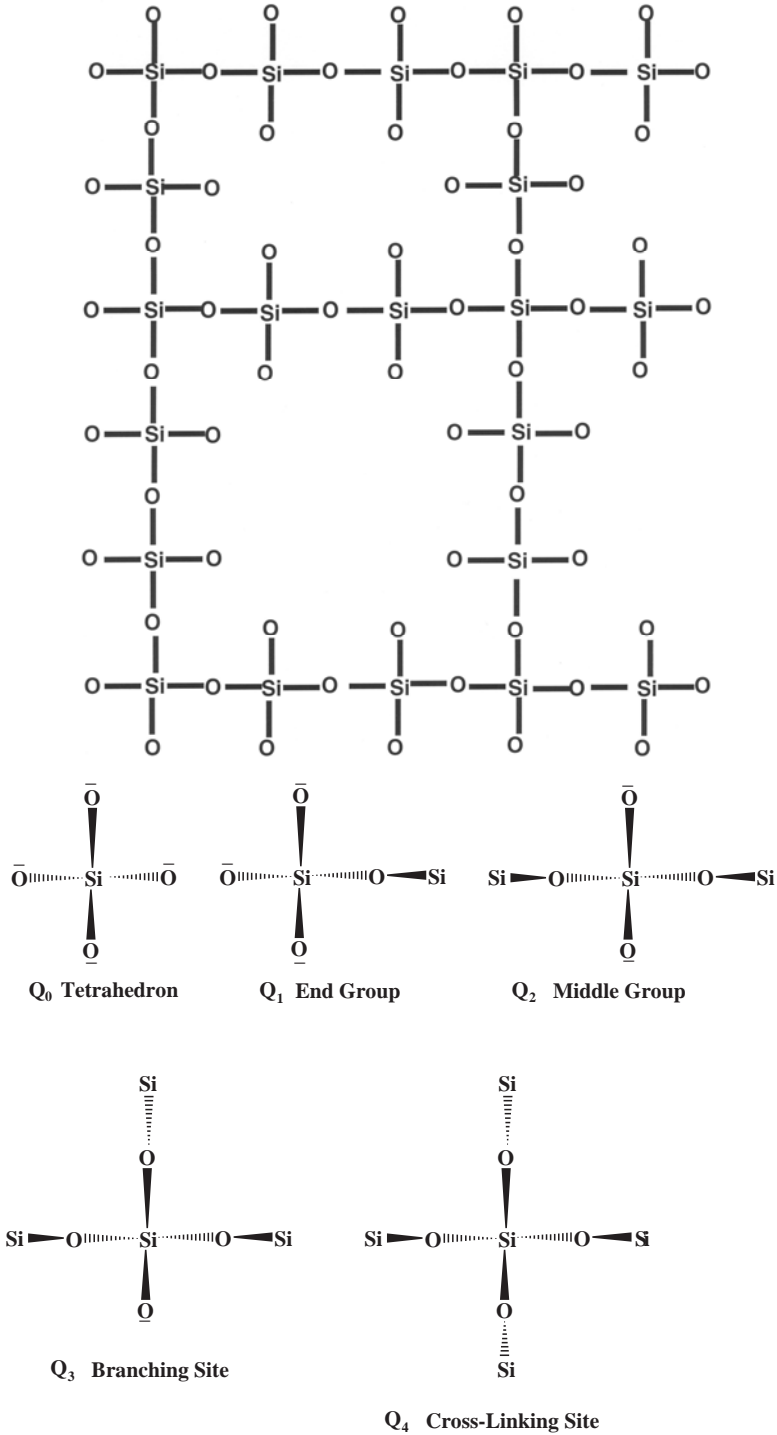Figure 1 ^{29}Si NMR spectra of four samples without Co loading

Figure 2. A stereo-chemical representation of the silica structural units, Q_n (lower portion of the figure), and a two dimensional portrayal of these units in an aerogel matrix (top portion of the figure).
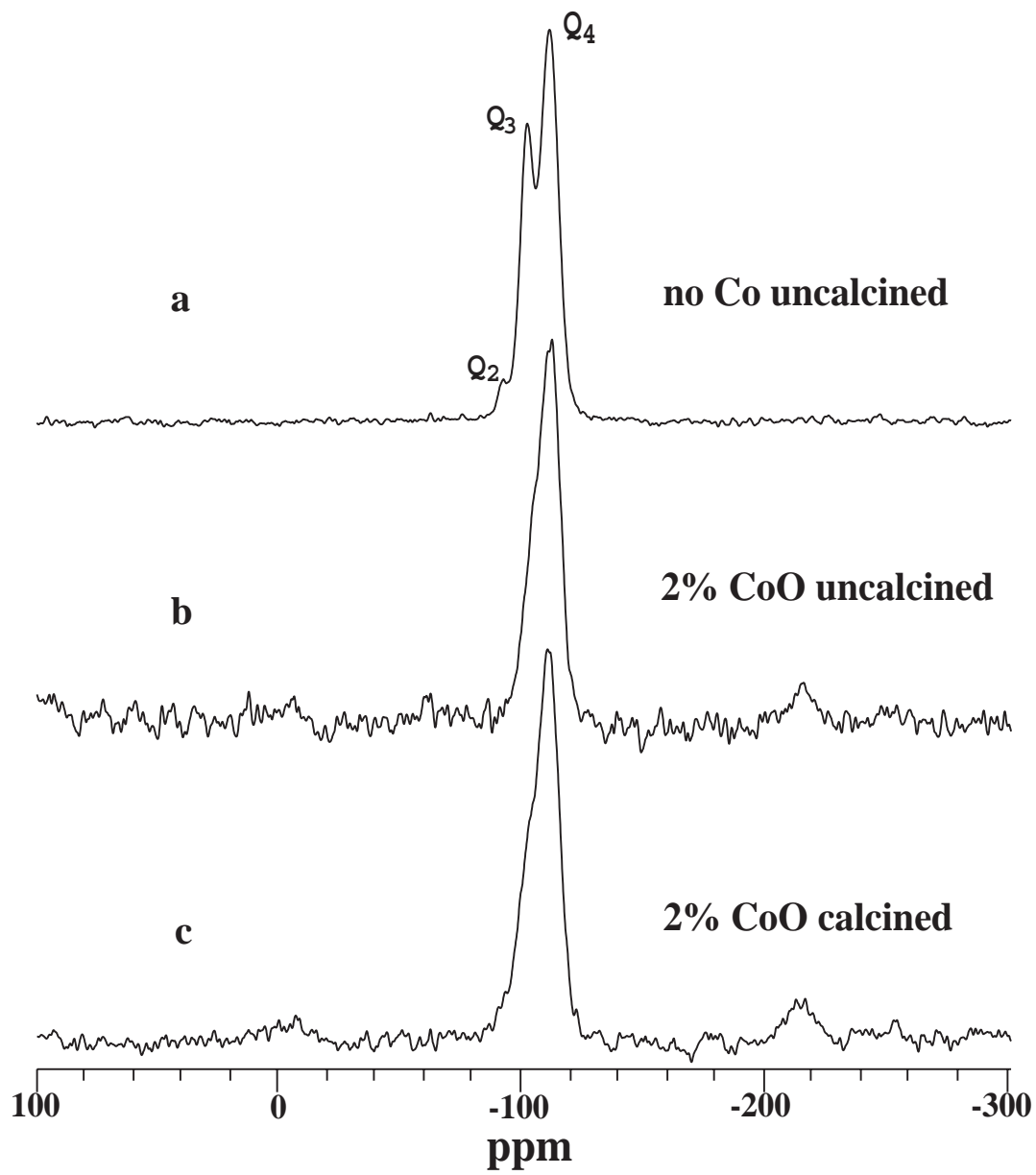
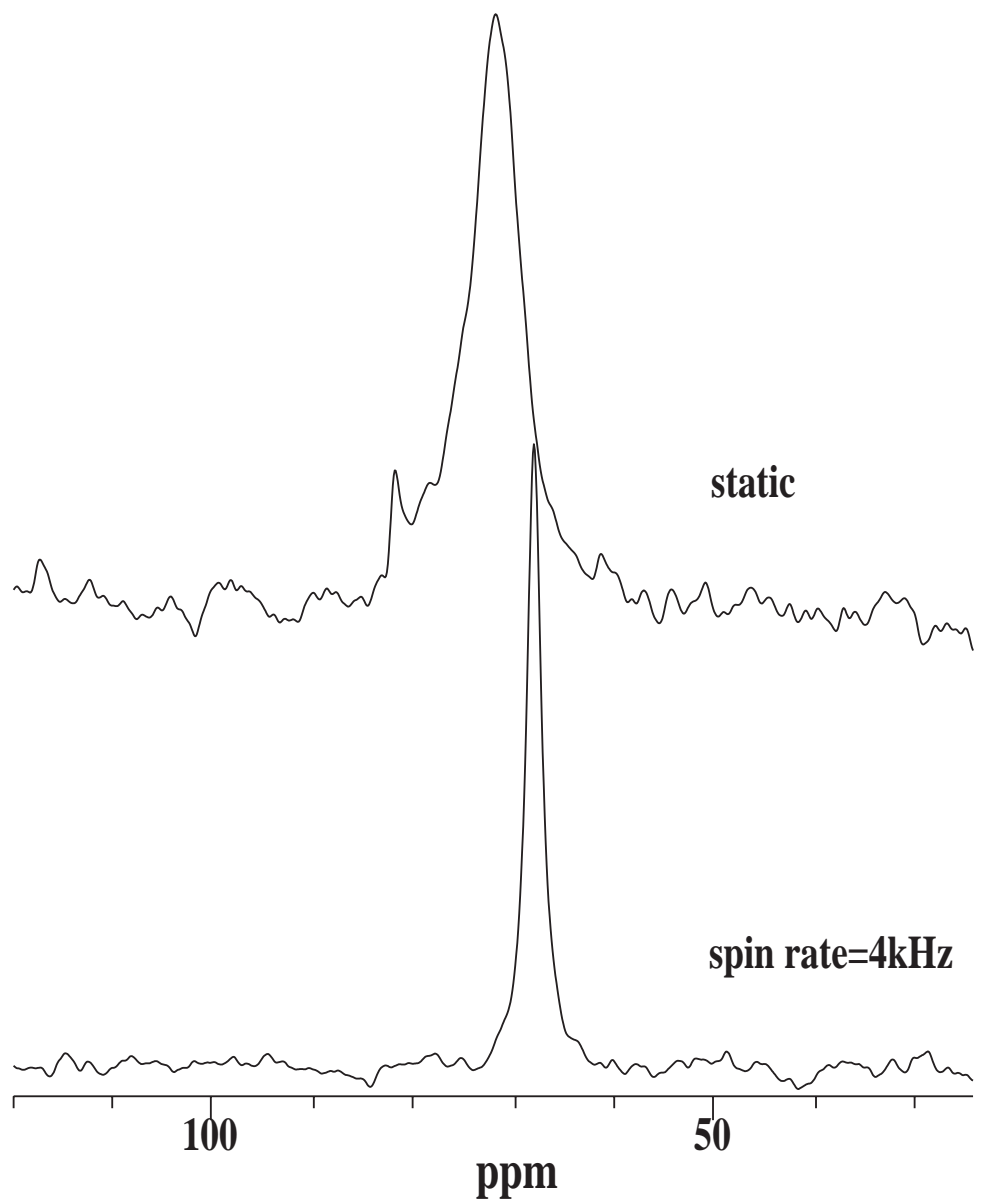Figure 3 ^{29}Si NMR spectra of three samples without and with Co

static

spin rate=4kHz

100   50

ppm

Figure 4 ^{13}C NMR spectra of ferrocene loaded in SiO_2 aerogel

Characterization of Molybdenum and Tungsten Alcohol-Synthesis Catalysts using Temperature-Programmed Reduction and X-Ray Diffraction

Edwin L. Kugler[1], Jonathan C. Hanson[2] and Dady B. Dadyburjor[1]

[1] Department of Chemical Engineering, West Virginia University

[2] Department of Chemistry, Brookhaven National Laboratory

Introduction

We have studied molybdenum and tungsten catalysts to synthesize higher alcohols from CO and H_2 feedstocks. Both catalysts are effective when supported on carbon and promoted with alkali metals. Molybdenum is a better catalyst than tungsten. Tungsten generates methanol and methane with low reaction rates. Molybdenum produces mixtures of C_1 to C_8 alcohols at significant rates. The differences in catalytic performance have led us to study the reduction characteristics of both catalysts. Molybdenum catalysts have been pretreated with hydrogen at 500 ^{o}C prior to being used for alcohol synthesis. Tungsten catalysts are inactive after a 500 degree pretreatment, requiring reduction at 600 ^{o}C for significant reaction rates.

A collaboration with Brookhaven National Laboratory was initiated in 2002 to study temperature-programmed reduction in an x-ray beam. Brookhaven has a unique facility for this experiment. Time-resolved diffraction patterns were obtained that show how molybdenum and tungsten oxides are reduced when supported on carbon. Changes in x-ray diffraction patterns occur at temperatures corresponding to catalyst pretreatment conditions.

Experimental Methods

Time-resolved diffraction data were collected at the National Synchrotron Light Source, Brookhaven National Laboratory on beam line X7B. The molybdenum and tungsten-on-carbon samples studied were prepared by incipient-wetness impregnation and thermal pretreatment in a nitrogen atmosphere using methods described in reference 1. Catalyst samples were loaded into an open sapphire capillary tube that was attached to a flow reactor cell similar to one described in reference 2. The capillary was connected to the reactor with 1/16 inch Swagelok fittings and vespel/carbon ferrules. A 0.010 inch chromel-alumel thermocouple was inserted into the capillary near the catalyst sample. The sample (approximately 1 mg) was heated using a small resistance heater wrapped around the capillary. Diffraction patterns were recorded in the range 25-875 ^{o}C under a 5%H_2 – 95% He gas mixture with flow rates of 10-20 cm^3/min. Samples were heated at 5 ^{o}C/min. X-ray patterns were collected with a MAR345 detector at 5 minute intervals for tungsten and 6 minute intervals for molybdenum. The powder rings were integrated using FIT2D software. Diffraction patterns were identified using the PDF-4 database (International Center for Diffraction Data, ICDD) and JADE software.

Results

Figure 1 shows the x-ray diffraction patterns of a tungsten-on-carbon catalyst that was reduced with 5% hydrogen from 525 to 925 ^{o}C. No changes occurred at lower temperature so that the figure focuses on the temperature range where phase changes occur. The diffraction lines at

lower temperatures are produced by silicon dioxide and non-stochiometric tungsten oxides. The silicon dioxide is an impurity in the carbon support. The tungsten oxides are reduced to metallic tungsten at about 800 ^{o}C.
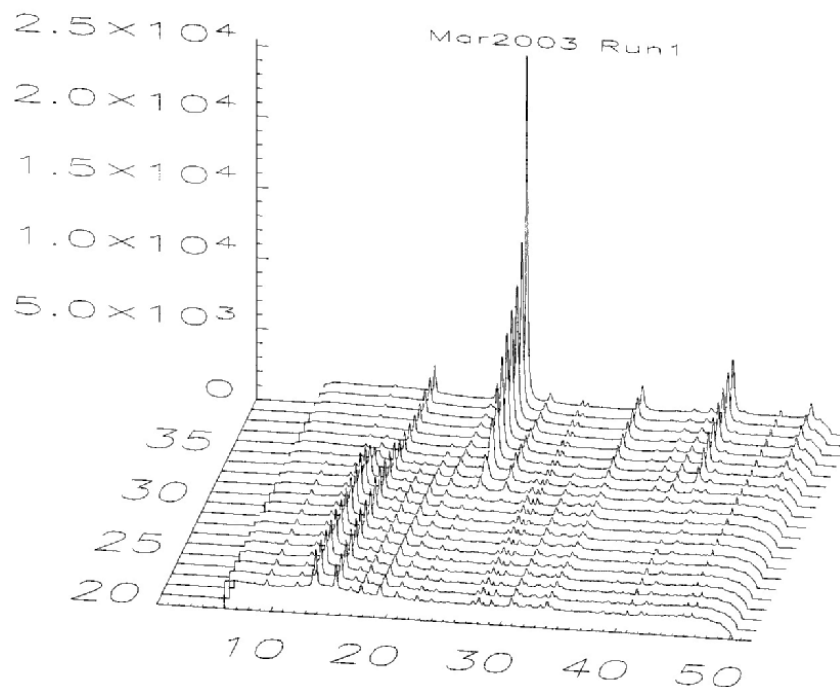

Figure 1. X-Ray diffraction patterns of tungsten-on-carbon measured during hydrogen reduction over the temperature range of 525-925 ^{o}C.

Figure 2 shows the pattern measured at 875 ^{o}C. The strongest peaks are produced by metallic tungsten. Other peaks are produced by the silicon dioxide impurity and by an unidentified phase that can be indexed as α-tungsten or the carbide W_3C. Either phase would be reasonable for a tungsten-on-carbon catalyst. Interestingly, nothing seems to happen to the tungsten oxide diffraction pattern until tungsten is reduced to metallic tungsten. The identified peak may be an intermediate. Additional work is needed to determine if these lines are produced by a tungsten carbide or another phase of metallic tungsten.
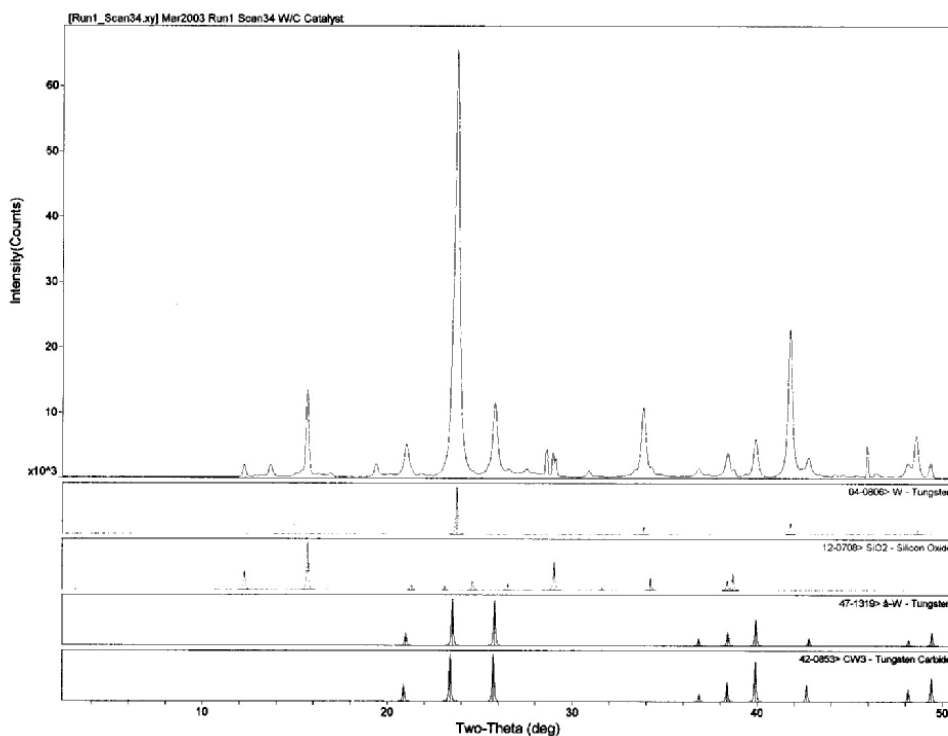
Figure 2. Identification of phases in tungsten-on-carbon catalyst reduced at 875 °C.

Molybdenum on carbon catalysts show a totally different type of behavior when reduced with hydrogen. Figure 3 shows the x-ray diffraction patterns of a potassium promoted, molybdenum-on-carbon catalyst that was reduced with 5% hydrogen from 25 to 875 °C. The diffraction patterns show KMoO4 at low temperatures, reduction to Mo(III) and Mo(IV) oxides at about 500 °C, and finally reduction to Mo_2C at high temperature. The pattern for Mo_2C is shown in Figure 4. The molybdenum carbide is produced directly from molybdenum oxides, with no indication that metallic molybdenum is present. The Mo2C exists as small particles, with an estimated average-particle-size of 3 nm.

All of the molybdenum-on-carbon catalysts studied showed reduction at high temperature to Mo_2C with no evidence of the formation of metallic molybdenum. All potassium promoted, molybdenum-on-carbon catalysts showed the formation of intermediate Mo(III) and Mo(IV) oxides at about 500 °C. These intermediate oxides may be important in alcohol synthesis. Studies during the next year should help to elucidate the important of these phases.
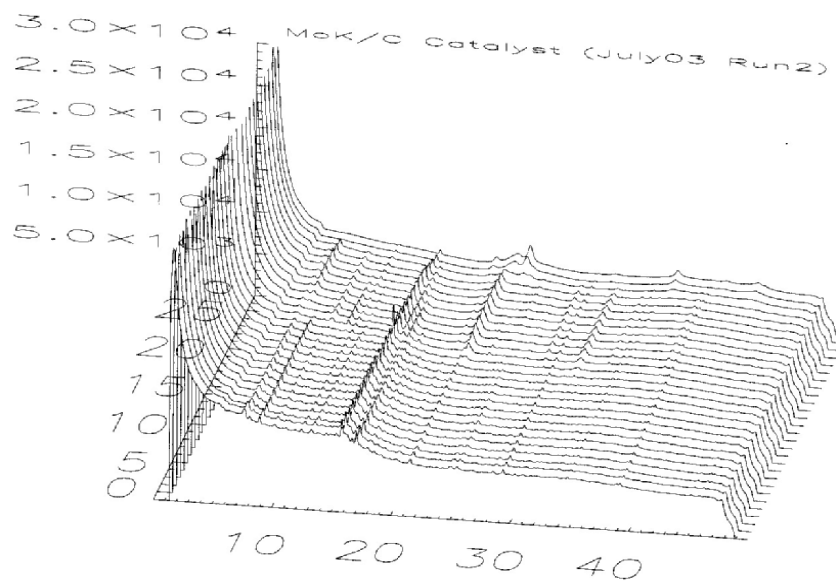
Figure 3. X-Ray diffraction patterns of potassium promoted, molybdenum-on-carbon catalyst measured during hydrogen reduction over the temperature range of 25-875 ^{o}C.
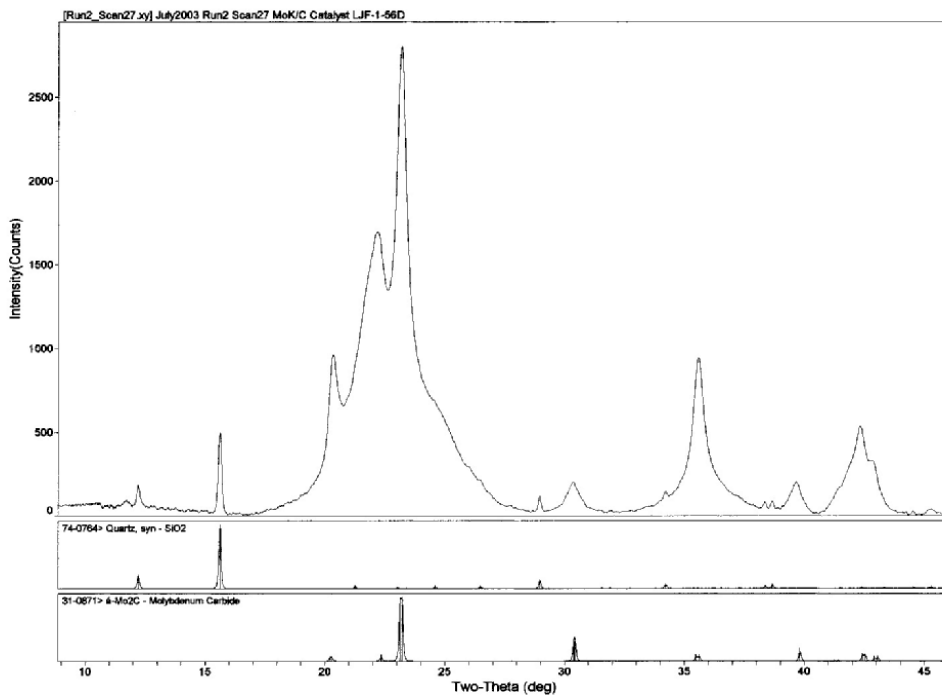

Figure 4. Identification of phases in potassium promoted, molybdenum-on-carbon catalyst reduced at 875 ^{o}C.

Conclusions

In situ x-ray diffraction has shown how several molybdenum and tungsten alcohol-synthesis catalysts are reduced stepwise from the starting oxides to metals and metal carbides. Potassium promoted molybdenum-on-carbon catalysts show intermediate Mo(III) and Mo(IV) oxides which are absent when potassium is absent. The alkali metal appears to stabilize these oxides. The alkali metal is also necessary to produce alcohols with molybdenum catalysts. Without an alkali promoter, only hydrocarbons are produced. This correlation suggests that the observed Mo(III) and Mo(IV) oxide phases are important in alcohol synthesis.

Future Work

Molybdenum-on-carbon catalysts will be prepared to maximize the concentration of phases identified with the *in situ* x-ray diffraction techniques to determine the importance of these materials in higher alcohol synthesis.

References

1. L. Feng, X. Li, D. B. Dadyburjor and E. L. Kugler, J. Catal. **2000**, 190, 1
2. P. J. Chupas, M. F. Ciraolo, J. C. Hanson and C. P. Grey, J. Am. Chem. Soc. **2001**, 123, 1694

Publications and Presentations in Current Year

1. Iyer, M. V., L. P. Norcio, A. Punnoose, E. L. Kugler, M. S. Seehra and D. B. Dadyburjor, Catal. Lett., accepted for publication.
2. Iyer, M. V., L. P. Norcio, E. L. Kugler and D. B. Dadyburjor, Ind. & Eng. Chem. Res. 42, 2712 (2003)
3. Shao, H.-F., E. L. Kugler, M. V. Iyer and D. B. Dadyburjor, in Proc. Fuel Cell Topical Conference, American Institute of Chemical Engineers (2003)
4. D. B. Dadyburjor, Catalysis for Synthesis-Gas Formation from Reforming of Methane, invited lecture at 16th National Symposium, Catalysis Society of India, February 2003